

3.9 DRIFT SEEPAGE MODELS

3.9.1 Introduction

This section summarizes modeling studies performed to estimate seepage of liquid water into waste emplacement drifts. These seepage-related studies are discussed in detail in three AMRs: (1) the development of a seepage process model and its calibration, described in AMR *Seepage Calibration Model and Seepage Testing Data* (CRWMS M&O 2000, U0080), (2) the application of the model to predict seepage under a variety of conditions, described in AMR *Seepage Model for PA* (CRWMS M&O 2000, U0075), and (3) the seepage abstraction process, described in AMR *Abstraction of Drift Seepage* (CRWMS M&O 2000, U0120).

Potential seepage of water into waste emplacement drifts has been identified by YMP as a principal factor that may affect the overall performance of the potential high-level nuclear-waste repository at Yucca Mountain, Nevada (Section 1.2.2). The number of waste packages contacted by water, the corrosion rate of drip shields and waste packages, the dissolution and mobilization of radioactive contaminants, and their release and migration towards the accessible environment all depend on the rate, the chemical composition, and the spatial and temporal distribution of water seeping into the waste emplacement drifts. Consequently, the design requirements of the engineered barriers (CRWMS M&O, 1998h) are affected by the presence or absence, rate, and distribution of drift seepage.

Seepage is defined here as flow of liquid water into an underground opening such as a niche, alcove, or waste emplacement drift. According to this definition, seepage does not include vapor diffusion into the opening or condensation of water vapor within the drift. *Seepage flux* is defined as the rate of seepage per unit area. *Seepage percentage* is defined as the ratio of seepage flux divided by percolation flux. In the context of liquid-release tests, seepage percentage is the ratio of the amount of water that seeped into the niche divided by the total amount of water released. *Seepage threshold* is defined as a critical percolation flux below which no seepage occurs. *Seepage fraction* is defined as the fraction of waste packages affected by seepage. This is equivalent to the number of 5 m drift sections that exhibit a nonzero seepage percentage.

Estimating seepage into underground openings excavated from an unsaturated fractured formation requires process understanding on a wide range of scales, from the mountain-scale distribution of percolation flux to the intermediate-scale channeling or dispersion of flow in an unsaturated fracture network, to the small-scale capillary-barrier effect, to the micro-scale phenomena within fractures and specifically at the drift wall. Moreover, the thermodynamic environment in the drift (temperature, relative humidity, ventilation regime, etc.) must be considered.

The schematic in Figure 3.9-1 illustrates some of the seepage-relevant phenomena and processes. The factors affecting drift seepage can be described as follows:

1. *Capillary-Barrier Effect, Flow Diversion*: Under unsaturated conditions, the rate of water dripping into the opening is expected to be less than the downward percolation rate because the cavity acts as a capillary barrier (Philip et al. 1989, pp. 16–28). (A capillary barrier is sometimes also referred to as a Richards barrier

or cavity effect.) If percolating water encounters the cavity, the relatively strong capillary forces in the formation retain the water, preventing it from seeping into the drift. Water accumulates at the drift ceiling, where the increase in saturation leads to capillary pressures that are locally less negative than in the surrounding rock, allowing water to be diverted around the drift. If the lateral hydraulic conductivity is insufficient to divert the water, fully saturated conditions are reached locally, and seepage occurs as the capillary barrier fails. In an anisotropic fracture network, the orientation of an individual fracture determines which of its hydraulic properties affects seepage most. The effectiveness of the capillary barrier is determined by the capillarity of the vertical fractures and by the permeability and connectivity laterally within the fractures. Note that even though the capillary barrier fails and seepage occurs, the seepage flux is (perhaps significantly) lower than the percolation flux. The seepage threshold and the seepage rate are strongly affected by the drift geometry and formation properties, especially the capillary-pressure and unsaturated hydraulic-conductivity functions. The capillary-barrier effect generally leads to a saturation increase at the apex (crown) of the drift. Flow rates and liquid saturations below the drift are usually lower as a result of the capillary barrier effect, but may be locally increased depending on the drainage system.

2. *Distribution of Percolation Flux, Flow Channeling:* As water percolates through the layered, unsaturated, fractured porous system at Yucca Mountain, it is likely to be redirected and focused into flow channels, which may again be dispersed at fracture intersections. The distribution of flow channels, their frequency, width, and hydrologic properties determine the seepage probability and thus the number of emplacement drifts and waste packages affected by seepage. The spatial distribution of flow channels may change with average percolation flux and potentially with time. Note that calcite deposits suggest that flow channels do not change significantly with time (CRWMS M&O 2000, U0085, Section 6.10.3). Flow focusing is estimated based on the active fracture concept (CRWMS M&O 2000, U0120, Section 6.3.3); these estimates are consistent with an observation of a damped feature in Niche 3566 (Section 2.2.2.2.1). Depending on the flux within an individual flow channel, the seepage threshold may or may not be exceeded locally. A general discussion of channeling effects under unsaturated flow conditions can be found in Birkholzer and Tsang (1997, pp. 2221–2238). Flow focusing occurs and must be accounted for on a variety of scales, as discussed in Section 3.9.3.1.
3. *Hierarchical Fracture Network:* The geometric and hydrologic characteristics of the fracture network affect seepage as they determine the flux distribution and the effectiveness of the capillary barrier. The intermediate-scale (between mountain and drift scale) characteristics of the fracture network affect seep development, potential compartmentalization of the flow field, and effective anisotropy. All these factors determine the spatial distribution of flow channels and the flux within one of those channels. Heterogeneities of the fracture network on different scales and within individual fractures affect local percolation fluxes, and therefore seepage. The capillary-barrier effect is governed by the connectivity of the

fracture network and its capillary strength. Small fractures and microfractures, if interconnected, have the potential to reduce seepage because they have sufficient capillary strength to hold the water, preventing it from freely seeping into the opening. At the same time they have—unlike the matrix—sufficient permeability to facilitate flow diversion around the drift. The question arises whether seepage-relevant fracture properties can be derived from fracture-trace maps, considering that the mapped geometric characteristics and hydraulic properties are not necessarily related. Model calibration is the approach relied upon to determine effective parameters that include the potential effects of individual fractures and microfractures on seepage. Simulations with multiple realizations of a heterogeneous property field are performed to account for the random nature of the fracture network (CRWMS M&O 2000, U0075).

4. *Drift Geometry, Roughness, Breakouts* The geometry (shape, size) of the underground opening (waste emplacement drift, alcove, niche) determines the likelihood of encountering seeps and the ease with which water can be diverted around it as a result of the capillary barrier effect. Analytical solutions examining the impact of drift geometry on seepage threshold were developed by Philip et al. (1989, pp. 16–28). The geometry of drift-wall roughness and the characteristics of the surface (wettability, micro-roughness, dust, and coating) partially control local water accumulation, droplet formation, the potential for film flow along the drift wall, and eventually dripping locations. The frequency, location, size, and geometry of breakouts (locations with a cavity in the drift wall because rock has fallen out) and partial drift collapse affect the integrity of the capillary barrier. Breakouts may lead to distinct topographic lows, which increase seepage, or they make the drift more cone-shaped, which promotes flow diversion and thus decreases seepage.
5. *Ventilation, Evaporation/Condensation*: The temperature and humidity conditions in the drift and their regulation by ventilation determine evaporation and condensation effects. Evaporation at the drift wall generally reduces drop formation and dripping (Ho 1997a, pp. 2665–2671), and creates a dry-out zone around the drift. If relative humidity in the drift is kept below 100% by ventilation, seepage of liquid water is reduced, whereas vapor diffusion into the drift is increased. The moisture from the increased vapor influx is effectively removed by ventilation. Nevertheless, local differences or temporal changes in drift temperature may lead to condensation of vapor, causing droplet formation at the drift wall and other surfaces within the drift. Accumulation of condensate may lead to dripping.
6. *Excavation-Disturbed Zone, Dry-Out Zone*: The properties of the fractured rock in the immediate vicinity of the drift wall control the capillary-barrier effect, which occurs within a relatively small region around the opening. The extent of this zone is approximately given by the height to which water rises on account of capillarity. The zone governing seepage is likely to be smaller than the zone affected by excavation-induced stress redistribution and related rock deformations (opening and closing of existing fractures, generation of new microfractures and

cracks) resulting from drift excavation. Moreover, drift ventilation and/or heating lead to a dry-out zone with associated dissolution and precipitation of minerals (CRWMS M&O 2000, N0120/U0110). The hydrologic properties of this zone, its extent, and the characteristics of its transition to the undisturbed formation potentially impact seepage.

7. *Design*: The layout and design of the potential repository and the engineered barrier system affect the probability of seepage water contacting waste packages.

The complex physical processes affecting drift seepage cannot be addressed comprehensively in an analytical or numerical model, mainly because it is impossible to obtain sufficient characterization data over many scales to describe all the relevant geometric features and hydrologic properties. The characterization and modeling approach presented here focuses on obtaining effective parameters based on seepage-relevant hydraulic data. The abstraction of seepage for Total System Performance Assessment (TSPA) aims at yielding robust, conservative seepage estimates over a wide range of hydrologic conditions (CRWMS M&O 2000, U0120).

3.9.2 Objectives and General Modeling Approach

Seepage predictions are based on and provide information for a suite of models and analyses:

- Site-Scale UZ Flow Model (UZFM) (CRWMS M&O 2000, U0050)
- Calibrated Properties Model (CPM) (CRWMS M&O 2000, U0035)
- Seepage Calibration Model (SCM) (CRWMS M&O 2000, U0080)
- Thermal-Hydrological-Chemical Seepage Model (THC Seepage Model) (CRWMS M&O 2000, N0120/U0110)
- Seepage Model for Performance Assessment (SMPA) (CRWMS M&O 2000, U0075)
- Seepage abstraction (CRWMS M&O 2000, U0120)
- TSPA

The site-scale UZ Flow Model provides (among other quantities) the large-scale distribution of percolation fluxes at the potential repository horizon (Sections 3.7.4.1 through 3.7.4.3). The Calibrated Properties Model (Section 3.6) provides estimates for some of the parameters input to the drift-scale seepage process models. The purpose of the Seepage Calibration Model (SCM) is to present a methodology for the subsequent development of seepage process models (Section 3.9.4). The purpose of the Seepage Model for PA (SMPA) is to provide seepage estimates for a variety of hydrologic properties and drift shapes (Section 3.9.5). The purpose of the THC Seepage Model (Section 3.10) is to analyze the impact of thermal and chemical effects on seepage and to predict the chemical composition of water and gas that may seep into waste emplacement drifts. The purpose of the seepage abstraction is to provide the framework for evaluating seepage into potential repository emplacement drifts for TSPA simulations and to

generate probability distributions that represent the uncertainty and spatial variability of seepage (Section 3.9.6). This information is then used in TSPA calculations for SR.

Figure 3.9-2 schematically shows the relationships between the different seepage models as well as data input and the exchange of information. Air-permeability and liquid-release-test data enter the development and calibration of the SCM, which also uses parameters developed by the CPM. The modeling approach and some of the seepage-relevant parameters from the SCM are used to develop the SMPA, which also evaluates various drift-degradation scenarios. The seepage data calculated with the SMPA enter the seepage abstraction process, which incorporates results from the mountain-scale percolation flux modeling as well as drift-scale THC modeling to arrive at defensible seepage values to be used in the TSPA calculation. This section of the PMR describes the SCM and SMPA as well as the seepage abstraction.

Given the objectives outlined above, the current seepage models are not expected to accurately predict individual seepage events or the precise spatial distribution along the emplacement-drift axis or the drift ceiling. Instead, the seepage models are intended to provide estimates of the seepage flux averaged over a 5 m drift segment (the approximate length of a waste package) as a function of the percolation flux on the drift scale. Once seepage rates are known deterministically for a wide range of conditions, a probabilistic analysis is performed to include uncertainty and spatial variability. In addition, the seepage models improve our understanding of seepage in fractured formations and the relative importance of certain factors (such as drift deformation, variability in the permeability field, and the correlation between permeability and capillary strength).

Seepage models are simplifications and abstractions of the recognized seepage-relevant processes and features summarized in Section 3.9.1. The selection of processes being included in a specific seepage model is guided by their expected significance. Experiments are designed to identify, understand, and characterize significant processes and parameters. Remaining uncertainties and property variabilities are considered either by stochastic simulations and uncertainty propagation analyses, or by assuming large parameter uncertainties in the TSPA calculations. Conservative assumptions are made for effects that cannot be accounted for because of a lack of characterization data.

The following premises guide the seepage modeling approach:

1. Seepage amounts and seepage locations are sensitive to magnitude and local distribution of percolation flux as well as the heterogeneity in fracture properties around the drifts. The heterogeneity cannot be captured deterministically, but rather through geostatistical description, stochastic simulations, and the estimation of effective parameters.
2. Parameters affecting seepage are best derived from tests that reveal seepage-relevant processes. The effective parameters determined in such a manner are process specific, scale dependent, and model related.

3. Uncertainties in the parameters defining the geostatistical model and mean hydrogeologic properties are accounted for in a probabilistic uncertainty propagation analysis.
4. The seepage models must be consistent and compatible with the suite of UZ flow and transport models.

Finally, independent evidence from analog sites is examined and alternative conceptual models are studied to guard against potential flaws in the conceptual models.

As mentioned in Section 3.9.1, seepage is affected by features and processes occurring on a multitude of scales, which cannot be captured in a single model. The model hierarchy presented here assures that each scale is appropriately represented. The site-scale UZ Flow Model provides the large-scale distribution of percolation fluxes (Sections 3.7.4.1 through 3.7.4.3). Flow focusing factors are calculated (Section 3.9.6.3) to account for channeling effects occurring on the drift scale. The heterogeneity in the seepage process models (Sections 3.9.4 and 3.9.5) leads to further flow focusing down to the sub-meter scale. Finally, the estimation of effective parameters through calibration against seepage-relevant data (Section 3.9.4) takes into account the effects of sub-grid-block channeling and other small-scale flow phenomena.

3.9.3 Key Issues and Corresponding Modeling Assumptions

The following is a discussion of key issues pertaining to seepage (see Figure 3.9-3); their relevance (given the objectives described in Section 3.9.2) is discussed, and the simplifying assumptions made in the seepage process models and seepage abstraction are presented in the remainder of this subsection.

3.9.3.1 Percolation Flux and Channeling Effects

Flux and spatial distribution of downward percolating water is the most important factor affecting seepage rates and locations. Water movement is controlled by net infiltration at the surface and subsequent multiscale moisture redistribution either by channeling (flow focusing) or bifurcation (flow dispersion). Large-scale geological units and features such as the PTn and faults lead to a redistribution of percolation fluxes. On an intermediate scale, flow through the fracture network may be focused as a result of flow channeling effects. This leads to zones of locally higher percolation fluxes and (in between them) areas of reduced water flow. Water within such a high-flux zone (weep) may be further channeled by small-scale heterogeneities of the fracture network. Finally, heterogeneity and flow instabilities within individual fractures lead to small-scale flow channels (rivulets or fingers). Since flow diversion and average seepage flux are determined by the characteristics of these rivulets as they encounter the drift wall, it is important to estimate channeling effects on all scales.

A single numerical model cannot possibly account for multiscale heterogeneity and channeling effects—from large-scale flow redistributions to small-scale rivulet formation. Therefore, a series of models was developed, each addressing flow channeling on its assigned scale. The model hierarchy can be described as follows:

1. Flow redistribution on account of large-scale features is considered in the site-scale UZ Flow Model (Section 3.7.2). This model provides average percolation fluxes on the scale of hundreds of meters (CRWMS M&O 2000, U0050).
2. Potential concentration of flow from the large-scale averages to the scale of an individual drift segment (an area of tens of square meters) is accounted for by multiplying the average flux with a stochastic flow-focusing factor, taking into account the fact that flow is reduced in other areas. These flow-focusing factors are estimated using the active fracture concept of Liu et al. (1998, pp. 2633–2646) and geometric arguments. The approach is described in Section 3.9.6.3 and CRWMS M&O (2000, U0120, Section 6.3.3).
3. Flow redistribution on the scale of a few meters or less is simulated in the drift-scale seepage process models (Sections 3.9.4 and 3.9.5), in which heterogeneities in the fracture continuum are explicitly represented based on geostatistical analysis of air-permeability values (Sections 3.9.4.4 and 3.9.5.2). Seepage is then calculated for multiple realizations of stochastically generated property fields.
4. Phenomena and processes that occur on a scale smaller than the gridblock size of the numerical model are accounted for by estimating effective parameters through inverse modeling. The impact of rivulets on seepage and other small-scale effects are not modeled explicitly, but are implicitly considered by estimating seepage-relevant parameters. Specifically, if water from a small-scale rivulet or through film flow seeps into the opening during a liquid-release test, it is reflected in the corresponding seepage data point. By adjusting parameters during the calibration process to match these data points, the small-scale effects are automatically accounted for in an integrated way.

In summary, percolation flux used in the seepage process models is taken to be the large-scale average flux multiplied by flow-focusing factors. This increased flux is applied uniformly at the top boundary of the model, and additional focusing occurs as water percolates through the heterogeneous property field of the model. The calculated seepage fraction is finally determined based on property values determined in an inversion of seepage-relevant data that include small-scale effects.

3.9.3.2 Episodic Flow

Percolation flux is not expected to be constant with time, but may increase episodically as a result of high-infiltration events, seasonal variations, and climate changes (Section 3.7.2). Episodic flow events may affect seepage in two ways:

1. Episodic flow events lead to periods when percolation fluxes (and thus seepage rates) are greater than the corresponding average values.
2. Episodic flow events lead to transient effects (such as storage and hysteresis).

Temporally increased percolation fluxes can be handled by applying episodic-flow factors in a way similar to the flow-focusing factors discussed in Section 3.9.3.1 (see also CRWMS M&O

(2000, U0120, Section 6.3.4)). Currently, there is no evidence that high-frequency fluctuations (a few years or shorter) penetrate to the depth of the potential repository. Flow simulations have shown that the PTn effectively damps out flow transients (Section 3.7.3.1). Note that increased percolation from long-term transients (climate change) is explicitly accounted for in the TSPA analysis (CRWMS M&O 2000, U0120).

Seepage is controlled by the properties of a small zone surrounding the drift. Consequently, storage effects as a result of episodic flow events are negligible if the event is longer than the time required to change the saturation in the available pore space in that zone. High-frequency, large-amplitude net infiltration events are damped as they travel through the mountain to the extent that they arrive as diffuse fronts of small amplitude at the potential repository horizon, making storage effects in the seepage-controlling zone negligible. An episodic-flow scenario is discussed in CRWMS M&O (2000, U0075, Section 6.6.7). Additional documentation on the implications of episodic flow for seepage is presented in CRWMS M&O (2000, U0170, FEP number 2.2.07.05.00).

The parameters of the capillary pressure curve are determined by inversion of liquid-release tests (Section 3.9.4). These tests are imbibition experiments, yielding a wetting branch of a hysteretic capillary pressure curve. If hysteresis were important, this approach would lead to a conservative estimate of capillary strength. Potential hysteresis effects, however, are neglected because these effects are considered to be small in comparison to the uncertainty inherent in the empirically determined capillary pressure relations.

3.9.3.3 Ventilation, Evaporation, and Condensation Effects

Ventilation leads to reduced relative humidity in the drift and forced advective removal of water vapor. The potential impact on seepage and seepage experiments are as follows:

1. Water evaporates at the drift wall, reducing the rate of liquid water seeping into the opening.
2. Diffusive vapor transport into the drift increases, potentially creating a dry-out zone around the opening.
3. Water collected in the capture system during liquid-release tests evaporates, leading to apparently smaller seepage rates.
4. Spatial or temporal temperature changes may lead to condensation of water at the drift wall.

Evaporation of water at the drift wall reduces seepage. This effect may be significant during ventilation periods, when the evaporation rate exceeds the potential seepage rate, preventing the development of liquid droplets that drip into the opening. Ho (1997a, pp. 2665–2671) provides a detailed description of evaporation mechanisms on the scale of individual water droplets within or emerging from fractures. The fact that no natural seepage is currently observed in the ESF could be attributed to ventilation effects. (Note that, because of the capillary-barrier effect, zero seepage may result even if the relative humidity in the ESF were 100%.) Neglecting ventilation and evaporation effects in a numerical seepage prediction is conservative because omitting them

increases predicted seepage of liquid water. Therefore, the assumption is made that the relative humidity in the drift is 100% (i.e., there is a zero-capillary-pressure boundary condition applied at the drift wall). In a ventilated drift, the development of a dry-out zone increases the capillary pressure and local storage volume and thus reduces the risk of reaching seepage conditions; the assumption of 100% relative humidity in the drift is again conservative. The assumption is also reasonable for the time when ventilation is stopped and the drift is closed.

The reduced relative humidity in a ventilated drift increases diffusive vapor flow from the rock into the opening. However, the underestimation of diffusive vapor flow in a model with 100% relative humidity is irrelevant, because the assumption already implies that the moisture content in the drift environment is at its maximum. The assumption of 100% relative humidity is conservative since it maximizes the amount of moisture that can condense within the drift. While condensation is a potentially important effect, no estimates of drip formation as a result of condensation due to temperature variations or in-drift movement of moist air are presented here.

Evaporation of water collected in the seepage-test capture system leads to an underestimation of seepage rates during a liquid-release test and is therefore not conservative. Parameters are adjusted during the inversion such that the model reproduces the observed seepage percentage, which is likely to be too small. This issue is currently addressed by monitoring relative humidity in the niche and directly measuring evaporation rates. Moreover, the estimation of seepage-relevant parameters is predominantly based on data from short-term liquid-release tests that were performed at rates significantly higher than the potential evaporation rate.

For these reasons, drift ventilation effects are neglected in the current seepage process models. Note that evaporation and condensation in the rock as a result of waste-generated heat is accounted for in the THC Seepage Model (Section 3.10.5; CRWMS M&O 2000, N0120/U0110). In-drift evaporation and condensation effects are not considered here.

3.9.3.4 Excavation Effects, Surface Roughness, and Drift Degradation

Drift excavation induces mechanical disturbance and stress redistribution in the surrounding rock, creating a zone with altered formation properties. Surface roughness at the drift wall, breakouts and rock fall from the drift ceiling, and changes in drift geometry as a result of partial drift collapse may result in local topographic lows along the drift ceiling, where water tends to accumulate. These features have the following impact on seepage:

1. Increased fracturing, fracture dilatation, and fracture compression affect the hydrologic properties of the excavation-disturbed zone (EDZ), and may increase or decrease seepage.
2. Small-scale roughness increases local ponding probability and thus increases seepage.
3. Depending on the location of rock fall along the drift perimeter and the geometry of the breakouts, these intermediate-scale changes in drift-wall geometry tend to promote seepage as water may be channeled into rock wedges from which it

cannot escape. The frequency, location, and geometry of breakouts determine their overall impact on total seepage.

4. Depending on the final shape of the drift, partial or complete drift collapse may either increase or decrease seepage into the remnants of the opening. Since breakouts tend to produce local topographic lows along the drift wall, it is more likely that drift collapse leads to an increase in seepage.

Existing fractures may be opened or compressed as a result of drift excavation. The mechanism leading to either opening or closing of fractures depends on the location of the drift in relation to major geologic features, the position along the drift circumference (crown, spring line, invert), the local stress condition, the fracture orientation and fracture network characteristics, the rock-mechanical properties of the fractures and the matrix, and the rock-mechanical behavior during the deformation (elastic, inelastic). Fracture dilatation leads to an increase in permeability, which tends to reduce seepage, and at the same time to a decrease in capillary strength, which tends to increase seepage. Conversely, reduced permeability as a result of fracture compression tends to promote seepage, but at the same time the increased capillary strength enhances the water retention capability, reducing seepage. This counteracting effects reduce the overall impact of fracture deformation on seepage. A detailed analysis of the coupled hydrologic-mechanical behavior as a result of drift excavation and its effect on seepage is difficult to perform. Note that the approach described in this section relies on the calibration of data from seepage experiments that were performed in the excavation-disturbed zone. The data thus reflect potential effects of fracture dilatation or compression on seepage. Matching these data through inverse modeling yields effective parameters that include potential excavation effects.

The extent of the EDZ is likely to exceed the thickness of the zone that determines seepage. This is confirmed by modeling (Bidaux and Tsang 1991, pp. 2993–3008) and experimentation (Wang and Elsworth 1999, pp. 751–757). The seepage-relevant properties of this zone are determined by calibration against liquid-release-test data. As a result of this approach, the potential impact of the EDZ on seepage is automatically accounted for in a calibrated seepage process model. Note that excavation-induced (micro-) fracturing around the drift increases permeability without significantly reducing the effective capillary strength. This reduces seepage by promoting flow diversion. On the other hand, dilatation of existing fractures is accompanied by a reduction in capillary strength, offsetting the advantage of increased permeability by a reduced strength of the capillary barrier.

If the amplitude of small-scale surface roughness reaches a significant fraction of the capillary head, small-scale lateral flow diversion is impeded and saturation in the troughs of the wavy or jagged surface is elevated, leading to increased seepage. The impact of small-scale, sub-gridblock surface roughness is automatically accounted for through the estimation of effective seepage parameters.

A breakout can be described as an intermediate-scale surface roughness. Water is accumulated in topographic lows created by the breakout, leading to increased local seepage if no opportunities or insufficient opportunities for flow diversion exist. The impact of breakouts on seepage depends on block size and rock fall frequency, which in turn is functions of fracturing and stress

conditions. Examples of 3-D seepage simulations with discrete breakouts are presented by CRWMS M&O (2000, U0075, Sections 6.4.2 and 6.6.5).

Extended rock failure and partial drift collapse may change the shape of the opening in a way that promotes or reduces seepage. One example yielding increased seepage is shown in Section 6.4.3 and CRWMS M&O (2000, U0075, Sections 6.4.3 and 6.6.5). The composite effects of drift degradation are accounted for in the seepage abstraction (Section 3.9.6) through application of a seepage-rate enhancement factor (CRWMS M&O 2000, U0120, Section 6.3.1).

3.9.3.5 Capillary Barrier and Seepage Threshold

The capillary-barrier effect has been described in Section 3.9.1, Point 1. While the development of a capillary barrier and the existence of a seepage threshold are the result of the fundamental behavior of fluids in unsaturated media and are well-understood features of a hydrogeologic system (see, for example, Frind et al. (1977, pp. 3133–3163); Philip et al. (1989, pp. 16–28); Oldenburg and Pruess (1993, pp. 1045–1056); Birkholzer et al. (1999, pp. 349–384)), the effectiveness of the capillary barrier at a specific location is difficult to determine. It specifically depends on the permeability and capillary strength near the opening. Moreover, the performance of a capillary barrier must be assessed as a total system (here on the scale of the cross section of a waste emplacement drift) that considers all the factors discussed in Sections 3.9.3.1 through 3.9.3.4.

A detailed characterization of seepage-relevant, small-scale hydrogeologic properties near the drift wall appears unfeasible. Fracture-trace maps are likely to be biased because they exclude small fractures and microfractures, which may be crucial for the performance of the capillary barrier. In addition, it is difficult to relate the mapped geometric characteristics to the hydraulic properties governing seepage. For these reasons, no use of geometric fracture network information is made, because it would require making numerous simplifying assumptions to arrive at the hydrogeologic properties controlling seepage. Instead, seepage-relevant properties are determined, and the overall performance of the drift as a capillary barrier is assessed by conducting and analyzing liquid-release tests. As water injected from a borehole reaches the opening at the drift crown, the capillary barrier comes into effect. Some of the water may seep into the opening, whereas the rest is diverted laterally, eventually flowing around the drift. Analyzing data from this experiment ensures that the capillary barrier is tested on the appropriate scale, in the relevant zone, and using the pertinent physical processes such as water retention and pressure build-up in the fractures, flow diversion through microfractures, local failing of the capillary barrier in discrete fracture segments intersected by the opening, and seepage as a result of film flow. Nevertheless, numerical modeling is required to estimate seepage under changed conditions, namely lower percolation fluxes. Currently, the validity of such an extrapolation cannot be assessed experimentally. The synthetic modeling study presented in CRWMS M&O (2000, U0080, Section 5.3) suggests that reasonable predictions of seepage for lower percolation fluxes can be obtained when following the approach described here and in Section 3.9.4 below. It should be realized that applying a numerical model to conditions and time scales different from those encountered during model calibration always bears a risk, because the underlying mechanisms significant to seepage may change.

The seepage threshold may be considered a characteristic point describing the performance of a capillary barrier. It indicates whether or not water seeps into the opening for a given local percolation flux. However, performance assessment requires predicting seepage rates over the entire range of expected percolation fluxes. Even if seepage-threshold estimates remain uncertain, the reduction of drift influx at percolation fluxes above the seepage threshold is an important aspect of the seepage problem. The relative difficulty of accurately determining the seepage threshold does not invalidate the calculation of seepage fluxes.

3.9.4 Seepage Calibration Model

3.9.4.1 Objectives and General Approach

In this section the development, calibration, and validation of the Seepage Calibration Model is described. The purpose of the SCM is to present a methodology for the subsequent development of seepage process models such as the Seepage Model for Performance Assessment (Section 3.9.5). The SCM is a template, heterogeneous fracture-continuum model that is developed based on air-permeability and liquid-release-test data from the experiments performed in Niche 3650 of the ESF at Yucca Mountain. The steps involved in the development of the SCM are schematically shown in Figure 3.9-4. A geostatistical analysis of post-excavation air-permeability data provides the basis for the generation of a heterogeneous property field, which is mapped onto the model grid. Liquid-release tests are simulated to calibrate the model against measured cumulative-seepage data. The calibrated SCM is then validated using data from additional liquid-release tests. The development of the SCM is documented in CRWMS M&O (2000, U0080).

The scope of this modeling study is limited to an analysis of seepage data from Niche 3650. The parameters estimated by the SCM are thus only representative for isothermal seepage into an uncollapsed opening excavated in the middle nonlithophysal zone of the Topopah Spring welded tuffs at Yucca Mountain.

3.9.4.2 Air-Permeability and Liquid-Release-Test Data

Air-injection tests were performed in boreholes drilled above Niche 3650, and air-permeability values were determined (CRWMS M&O 2000, U0015, Section 6.1). A geostatistical analysis of these post-excavation air permeabilities provided a measure of statistical variability and spatial correlation (see variogram in the top panel of Figure 3.9-4). The air-permeability field is essentially random, without a noticeable spatial correlation.

A series of short-duration liquid-release tests was performed at Niche 3650. The seepage tests were conducted after niche excavation by introducing water into select test intervals in boreholes located above the niche. The tests were performed by sealing a short section of borehole (using an inflatable packer system) and then releasing water at a constant rate into the isolated test interval. Any water that migrated from the borehole to the niche ceiling and dripped into the opening was captured and weighed. The seepage percentage, defined as the mass of water that dripped into the capture system divided by the mass of water released into the borehole interval, was used to quantify seepage into the drift from a localized water source of known duration and

flow rate. Details about the liquid-release tests can be found in CRWMS M&O (2000, U0015, Section 6.2).

The heterogeneous property field of the SCM was developed based on the geostatistical characteristics of the air-permeability data (Section 3.9.4.4). The seepage-relevant hydrologic properties were determined by calibrating the SCM against the liquid-release-test data (Section 3.9.4.5).

3.9.4.3 Model Assumptions

The basic assumptions of the SCM are consistent with those of other submodels of the UZ Flow and Transport Model (see Section 1 for list of submodels; see CRWMS M&O (2000, U0050, Sections 5 and 6.1.2) for assumptions and modeling approach); the submodel of specific concern is the SMPA described in Section 3.9.5. Consistency and compatibility are essential requirements because the concepts and parameters derived with the SCM are only valid and useful for subsequent seepage calculations if they refer to similar conceptual models. The key assumptions are summarized below; additional assumptions and a more detailed discussion of why they are considered valid or reasonable can be found in CRWMS M&O (2000, U0080, Section 5).

It is assumed that the continuum approach is a valid concept to calculate percolation flux and drift seepage at Yucca Mountain. This assumption is based on the observation that the fracture network in the Topopah Spring middle nonlithophysal unit at Yucca Mountain is well connected (CRWMS M&O 2000, U0075, Section 6.7). In addition, the synthetic study presented in CRWMS M&O (2000, U0080, Section 5.3) demonstrates that simulating seepage into underground openings excavated from a highly fractured formation can be performed using a model that is based on the continuum assumption, provided that the model is calibrated against seepage-relevant data such as data from a liquid-release test. Synthetically generated data from a model that exhibits discrete flow and seepage behavior were used to calibrate a simplified fracture-continuum model. Seepage predictions for low percolation fluxes made with the calibrated fracture-continuum model were consistent with the synthetically generated data from the discrete-feature model. The appropriateness of using the continuum approach to simulate flow through fractured rock was also studied by Jackson et al. (2000, pp. 189–202) using synthetic and actual field data. They concluded that heterogeneous continuum representations of fractured media are self-consistent, i.e., appropriately estimated effective continuum parameters are able to represent the underlying fracture network characteristics.

Adopting the continuum approach, water flow under unsaturated conditions is assumed to be governed by Richards' equation (Richards 1931, pp. 318–333). Relative permeability and capillary pressure are described as continuous functions of effective liquid saturation according to the expressions given by the van Genuchten-Mualem model (Luckner et al. 1989, pp. 2191–2192). Within the heterogeneous property field, capillary strength is correlated to absolute permeability according to the Leverett scaling rule (Leverett 1941, p. 159).

3.9.4.4 Model Development

Because the SCM was to be calibrated against liquid-release-test data obtained in Niche 3650, the model was discretized to include the approximate geometry of the niche and its boreholes. A permeability field was generated, conditioned on and following the geostatistical properties of the post-excavation air-permeability data measured in various intervals of the three boreholes drilled above the niche. The resulting permeability field was mapped onto the numerical grid of the SCM, and the capillary-strength parameter was correlated to the permeability in each grid block according to Leverett's scaling rule (Leverett 1941, p. 159). The location of Niche 3650, its layout, and the corresponding numerical grid and log-permeability field of the 3-D heterogeneous SCM are shown in Figure 3.9-5. Simplified versions of the SCM include a 2-D X-Z cross section and homogeneous versions of the model in two and three dimensions.

A free-drainage boundary condition was applied at the bottom of the model. The niche itself was set at a reference pressure of 1 bar. No capillary suction was applied in the niche, i.e., it was assumed that the air at the niche wall was of 100% relative humidity (see discussion in Section 3.9.3.3). Water was allowed to enter, but was prevented from exiting the niche. Thus, the temporal change of water in the niche element represented the cumulative seepage collected in the capture system installed during the liquid-release tests in Niche 3650. No-flow boundary conditions were specified at the left, right, back, and front sides of the model. Initial parameter estimates were obtained from the Calibrated Properties Model (CRWMS M&O 2000, U0035), and a steady-state simulation was performed to obtain the initial saturation distribution. More details about the development of the SCM can be found in Section 6.3 of CRWMS M&O (2000, U0080).

3.9.4.5 Model Calibration

Data from five liquid-release tests (CRWMS M&O 2000, U0080, Table 6) were selected for calibration of the seepage model by means of inverse modeling. The five tests were conducted in 30 cm long borehole intervals at various injection rates (ranging from approximately 120 ml/min for the first test to 1 ml/min for the last test), revealing the dependence of seepage on flux. Approximately 1 liter of water was injected in each test. The inactive time between individual test events ranged from approximately 2 hours between the second and third test, to 20 days between the first and the second test. This reveals potential memory effects such as the increased seepage percentage in the third test, which is a result of reduced storage because the pore space is occupied by water injected during the previous test. The seepage percentages observed at the end of each test (ranging from approximately 56% for the third test to 0% for the last test) are thus expected to reveal a number of seepage-relevant processes, including storage effects and rates below and above the seepage threshold.

Using the measured amount of water collected during the five seepage tests, two parameters were determined by inverse modeling. The two parameters are the porosity (ϕ) and the reference capillary-strength parameter ($1/\alpha$). These parameters were selected because of their sensitivity to the observed data and their correlation to other parameters. In a transient seepage experiment with only a small volume released, the amount of water seeping into the niche depends mainly on the following three factors:

1. The ability of the formation to hold the water by capillary forces, here expressed through an effective van Genuchten parameter α
2. The ability of the formation to store the finite amount of water released, here expressed through an effective porosity ϕ , which may include effects of matrix imbibition
3. The ability of the formation to divert water around the opening, here expressed through an effective permeability k .

The simulated seepage mass can be increased by decreasing either capillary strength, $1/\alpha$, porosity, ϕ , or permeability, k . Consequently, all possible parameter pairs are negatively correlated if inversely determined from seepage data. Because only seepage-mass data are available for calibration, the parameter correlations are expected to be strong; that is, it is unlikely that they can be determined independently from one another and with a reasonably low estimation uncertainty. The parameters to be determined are the porosity (ϕ) and the reference capillary-strength parameter ($1/\alpha$) while permeability (k) is fixed at the value estimated from the air-injection tests. A joint inversion of all five tests using iTOUGH2 V4.0 (STN: 10003-4.0-00) (Section 1.3.3.2) yielded a good match and reasonable parameter estimates. As shown in Figure 3.9-6, the heterogeneous three-dimensional SCM matches the observed seepage-mass data well and better than the two-dimensional or homogeneous alternatives.

The estimated reference capillary-strength parameter of $1/\alpha = 66$ Pa is low relative to values derived from calibration against saturation and water-potential data (CRWMS M&O 2000, U0035, Section 6.1.2). This is mainly because the injected water preferentially flowed through the relatively large fractures, which exhibit weak capillarity. In addition, the apertures of these fractures are likely to be larger in the excavation-disturbed zone as opposed to the undisturbed rock, leading to weaker capillarity. Moreover, the low estimate results from the fractures not being modeled as discrete features but as a continuum. Discrete fractures intersecting the niche promote seepage (i.e., for some flow paths, diversion around the drift is not possible). Consequently, the absence of discrete fractures in the model is partly compensated by a reduction of the estimated $1/\alpha$ value, which has the effect of weakening the capillary barrier and thus increasing seepage. The porosity estimate of $\phi = 0.0013$ seems reasonable (CRWMS M&O 2000, U0090, Section 6.1); it comprises all fractures involved in the flow and seepage process, including microfractures and the pore space affected by matrix imbibition. Note that porosity is of no importance for the prediction of long-term, near-steady-state seepage. More details about the calibration of the SCM can be found in CRWMS M&O (2000, U0080, Section 6.4).

3.9.4.6 Model Validation

The purpose of the SCM is to provide a general modeling approach that can be used for the subsequent development of process models for seepage predictions. These predictions are performed with the Seepage Model for Performance Assessment (SMPA), which develops the data basis for the seepage abstraction. Confidence into the SCM and the modeling approach can be gained by demonstrating that seepage-relevant processes and seepage-relevant parameters are identified to the degree required by the objectives of the downstream models. The SMPA evaluates seepage over a wide range of parameter values to accommodate spatial variability and

uncertainty (Section 3.9.5). Moreover, uncertainty is accounted for during the abstraction process by choosing appropriate distribution functions for the input parameters and by applying safety factors based on conservative assumptions (Section 3.9.6).

Given the objectives of the downstream models, the following testing of the SCM was considered sufficient and appropriate. The calibrated SCM was used to make predictions of observed seepage percentages from liquid-release tests that were performed in a different borehole interval using different injection rates and varying inactive time periods in between the individual test events. The uncertainty of the model predictions was evaluated using linear error propagation analysis and Monte Carlo simulations. This approach reflects the intended use of the downstream models, in which seepage is treated as a stochastic process. The observed seepage percentages lay within the uncertainty range of the model predictions, i.e., a correct probabilistic statement would have been made regarding the predicted seepage value. This favorable result increased confidence in the appropriateness of the chosen approach to seepage modeling. The relevant processes are understood and the key factors affecting seepage are identified. The proposed modeling approach, which includes the conceptual model development and the calibration against seepage-relevant data, is appropriate for evaluating seepage into waste emplacement drifts. The model is thus validated for its intended use. More details about the testing of the SCM can be found in CRWMS M&O (2000, U0080, Section 6.5).

3.9.4.7 Seepage Threshold Prediction

Steady-state seepage simulations were performed with the calibrated SCM (CRWMS M&O 2000, U0080, Section 6.6). The percolation flux applied at the top of the model was varied over a large range. Starting from a small value yielding zero seepage, the percolation flux was increased stepwise until seepage occurred, at which point the seepage threshold was identified. Further increasing the flux at the top model boundary provided estimates of seepage percentage as a function of percolation flux. A seepage threshold of approximately 200 mm/yr was obtained for the middle nonlithophysal unit of the Topopah Spring tuff. Note that this value applies to an opening of the size and geometry of Niche 3650; thus, the estimate cannot be directly applied to seepage into waste emplacement drifts because they are of a different geometry and—more importantly—are predominantly located in a different stratigraphic unit. Furthermore, seepage threshold predictions are expected to be highly uncertain and variable with location. Conservatively estimated distributions of seepage thresholds for the potential repository horizon are presented in Section 3.9.6.4. The preliminary seepage-threshold prediction obtained for Niche 3650 suggests that a potentially significant amount of water percolating under natural flow conditions is diverted around the drift.

3.9.4.8 Summary

The calibration and validation of the SCM demonstrate that simulations of seepage into underground openings excavated from a highly fractured formation can be performed using a heterogeneous fracture-continuum model, provided that the model is calibrated against seepage-relevant data. The calibration process yields scale-dependent, seepage-specific, and model-related effective parameters that partly reflect the discreteness of the fracture network. The modeling and calibration approach was successfully applied to seepage data from liquid-release

tests performed in Niche 3650 in the ESF. The calibrated model can be used to predict seepage threshold and seepage percentages for different percolation fluxes, as described in Section 3.9.5.

3.9.5 Seepage Model for PA

3.9.5.1 Objectives and General Approach

This section contains a description of the simulations performed with the Seepage Model or Performance Assessment (SMPA) and its submodel, the Disturbed Drift Seepage Model (DDSM). The main purpose of the SMPA is to evaluate long-term drift seepage over a large range of hydrogeologic parameters and for a variety of percolation fluxes. In addition to these parameter sensitivity studies, the SMPA is also used to examine certain scenarios described below (Section 3.9.5.3). The SMPA is run for multiple realizations of heterogeneous rock properties. Effects of episodic flow events and changed drift geometry on account of drift degradation are also evaluated. The results of these simulations are to be used by TSPA to develop the probability distributions of water seepage into waste emplacement drifts (Section 3.9.6). The SMPA is documented in CRWMS M&O (2000, U0075).

The SMPA simulations are based on the current repository design, using hydrogeologic information and seepage-related data from the middle nonlithophysal unit of the Topopah Spring tuff. Moreover, it only considers seepage under ambient thermal conditions. These limitations require the use of relatively large uncertainties in the subsequent TSPA calculations (Section 3.9.6).

3.9.5.2 Model Development

The SMPA follows the approach of the SCM (see Section 3.9.4 and CRWMS M&O (2000, U0080)) and the modeling framework described in Birkholzer et al. (1999, pp. 358–362) (CRWMS M&O 2000, U0075, Section 5). The model is based on the same assumptions already discussed in Section 3.9.4.3. The SMPA is a three-dimensional, heterogeneous fracture-continuum model 5.23 m long (corresponding to the waste package length plus 0.1 m spacing), 15 m wide (drift diameter is 5.5 m), and 20 m high. Gridblock size is 0.5 m × 0.5 m × 0.5 m. Additional information about the development of the SMPA can be found in CRWMS M&O (2000, U0075, Section 6.3).

3.9.5.3 Selection of Parameter Ranges and Case Studies

Table 3.9-1 shows four parameters identified as being relevant for long-term seepage predictions. Seepage is evaluated for each parameter combination at discrete points within the ranges indicated; three realizations of the heterogeneous property field were generated for each point in the four-dimensional parameter space. This can be considered an extensive sensitivity analysis. No probability distributions or parameter correlations need to be specified here; during the seepage abstraction (Section 3.9.6) and TSPA calculations, correlations are identified, and the seepage rates developed here are sampled following the probability distributions of the input parameters.

Table 3.9-1. Parameter Ranges for Which Seepage Is Evaluated Using the SMPA (Adapted from CRWMS M&O 2000, U0075, Section 6.3)

Parameter	Minimum	Maximum	Parameter Description
k, m^2	0.9×10^{-14}	0.9×10^{-11}	Mean permeability of fracture-continuum
$1/\alpha, Pa$	30	1000	van Genuchten's capillary-strength parameter
$\sigma_{\ln(k)}$	1.66	2.50	Standard deviation of log-permeability field
$Q_p, mm/yr$	5	500	Percolation flux

The permeability range is based on a review of air-permeability data from the niche studies (CRWMS M&O 2000, U0015, Section 6.1), the Single Heater Test area (Tsang and Birkholzer 1999, p. 393), pneumatic pressure signal analyses (Ahlers et al. 1999, pp. 47–68), and air-injection tests in four surface-based boreholes (LeCain 1997, pp. 2, 11–14) (CRWMS M&O 2000, U0075, Section 6.3.2).

The range of the capillary-strength parameter $1/\alpha$ covers the values obtained with the SCM (CRWMS M&O 2000, U0080, Table 10) and previously published values by Birkholzer et al. (1999, p. 354) (CRWMS M&O 2000, U0075, Section 6.3.4). The lower bound for the $\sigma_{\ln(k)}$ parameter, which reflects the degree of heterogeneity, is taken from the geostatistical analysis of post-excavation air-permeability data at Niche 3650 (CRWMS M&O 2000, U0080, Section 6.2.3).

Seepage is expected to increase with increasing variability in the heterogeneous permeability field, because local channeling effects and ponding probabilities are increased. Consequently, the range of $\sigma_{\ln(k)}$, which is a measure of heterogeneity, is examined for values higher than that obtained from the geostatistical analysis of the air-permeability data (CRWMS M&O 2000, U0075, Section 6.3.5).

Finally, seepage is evaluated for percolation fluxes as low as 5 mm/yr and as high as 500 mm/yr (CRWMS M&O 2000, U0075, Section 6.3.6). The latter accounts for a pluvial climate scenario as well as spatial and temporal focusing effects (Sections 3.9.3.1, 3.9.3.2, and 3.9.6.4). The rationale for selecting the parameter ranges shown in Table 3.9-1 is further discussed in Sections 6.3.2 through 6.3.4 of the AMR CRWMS M&O (2000, U0075).

Two parameter combinations were singled out for additional sensitivity studies. Parameter Set A is close to the base-case set given in Birkholzer et al. (1999, Table 1); Set B is close to the best-estimate parameter set obtained with the SCM, reflecting parameters of the EDZ (CRWMS M&O 2000, U0075, Section 6.3.5). Sensitivity studies were performed to examine the following parameters, processes, and features:

- The correlation length of the heterogeneous permeability field (three λ values).
- The van Genuchten parameter n (two n values).
- Correlation between capillary-strength parameter and permeability (Leverett scaling).
- Drift degradation (four scenarios).
- Episodic flow events.

Details about the different scenarios can be found in CRWMS M&O (2000, U0075, Sections 4.1, 6.3.5, 6.4, and 6.5).

3.9.5.4 Results

The seepage percentage—defined as the seepage flux divided by the average percolation flux over the drift footprint—is evaluated for three realizations of the permeability field at 240 points in the four-dimensional parameter space described in Section 3.9.5.3. The results confirm the expected behavior where seepage increases with decreasing permeability, decreasing capillary strength, and increasing percolation flux. The seepage flux is high and approaches the percolation flux only if the capillary barrier is weak (i.e., $1/\alpha$ is small), permeability is relatively low (smaller than 10^{-12} m²), or percolation flux is high. In all other cases, the capillary barrier effect results in seepage fluxes that are substantially lower than the corresponding percolation fluxes. Zero seepage is obtained for a relatively large portion of the examined parameter space.

The various sensitivity studies indicate the following trends:

- Seepage increases with increasing correlation length λ (CRWMS M&O 2000, U0075, Section 6.6.2). Note that the geostatistical analysis of the post-excavation air-permeability data (CRWMS M&O 2000, U0080, Section 6.2.2) support the choice of the base-case value with the smallest correlation length.
- Seepage is relatively insensitive to the van Genuchten parameter n (CRWMS M&O 2000, U0075, Section 6.6.3).
- Seepage tends to be higher if the capillary strength is correlated to permeability according to the Leverett scaling rule (CRWMS M&O 2000, U0075, Section 6.6.4).
- Drift degradation leads to increased seepage (CRWMS M&O 2000, U0075, Section 6.6.5).
- Episodic flow events result in averaged seepage fluxes that are higher than those obtained with constant percolation flux. However, transient effects from episodic flow events are not expected to be significant over most of the potential repository.

The detailed results can be obtained from Tables 6 through 8 of the report CRWMS M&O (2000, U0075). They are summarized and condensed as part of the PA seepage abstraction (see CRWMS M&O (2000, U0120) and Section 3.9.6 below).

3.9.6 Abstraction of Seepage into Drifts

3.9.6.1 Introduction and Objectives

Evaluating the impact of drift seepage on repository performance is complex because many of the effects previously discussed counteract one another. For example, seepage is more likely to occur (and seepage rate is generally higher) if the water percolating through the rock is focused into discrete flow channels. On the other hand, the stronger the focusing effect, the fewer

channels are developed, reducing the number of waste packages being affected by seepage. Similarly, the ability of the capillary barrier forming at the drift wall to divert some of the water around the opening is reduced if permeability is low, leading to higher seepage rates. At the same time, low-permeability rocks tend to exhibit stronger capillary forces, which increase the capillary-barrier effect, leading to reduced seepage rates. Because of this negative correlation, it is difficult to predict whether competent rock with few fractures leads to higher or lower seepage than less competent rock with a high fracture density or larger fracture apertures.

The situation is further complicated by the fact that the relationships between the degree of channeling and flow rate within an individual channel, the flow rate in a channel and seepage, seepage and corrosive damage, and finally corrosive damage and contaminant release are strongly nonlinear. Moreover, each of these relationships exhibits conceptual and parametric uncertainties.

Figure 3.9-7 shows schematically the relationships between some of the major seepage-relevant factors and their impact on repository performance. For example, if a given percolation flux is focused into a few flow channels (i.e., low seep frequency) the flux in each flow channel is relatively high (Figure 3.9-7a). This has the following two effects: (1) the number of waste packages affected by seepage is relatively small (Figure 3.9-7b), potentially reducing the negative impact of seepage; on the other hand, (2) the seepage threshold is likely to be exceeded and seepage fluxes in the affected area are relatively high (Figure 3.9-7c). High seepage rates can promote corrosion of engineered barriers, waste dissolution, and contaminant release from the affected waste package (Figure 3.9-7d). The total release of radionuclides is the product of the relatively high release rate and the relatively small number of waste packages being affected by seepage.

On the other hand, flow dispersion lead to relatively small local percolation fluxes that are potentially below the seepage threshold. As a result, seep flow rates can be expected to be low, and—depending on the distribution of percolation flux and seepage threshold—the seepage fraction is smaller or larger compared to the scenario with strong flow focusing. A detailed performance-assessment calculation must determine which of these factors dominate. Moreover, local conditions, uncertainties, and spatial variabilities must be propagated through these models to arrive at seepage probabilities and distributions for use in downstream TSPA models.

The seepage models discussed in Sections 3.9.4 and 3.9.5 focus on the determination of the seepage threshold and seepage rates for a given percolation flux (i.e., the relationship schematically shown in Figure 3.9-7c). Flow focusing and seep frequency (Figure 3.9-7a) and their impact on seepage fraction (Figure 3.9-7b) are accounted for in the abstraction (Section 3.9.6.4).

The presumption that seepage events are not localized and occur everywhere in the waste emplacement drifts (i.e., all waste packages encounter seepage), and that the seepage rate is equal to the percolation rate (i.e., no capillary-barrier effect exists, leading to maximum seepage rates), would be overly conservative. Consideration of a seepage threshold is beneficial for TSPA even if the seepage threshold value remains highly uncertain. Essentially, the occurrence of seepage is the product of two probabilities, namely the probability of experiencing high local percolation fluxes and the probability of encountering a drift segment with a low seepage

threshold. The situation is schematically shown in Figure 3.9-8. Given a certain percolation flux, the conditional probability for the capillary barrier to fail is indicated by the shaded area. While the failure probability increases with increasing percolation flux, the probability for reaching such high percolation fluxes decreases. The probability that the capillary barrier fails and seepage occurs can be determined by independently sampling from both the percolation-flux and seepage-threshold distribution, and by counting the number of realizations in which the percolation flux exceeded the seepage threshold. Even assuming a large uncertainty in the seepage threshold, the resulting seepage fraction will be less than one (the seepage fraction obtained by neglecting capillary-barrier effects).

A good understanding of seepage processes, an accurate determination of seepage-relevant formation parameters, and a careful estimation of seepage rates and seepage distribution are therefore some of the main objectives of the experimental, numerical, and analytical UZ studies at Yucca Mountain. A more detailed discussion of PA-related aspects of seepage can be found in CRWMS M&O (2000, U0120).

The purpose of the seepage abstraction is to put the information generated by the seepage process modeling in a form appropriate for use in TSPA for SR. The abstraction method is an extension of that employed for the TSPA for VA (DOE 1998, Sections 3.1.1.4, 3.1.2.4, and 3.1.3.3; CRWMS M&O 1998g, Sections 2.2.4, 2.4.4, and 2.5.2). The objective is to develop the framework for evaluating the amount of seepage of liquid water into potential repository emplacement drifts for TSPA simulations. Seepage is treated as a stochastic quantity in TSPA simulations by sampling values from generated probability distributions that represent the uncertainty and spatial variability of seepage. The process is schematically shown in Figure 3.9-9. Seepage has been evaluated as a function of percolation flux and k/α , a lumped parameter capturing the effectiveness of the capillary barrier. Probability density functions are prescribed for each of the two parameters. During a TSPA simulation, a large number of random values are generated based on these distributions. The seepage rate corresponding to each pair of random parameter values yields the probability density function of seepage into waste emplacement drifts. Note that the actual sampling procedure is more complicated as the potential repository is located in multiple units, and additional constraints and correlations must be observed.

The Monte Carlo simulation is basically an uncertainty analysis: each realization is taken to be equally likely, so any one of the realizations could be the "correct" one. The differences between one realization and another are within the range of uncertainty about each parameter that is varied. Some parameters, like fracture permeability or α parameter, are uncertain, so they vary from one TSPA realization to another; but they are also spatially variable, so they vary from location to location within each TSPA realization. TSPA calculations thus account for both uncertainty and spatial variability.

In Section 3.9.6.2, probability distributions of seepage are developed, combining the results of the SMPA with information about the relative likelihood of the various parameter combinations. In Section 3.9.6.3, adjustments for several perturbing physical processes are introduced. In Section 3.9.6.4, the results of the abstraction of drift seepage are summarized.

3.9.6.2 Initial Abstraction of Seepage Results

The SMPA was used to simulate seepage for a large number of parameter combinations (Section 3.9.5). Examination of the results reveals that seepage percentages are not strongly dependent on the standard deviation of the heterogeneous permeability field. In addition, similar seepage percentages were obtained for simulations with the same value of k/α (and common values of other parameters). Thus, for the abstraction analysis, seepage is treated as a function of k/α rather than of k and α separately. With these simplifications, seepage can be treated as a function of just two variables, namely k/α and percolation flux q .

The abstraction analysis focuses on two quantities: (1) the *seepage fraction*, f_s , which is the fraction of waste-package locations (model simulations) that have seepage (i.e., that have nonzero seepage percentage); and (2) the *seep flow rate*, Q_s , which is the volumetric flow rate of seepage in a drift segment. The seep flow rate is obtained from the seepage percentage by multiplying by the percolation flux and the area of a drift segment. For each modeled percolation flux q , and for all simulations with a common value of k/α , the seepage fraction and the mean and standard deviation of the seep flow rate are calculated.

The next step in the abstraction is to assign probabilities, or weights, to the two parameters. The distribution for k/α is obtained from the means and standard deviations of k (based on air-injection data) and α (based on SCM calibration results). Details of this procedure can be found in CRWMS M&O (2000, U0120, Section 6.2.2). The mean of k/α was determined to be $6 \times 10^{-11} \text{ m}^2 \text{ Pa}$. To account for uncertainty, a range of values is considered. The available information indicates that our uncertainty increases at higher values of k/α , so the range considered is skewed to higher values: values of k/α from one-half order of magnitude lower to one order of magnitude higher than $6 \times 10^{-11} \text{ m}^2 \text{ Pa}$ are considered. This is the range of values for the geometric mean of the distribution of k/α from location to location; in each case the standard deviation of the distribution of $\log(k/\alpha)$ from location to location is taken to be 0.32. As is implied by the use of logs, the spatial distribution of k/α values is taken to be log-normal.

Percolation flux q is not weighted at this stage. Percolation information is supplied with the appropriate spatial and temporal distribution during the actual TSPA simulations. All the results are thus given as a function of percolation flux. Given a distribution for k/α , a corresponding distribution can be developed for seepage. When the seepage information from the Seepage Model for PA is combined with the discrete distribution of k/α , weighted seepage statistics are obtained, representing the distribution of spatial variability of seepage within a TSPA realization.

3.9.6.3 Adjustments

The following adjustment are made to account for certain effects:

1. Distributions for the amount of seepage as a function of percolation flux are derived directly from seepage process-model results (CRWMS M&O 2000, U0075) and are constrained by measurements of permeability around three niches in the ESF (CRWMS M&O 2000, U0015, Section 6.1) and calibration of seepage tests conducted in one niche in the ESF (CRWMS M&O 2000, U0080,

Section 6.4). The derived distributions are summarized in Section 3.9.6.4; more details can be found in CRWMS M&O (2000, U0120, Section 6.2.4).

2. Seepage calculations for drifts with breakouts in the drift wall were performed with the SMPA (CRWMS M&O 2000, U0075, Section 6.4.3). These simulations suggested a moderate increase of drift seepage as a result of partial drift degradation. In the abstraction, seep flow rates calculated with the SMPA were increased by a conservative factor of 1.55 to account for the effects from partial drift degradation and rock bolts (CRWMS M&O 2000, U0120, Section 6.3.1).
3. The impact of the correlation between permeability and capillary strength on seepage was evaluated by the SMPA (CRWMS M&O 2000, U0075, Section 6.6.4). Using the Leverett scaling rule (Leverett 1941, p. 159) to relate capillary strength to local permeability variations yielded slightly higher seepage rates as compared to the rates obtained with a spatially constant α value. Seep flow rates calculated with the SMPA were therefore increased by 10% as an adjustment for the potential correlation of k and α (CRWMS M&O 2000, U0120, Section 6.3.2).
4. Distributions of the degree of flow focusing above the drifts are determined based on estimates of “weep” spacings implied by the active fracture model of UZ flow. Weep spacings were calculated by two methods to estimate lower and upper bounds for three net infiltration levels (mean, lower, and upper; see CRWMS M&O (2000, U0120, Section 6.3.3.1)). Both methods generate weep spacings that are approximately log-normally distributed. The distributions of weep spacings are used to define distributions of the flow-focusing factor, which is a multiplicative factor describing how much percolation flux might be increased over its average value at any given location. The flow-focusing factor is used to scale the percolation flux and the seepage fraction; it is log-uniformly distributed, with minimum of 1 in each case and maximum of 47 for the low-infiltration case, 22 for the base-infiltration case, and 9.7 for the high-infiltration case. This distribution of flow-focusing factors is an uncertainty distribution, which means that one value of it is sampled for each TSPA realization. That value is then applied to modify the spatial variability of seepage within the realization. Details can be found in CRWMS M&O (2000, U0120, Section 6.3.3.2).
5. Episodic flow could be accounted for through application of temporally varying percolation fluxes during the TSPA calculations in analogy to the use of spatial flow focusing factors. Since episodic flow events are damped by the PTn and are not expected to penetrate to the potential repository horizon, no adjustment is currently made.
6. Coupled processes (thermal-hydrologic, thermal-hydrologic-mechanical, and thermal-hydrologic-chemical) have generally been found to have limited impact (in terms of magnitude and time scale) on seepage or are beneficial. Currently, no adjustments are being made (see Section 4.2.1.1 and CRWMS M&O (2000, U0120, Sections 5 and 6.3.5)).

3.9.6.4 Abstraction Results

As discussed in Section 3.9.6.2, seepage is mainly a function of the ratio of geometric-mean fracture permeability k to fracture α parameter, k/α , and the uncertainty in this ratio is taken to be one order of magnitude above and one-half order of magnitude below the best-estimate value, which is $6 \times 10^{-11} \text{ m}^2 \text{ Pa}$. A triangular shape is chosen for the seepage uncertainty distributions. This distribution appropriately represents the key features desired, which are that seepage values for $k/\alpha = 6 \times 10^{-11} \text{ m}^2 \text{ Pa}$ are most likely and that k/α could be higher or lower, but those values are less likely to be representative of potential repository conditions.

Table 3.9-2 summarizes the seepage distributions as they vary with percolation flux. A seepage threshold of approximately 200 mm/yr, 15 mm/yr, and 5 mm/yr was found for minimum, peak, and maximum k/α values, respectively. Note that these values are the abstracted, conservatively estimated seepage rates, seepage fractions, and seepage thresholds for a waste emplacement drift with a 5.5 m diameter, taking into account uncertainty and spatial variability of the entire potential repository horizon. This has to be distinguished from the previously reported seepage-threshold estimate of 200 mm/yr (Section 3.9.4.7), which referred to a single location in the middle nonlithophysal zone and for an opening smaller than a waste emplacement drift. Additional details on the derivation of the values in this table and their interpretation may be found in CRWMS M&O (2000, U0120, Section 6.4). For values of percolation flux not in the table, linear interpolation or extrapolation was used.

Table 3.9-2. Uncertainty in Seepage Parameters as Function of Percolation (Table from CRWMS M&O 2000, U0120, Table 11)

q (mm/yr)	Minimum Value of k/α			Peak Value of k/α			Maximum Value of k/α		
	f_s	Mean $Q_s \text{ (m}^3/\text{yr)}$	Std. Dev. $Q_s \text{ (m}^3/\text{yr)}$	f_s	Mean $Q_s \text{ (m}^3/\text{yr)}$	Std. Dev. $Q_s \text{ (m}^3/\text{yr)}$	f_s	Mean $Q_s \text{ (m}^3/\text{yr)}$	Std. Dev. $Q_s \text{ (m}^3/\text{yr)}$
5	0	0	0	0	0	0	1.97×10^{-3}	3.21×10^{-3}	3.16×10^{-3}
14.6	0	0	0	2.45×10^{-3}	7.95×10^{-3}	7.09×10^{-3}	5.75×10^{-2}	2.26×10^{-2}	2.45×10^{-2}
73.2	0	0	0	0.250	0.106	0.198	0.744	0.404	0.409
213	4.91×10^{-3}	0.284	0.188	0.487	1.51	1.15	0.944	3.31	2.24
500	6.01×10^{-2}	0.992	1.05	0.925	5.50	4.48	0.999	13.0	5.74

NOTE: q is percolation flux, f_s is seepage fraction, and Q_s is seep flow rate.

The standard deviations of seep flow rate in Table 3.9-2 are relatively large. These large standard deviations result from the large differences in seepage from one set of simulations to another. For example, the weighted mean and standard deviation for $k/\alpha = 6 \times 10^{-11} \text{ m}^2 \text{ Pa}$ are a combination of the results for k/α values from 9×10^{-12} to $2.7 \times 10^{-10} \text{ m}^2 \text{ Pa}$ and over that range of k/α the mean seep flow rate at 73.2 mm/yr goes from zero to 0.408 m^3/yr . Thus, an amount of spatial variability in k/α corresponding to a log standard deviation of 0.32 (Section 3.9.6.2) translates into a relatively large spatial variability of seepage. This is consistent with the concept of seepage as a random process.

The effect of flow focusing is illustrated in Figures 3.9-10 and 3.9-11 for seepage fraction and mean seep flow rate, respectively. Each plot has four curves, for the flow-focusing factor F equal to 1 (no flow focusing), 5, 15, and 45. The $F = 1$ curves are based on the mean of the respective uncertainty distributions (for a triangular distribution, the mean is $(\text{min} + \text{peak} + \text{max})/3$, with min, peak, and max as listed in Table 3.9-2). The curves with higher values of F are generated from the $F = 1$ curves as described in CRWMS M&O (2000, U0120, Section 6.3.3.2). Increased flow focusing results in lower seepage fractions and higher seep flow rates. Note, however, that at very low percolation fluxes the seepage fraction is higher for higher focusing factors, because a percolation flux below the threshold for seepage can be boosted above the threshold by the focusing multiplier (CRWMS M&O (2000, U0120, Section 6.3.4)

3.9.7 Corroborative Evidence and Analog Studies

3.9.7.1 Calcite Depositions in Lithophysal Cavities

Observations of calcite and opal in lithophysal cavities in the Topopah Spring tuff were used to estimate long-term seepage rates into these small openings (CWRMS M&O 2000, U0085, Section 6.10.3). Calcite is assumed to precipitate from downward-percolating meteoric water because of (1) evaporation, (2) CO_2 outgassing as a result of the geothermal gradient, and (3) interaction with a gas phase containing less CO_2 than the gas with which the water was last equilibrated. Considering these calcite-precipitation mechanisms and assuming certain water-to-calcite ratios, seepage into lithophysal cavities was estimated from calcite-deposition data. This analysis shows that (1) not all lithophysal cavities encountered seepage and (2) seepage flux is a very small fraction of percolation flux. Both conclusions corroborate the general concept and the findings of the drift-seepage studies discussed in Sections 3.9.1 through 3.9.5. Specifically, they support the concept of a capillary barrier reducing seepage over percolation flux. Note that the seepage threshold for small cavities may be significantly higher than for a large waste emplacement drift.

The presence of lithophysal cavities does not directly impact seepage into a waste emplacement drift. However, there is a second-order, indirect effect. On account of the capillary barrier effect, lithophysal cavities are partial obstacles to downward flow of water. Consequently, their presence may lead to local, small-scale flow channeling, which could induce increased seepage. Lithophysal cavities also increase the roughness of the drift wall. Both effects are accounted for through the use of conservative flow focusing factors and safety factors for drift roughness.

3.9.7.2 Rainier Mesa

Rainier Mesa, located approximately 30 km northeast of Yucca Mountain, is underlain by a sequence of welded and nonwelded tuffs similar to those that underlie Yucca Mountain. Precipitation is about double the mean at Yucca Mountain, and percolation is estimated to be about eight percent of precipitation (Wang et al. 1993, p. 676). Most of the Rainier Mesa tunnels were constructed in the zeolitic tuffs, which are believed to be near full saturation. Faults and joints are abundant in these zeolitic-bedded tuffs. When intersected by tunnels, some of these joints and especially through-going faults have yielded significant amounts of water. The seeping features are thought to be pathways for flow from a perched water zone above the zeolitic horizon. Seepage water is geochemically similar to meteoric water and is associated with fast-

flow paths. Seepage at Rainier Mesa occurs only in tunnels constructed in the zeolites; no seepage is observed in the tunnel intersecting the vitric tuff units. These observations suggest that seepage into tunnels may be localized and restricted to certain flow paths and units. This corroborates the modeling results, which indicate that the seepage fractions are less than one. More details can be found in CRWMS M&O (2000, U0135, Section 6.5.1.2) and Wang et al. (1993, pp. 675–681).

3.9.7.3 Altamira

Seepage into caves can be used as a natural analog for seepage into waste emplacement drifts. Unfortunately, most caves are part of a karst system found in limestone formations in the saturated zone or in zones of significantly higher percolation fluxes than those expected at Yucca Mountain. The caves near Altamira, Spain are located in the unsaturated zone of a fractured limestone bedrock with clay-rich layers. Precipitation is approximately ten times higher than at Yucca Mountain. Nevertheless, seepage rates into the caves are estimated to be a small fraction of the expected percolation flux. Moreover, there are essentially no fluctuations in the observed seepage rates despite the fact that the unsaturated zone is only about 7 m thick and evapotranspiration is expected to exceed precipitation for a few months out of the year. More details can be found in Villar et al. (1985, pp. 21–24).

3.9.7.4 Absence of Seepage into Sealed Drift Segments

Currently, no natural seepage into the ESF has been observed. Furthermore, no construction water was observed to seep into the ESF Main Drift as the tunnel boring machine passed the cross-over point during the excavation of the ECRB Cross Drift. However, evaporation and moisture removal through ventilation of the ESF is likely to be larger than potential seepage rates, preventing direct observation of liquid water dripping into the drift.

As described in Section 2.2.2.2.1, an approximately 100 m long segment of Alcove 7 and an approximately 1,000 m long segment of the ECRB Cross Drift have been sealed by bulkheads to isolate them from ventilation. No seepage has been observed so far in either of these two drift segments. The absence of visible seepage in sealed-off drift segments corroborates the modeling results which estimate that present-day percolation fluxes are likely to be smaller than the prevailing seepage thresholds.

3.9.8 Alternative Conceptual Models

3.9.8.1 Discrete Fracture Network Model

A discrete fracture network model (DFNM) is an alternative conceptual model to the heterogeneous fracture continuum model (Pruess et al. 1999, pp. 307–309). The DFNM has the advantage of being intuitively more appealing for seepage predictions. A high-resolution DFNM model is capable of generating channelized flow and discrete seepage events. The development of a defensible DFNM requires collecting a very large amount of geometric and unsaturated hydrologic property data. While part of the required geometric information can be obtained from fracture mappings, the description of the network remains incomplete and potentially biased. Moreover, unsaturated hydrologic parameters on the scale of individual fractures are required, along with conceptual models and simplifying assumptions regarding unsaturated flow within

fractures and across fracture intersections. These databases required to develop a DFNM are currently not available. As a result, the cumulative effect of all the input uncertainties is likely to outweigh the apparent advantage of a detailed representation of the fracture network.

In general, the choice of a conceptual model for seepage predictions should be based on a careful consideration of the study objectives, the available database in comparison with the data needs, the uncertainties in the input parameters, and the corresponding prediction uncertainties, as well as computational aspects. The appropriateness of using a fracture-continuum model for the prediction of effective seepage quantities was demonstrated in CRWMS M&O (2000, U0080, Section 5.3).

3.9.8.2 Seepage Governed by Ponding Probability

As an alternative conceptual model to a seepage process model, Birkholzer et al. (1999, pp. 372–379) related seepage to the local ponding probability, which was derived from the variability of the permeability field. Their approach assumed that in strongly heterogeneous formations, seepage is predominantly affected by pressure variations governed by local heterogeneity rather than the presence and geometry of the capillary barrier. This is different from the behavior in a homogeneous system, where the geometry of the capillary barrier has a strong impact on seepage (Philip et al. 1989, pp. 16–28). Strong medium- to small-scale heterogeneities tend to increase seepage as they increase channeling and local ponding. This effect is included in the current seepage process models through the estimation of effective, seepage-specific parameters. While the approach presented by Birkholzer et al. (1999, pp. 372–379) and discussed in CRWMS M&O (2000, U0075, Section 6.7) may provide guidelines for how to extrapolate seepage predictions to other units or drift geometries, it nonetheless requires a calibration step similar to that described in Section 3.9.4.

3.9.9 Summary and Conclusions

Seepage into waste emplacement drifts is considered a key factor affecting the performance of a potential high-level nuclear waste repository at Yucca Mountain, Nevada. Theoretical analyses, numerical modeling studies, field testing, and observations at analog sites suggest that seepage into underground openings excavated in unsaturated formations is smaller than the local percolation flux. This is mainly a result of capillary pressure holding water in the formation, diverting it around and preventing it from entering the openings. The effectiveness of this capillary barrier depends on the percolation flux itself, the hydrogeologic properties of the formation, and the geometry of the drift.

A sequence of models was used to predict seepage fraction, seepage threshold, and seep flow rate for waste emplacement drifts. A seepage process model was calibrated against seepage-relevant data from liquid-release tests. Seepage rates were then calculated over a wide range of parameter values and compiled in an abstraction process. Finally, probability distributions of the key parameters were introduced and conservative assumptions were made to arrive at probabilities for seepage into waste emplacement drifts.

These analyses indicate that seepage fluxes are lower than percolation fluxes, even under conservative assumptions, and that only a fraction of the waste packages will encounter seepage. However, seepage predictions remain uncertain.

Figure 3.9-12 summarizes qualitative and quantitative results pertaining to the issues discussed in Section 3.9.3. The results reflect the values obtained after the TSPA abstraction.

3.10 DRIFT-SCALE THERMAL-HYDROLOGICAL-CHEMICAL PROCESSES AND MODELS

3.10.1 Introduction

The purpose of this section is to describe (1) the conceptual model and input data for coupled thermal, hydrological, and chemical (THC) processes; (2) the Drift Scale Test (DST) THC Model; (3) the THC Seepage Model; and (4) the abstractions done by Performance Assessment on the results of the THC Seepage Model. The conceptual model for THC processes provides a comprehensive basis for modeling the pertinent mineral-water-gas reactions in the host rock under thermal loading conditions, as they influence the water and gas chemistry that may enter drifts over 100,000 years. The purpose of the DST THC Model is to validate the conceptual model and input data by comparison of measured gas and water chemistry from the DST to the results of simulations. The purpose of the THC Seepage Model is to evaluate the effects of THC processes in the rock around emplacement drifts on the possible seepage-water chemistry, gas-phase composition, and the potential effects of THC processes on unsaturated zone (UZ) flow and transport. This model was used to evaluate the effects of mineral dissolution and precipitation, the effects of CO₂ exsolution and transport in the region surrounding the drift, the potential for forming zones of calcite, silica, or other minerals, the resulting changes to porosity, permeability, and the potential effects on seepage. The THC Seepage Model and validation of the data and processes using the DST are treated in the Analysis/Model Report (AMR) *Drift-Scale Coupled Processes (DST and THC Seepage) Models* (CRWMS M&O 2000, N0120/U0110).

3.10.2 Thermal-Hydrological-Chemical Conceptual Model

The THC conceptual model underlies the numerical simulations of THC processes in the DST THC Model and in the THC Seepage Model. The conceptual model must be able to describe processes involving liquid and vapor flow, heat transport, and thermal effects resulting from boiling and condensation, transport of aqueous and gaseous species, mineralogical characteristics and changes, and aqueous and gaseous chemistry. A conceptual model of reaction-transport processes in the fractured welded tuffs of the potential repository host rock must also account for the different rates of transport in very permeable fractures compared to the much less permeable rock matrix (see for example, Steefel and Lichtner 1998, pp. 186–187).

In addition to the unsaturated hydrological properties required to simulate THC processes in the UZ, the data necessary for the evaluation of THC processes include the initial and boundary water and gas chemistry, the initial mineralogy, mineral volume fractions, reactive surface areas, equilibrium thermodynamic data for minerals, aqueous and gaseous species, kinetic data for mineral-water reactions, and diffusion coefficients for aqueous and gaseous species. The following subsections describe the conceptual model for thermal-hydrological (TH), geochemical, and coupled THC processes in the fractured tuffs.

3.10.2.1 TH Processes

TH processes in the fractured welded tuffs at Yucca Mountain have been examined theoretically and experimentally since the early 1980s (Pruess et al. 1984; Pruess et al. 1990a, pp. 1235–1248;

Buscheck and Nitao 1993, pp. 418–448; Pruess 1997, pp. 335–372; Tsang and Birkholzer 1999, pp. 385–425; Kneafsey and Pruess 1998, pp. 3349–3367). A conceptual model showing the important TH processes occurring around a drift (as derived through these studies and through observations of the Single Heater Test and the DST) is shown in Figure 3.10-1. To summarize the processes as depicted in the figure, heat conduction from the drift wall into the rock matrix results in vaporization and boiling, with vapor migration out of matrix blocks into fractures. The vapor moves away from the drift through the permeable fracture network by buoyancy, by the increased vapor pressure caused by heating and boiling, and through local convection. In cooler regions, the vapor condenses on fracture walls, where it drains through the fracture network either down toward the heat source from above or away from the drift into the zone underlying the heat source. Slow imbibition of water from fractures into the matrix gradually leads to increases in the liquid saturation in the rock matrix. Under conditions of continuous heat loading, a dryout zone may develop closest to the heat source separated from the condensation zone by a nearly isothermal zone maintained at about the boiling temperature. Where this nearly isothermal zone is characterized by a continuous process of boiling, vapor transport, condensation, and migration of water back to the heat source (either by capillary forces or gravity drainage), this zone may be termed a heat pipe (Pruess et al. 1990a, pp. 1235–1248).

The design shown in Figure 3.10-1 includes backfill; however, this conceptual model is not dependent on the presence of backfill. A design change was made in January 2000 that removed backfill from the reference design. Qualitatively, this change does not affect the TH processes occurring in the rock around the drifts; however, the absence of backfill may result in a different temperature distribution at the drift wall and different times of maximum drift-wall temperature, maximum dryout and rewetting. These different rates of heating would affect the time variation of water and gas chemistry around the drifts.

3.10.2.2 Effects of TH Processes (Boiling, Condensation, and Drainage) on Water and Gas Chemistry and Mineral Evolution

The chemical evolution of waters, gases, and minerals is intimately coupled to the TH processes discussed in the previous section. The distribution of condensate in the fracture system determines where mineral dissolution and precipitation can occur in the fractures and where there can be direct interaction (via diffusion) between matrix pore waters and fracture waters. Figure 3.10-2 shows schematically the relationships between TH and geochemical processes in the zones of boiling, condensation, and drainage in the rock mass outside of the drift and above the heat source.

One important aspect of the system is the exsolution of CO_2 out of the liquid phase as temperature increases. The exsolution and transport of CO_2 out of the boiling zone results in a local increase in pH and a decrease in pH in the condensation zone into which the vapor enriched in CO_2 is transported. The extent to which the pH is shifted depends strongly on the rates of mineral-water reactions, which can buffer the change in pH. Because the diffusivities of gaseous species are several orders of magnitude greater than those of aqueous species, and because the advective transport of gases can be more rapid than that of liquids, the region where CO_2 degassing affects water and gas chemistry could be much larger than the region affected by transport of aqueous species.

Effects of TH processes on water chemistry are varied and depend on the behavior of the dissolved species and their relation to mineral-water reactions. Conservative species (i.e., those that are unreactive and nonvolatile), such as chloride (Cl^-), become concentrated in waters undergoing vaporization or boiling, but are absent from the vapor condensing in the fractures. Therefore, the concentration in the draining condensate waters is determined by mixing with fracture pore waters and interaction with matrix pore waters via diffusion. Concentrations of aqueous species, such as Ca^{+2} , are also affected by calcite dissolution or precipitation as well as reactions involving Ca-bearing zeolites, clays, and plagioclase feldspar.

Zonation in the distribution of mineral species may occur as a result of varied temperature effects on mineral solubility. The inverse relation between temperature and calcite solubility (as opposed to the silica phases, which are much more soluble at higher temperatures) may cause zonation in the distribution of these phases in the condensation and boiling zones (Figure 3.10-2). Precipitation of amorphous silica or another silica phase is likely to be confined to a narrower zone where evaporative concentration from boiling exceeds its solubility. Hence, calcite may precipitate in fractures over a broad zone of elevated temperature and where CO_2 has exsolved due to temperature increases or boiling. Alteration of feldspars to clays and zeolites is likely to be most rapid in the boiling zone because of their increased solubility (as well as dissolution and precipitation rates) at higher temperatures (Lasaga 1998, p. 66). In drainage zones, there may also be zonation in mineral alteration within the rock matrix adjacent to the fracture similar to that observed as a function of distance along the transport path (Steefel and Lichtner 1998, pp. 186–199).

3.10.2.3 Effects of Infiltration and Climate Changes on THC Processes

Early in the thermal history of the potential repository, much of the chemistry of the UZ around drifts will be constrained by the chemistry of ambient fracture and matrix pore water, which may change the concentration as a result of boiling, by dilution with condensate water, or by mineral-water-gas reactions. Once the peak thermal period has subsided, percolating water mixes with the condensate water above the potential repository and eventually rewets the dryout zone. The composition of the percolating waters (before mixing) may be similar to that presently found above the potential repository as matrix pore water, or it may reflect more dilute water, from a wetter climate, that has traveled through fractures. Changes in the percolation flux also affect the extent of mineral deposition and dissolution, because of the changes in the flux of dissolved species to the region around drifts. For example, the greater the flux of Ca, the more calcite would be precipitated, at a given concentration. Higher percolation fluxes could increase the dissolution rates of minerals that are undersaturated in the fluid, because it can increase the degree to which the mineral is undersaturated.

3.10.2.4 Hydrologic Property Changes in Fractures and Matrix

Mineral precipitation and dissolution in fractures and matrix have the potential for modifying the porosity, permeability, and unsaturated hydrologic properties of the system. Because the molar volumes of minerals created by hydrolysis reactions (i.e., anhydrous phases, such as feldspars, reacting with aqueous fluids to form hydrous minerals, such as zeolites or clays) are often larger than the molar volumes of the primary reactant minerals, dissolution-precipitation reactions can often lead to porosity reductions. The extent of mineral-water reactions is controlled by the

surface areas of the mineral phases in contact with the aqueous fluid, and the distribution of minerals in the fractures is heterogeneous. Therefore, changes in porosity and permeability caused by these processes may also be heterogeneously distributed. Other factors that may lead to heterogeneity in property changes are the distribution of liquid saturation in fractures, the proportion of fractures having actively flowing water, and the rates of evaporative concentration due to boiling, which may change the dominant mechanisms of crystal growth and nucleation.

As summarized in the preceeding subsection, the conceptual model for THC processes incorporates a wide range of coupled physical and chemical processes. The following subsection deals with the implementation of this conceptual framework into a quantitative numerical model.

3.10.3 Modeling Approach, Assumptions, Inputs and Outputs

The flow of information between various models and data sources and the DST THC Model and THC Seepage Model is presented in Figure 3.10-3. The DST THC Model takes its inputs from the DST TH Model, the Calibrated Properties Model (CPM; CRWMS M&O 2000, U0035), and numerous sources of geochemical data (Geochemical Data) as discussed in CRWMS M&O (2000, N0120/U0110). Geochemical Data include mineral abundances and compositions, and water and gas chemistry. The THC Seepage Model obtains its inputs from the Calibrated Properties Model (CPM), Geochemical Data, and also Repository Design (CRWMS M&O 1999e; CRWMS M&O, EBS PMR, Section 2.5) and the UZ Flow and Transport Model (Flow and Transport; CRWMS M&O 2000, U0050). Repository Design provides the data on in-drift geometry and drift spacing, and the thermal and hydrological properties of Engineered Barrier System components. The UZ Flow and Transport Model provides the hydrogeologic layer boundaries and pressure and temperature boundary conditions. Results of sensitivity studies on mineral assemblages and conceptual model validation in the DST are used to guide the development and analysis of the THC Seepage Model. However, direct numerical output from the DST THC Model is not used in the THC Seepage Model. Output data from the THC Seepage Model are abstracted for use in Total System Performance Assessment (TSPA) and discussed further in Section 3.10.11.

The following subsections describe in more detail the implementation of the conceptual model as a mathematical description of THC processes in the fractured tuffs. Data that form the basis of the DST THC and THC Seepage models are also discussed.

3.10.3.1 Dual-Permeability Model For Reaction-Transport Processes

To handle separate yet interacting processes in fractures and matrix, the dual-permeability method was adopted for all aspects of the system (flow, transport, and reaction). Transport rates greater than the rate of chemical equilibration via diffusion necessarily lead to disequilibrium in water chemistry between fractures and matrix. This can lead to differences in dissolution/precipitation rates and therefore the rate of change in porosity and permeability between the two media. Because the system is unsaturated and undergoes boiling, the transport of gaseous species is an important consideration. The model must also capture the differences between initial mineralogy in fractures and matrix and their evolution. In the dual-permeability method, each gridblock is separated into a matrix and fracture continuum, each of which is

characterized by its own pressure, temperature, liquid saturation, water and gas chemistry, and mineralogy.

The fracture continuum is considered as separate from but interacting with the matrix continuum, in terms of the flow of heat, water, and vapor through advection and conduction. Aqueous and gaseous species are transported via advection and molecular diffusion between fractures and matrix. It is assumed that the dual-permeability approach, with appropriate material and fracture properties and an appropriate discretization of time and space, is a sufficiently accurate approximation of the real world for the spatial scales of interest. The dual-permeability approach for modeling hydrologic processes in fractured porous media is also discussed in Section 3.4. This approach is validated by the comparison of measured geochemical data to results of simulations presented in CRWMS M&O (2000, N0120/U0110), and as discussed in Section 3.10.4.

3.10.3.2 Active Fracture Model For Reaction-Transport Processes

The active fracture model (Liu et al. 1998; CRWMS M&O 2000, U0030, Section 6.4.5) has been used in many of the modeling studies described in this report. Because a major intent of the method is to modify the fracture-matrix area for the liquid phase as a function of the liquid saturation, for consistency the active fracture model should also be used for the calculation of the surface area of minerals on fracture walls in contact with the liquid phase. The reference saturation for the active fracture model is the residual liquid saturation, below which flow is considered to be absent. However, mineral-water reactions are expected to occur at all saturations above zero. Therefore, a modification of the active fracture model was implemented for mineral-water reactions, such that the reference saturation was taken as a small value (1×10^{-4}), consistent with that implemented for mineral-water reactions and transport near conditions of complete dryout. This value is approximately a cutoff at which evaporative concentration increases the ionic strength of the residual porewater to values outside the range of the validity of thermodynamic relationships for dilute systems.

3.10.3.3 Equilibrium and Kinetic Models for Mineral–Water–Gas Reactions

Mineral-water reactions are considered to take place under kinetic or equilibrium conditions. The methods used to express the kinetic and equilibrium reactions are described in CRWMS M&O (2000, N0120/U0110) and are similar to those described in Reed (1982, pp. 513–528) and Steefel and Lasaga (1994, pp. 529–592). Because the dissolution rates of many mineral-water reactions are quite slow, most phases were treated using pseudo-first-order reaction kinetics. Data for kinetic mineral-water reactions were derived from published experimental data. Gas species, such as CO_2 , were treated as ideal mixtures of gases in equilibrium with the aqueous solution.

3.10.3.4 Initial and Infiltrating Water and Gas Chemistry and Mineralogy

The initial water chemistry for the DST THC Model and the THC Seepage Model was an average of measurements made of pore waters from Alcove 5, near the Drift Scale Test (CRWMS M&O 2000, N0120/U0110, Section 6.1.2). The chemistry of this water is given in Table 3.10-1.

Table 3.10-1. TSw Porewater Composition and CO₂ Partial Pressure (CRWMS M&O 2000, N0120/U0110, Table 3)

Parameter	Units	Concentration
pH (at 25°C)	pH Units	8.32
Na	mg/L	61.3
SiO ₂ (aq)	mg/L	70.5
Ca	mg/L	101
K	mg/L	8.0
Mg	mg/L	17
Al	mg/L	9.92x10 ⁻⁷ (1)
Fe	mg/L	6.46x10 ⁻⁸ (2)
HCO ₃ (3)	mg/L	200
Cl	mg/L	117
SO ₄	mg/L	116
F	mg/L	0.86
CO ₂ (gas) (4)	Pa	85.2

NOTES: (1) Calculated by equilibrating with Ca-smectite at 25°C.

(2) Calculated by equilibrating with hematite at 25°C.

(3) Total aqueous carbonate as HCO₃⁻, calculated from charge balance.

(4) Calculated at equilibrium with the solution at 25°C.

The infiltrating water chemistry could be chosen from either the porewater chemistry in the UZ at or above the potential repository horizon or from a more dilute composition found in the perched water or saturated zone (e.g., J-13 water). The perched waters are much more dilute than UZ pore waters (CRWMS M&O 2000, U0085, Tables 6 and 8), and isotopic compositions (³⁶Cl/Cl, ¹⁸O/¹⁶O, D/H, ¹⁴C) and Cl concentrations also suggest the presence of a large proportion of late Pleistocene/early Holocene water (Levy et al. 1997, p. 906; Sonnenthal and Bodvarsson 1999, pp. 107–108; CRWMS M&O 2000, U0085, Table 9). Consequently, we assume that the infiltrating water and the water in the fractures have the same chemical composition as the matrix pore water. The sample chosen was collected from Alcove 5 near the DST and is listed in Table 3.10-1. Analyses of PTn pore waters (and some at the top of the TSw) and many Cl analyses of TSw pore waters are consistent with this interpretation (Sonnenthal and Bodvarsson 1999, pp. 140–141; CRWMS M&O 2000, U0085, Table 6).

The minerals, aqueous and gaseous species shown in Table 3.10-2 include the major phases found in fractures and the matrix in the TSw and others that are likely to occur under thermally perturbed conditions, based on their occurrence in deeper zeolitized units (denoted Case 1). Two sets of geochemical species were chosen, so that the sensitivity to the mineral assemblage could be evaluated, and additional information could be obtained for PA abstractions. Case 2 represents a smaller set of species and minerals (calcite, gypsum, silica phases) that captures

many basic aspects of the DST water and gas chemical evolution, such as the pH and gas-phase CO_2 concentrations, but neglects Al, Fe, and F-bearing aqueous species and minerals. Simulations of the DST and the THC Seepage Model considered both geochemical cases.

Table 3.10-2. Model Mineral Assemblage, Aqueous and Gas Species (Full Geochemical System; CRWMS M&O 2000, N0120/U0110, Table 7)

Species	Minerals
Aqueous:	
H_2O	Calcite
H^+	Tridymite
Na^+	α -Cristobalite
K^+	Quartz
Ca^{+2}	Amorphous Silica
Mg^{+2}	Hematite
SiO_2	Fluorite
AlO_2^-	Gypsum
HFeO_2^{+3}	Goethite
HCO_3^-	Albite
Cl^-	Microcline
SO_4^{-2}	Anorthite
F^-	Ca-Smectite
	Mg-Smectite
Species	
Gas:	
	Na-Smectite
CO_2	K-Smectite
	Illite
	Kaolinite
	Sepiolite
	Stellerite
	Heulandite
	Mordenite
	Clinoptilolite
	Volcanic Glass

3.10.3.5 Relations for Mineral Reactive Surface Areas

Reactive surface areas of minerals on fracture walls were calculated from the fracture-matrix interface area/volume ratio, the fracture porosity, and the derived mineral volume fractions (CRWMS M&O 2000, N0120/U0110; Section 6.1.5.1). The fracture-matrix interface areas and

fracture porosities for each unit were taken from the drift-scale calibrated properties set (CRWMS M&O 2000, U0050, Section 6.2). These areas were based on the fracture densities, fracture porosities, and mean fracture diameter. The wall of the fracture is treated as a surface covered by mineral grains having the form of uniform hemispheres.

Mineral surface areas in the rock matrix were calculated using the geometric area of a cubic array of truncated spheres that make up the framework of the rock (CRWMS M&O 2000, N0120/U0110, Section 6.1.5.2). Clay minerals are considered as coatings of plate-like grains. The grains forming the framework of the rock matrix are considered to be the primary high-temperature phases of the tuff (i.e., quartz, cristobalite, tridymite, and feldspars). The abundance of secondary phases (i.e., those that formed as alteration products or low-temperature coatings on the primary assemblage), such as clay minerals, is used to reduce the free surface area of the framework grains.

3.10.3.6 Relations for Hydrological Property Changes

Changes in porosity, permeability, and capillary pressure as a result of mineral precipitation and dissolution are treated in CRWMS M&O (2000, N0120/U0110, Sections 6.1.6.2–6.1.6.3). Porosity changes in matrix and fractures are directly tied to the volume changes resulting from mineral precipitation and dissolution. Fracture-permeability changes are approximated using the porosity change and an assumption of plane parallel, fractures of uniform aperture (cubic law; Steefel and Lasaga 1994, p. 556). Although this is a gross simplification of the fracture geometry, it is not possible to predict the actual form and distribution of mineral precipitates at a very small scale. This is because of the many complexities of the fracture geometry and the very complex nature of mineral nucleation and growth under changing physical and chemical conditions. Thus, the permeability changes are only approximate. Matrix permeability changes are calculated from changes in porosity using ratios of permeabilities calculated from the Carmen-Kozeny relation (Bear 1988, p. 166) and ignoring changes in grain size, tortuosity, and specific surface area. Because of the exceedingly small initial matrix permeabilities of the welded Topopah Spring tuff, simplification in the matrix relations is immaterial. If mineral precipitation caused very substantial changes in permeability, or the permeability of the fracture system was already very low, then it would be necessary to treat the relations between permeability changes and porosity changes more rigorously. Changing permeability and porosity also induces changes in the unsaturated flow properties of the rock. Therefore, the capillary pressure is modified using the Leverett scaling relation (Slider 1976, p. 280).

3.10.3.7 Basis for Numerical Code TOUGHREACT V2.2

The geochemical module incorporated in TOUGHREACT V2.2 (described in Section 1.3.2.3) simultaneously solves a set of chemical mass-action, kinetic-rate expressions for mineral dissolution/precipitation, and mass-balance equations. Implementation of multiphase flow and heat transport for dual-permeability media is equivalent to TOUGH2 V1.4, which was used for other UZ flow calculations and TH calculations (CRWMS M&O 2000, U0050) and for TH calculations of the DST. TOUGHREACT V2.2 provides the extent of reaction and mass transfer between a set of given aqueous species, minerals, and gases at each gridblock of the flow model (Xu and Pruess 1998; Xu et al. 1998). Equations for heat, liquid and gas flow, aqueous and gaseous species transport, chemical reactions, and permeability/porosity changes are solved

sequentially (e.g., Steefel and Lasaga 1994, p. 550). It is assumed that the physical properties of the gas phase are unaffected by changes in the partial pressure of CO_2 resulting from heating, calcite reactions, and gas-phase transport. This assumption is justified by the results of the DST and THC Seepage Model runs, which show that the volume fraction of CO_2 is generally less than 5% and always less than 10% (CRWMS M&O 2000, N0120/U0110).

3.10.4 DST THC Model Results and Validation

The DST is the second underground thermal test being carried out in the Exploratory Studies Facility (ESF) at Yucca Mountain, Nevada. The purpose of the test is to evaluate the coupled thermal, hydrological, chemical and mechanical processes that take place in unsaturated fractured tuff over a range of temperatures from approximately 25°C to 200°C. The heaters were activated in December 1997 and are planned to run for 4 years followed by a 4 year cooling period.

Simulation of DST THC processes provides an important validation test for the THC conceptual models and input data used in the THC Seepage Model (Figure 3.10-3) for a much longer time scale. Geochemical input parameters have not been calibrated to measured data collected during the DST and therefore the DST THC Model simulations are an independent test of the conceptual model and input data used also in the THC Seepage Model. Detailed analysis of THC processes in the DST and validation tests are presented in CRWMS M&O (2000, N0120/U0110). This validation process involves examination of areas of modeled fracture drainage compared to the locations where water was collected during the test, the comparison of CO_2 concentrations collected from sampled gases, and comparison of the chemistry of waters collected from boreholes over time. These validation exercises are continuing as more data are collected from the DST and the models are improved to represent the physical and chemical processes more accurately. The following subsection compares modeling results to measured CO_2 concentrations collected from boreholes. Brief descriptions of the evolution of the water chemistry and mineralogy follow.

3.10.4.1 Gas-Phase CO_2 Evolution

In the first test, CO_2 concentrations measured in gas samples taken from boreholes during the DST are compared to simulation results using the DST THC Model. It is very important to capture changes in gas-phase CO_2 concentrations because they strongly control the pH of condensate waters, they are sensitive to temperature, and CO_2 transport is sensitive to the fracture hydrologic properties. CO_2 also affects HCO_3^- concentrations in fracture waters, which are important for the in-drift geochemical environment. Modeled distributions of CO_2 concentrations and temperature in fractures and matrix are shown after 6 and 20 months of heating (which are also times for which CO_2 measurements are available) in Figure 3.10-4 for the calcite-silica-gypsum geochemical system (Case 2). At both times, and in both fractures and matrix, a halo of increased CO_2 concentrations appears centered approximately at the 60°C isotherm. Over the 14-month period, between 6 months and 20 months, the halo increases considerably in extent and magnitude.

To evaluate how the model predicts the time evolution of CO_2 concentrations in the gas phase, measured CO_2 concentrations from intervals that were repeatedly sampled from February 1998

to August 1999 (20 months) are compared to model results for the same times. Figure 3.10-5 shows the time evolution of CO₂ concentrations in borehole intervals 74-3, 75-3, 76-3, and 78-3 (see Figure 3.10-4 for locations of borehole intervals). In borehole interval 74-3, there were only grid nodes above (cooler side) and below (hotter side) the interval, and therefore results from both nodes are plotted to see if they bracket the measured compositions. In borehole interval 78-3, two locations (center and end) were chosen, because of the strong thermal gradient across this region. The comparison shows that the simulations generally follow the trends in measured CO₂ concentrations. Two exceptions are when a known heater power loss occurred (around 19 months; see slope change in 74-3 and 75-3 at 20 months) or when the samples were at boiling temperatures and were nearly all water vapor (instead of air) and had much of the water condensed out during sampling (76-3 and 78-3, largest peaks). In the latter case, the modeling results should diverge from the measured data, because they reflect the CO₂ concentration for the full water vapor-air mixture. This effect is discussed in CRWMS M&O (2000, N0120/U0110, Section 6.2.7.2).

3.10.4.2 Water Chemistry Evolution

The modeled chemistry of waters in fractures is shifted from an initial pH of about 8.3 to 6.5, and is captured as changes in time and space. The lowest modeled pH values are in the region of highest gas-phase CO₂ concentrations. The shift in pH in the modeled fracture water is similar to that observed in the water collected from hydrology boreholes at the same times and in the expected regions during the DST (CRWMS M&O 2000, N0120/U0110), which were also areas of high gas-phase CO₂ concentrations. Chloride concentrations in waters collected from hydrology boreholes are considerably more dilute (a factor of 5 to 10) than the matrix pore water, which was also predicted by the modeling. Other species such as Ca and Si show similar trends in the modeled fracture water compositions compared to measured water compositions. Additional information on water chemistry can be found in CRWMS M&O (2000, N0120/U0110).

3.10.4.3 Mineralogical Changes

In the model simulations, calcite is the major phase forming in the zone above the heaters, although the abundances are exceedingly small. Secondly, amorphous silica also precipitates, but is much less abundant compared to calcite. No direct observation of the precipitation or dissolution of calcite has been found because the DST is ongoing; however, trends such as decreasing Ca in water found in boreholes with increasing temperature, pH and silica concentrations are strongly suggestive of calcite precipitation (CRWMS M&O 2000, N0120/U0110, Table 9). Fracture porosity changes in the DST simulations are very small after 20 months of simulation (on the order of 0.01%) and follow closely the area of calcite precipitation (CRWMS M&O 2000, N0120/U0110, Figure 17). Such small changes likely have no measurable effect on the hydrologic properties of the rock. More data are being collected from the DST, including ¹⁴C concentrations in gas-phase CO₂ and hydrogen, carbon, oxygen, strontium, and uranium isotopic measurements that will allow for more careful testing of the DST THC Model.

3.10.5 THC Seepage Model

This subsection describes the THC Seepage Model and the results of predictions of water and gas chemistry that may seep into drifts over the next 100,000 years. This model also considers any changes in the hydrological properties as a result of mineral precipitation and dissolution.

3.10.5.1 THC Seepage Model Description

A THC Seepage Model incorporates the elements of the EDA II (Enhanced Design Alternatives; Wilkins and Heath 1999, Enclosure 2) to represent waste package heating over time, changes in heat load due to ventilation, the effective heat transfer within the drift, the addition of backfill after 50 years, and THC processes. This two-dimensional model incorporated the initial layering in hydrologic and thermal properties and mineralogy from the surface to the Calico Hills zeolitic unit, along with different initial mineralogy and reactive surface areas in fractures and matrix (Figure 3.10-6). A number of cases were evaluated for different calibrated property sets, climate change scenarios, and geochemical systems. The climate scenarios were constructed from average values of the present-day infiltration, monsoon and glacial transition climates along with the upper and lower bounds. These averages were calculated from about 30 TH chimney models in the potential repository footprint. Predictions were presented of the water and gas chemistry that may enter the drifts for a period of 100,000 years, including a preclosure period of 50 years with 70% heat removal by ventilation.

3.10.5.2 TH Effects

TH effects on liquid saturation and flow around drifts were investigated in CRWMS M&O (2000, N0120/U0110). The TH effects on liquid saturation and temperature around drifts are a function of the infiltration rate and the initial liquid saturations calculated from steady-state simulations using specific calibrated property sets (CRWMS M&O 2000, U0035). Liquid saturations and temperature are shown around the drifts at 600 years, which is approximately the time of maximum dryout extent for the three climate cases investigated (Figure 3.10-7). These climate cases considered three time periods (0–600, 600–2,000, and 2,000–100,000 years) and different infiltration rates for each period (0.6/6/3, 6/16/25, and 15/26/47 mm/yr) for a lower, mean, and upper bound, respectively (CRWMS M&O 2000, N0120/U0110). The dryout zone is asymmetric around the drift as a result of the position of the waste package and backfill, and the effect of infiltration above the drift. The smaller dryout zone in the lowest infiltration case compared to the mean infiltration case is apparently the result of the differing property sets rather than differences in the infiltration rate. Higher liquid saturations in the pillar region are a result of water being diverted around the drift.

3.10.5.3 Gas-Phase CO₂ Evolution

The CO₂ evolution in the gas phase is a controlling factor for the pH and mineral-water reactions. Time profiles for gas-phase CO₂ concentrations at three locations around the drift are shown in Figure 3.10-8 for the Case 2 (calcite-silica-gypsum) geochemical system. Carbon dioxide concentrations in fractures drop significantly during dryout and increase again during rewetting. The increase in CO₂ concentrations in the gas phase during rewetting is likely a result of heating of these waters as they approach the drift wall, as suggested by the high-infiltration

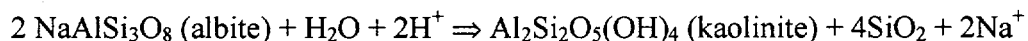
case showing the largest CO₂ concentration after rewetting (near 12,000 ppmV). The highest concentrations are similar to those observed during the DST, although rewetting has not taken place in the DST because it is still in the heating phase.

3.10.5.4 Water Chemistry Evolution

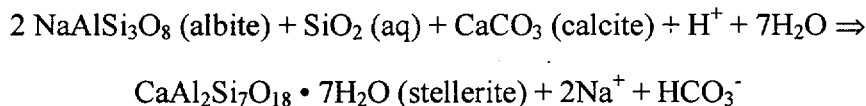
Chloride is a useful indicator of the extent of boiling or dilution, and interaction of condensate waters in fractures that are low in Cl with matrix pore waters having much higher chloride concentrations. Chloride concentrations are plotted in Figure 3.10-9 as a function of time at three locations around the drift. The gap in concentrations between about 75 and 1,000 years reflects the dryout period when no aqueous phase is present at the drift wall. Upon rewetting, chloride concentrations drop relatively quickly below 400 mg/L toward ambient values near 110 mg/L. There is no evidence of water with high concentrations of chloride at liquid saturations above residual saturation during the reflux period (after about 1,000 years). Therefore, waters that are most likely to seep into drifts will not be significantly more concentrated in chloride than the ambient pore water.

Predicted pH and total aqueous carbonate concentrations (as HCO₃⁻) in fracture pore water are shown in Figures 3.10-10 and 3.10-11 for the calcite-silica-gypsum system. The calculated pH is generally higher for the full geochemical system results (approximate range 8.5 to 9.8; shown in CRWMS M&O 2000, N0120/U0110, Figure 30) than for the calcite-silica-gypsum system (approximate range 7 to 8.5). The composition of waters reaching the drift wall during rewetting were roughly neutral in pH (7.2 to 8.3) for the smaller system, and approximately 8.6 to 9.0 for the full geochemical system. Total aqueous carbonate concentrations are higher in the full system at the drift crown (maximum, after rewetting, near 10,000 mg/L for the low infiltration case) than in the calcite-silica-gypsum system (near ambient values of 200 mg/L after rewetting).

The pH-carbonate-CO₂ data show different trends when aluminosilicates in the mineral assemblage are considered. The aluminosilicate reactions are sensitive to competing effects of infiltration rate and gas phase CO₂ diffusion relative to calcite dissolution/precipitation, feldspar dissolution, and calcium-zeolite precipitation. The dissolution of feldspars to form zeolites and clays directly affects the pH. For example, the dissolution of albite (Na-feldspar) to form kaolinite (clay) results in an increase in pH, as follows:



Feldspar dissolution also indirectly causes an increase in pH when Ca-rich zeolites precipitate, depleting calcium from solution and destabilizing calcite, as in the following reaction:



As a result, simulations that consider aluminosilicate reactions generally yield higher pH and total aqueous carbonate concentrations and generally lower CO₂ partial pressures than simulations with the simpler calcite-silica-gypsum system. Simulations of the DST show that results from the calcite-silica-gypsum system matches the observed pH, bicarbonate, and calcium

more closely than the more complex system. However, over longer and more stable periods of reflux and boiling, the system may trend toward the chemistry of the more complex system.

3.10.5.5 Porosity and Permeability Changes and Assessment of Precipitation Cap Formation

The calculated change in fracture porosity in the vicinity of the drift, at a simulation of 10,000 years, is shown in Figure 3.10-12 for the three climate scenarios and the calcite-silica-gypsum system. The maximum porosity reduction (negative in the plots) occurs for the high-infiltration case and is predominantly above the drift, adjacent to the tsw33 and tsw34 hydrogeologic unit contact. In all cases, the porosity change is relatively small (less than 1% of the initial porosity) and mostly to smaller values. The porosity decrease results primarily from calcite precipitation (as in the DST simulations). In the full geochemical system, the fracture porosity change is similarly small, but is dominated by zeolite reactions. Because the fracture porosity changes are exceedingly small, and permeability changes are negligible, TH processes are not significantly affected by mineral precipitation or dissolution.

3.10.6 Uncertainties and Limitations

Many uncertainties exist in the thermodynamic and kinetic parameters used to describe mineral precipitation and dissolution. Limitations also arise under specific geochemical and/or physical conditions. For example, as the concentrations of dissolved solutes increase during boiling of porewater, the activity coefficients of the dissolved species may deviate significantly from unity, and the ionic strength at which the models yield reasonable results is exceeded. Rapid boiling can also lead to mineral supersaturation outside the range of the pseudo-first-order kinetic models employed, which are generally reasonable under near-equilibrium conditions. Mineral precipitation may then be controlled by nucleation kinetics and other surface-energy-related phenomena. These uncertainties and limitations are generally difficult to quantify, because the models also introduce simplifications in the process of using these data, and the physical regimes under which the model breaks down may not be important for the overall dynamics of the system. Geochemical reactions are a strong function of temperature and the presence of water, which are better constrained than the rates of reaction and may control the spatial distribution of mineral precipitation, even if the exact quantities of the minerals at a given time are uncertain.

Relations between permeability changes and porosity changes are also highly uncertain. These uncertainties are difficult to quantify because they depend on the detailed geometry of the pore space and throats; however, some methods have succeeded in quantifying this effect in diagenetically altered rocks (Ehrlich et al. 1991, pp. 1579–1592). The effect of porosity reductions in fractures on the fracture permeability is even more uncertain.

The model is also limited to the middle nonlithophysal unit of the Topopah Spring tuff. Lithophysal units may exhibit different TH behavior that would change the interaction of fracture and matrix waters. Differences in the mineralogy of fractures and lithophysae could change the chemistry of the system somewhat, although the bulk rock chemistry is very similar for all of the welded TSw units. More important than small differences in mineral abundances is the effective reactive surface area which could be larger in lithophysal units because of the

greater abundance of vapor-phase minerals and as result of the interaction of waters flowing between fractures and lithophysae.

These uncertainties do not, in general, limit the applicability of the models because of the ability to calibrate effective reaction rates to fit the results of laboratory and in-situ experiments (i.e., thermal tests). Some of the uncertainties inherent in the thermodynamic and kinetic data have been addressed by the consideration of a simplified and a more complex mineral assemblage. Validation of the model by comparison to geochemical data from the DST provides the best degree of confidence building, and these comparisons have shown that the model is reasonable. Differences in the model results between the two geochemical systems, showing that the pH and CO₂ concentration in the gas phase for the simpler system compare more favorably to data from the DST shows that the model does provide important bounds on reaction rates. Results from the more complete system yield a higher pH than in the measured waters from the DST, which is due to a greater calculated reaction rate for feldspars. Therefore, porosity reductions as a result of feldspars altering to clays and zeolites likely take place at rates less than that given by model, giving an important upper bound.

3.10.7 Alternative Conceptual Models

A model proposed by Matyskiela (1997, pp. 1115–1118) suggests that silica precipitation in the rock matrix adjoining fractures will strongly reduce the permeability of the matrix, resulting in significantly decreased imbibition of percolating waters. The times for strong silica sealing of the matrix wall for a vitric tuff were 5 years for a solution having 350 ppm SiO₂ and 105 years for a solution having 125 ppm SiO₂. For a devitrified tuff, it was estimated that cristobalite dissolution followed by quartz precipitation would lead to a 1 mm thick quartz margin in about 30 years. It is clear that several factors would immediately reduce the magnitude of the effects described. First, the potential repository would be located in a devitrified tuff where the rates of reaction are orders of magnitude slower than for volcanic glasses. Second, the proposed model considered the system as fully saturated, maximizing the reactive surface area, the water available for reaction, and the diffusion coefficient. In an unsaturated system, only a part of the fracture area would be contacted by water, so that the process would have to take place for much longer periods to actually affect a large part of the fracture surfaces. Third, it is considered that the fracture water will have higher silica concentrations than a matrix porewater, thus leading to a diffusion gradient into the matrix. However, no clear reason exists why the fracture water should have a higher silica concentration, because it originated as pure condensate (zero SiO₂) that has drained back toward the heat source, increasing its silica content through wall rock reactions. Because the system is unsaturated, there is little driving force for convection as in a single-phase hydrothermal system. A quantitative analysis of this problem was explored by Lichtner et al. (1999) which also questioned the interpretations and conclusions presented in the Matyskiela (1997, pp. 1115–1118) paper (see CRWMS M&O 2000, U0135) and in Section 3.10.9 below.

3.10.8 Corroborative Evidence

Water and gas chemistry collected from the ongoing DST has been invaluable in the testing of the models developed for the prediction of potential long-term repository performance. No other data can be used to directly corroborate the model because of the uniqueness of the system.

However studies from natural geothermal analogs has been used as corroborative evidence, as discussed in Section 3.10.9.

3.10.9 Analogs

THC processes are better constrained through analysis of selected intrusive complexes hosted in unsaturated tuffaceous rock. The ideal intrusion to serve as a natural analog to THC processes anticipated at a potential Yucca Mountain repository should have been emplaced above the water table, should be of sufficient size to have produced enough heat to sustain boiling conditions for times on the order of several thousand years (~30 m width), and should occur in host rock of similar composition and characteristics to the Topopah Spring tuff.

An analogy for understanding future behavior of a potential repository is the fossil hydrothermal system at Yucca Mountain itself (Bish and Aronson 1993, pp. 148–161). After formation of the major zeolitic horizons (13–11.6 Ma), deep-seated hydrothermal activity persisted until about 10 million years ago (Ma). This activity was limited to temperatures of 90–100°C, the zeolite stability limit. Conceptual models for mineral evolution at Yucca Mountain (CRWMS M&O 2000, I0045, Section 6.3) suggest that the most likely mineralogical reactions caused by potential repository heating would include dissolution of volcanic glass and precipitation of clinoptilolite, clay, and opal-CT; dissolution and precipitation of silica polymorphs (cristobalite, opal-CT, tridymite, and quartz); alteration of feldspars to clays; and, finally, reactions involving calcite and zeolites. Present-day temperatures in borehole G-3, within the potential repository block, compare closely to inferred paleotemperatures. In contrast, increasingly higher paleotemperatures are inferred for boreholes G-1 and G-2, which are closer to the center of the Timber Mountain caldera source of eruption (G-2 being the farthest north). Mineral abundances in G-1 and G-2 cores indicate a northward progression of an increasing abundance of clays and zeolites along with decreased abundance of glass. This is consistent with the reactions stated above.

In addition to considering Yucca Mountain as a self-analog, contacts between igneous intrusions and host rock may provide useful information as coupled-process analogs. The Banco Bonito obsidian flow filled a steep-walled canyon cut in the Battleship Rock tuff on the southwest rim of the Valles Caldera, New Mexico, about 400,000 years ago. The obsidian, initially at temperatures of 850°C, heated the porous tuff in the canyon walls to 150–350°C for decades, and, according to models, vaporized much of the pore water, and caused refluxing of water (Stockman et al. 1994). Contact effects include a reddish “baked” zone extending several meters into the tuffs. No evidence of hydrothermal alteration was noted, suggesting that the area was unsaturated at the time of contact. Apart from devitrification, the principal mineralogic change in tuff near the contact was the development of feldspar-silica linings on voids in the pumiceous tuff matrix; no significant development of zeolites was found. Stockman et al. (1994) concluded that overall, the effects of heating in this unsaturated environment appeared to have been slight and were limited to the tuff nearest the contact.

At Grants Ridge, New Mexico, a 2.6 Ma basalt plug intruded into 3.3 Ma non-welded, pumice-rich, compositionally homogeneous, rhyolitic tuff and volcanoclastic sediments (WoldeGabriel et al. 1999, pp. 389–411). A 10 m wide aureole characterized by color variation, contact welding, brecciation, partial melting, and stoping developed around the 150 m wide basalt plug. Despite

the high-temperature ($> 700^{\circ}\text{C}$) basaltic intrusion, there was no evidence of pervasive hydrothermal circulation and alteration of the country rock. WoldeGabriel et al. (1999, pp. 389–411) postulated that vapor-phase expulsion of elemental species could have been responsible for the minor depletion of elements at the contact during devitrification of the silicic glass at near-solidus temperature related to the basaltic intrusion. Because devitrification is generally enhanced by the presence of aqueous fluids, the abundance of volcanic glass within a short distance (~ 10 m) from the plug is consistent with the inference of WoldeGabriel et al. (1999, pp. 389–411) that the plug intruded into an unsaturated environment.

In the Paiute Ridge area of the Nevada Test Site, late Miocene basaltic magma intruded a sequence of 22 to 11 Ma tuffs in a single magmatic pulse as dikes, sills, and lopoliths (Lichtner et al. 1999). A contact aureole ~ 3 m wide surrounds the intrusions. Matyskiela (1997, pp. 1115–1118) studied alteration surrounding one intrusion, the 50 m wide Papoose Lake sill. His major finding was alteration of glass shards to cristobalite and clinoptilolite within 60 m of the intrusion, which he interpreted as resulting from emplacement of the intrusion. Most significant was his observation of complete filling of pore spaces with silica at fracture-matrix interfaces, thus reducing fracture-matrix interaction and forcing infiltrating water to flow within fractures. Matyskiela (1997) estimated enhanced fracture flow to be as much as five times ambient conditions. This is the opposite behavior to formation of a silica cap, as predicted by recent simulations conducted for Yucca Mountain (Nitao 1998) in which fractures would become filled with quartz or chalcedony, thus inhibiting further flow. An issue is the extent to which a fracture can be filled by the silica contained in matrix pore water. Lichtner et al. (1999) shows that for a given matrix porosity, the degree of sealing of the fracture depends on the fracture porosity and the particular silica polymorph that precipitates. The two-phase numerical simulation results of Lichtner et al. (1999) suggest that at distances of tens of meters from the larger Paiute Ridge intrusion in their study (width ≥ 39 m), prolonged boiling conditions were established for times on the order of several thousands of years. Amorphous silica, with its higher solubility, gives the largest fracture filling, followed by chalcedony and quartz. For complete sealing of the fracture, a very small fracture porosity is necessary.

Some other questions arise regarding the effect of the sill on the host rocks. First, it is stated that the basaltic magma was particularly dry because hydrous phases (such as amphibole) were not found and because it was nonvesiculated (Matyskiela 1997, p. 1115). However, the absence of amphibole in this sill is not evidence for a lack of water in the melt because amphiboles are not stable phases at low pressures in basaltic melts (Ehlers 1972, p. 161). Also, this igneous body is a sill and not a flow; the slower cooling allows water degassing without obvious vesiculation (as in a lava flow). Basaltic magmas also can exsolve significant quantities of CO_2 in addition to H_2O , and therefore the geochemical environment was not clearly analogous to that around a potential repository drift.

In summary, in both the Banco Bonito flow and the Grants Ridge basaltic intrusion, the effects of high temperature on unsaturated environments appeared to have been slight, were limited to within about 10 m of the contact, and showed no evidence of fluid-driven convective heat transfer or pervasive hydrothermal alteration of the country rock. These field studies provide a limiting-case natural analog for evaluating effects of heat from decay of radioactive waste in an unsaturated environment.

3.10.10 Model Validation

The drift-scale THC models have been extensively validated by comparison of gas and water geochemical data collected during the DST, as discussed in Section 3.10.4 and described in detail in CRWMS M&O (2000, N0120/U0110). These comparisons include gas-phase CO₂ concentrations as a function of time and space, the pH of waters collected in boreholes, and general observations on changes in concentrations of Cl and other aqueous species. The model can be considered validated for its intended use.

The thermal tests provide the only field-scale experiments that have produced seepage under thermally perturbed conditions. Numerous samples of water have been collected from several borehole intervals during the DST, and previously a few samples were collected in the Single Heater Test.

Prediction and comparison to data from thermal tests and experimental studies have allowed for validation of the models describing coupled THC processes. However, it is not possible to validate all aspects of the model over a 100,000 year period. Yet reasonable bounds on the system behavior were made based on validation over relatively short time scales using the DST as described in this section and in CRWMS M&O 2000, N0120/U0110. The model has provided bounds on the gas and water chemistry over time (i.e., CO₂ and pH) as well as changes in porosity, as discussed in Section 3.10.6. For example, the composition of waters reaching the drift wall during rewetting was roughly neutral in pH (7–8.5) for the smaller geochemical system (without aluminosilicates) and had a pH of approximately 8.6–9.0 for the more complete geochemical system.

3.10.11 Abstraction of Drift-Scale THC Modeling for TSPA-SR

The THC water chemistry and gas-phase composition abstraction represents the fracture waters impinging at the crown and sides of the potential emplacement drifts. The abstraction uses the detailed time-history results of the process-level THC model and discretizes them into four distinct geochemical periods for which compositional boundary conditions are provided for the potential in-drift geochemical environment for TSPA models. The abstraction compositional boundary conditions include constituents represented by five cations, six anions, and pH. In addition, this abstraction includes the partial pressure of carbon dioxide in the gas phase in fractures adjacent to the potential drifts (and, during the abstraction boiling period, the equilibration temperature used for that gas with the condensate water composition). These boundary conditions to the potential drifts allow incorporation of time varying, thermally perturbed water and gas compositions within the assessment of chemical interactions of the in-drift environment.

The abstracted use of the THC process model results from the Case 2 mineralogy is based on the fact that it reproduces more accurately the observed changes to water and gas compositions in the drift-scale heater test (CRWMS M&O 2000, N0120/U0110; Sections 6.1.7 and 6.2.7). This corresponds to using the mineralogic phase constraints represented in Case 2 to set the major element composition of the water and gas. This decision is supported by the THC process-level model validation with the DST results, for which the Case 2 results provide closer description of the ambient and thermally perturbed geochemical system (CRWMS M&O 2000, N0120/U0110;

Sections 6.1.7, 6.2.7 and 6.3.5). Therefore, the abstraction of aqueous water chemistry of the major chemical species (which are contained in both Case 1 and Case 2 representations) is from Case 2 only.

For the constituents included in both those chemical systems, the major differences between results (for PA purposes this is defined as a factor of 10—or one log unit—or more) are limited to Ca^{2+} , Na^+ , and HCO_3^- . These represent differences that result primarily from the more uncertain kinetic representation of the more complex chemical system (CRWMS M&O 2000, N0120/U0110; Sections 6.1.7, 6.2.7, and 6.3.5). As discussed therein, the uncertain precipitation rates of the alumino-silicates create a feedback to the carbonate system by removing Ca from solution, impacting the carbonate system through the changes in calcite saturation state. However, estimates of the additional constituents included only within the Case 1 results should be reasonably obtained from those results. This is because the primary differences in the systems are those constituents listed above and the variations in pH, that may impact mineral equilibria in the more complex chemical system, are of lesser magnitude. The process model Case 1 results for F⁻ are assessed to be relatively insensitive to the possible changes (CRWMS M&O 2000, N0120/U0110; Section 6.3.5). The phase constraints applied within the Case 1 representation for these additional constituents should be largely unchanged (although more accurate kinetic parameter sets should prevent them from impacting the carbonate subsystem) and these are all trace constituents compared to the major constituents included within both Case 1 and Case 2. Given this, the values for the additional constituents from the Case 1 representation should provide at least order-of-magnitude estimates for incorporating abstracted first approximations for these constituents. In the abstraction these values are combined with the constituents from the Case 2 results to describe a more comprehensive water composition (Table 3.10.3). Addition of these values to these abstracted water compositions should have only minor effects on charge balance, because these additional aqueous species are trace constituents compared to the major elements given within the Case 2 representation.

Table 3.10.3 represents the THC abstraction of water and gas compositions for the THC boundary conditions adjacent to the drift wall. Each of the time periods defined below has a defined composition of gas and water that represent those constituents that can enter the drift during those times based on the process-level THC models for the thermally perturbed geosphere. Four periods were defined based on the examination of the process-level results. Each of these periods was evaluated to define constant representative values (as discussed above) for all constituents during that period with step (i.e., instantaneous) changes between the periods. The first period defined goes from 0 to 50 years and is the entire preclosure period. This is followed by the defined boiling period 2, during which the fractures are calculated to have zero saturation. The water that may enter the drift through these fractures would be that moving rapidly down from the condensate zone. This boiling period is followed by a transitional cooldown period from 1000 to 2000 years during which the temperature is still high, but below boiling. Finally an extended cool-down period 4 is defined from 2000 to 100,000 years, over which the temperatures return to ambient and water compositions change gradually.

Although the preclosure period (50 years) is included in the process models, the postclosure performance assessment starts at the end of this initial period. Abstracted results for Period 1 preclosure are included only for complete coverage of the time of the process-level results. The process model results do not include the chemical effects of pre-closure ventilation, so the gas

composition and water chemistry within this period may not be very representative of those that could enter the drifts. These abstracted values for Period 1 preclosure are not used within the performance assessment analyses. Because the preclosure period is not being used within the performance assessment, the values for the 0-50 year period are more coarsely abstracted and chosen to be roughly representative of the first 50 years. This period will not be used further in this abstraction. The abstracted boiling period 2 directly follows the preclosure abstraction period 1. During the second abstraction period, the boiling period, the fracture saturation around the drifts is calculated to be zero in the THC process model results. The chemical composition of the condensate water, calculated to be in the zone of highest saturation above the fracture dryout, is used to represent the water that may flow rapidly through the fractures during the boiling period. The values for such water are given below in Table 3.10.3 with the value of the partial pressure of CO_2 in the gas surrounding the drift wall during that dryout time. The flux of such water would be at a minimum during this period, so that the fracture gas composition at the drift wall during the dryout period should be the appropriate composition with which to equilibrate the condensate liquid. This value ($\log \text{CO}_2$, volume fraction = -6.5) is given in Table 3.10.3 below. This gas composition, and associated boiling temperature, should be used to equilibrate with the abstracted condensate water composition shown for this period in Table 3.10.3. This represents the abstracted water that may flow rapidly down fractures into the dryout zone from the overlying condensate zone.

It is re-emphasized that during the abstracted boiling period (50-1000 years), denoted as period 2 in Table 3.10.3, the abstracted aqueous concentrations and pH are obtained from the process-level model results from `satmax_summary.xls` (DTN: LB991200DSTTHC.002), not the results for locations at the drift wall. These latter water compositions are artifacts of the point at which the water chemistry representation was shut off either due to high ionic strength or low saturations. However, the gas composition (CO_2 , gas) is obtained from the appropriate results for the crown fractures at the drift wall because the process-level THC gas chemistry calculation is continuous through this period (see Figure 29, CRWMS M&O 2000, N0120/U0110). The boiling period abstracted water composition is based on the condensate water chemistry above the dryout zone, representing water that would flow rapidly down the fracture if possible.

The remaining two THC periods, the transitional and extended cool-down periods, are abstractions of the chemistry results obtained from the process-level THC model in the same manner as that for the pre-closure period (0-50 years). However, because the changes are more gradual for most constituents in these time periods, it was possible to identify a result at a specific time given by the process model that corresponded to a reasonable representation for the compositional parameters needed in the abstraction. Using specific calculated results from the THC process model ensures that issues of charge balance and phase equilibria are maintained completely consistently within the abstracted representation.

It is noted that the abstracted temperatures listed in Table 3.10.3 are given for use as a guide only, especially in Period 4 in which the temperature changes gradually from about 90°C to 25°C over 98,000 years. Only the temperature in the Boiling Period 2 should be used in process models to calculate re-equilibration of the condensate-zone water composition with the abstracted CO_2 gas composition in the fractures at the drift crown for that period of time. For further Performance Assessment model abstractions, the temperatures given in Table 3.10.3 can be used as the representative values for the temperature of the abstracted compositions, but

should be tied to the thermal variation of the repository system as abstracted for the total system performance assessment.

The following should be noted for the abstraction shown in Table 3.10.3:

- The first 50 years represents the repository preclosure period with 70% heat removal via ventilation. However, because the Performance Assessment only starts at closure, these values are not used there and are only provided for completeness of the time span. It is emphasized that the values probably would not be representative of preclosure conditions because the potential chemical effects of ventilation are not included in the process model.
- The values for abstraction period 3, correspond to the process-level model results at 2000 years after initial waste emplacement. This is because as soon as the drift wall rock resaturates, the CO_2 very rapidly approaches about 1×10^{-3} bars and the pH and water composition are taken consistently with this gas chemistry.
- The 10,000-year process-level model results are used for the abstraction values in the last period as a reasonable approximation of the water composition average for that whole period.
- The additional constituents taken from the results of the more detailed chemical system are, in general, trace constituents compared to those taken from the less detailed chemical system. Even though combination of these results may lead to discrepancies of the trace constituents that could be large in a relative sense, their contributions to the absolute uncertainties will remain small because of their trace abundances. Only potassium approaches the concentrations of the constituents taken from the less detailed chemical system, and even it is one to two orders of magnitude lower in concentration than the major cation species Ca^{+2} and Na^{+} included in Case 2 results.

Table 3.10-3. THC Abstraction for the Mean Infiltration Rate Case with Climate Change (CRWMS M&O 2000, N0125, Table 3)

Constituents from Simplified Chemical System (Calcite-Silica-Gypsum)				
	Preclosure	Boiling	Transitional Cool-Down	Extended Cool-Down
	Period 1	Period 2	Period 3	Period 4
Parameter	Abstracted Values	Abstracted Values	Abstracted Values	Abstracted Values
Time	0 - 50 years	50 - 1,000 years	1,000 - 2,000 years	2,000 - 100,000 years
Temperature, °C	80	96	90	50
log CO ₂ , vol. frac.	-2.8	-6.5	-3.0	-2.0
pH	8.2	8.1	7.8	7.3
Ca ²⁺ , molal	1.7E-03	6.4E-04	1.0E-03	1.8E-03
Na ⁺ , molal	3.0E-03	1.4E-03	2.6E-03	2.6E-03
SiO ₂ , molal	1.5E-03	1.5E-03	2.1E-03	1.2E-03
Cl ⁻ , molal	3.7E-03	1.8E-03	3.2E-03	3.3E-03
HCO ₃ ⁻ , molal	1.3E-03	1.9E-04	3.0E-04	2.1E-03
SO ₄ ²⁻ , molal	1.3E-03	6.6E-04	1.2E-03	1.2E-03
Additional Constituents from Full Chemical System				
Mg ²⁺ , molal	4.0E-06	3.2E-07	1.6E-06	7.8E-06
K ⁺ , molal	5.5E-05	8.5E-05	3.1E-04	1.0E-04
AlO ₂ ⁻ , molal	1.0E-10	2.7E-07	6.8E-08	2.0E-09
HFeO ₂ ⁻ , molal	1.1E-10	7.9E-10	4.1E-10	2.4E-11
F ⁻ , molal	5.0E-05	2.5E-05	4.5E-05	4.5E-05

3.10.12 Summary and Conclusions

The conceptual model for THC processes provides a comprehensive basis for modeling the pertinent mineral-water-gas reactions in the host rock, under thermal loading conditions, as they influence the water and gas chemistry that may enter drifts over 100,000 years. Data are incorporated from the drift-scale calibrated property sets, the UZ Flow and Transport Model, geochemical data (fracture and matrix mineralogy, aqueous geochemistry, and gas chemistry), thermodynamic data (minerals, gases, and aqueous species), data for mineral-water reaction kinetics, and transport data. Simulations of THC processes included coupling between heat, water, and vapor flow, aqueous and gaseous species transport, kinetic and equilibrium mineral-water reactions, and feedback of mineral precipitation/dissolution on porosity, permeability, and capillary pressure (hydrologic properties) for a dual-permeability (fracture-matrix) system. The effect of these coupled THC processes on the time evolution of flow fields in the UZ around drifts has been investigated for different climate change scenarios, calibrated property sets, and initial mineralogy. Validation of the model was done by comparison of measured gas and water chemistry from the Drift Scale Test (DST) to the results of simulations using the DST THC

Model. In particular, simulation results were compared to measured gas-phase CO_2 concentrations and the chemistry of waters collected from hydrology boreholes collected during the test.

Comparisons of water chemistry (pH) and CO_2 concentrations in the gas phase from the DST indicate that a smaller set of aqueous species and minerals (calcite, silica phases, gypsum), but including gaseous CO_2 , can describe the general evolution of DST water quite closely. Including a wide range of aluminosilicates, such as feldspars, clays, and zeolites yields information on additional species (i.e., Al, Fe, F), but their inclusion causes shifts in the water and gas chemistry that are more rapid than observed. These effects may be more important over longer time periods, leading to similar but less rapid changes (i.e., a slightly closer approach to equilibrium). However, over the time scale of the DST, the effective reaction rates and/or thermodynamic properties of these phases will clearly require some refinement.

The THC Seepage Model incorporates the elements of the EDA II design to represent waste package heating over time, changes in heat load due to ventilation, the effective heat transfer within the drift, the addition of backfill after 50 years, and THC processes in the unsaturated zone. A number of cases were evaluated for different calibrated property sets, climate-change scenarios, and geochemical systems. The THC seepage simulations indicate that there may be an increase in the CO_2 gas and aqueous carbonate concentrations around the drift during rewetting. The extent of the dryout zone and the time of rewetting were different for each climate history and calibrated property set, although the general character was unchanged. As in the Drift Scale Test THC simulations, some notable differences in the pH and CO_2 concentrations appeared in the two geochemical systems. The composition of waters reaching the drift wall during rewetting were roughly neutral in pH (7–8.5) for the smaller geochemical system (without aluminosilicates) and approximately 8.6–9.0 for the more complete geochemical system. Predicted pH and HCO_3^- concentrations in the smaller geochemical system simulations are supported by the data from the DST; however, the long term evolution could trend in the direction of the more complex system chemistry, if the slow reaction rates of the aluminosilicates limit the changes in water chemistry that can be observed over the short heating time of the DST.

Even with the apparently overestimated reaction rates for the full mineral assemblage, the changes in porosity and permeability around drifts over 100,000 years were small (less than 1% of the total fracture porosity), and therefore effects on flow and transport are considered negligible. A summary of important results as related to the conceptual model of drift-scale THC processes is shown in Figure 3.10-13.

In the abstraction for TSPA-SR calculations, the transient water and gas compositions are averaged over four discrete time periods from 0 to 100,000 years. Only the mean infiltration cases are selected because the results of the low and high infiltration cases showed similar behavior in general. The results that are passed to the in-drift geochemical models in TSPA are aqueous concentrations for five cations and six anions, pH, and partial pressure of carbon dioxide during the four discrete periods. These results are used to determine the in-drift environment and the corrosion of the drip shields and waste packages over time.

3.11 UZ TRANSPORT MODEL

3.11.1 Introduction

The evaluation of possible radionuclide transport from the potential repository horizon to the groundwater in the saturated zone is key to assessing the performance of the potential repository. This section describes the issues, approach, assumptions, and understanding of the relevant physical processes, and input parameters used to develop the Transport Model in the UZ. The Transport Model utilizes the understanding of the complex flow processes from the Flow Model (Section 3.7) and accounts for the transport of aqueous/colloidal radionuclide species in both the fracture and matrix continua, with exchange between continua resulting from advective and/or diffusive processes, as well as sorption in the matrix. Results of 2-D vertical cross sections, 3-D site-scale simulations of the important radionuclides and daughter products, and 3-D simulations of tracer breakthrough at the water table are presented for different climate scenarios developed in Section 3.5. These results are analyzed to identify the major transport mechanisms and breakthrough times through the different hydrogeologic units and the effects of the major hydrogeologic features (faults and perched water). Model validation using the results of the ESF Alcove 1 and Busted Butte tracer tests is summarized. Review of known analog sites for UZ transport indicates that unsaturated systems in arid environments may provide favorable sites for geologic disposal of radioactive waste. The abstraction of the Transport Model used for calculations of radionuclide transport in TSPA is then discussed. Finally, this section ends with conclusions regarding the important issues identified for radionuclide transport at Yucca Mountain.

3.11.1.1 Issues

The Transport Model evaluates a suite of factors that control potential radionuclide transport to determine their effects on radionuclide breakthrough times and concentrations at the groundwater table. A schematic representation of the key issues for the Transport Model is shown in Figure 3.11-1. The flow of water from the potential repository horizon to the groundwater table can transport both aqueous and colloidal phase radionuclides. The concentration of radionuclides and their daughter products are diminished according to their radioactive decay rates, dilution due to mixing (i.e., dispersion), and the extent of sorption onto the solid phase. The flow pathways are determined by the characteristics of the faults, hydrogeologic units, and the presence of perched water. These characteristics control the extent of downward versus lateral flow, fracture-matrix interaction, and the partitioning of flow between fractures and rock matrix. Fractures and faults can be fast flow paths, where fluid contact time and surface area are small relative to the matrix and limit the extent of rock-water interaction relative to the slower-moving matrix flow. Fracture properties, such as aperture, frequency, mineralogy and saturation, affect fracture-matrix interactions, dispersion, sorption and the transport of aqueous and colloidal species. Matrix porosity, saturation, and mineralogy affect the extent of diffusion and sorption of species. The transport of colloidal species is further affected by their size, which determines the nature of pore exclusion, and filtration processes. More detailed discussions of these issues follow in Section 3.11.2.

3.11.1.2 Approach

Transport modeling studies of representative radionuclide and colloids are conducted in 2-D vertical cross sections and 3-D site-scale models of the UZ to:

- Evaluate the effectiveness of matrix diffusion and sorption/filtration as retardation mechanisms in the various hydrogeologic units
- Determine the dominant transport features and mechanisms
- Estimate transport breakthrough from the potential repository to the water table
- Evaluate the importance of decay daughter products on transport.

Relationships of other models and data feeds to the Transport Model are schematically shown in Figure 3.11-2.

3.11.1.3 Assumptions

The key assumptions for the Transport Model in the UZ are listed here. The complete list of assumptions for the Transport Model and the discussion of the supporting rationale are in CRWMS M&O (2000, U0060, Section 5).

- Flow component assumptions are the same as for the Flow Model described in Section 3.7 (e.g., isothermal water flow, dual continuum, active fracture concept, van Genuchten-Mualem model for relative permeability and capillary-pressure constitutive relationships).
- The processes governing the transport of dissolved and/or colloidal species include advection, molecular and surface diffusion, hydrodynamic dispersion, sorption, radioactive decay, colloid filtration, and colloid-assisted solute transport.
- Colloid filtration does not affect the medium's porosity and permeability on account of the anticipated low colloid concentrations.
- The initial radionuclide (solute or colloidal species) concentrations are constant in the gridblocks corresponding to the potential repository and zero throughout the rest of the UZ model domain.

Section 3.11.2 provides a detailed discussion of the transport processes and other major factors affecting UZ transport.

3.11.2 Physical Processes

3.11.2.1 Flow Processes

Transport is closely tied to water flow. A detailed discussion about hydrology in the UZ is presented in Section 3.3, and transport modeling is based on the Flow Model discussed in Section 3.7. In addition to the advective flow processes, transport of radioactive solutes and/or colloids involves hydrodynamic dispersion, sorption (solutes) or filtration (colloids), matrix diffusion, and radioactive decay. The effects of these processes on UZ transport are discussed below.

3.11.2.2 Advection

Advection is the movement of dissolved or colloidal species resulting from the bulk flow of fluid (Fetter 1993, p. 47). In advective transport, the flowing water carries contaminants, and transport pathways coincide with flow pathways determined by the characteristics of the faults, hydrogeologic units, and perched water (Section 3.3). As flow in Yucca Mountain is predominately downward because of gravity, so is advective transport. The presence of perched water bodies may result in lateral flow and subsequent transport of the radionuclides.

Advection is probably the most important mechanism for fast radionuclide transport through the UZ to the water table. Advection through fractures is expected to dominate transport behavior in welded units because water flows largely through fracture networks. Dominant fracture flow in the zeolitic portions of the CHn and CFu also provides relatively short transport times to the water table, whereas the dominant matrix flow in the vitric CHn leads to much longer transport times.

3.11.2.3 Hydrodynamic Dispersion

Hydrodynamic dispersion includes both mechanical dispersion arising from local velocity variations and molecular diffusion driven by concentration gradients. Dispersion of the radionuclides occurs both along (longitudinal) and transverse to the average flow direction. Hydrodynamic dispersion dilutes and smears sharp concentration gradients and reduces the breakthrough time of radionuclides to the water table. The dispersion coefficient is a function of dispersivity and flow velocity.

Values of dispersivity are difficult to determine without site-specific measurements. Dispersivity has been shown to increase as a function of observation scale, attributed mainly to mixing as more heterogeneities are sampled at larger scales (e.g., Gelhar et al. 1992, pp. 1955–1974; Fetter 1993, pp. 65–66). Furthermore, the reported field measurements of transverse dispersivity show it to be significantly less than longitudinal dispersivity (Fetter 1993, pp. 65–66).

Hydrodynamic dispersion is not expected to play an important role in UZ transport. First, dispersion effects are implicitly accounted for by the fracture–matrix dual-continuum approach, which explicitly models local velocity variations. Second, the potential repository emplacement area is very broad (relative to the distance to the water table), which tends to suppress dispersion effects (CRWMS M&O 2000, U0030, Section 6.2).

3.11.2.4 Sorption

Sorption is a general term to describe the binding of a solute (radionuclide) onto the sorbent (either the immobile rock matrix or colloids). As a result of sorption onto the rock matrix, the advancing rate of sorbing radionuclides is retarded. On the other hand, the attachment of sorbing radionuclides onto colloids can potentially facilitate their transport, which is to be discussed in Section 3.11.2.7.

In Yucca Mountain studies, the effective sorption distribution coefficient (K_d) approach is employed to quantify the extent of radionuclide-sorbent interactions. This approach does not require identifying the specific underlying processes of sorption, such as surface adsorption, precipitation, and ion exchange. While the use of K_d to describe the complex radionuclide-sorbent interactions in a flowing fluid of variable chemistry is a simplification, the results from numerous laboratory batch and column experiments have not produced recommendations to abandon the K_d approach for modeling radionuclide retardation in the YMP (CRWMS M&O 2000, U0100, Sections 6.4 to 6.6).

Experimentally determined K_d values have been predominantly derived from batch experiments using crushed tuff (with the sample size of 75–500 μm) under water-saturated conditions for a variety of rock types and radionuclides (K_d values are listed in Table 3.11-1 in Section 3.11.3.2). There are concerns that this experimental approach may overestimate the K_d values in UZ transport, as discussed in more detail in Section 3.11.10.2.

Sorption onto fracture surfaces will retard radionuclide migration. The minerals coating the fracture surfaces generally differ from the host-rock mineralogy as a result of different exposure to precipitation of hydrothermal or meteoric waters, or alteration of the pre-existing minerals (CRWMS M&O 2000, U0100, Section 6.5.3). Laboratory sorption experiments showed that trace minerals might be quite effective at retarding ^{237}Np (neptunium) transport when they are concentrated on fracture surfaces (CRWMS M&O 2000, U0100, Section 6.5.3). Numerical simulations also showed that the limited sorption on the fracture walls is sufficiently important to retard transport of strongly sorbing radionuclides [e.g., ^{239}Pu (plutonium)] (CRWMS M&O 2000, U0060, Section 6.17.1). However, sorption in the fractures is not considered in the TSPA transport evaluations because of the limited data and conservative nature of this assumption regarding the radionuclide transport to the water table.

3.11.2.5 Matrix Diffusion

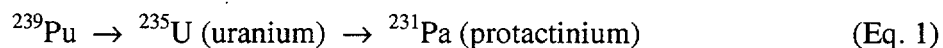
Matrix diffusion can play an important role in radionuclide exchange between the fractures and the rock matrix. Radionuclide diffusion into the rock matrix and away from the fracture surface is driven by a concentration gradient, and it will slow the advance of radionuclides by removing them from the faster flowing fractures. The significance of matrix diffusion depends mainly on factors such as effective contact area between fracture and matrix, the diffusion coefficient of the species, and characteristics of fracture networks (CRWMS M&O 2000, U0030, Section 6.2). The presence of inactive and relatively dry fractures, accounted for with the active fracture model (Section 3.4), could serve as barriers for matrix diffusion.

The effective diffusion coefficient, which is the product of the molecular diffusion coefficient, tortuosity, porosity, and water saturation, is used to account for rock geometry and saturation effects on matrix diffusion. Laboratory diffusion studies in porous geologic materials show that tortuosity values between about 0.5 and 0.01 are commonly observed (Fetter 1993, p. 44). Very limited experimental data exist on the tortuosity distribution in the various Yucca Mountain hydrogeologic units. CRWMS M&O (2000, U0060, Section 6.1.2) employed the approach of using the porosity value to approximate tortuosity, as suggested from the literature (Farrell et al. 1994, p. 64; Grathwohl 1998, pp. 28–35). Tortuosity measurements on devitrified tuffs showed good agreements with this approximation, thereby validating the approach (CRWMS M&O 2000, U0060, Section 6.1.2).

3.11.2.6 Radioactive Decay and Daughter Products

The decay of the radioactive species of interest and their half-lives are completely predictable and well documented. The production of daughter products from chain-decay adds complexity because transport simulations must compute the total radioactivity distribution, i.e., the sum of the concentrations of all the members of the radioactive decay chain. This is especially significant if the daughters have long half-lives. Daughter products with short half-lives relative to the simulation periods may not need to be considered.

The daughter products may have significantly different transport behavior than the parent radionuclide. Equation (1), for example, shows the ^{239}Pu decay chain.



This equation includes only the most important radioactive chain members and omits daughters with short half-lives. The daughter ^{235}U has significantly smaller K_d values compared to its parent ^{239}Pu (see Table 3.11-1).

3.11.2.7 Colloidal Transport

Colloids are very fine particles such as clay minerals, metal oxides, viruses, bacteria, and organic macromolecules that range in size from 1 to 10,000 nm (McCarthy and Zachara 1989, pp. 496–502). Generation and mobilization of colloids has become an important issue in the facilitated transport of radionuclides as intrinsic colloids [e.g., colloidal Pu (IV) and colloidal Pu (V)], or as radionuclide-bearing pseudocolloids for ^{239}Pu and ^{243}Am (americium). Colloidal transport differs from solute transport because of colloidal particle interactions (e.g., flocculation), pore exclusion, and surface reactions (e.g., deposition or attachment).

There is some field evidence of colloid-facilitated transport of radionuclides. In one case, the rapid migration of Pu and Am, attributed to colloidal transport, was found more than 30 m downward through unsaturated tuff over the course of approximately 30 years from a low-level waste site at Los Alamos National Laboratory (Buddemeier and Hunt 1988, p. 536). In a saturated zone study at the Nevada Test Site (NTS), $^{240}\text{Pu}/^{239}\text{Pu}$ isotope ratio “fingerprints” of the source of Pu in groundwater showed that it had been transported more than 1.3 km over a 30-year period, although Pu is strongly sorbing at the NTS and assumed to be immobile (Kersting et al. 1999, pp. 56–59). There was a direct finding that Pu was on colloidal material in samples

taken from the NTS through filtration of the groundwater samples. Note that the Pu observed at the NTS originated from an underground nuclear bomb test and that the effects of the underground blast on Pu transport are not fully understood. Microspheres are used as a colloidal tracer at the saturated C-Wells tests (CRWMS M&O 2000, AMR U0100, Section 6.9) and at the Busted Butte transport test in the unsaturated vitric Calico Hills Formation (CRWMS M&O 2000, AMR U0100, Section 6.8).

Colloid concentrations have been measured in several groundwater samples from Yucca Mountain and from other areas at the Nevada Test Site. The measured particle concentrations vary between 1.05×10^6 and 2.72×10^{10} particles/mL, with the lowest being for water from well J-13 and the highest for water from well U19q on Pahute Mesa (CRWMS M&O 2000, U0070, Section 6.2.2.2). These values are consistent with what has been reported in the literature for various groundwaters around the world.

In addition to natural colloids, anthropogenic colloids may be produced from the waste itself or from potential repository construction and sealing materials. This was demonstrated in a 50-month-duration experiment on simulated weathering of a high-level nuclear waste glass, where the amounts of Pu and Am released from waste forms were orders of magnitude greater than their respective concentrations in the dissolved phase (Bates et. al 1992, pp. 649–651). Constraints on these types of colloids are treated in the Waste Form Degradation (WFD) PMR (CRWMS M&O 2000, WFD PMR, Section 3.8).

3.11.3 Transport Properties

This section describes the transport properties used for the abstraction of UZ transport for TSPA evaluations, which is discussed in Section 3.11.13. Matrix diffusion and dispersivity values used for UZ transport modeling and validation, discussed in Sections 3.11.5-10, are different from those used for TSPA abstraction and will be explicitly identified.

3.11.3.1 Dispersion

No data are available to determine dispersivity in the UZ over the travel distance between the potential repository and the water table. In a transport simulation longitudinal dispersion results in earlier arrivals, but generally lower concentrations. Given this behavior, no simple conservative bound exists for the longitudinal dispersion. However, a dispersivity value of 20 m over the approximately 300 m UZ travel distance (in TSPA calculations) is consistent with the dispersivity versus scale correlation of Neuman (1990, pp. 1749–1758). Furthermore, the longitudinal dispersivity (primarily in the vertical direction) is not expected to have a large effect on radionuclide transport processes in the UZ because of the strong dispersive effects of fracture-matrix interactions that are explicitly captured in the Finite Element Heat and Mass Transfer (FEHM) particle-tracking calculation (see Section 3.11.13). Transverse dispersion acts only to reduce concentrations, with generally little effect on breakthrough time. Therefore, a conservative value of zero for transverse dispersivity is used. The base-case distribution for longitudinal dispersivity has been selected to be normal, with a mean of 20 m and a standard deviation of 5 m, which captures a range of 7.5 m to 32.5 m within the 99 percent probability limits. This dispersivity distribution applies to transport in all model units for both the fracture

and matrix continua, but values for fracture and matrix are sampled independently for TSPA calculations.

3.11.3.2 Sorption Coefficients

The main experimental program for sorption was carried out using batch sorption experiments. Table 3.11-1 gives the sorption distribution coefficients recommended for TSPA (CRWMS M&O 2000, U0100, Table 2a). For some radionuclides, specific sorption measurements using rock and water samples from Yucca Mountain have not been performed. For these radionuclides, sorption behavior has been evaluated on a theoretical basis.

Three assumptions were made to develop values of K_d for use in performance assessment (CRWMS M&O 2000, U0100, Section 5). First, the water compositions from wells J-13 and UE-25 p#1 are assumed to provide an adequate range of compositions to capture the influence of water compositional variability on sorption in the UZ. Potentially perturbed fluid compositions moving as plumes out of the potential drifts are not included in the evaluation of this assumption. Second, the effects of mineral variations on sorption in the UZ may be approximated using three rock types: devitrified tuff, vitric tuff, and zeolitic tuff. Finally, the effects of temperature are bounded by measurements of sorption at ambient temperature. However, the effects of mineral alteration because of thermal history are not included in the evaluation of this assumption.

The use of a linear, infinite-capacity sorption model is important for both describing sorption and for modeling the transport of sorbing radionuclides (see Section 3.11.13). Sorption of uranium shows nonlinear sorption behavior, in which the sorbed concentration is reduced from that of a linear model at higher concentrations (see CRWMS M&O 2000, U0100, Section 6.4.4.1.4.4). Linear sorption behavior is expected for the lower concentration levels that will constitute the earliest releases. At higher concentrations, nonlinear effects will act to "self-sharpen" the solute fronts (i.e., longitudinal dispersion is decreased). A linear sorption model may still be used for predicting radionuclide movements and breakthrough times in general, provided appropriate values of K_d are selected that account for the range of K_d s represented by the data at different solute concentrations. In this case, the range of K_d s as a function of concentration is incorporated as part of the frequency distribution defining the overall uncertainty in K_d .

Table 3.11-1. Sorption Coefficient Distributions for UZ Units (Adapted from CRWMS M&O 2000, U0100, Table 2a)

Element	Rock type	Min K_d (mL g ⁻¹)	Max K_d (mL g ⁻¹)	E[x]*	COV*	Distribution type
Americium (also Actinium, Samarium, Thorium, Zirconium)	Devitrified	100	2000	—	—	Uniform
	Vitric	100	1000	400	0.20	Beta
	Zeolitic	100	1000	—	—	Uniform
	Iron oxide	1000	5000	—	—	Uniform
Plutonium	Devitrified	5	70	—	—	Uniform
	Vitric	30	200	100	0.25	Beta
	Zeolitic	30	200	100	0.25	Beta
	Iron oxide	1000	5000	—	—	Uniform
Uranium	Devitrified	0	2.0	0.5	0.3	Beta
	Vitric	0	1.0	0.5	0.3	Beta
	Zeolitic	0	10.0	4.0	1.0	Beta (exp)
	Iron oxide	100	1000	—	—	Uniform
Neptunium	Devitrified	0	1.0	0.3	0.3	Beta
	Vitric	0	1.0	0.3	1.0	Beta (exp)
	Zeolitic	0	3.0	0.5	0.25	Beta
	Iron oxide	500	1000	—	—	Uniform
Radium	Devitrified	70	300	—	—	Uniform
	Vitric	50	100	—	—	Uniform
	Zeolitic	800	2000	—	—	Uniform
	Iron oxide	0	500	30	1.0	Beta (exp)
Cesium	Devitrified	10	700	—	—	Uniform
	Vitric	10	100	—	—	Uniform
	Zeolitic	300	3000	—	—	Uniform
	Iron oxide	0	300	30	1.0	Beta (exp)
Strontium	Devitrified	5	30	—	—	Uniform
	Vitric	0	20	—	—	Uniform
	Zeolitic	200	2000	—	—	Uniform
	Iron oxide	0	20	10	0.25	Beta
Nickel	Devitrified	0	200	50	0.33	Beta
	Vitric	0	50	30	0.33	Beta
	Zeolitic	0	200	50	0.33	Beta
	Iron oxide	0	500	—	—	Uniform
Lead	Devitrified	100	500	—	—	Uniform
	Vitric	100	500	—	—	Uniform
	Zeolitic	100	500	—	—	Uniform
	Iron oxide	100	1000	—	—	Uniform
Tin	Devitrified	20	200	—	—	Uniform
	Vitric	20	200	—	—	Uniform
	Zeolitic	100	300	—	—	Uniform
	Iron oxide	0	5000	—	—	Uniform
Protactinium	Devitrified	0	100	—	—	Uniform
	Vitric	0	100	—	—	Uniform
	Zeolitic	0	100	—	—	Uniform
	Iron oxide	500	1000	—	—	Uniform
Selenium	Devitrified	0	1	0.1	1.0	Beta (exp)
	Vitric	0	1	0.1	1.0	Beta (exp)
	Zeolitic	0	1	0.2	1.0	Beta (exp)
	Iron oxide	0	200	30	1.0	Beta (exp)
Carbon	Iron oxide	10	100	—	—	Uniform
Chlorine, Technetium, Iodine		0	0	—	—	—

NOTE: *Coefficient of variation: $COV = \sigma[x]/E[x]$; $E[x]$ is the expected value of K_d (mL g⁻¹).
 "—" means this parameter is not applicable.

3.11.3.3 Matrix Diffusion Coefficients

The matrix diffusion values for radionuclides are based on measured diffusion coefficients of tritium and Tc (technetium) (CRWMS M&O 2000, U0100, Section 6.6.1). The measurements (in water-saturated rock) showed that tritium diffused at a rate between $1 \times 10^{-10} \text{ m}^2/\text{s}$ and $3.5 \times 10^{-10} \text{ m}^2/\text{s}$ in several samples of devitrified tuff. For Tc, the matrix diffusion coefficient varied between $1 \times 10^{-11} \text{ m}^2/\text{s}$ and $4.9 \times 10^{-11} \text{ m}^2/\text{s}$, which is lower than that of tritium (CRWMS M&O 2000, U0100, Table 16). The lower diffusion rate is believed to be caused by exclusion from some matrix pores caused by the larger ion size and negative charge of the pertechnetate anion (TcO_4^- , the predominant aqueous species of Tc).

A distribution for Tc diffusion coefficients has been assigned to account for variations in rock type and water content. Using the measured Tc diffusion coefficients as a rough guide to the variability in the diffusion coefficient for different rock types, the overall range is estimated to be about a factor of 10. This range is roughly captured by the distribution shown in Table 3.11-2 for anionic radionuclides.

Predictions of radionuclide transport for cationic radionuclides (Np, barium, strontium, Am, cesium) using the diffusion coefficient for tritium and measured batch sorption coefficients were found to be conservative (i.e., faster than) relative to measured diffusion behavior (CRWMS M&O 2000, U0100, Section 6.6.1.3). Diffusion coefficient measured for tritium has been assigned to cationic radionuclides, and the combination of using a batch-sorption K_d value and the tritium diffusion coefficient provides a conservative model. As described above, the variations in rock type and water content are expected to result in variations in the diffusion coefficient of about one order of magnitude. This range is roughly captured by the distribution shown in Table 3.11-2 for cationic radionuclides.

Table 3.11-2. Summary of Diffusion Coefficient Data (CRWMS M&O 2000, U0100, Section 6.6.3)

Radionuclide Type	Mean (m^2/s)	Standard Deviation (m^2/s)	Maximum (m^2/s)	Minimum (m^2/s)	Distribution Type
Anionic	3.2×10^{-11}	1.0×10^{-11}	1×10^{-9}	0	Beta
Cationic	1.6×10^{-10}	0.5×10^{-10}	1×10^{-9}	0	Beta

3.11.3.4 Fracture Aperture and Spacing

Fracture aperture and spacing affect flow and transport between fractures and matrix. For a continuous, parallel fracture pattern, the inverse of the fracture aperture is half the area of contact between the fracture and matrix continua per unit volume of fracture pore space. Therefore, the larger the aperture, the less the diffusion (in a saturated system). For an unsaturated fracture the relevant volume (per unit matrix area) is not the fracture pore volume itself but the volume of water. In either case (saturated or unsaturated), specification of the aperture is necessary. Fracture spacing also affects the diffusion process because it sets the boundary for the depth of penetration from matrix diffusion.

The fracture apertures are derived from the fracture porosity and fracture-matrix connection area (see CRWMS M&O 2000, U0065, Section 6.2.1). Aperture distributions are described using a log-normal distribution of apertures for all the model layers beneath the potential repository. Apertures are sampled stochastically in the transport calculations for TSPA. The sensitivity of transport to fracture spacing is low, so a constant value for each layer is used.

3.11.3.5 Parameters for Colloid-Facilitated Radionuclide Transport

The association of radionuclides with colloids is modeled using two end-member representations: reversible equilibrium exchange with the aqueous phase and irreversible attachment. Radionuclides associated with colloids in either condition (reversible or irreversible) may be subject to size exclusion for fracture-matrix exchange. Colloids are excluded from moving from a fracture into matrix pores smaller than the colloid diameter. This tends to keep colloids (and the associated radionuclides) in the fractures, which leads to more rapid transport of the radionuclide. The chance of exclusion of a colloid from the matrix during fracture-matrix exchange is computed using a probabilistic method that considers different colloid sizes and pore size distribution (CRWMS M&O 2000, U0070, Section 6.1.2).

The description of reversible, colloid-facilitated radionuclide transport for the particle-tracking transport model used in performance assessment is quantified through two parameters (CRWMS M&O 2000, U0065, Section 6.1.4). One parameter, K_c , defines the equilibrium partitioning of radionuclides between the aqueous phase and colloids. The other parameter, R_c , is a retardation factor that captures the details of an equilibrium balance between colloid deposition and resuspension. The retardation factor in the colloid model abstraction applies to the transport through fractures. The distribution of retardation factors used is derived from C-Wells data for saturated-zone colloid transport (CRWMS M&O 2000, U0065, Section 6.2.5).

3.11.4 Geological Layers below the Potential Repository

The subsurface at Yucca Mountain consists of heterogeneous layers of anisotropic, fractured rocks consisting of alternating layers of welded and nonwelded ash flow and air fall tuffs. A more detailed discussion about the UZ geology is presented in Section 3.2; this section focuses on the effects of geological layers on transport.

The potential repository will be located in the TSw. The fractures in the TSw typically have permeabilities several orders of magnitude larger than the matrix permeabilities. Unsaturated flow in the TSw is primarily through the fractures, because the matrix permeability in many of the TSw subunits can support flows of only a few millimeters per year (Bodvarsson et al. 1999, p. 13).

The geological complexity of the underlying CHn results in heterogeneous distributions of fracture and matrix hydrological properties. These properties are expected to have pronounced effects on flow and transport of radionuclides in the UZ. The permeability of nonwelded tuffs is strongly dependent on the degree of alteration of the rock minerals into zeolites. The zeolitic alteration in the CHn (a common occurrence in its lower portions) can reduce the matrix permeability by orders of magnitude to the welded tuff permeability level (see Section 3.6).

Flow in the zeolitic portions of the Calico Hills Formation and surrounding bedded tuffs (CH) (CHz) (see Table 3.2-2) is dominated by fracture flow (similar to that in the TSw layers), although the fracture density is smaller in the CHz than that in TSw layers. In vitric portions of the Calico Hills Formation and overlying bedded tuff (CHv), the matrix and fracture permeabilities are on the same order. Thus, these layers behave as porous (rather than fractured) media, and flow is matrix-dominated, as confirmed from the Busted Butte field test results (discussed in more detail in Section 3.11.11.2). Below the potential repository horizon, both vitric and/or zeolitic layers are present. The existence of CHv layers below the repository has important implications in radionuclide transport because fracture flow originating in the TSw will be strongly attenuated, transport velocities significantly reduced, and contact of dissolved radionuclides with the rock matrix enhanced (which leads to more retardation for sorbing radionuclides).

Information about the zeolitic alteration of the Prow Pass Tuff and the underlying bedded tuffs (PP) is limited. Current understanding is that the model layers pp4 and pp1 are zeolitic and that pp3 and pp2 are devitrified and unaltered. Layers of pp4 and pp1, similar to the CHz layers, have small matrix permeabilities that are several orders of magnitude smaller than the fracture permeabilities (see Section 3.6). Permeability contrast between matrix and fracture in layers of pp3 and pp2 is small, similar to the CHv layers. Therefore, fracture flow may be dominant in pp4 and pp1 layers, while pp3 and pp2 behave like nonfractured porous media.

At some locations in the UZ (e.g., near borehole SD-6), Bullfrog Tuff layers may be present above the water table. There is limited information about the flow and transport behavior in these layers. Current understanding is that the bf3 model layer is devitrified and unaltered while the bf2 layer is zeolitic. According to the Calibrated Properties Model in Section 3.6, the permeability contrast between matrix and fracture in the bf3 layer is small; the bf3 layer might behave like a nonfractured porous medium. The bf2 layer has small matrix permeabilities that are several orders of magnitude smaller than the fracture permeabilities, and fracture flow may be dominant in the bf2 layer.

Based on the above discussions, conceptual schematics of flow and transport in two representative hydrogeologic sections are shown in Figure 3.11-3 to illustrate the effect of geologic layers on radionuclide migration below the potential repository. Borehole UZ-14 is located in the northern part of the potential repository site, while borehole SD-6 is located in the southern part. As radionuclides leave the potential repository, they could migrate through the TSw layers quickly, with limited matrix diffusion and sorption. CHv layers could be very effective in retarding migration because of the matrix-dominated flow in these layers. On the other hand, radionuclides could pass through CHz and zeolitic layers quickly, owing to the fracture-dominated flow. Devitrified layers pp3, pp2, and bf3 could also act as porous media and retard radionuclide migration effectively.

3.11.5 2-D Radionuclide Transport Simulations

Two vertical cross sections, representative of the geologic and mineralogical variability below the potential repository horizon, are used to study radionuclide transport from the potential repository to the groundwater of Yucca Mountain. These cross sections are located in the vicinity of the SD-6 and UZ-14 boreholes. The purpose of the transport simulations is to

evaluate the integrated transport performance of the complete geologic system as well as the individual important hydrogeologic units (i.e., TSw, CHv, CHz, and PP) beneath the potential repository. The simulations account for fracture aperture, fracture frequency, active fracture spacing, and saturation distribution (in the fractures and the matrix) across geologic formation interfaces.

3.11.5.1 2-D Semi-Analytical Code FRACL

FRACL V1.0 (see Table 1.3-1) can analyze transport of reactive solutes and colloids through layers of fractured and porous media. The transport equations in the matrix account for molecular and surface diffusion, mass transfer between the mobile and immobile water fractions, and physical, chemical, or combined sorption following a linear equilibrium, kinetic or irreversible isotherm. Radioactive decay, first order chemical reactions, and tracking of up to five products of radioactive decay or chemical reactions are also included in the solution. The transport equations in the fractures account for the same processes, in addition to advection and hydrodynamic dispersion. FRACL V1.0 accounts for the effects of different fracture spacing and it can accommodate layers of fractured rocks or a combination of fractured rock and nonfractured strata (CRWMS M&O 2000, U0060, Section 6.3.2).

3.11.5.2 Simulation Approach

Three representative radionuclides are considered: ^{99}Tc (nonsorbing), ^{237}Np (moderately sorbing), and ^{239}Pu (strongly sorbing). The radionuclides are released continuously at the top of the domain (which coincides with the location of the potential repository or the individual unit of interest), and the contaminant distribution is monitored over time. When occurring, sorption is assumed to follow a linear equilibrium isotherm (CRWMS M&O 2000, U0060, Section 6.5.2). Percolation rate is 6 mm/year, i.e., close to the mean present-day rate.

It is assumed that advection occurs only in fractures with the longitudinal dispersivity of 1 m (CRWMS M&O 2000, U0060, Table 6.7). The only mechanism of radionuclide transport from the fracture to the matrix is by matrix diffusion. In the transition between layers with nonaligned fractures and/or different fracture spacing, it is assumed that transport in the fracture continuum is continuous. Thus, the results represent the worst-case scenario, yielding the shortest possible breakthrough times of radionuclide transport (CRWMS M&O 2000, U0060, Section 6.5.4).

3.11.5.3 Transport in the Individual Hydrogeologic Unit

The TSw does not effectively retard radionuclide transport because of the dominance of fracture flow that reduces matrix diffusion and sorption (see Section 3.11.4). The breakthrough time for the radionuclides is in the order of $^{99}\text{Tc} < ^{237}\text{Np} < ^{239}\text{Pu}$, which corresponds to their difference in sorptive strength, K_d . In borehole SD-6, for example, breakthrough of the nonsorbing ^{99}Tc at the lower boundary of the TSw occurs in about 1 year. Breakthrough of the moderately sorbing ^{237}Np takes about 35 years, while for ^{239}Pu it occurs at about 300 years (CRWMS M&O 2000, U0060, Section 6.6).

Flow in the CHv is primarily matrix flow, and the unit behaves similarly to a nonfractured porous medium. The reduced flow velocity and increased contact time for matrix diffusion and sorption make the CHv an effective transport barrier (see Section 3.11.4). The CH in borehole

SD-6 consists of five vitric layers (i.e., ch1v, ch2v, ch3v, ch4v, and ch5v) and one zeolitic layer (ch6z) at the bottom. The ^{99}Tc front reaches the bottom of the ch5v in a few hundred years, while the ^{237}Np takes several thousand years. Advancement of ^{239}Pu is limited to the uppermost ch1v layer because of its strong sorptive tendency (CRWMS M&O 2000, U0060, Section 6.7).

Flow in the CHz is dominated by the fractures, and radionuclide transport through the unit is expected to be rapid, similar to that in TSw (see Section 3.11.4). The CH in borehole UZ-14 consists of six zeolitic layers (i.e., ch1z, ch2z, ch3z, ch4z, ch5z, and ch6z). The simulation results are consistent with the expected transport behavior. Both ^{99}Tc and ^{237}Np reach the bottom boundary in less than 10 years. Note that the value of K_d for ^{237}Np is 4 mL/g in the zeolitic tuffs as compared to 1 mL/g in the vitrified tuffs. The larger K_d value does not lead to more retardation in the CHz than the CHv, since the contact time for ^{237}Np with the tuffs is much shorter in the CHz because fracture flow is dominant. The strongly sorbing ^{239}Pu needs several thousands years to cover this distance (CRWMS M&O 2000, U0060, Section 6.7).

Within the PP, fracture flow may be dominant in pp4 and pp1 layers, while pp3 and pp2 layers behave like nonfractured porous media (Section 3.11.4). The top pp4 layer near SD-6 is breached in a short time, and then radionuclide transport is controlled by layers pp3 and pp2. These layers are quite efficient in retarding transport even for the nonsorbing ^{99}Tc , which takes more than 1,000 years. It takes several thousand years for ^{237}Np to reach the pp1 layer. The ^{239}Pu front does not cross the pp3 even after 10^5 years (CRWMS M&O 2000, U0060, Section 6.8).

3.11.5.4 Transport Simulations below the Potential Repository

Migration of radionuclides in borehole SD-6 is slow because of the presence of the CHv (see discussions in Section 3.11.4). The ^{99}Tc front takes several thousand years to reach the water table. The ^{237}Np breakthrough takes longer than 10^4 (but $<10^5$) years to reach the water table because of the moderate sorption (shown in Figure 3.11-4, where the right-side of the X-axis coincides with the location of water table). The strongly sorbing ^{239}Pu does not advance past the ch1v layer, less than 60 m from the point of release, even after 10^5 years (CRWMS M&O 2000, U0060, Section 6.9.2).

The ^{99}Tc transport in borehole UZ-14 shows a drastically different profile from that of SD-6. The extensive zeolitic zones of the CH at this location, where fracture flow is dominant, result in very rapid transport with a significant amount of ^{99}Tc reaching the water table in less than 10^3 years. Similarly, the ^{237}Np breakthrough at the water table takes substantially less than 10^4 years. Figure 3.11-4 compares the effects of the CHv and CHz on transport. The large portions of near-constant concentrations indicate the substantial impact of fracture-flow dominated CHz layers on transport (Figure 3.11-4). Even the strongly sorbing ^{239}Pu shows drastically enhanced migration by reaching a distance of about 255 m from the release point, yet it has not migrated past the pp3 layer after 10^5 years (CRWMS M&O 2000, U0060, Section 6.9.6).

3.11.6 3-D Site-Scale Radionuclide Transport

Modeling of radionuclide transport using large-scale 3-D grids was documented by CRWMS M&O (2000, U0060, Sections 6.10 to 6.14). The release rate of radionuclides at the potential repository was considered constant over time. Radionuclides of ^{99}Tc , ^{237}Np , and ^{239}Pu were

investigated, as well as the important members in the decay chains of ^{237}Np and ^{239}Pu . The grids and flow fields used for present-day infiltration and perched water model #1 were identical to those discussed by CRWMS M&O (2000, U0065, Section 6.2). The longitudinal dispersivity used was 1 m in the fractures and 0.1 m in the matrix as there is advective-dispersive transport through the matrix block (CRWMS M&O 2000, U0060, Table 6.14).

3.11.6.1 EOS9nT Code

EOS9nT V1.0 (see Section 1.3.2) is a TOUGH2 (V1.11) module for the simulation of an arbitrary number of solutes and/or colloids in the subsurface. The tracer transport equations account for advection, hydrodynamic dispersion, molecular diffusion, mass transfer between the mobile and immobile water fractions, sorption, radioactive decay, filtration (for colloids only), first-order chemical reactions, and colloid-facilitated transport. EOS9nT V1.0 considers equilibrium (linear, Freundlich, or Langmuir) sorption and kinetic sorption (linear, Freundlich, or Langmuir). Daughter products of radioactive decay can also be tracked.

EOS9nT V1.0 offers the option of a Laplace space formulation of the transport equations (in addition to conventional time-stepping) after the flow field becomes time-invariant. The Laplace transform formulation eliminates the need for time discretization, and an unlimited time-step size is thus possible without loss of accuracy or stability. It also completely linearizes all the kinetic transport equations and, thus, does not increase the order of the matrix to be solved. Additionally, the Laplace transform alleviates accuracy problems that may arise from the inaccurate weighting of the radioactive decay (CRWMS M&O 2000, U0060, Section 6.3.1). All the 3-D transport simulations are conducted by using the DeHoog implementation of the Laplace transform formulation of EOS9nT V1.0. Simulations are very fast and efficient, requiring 1,800–2,200 seconds of execution time to cover a simulation period of 10^6 years (CRWMS M&O 2000, U0060, Section 6.11.5).

3.11.6.2 Transport Simulation of ^{99}Tc

Breakthrough is described by the normalized release rate R , i.e., the ratio of radionuclide mass release rates at the groundwater versus that at the potential repository. The normalized release rate in Figure 3.11-5 shows a very strong dependence of ^{99}Tc transport on the infiltration regime. As the infiltration rate increases from lower bound to mean present-day level, the t_{10} time, defined as the time at which $R = 0.1$, decreases from about 10^4 years to about 300 years. The t_{50} , the time at which $R = 0.5$, decreases from about 45,000 years to about 4,000 years. Upper bound infiltration rate further reduces t_{10} (see Table 3.11-3). Figure 3.11-5 also shows that the maximum attainable R decreases with the infiltration rate, because lower bound infiltration results in lower velocities and longer times for transport, thus higher radioactive decay.

3.11.6.3 Transport Simulations of ^{237}Np and its Daughters

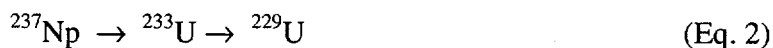
The sorption of ^{237}Np retards its transport through the UZ system, as compared to ^{99}Tc (Figure 3.11-5). From the values of t_{10} and t_{50} , the moderate sorption of ^{237}Np is sufficient to increase the time to reach the water table by a factor of about 40 (Table 3.11-3). Because of significant retardation, the maximum attainable R varies over a large range, and $R = 1.0$ is not achieved

within the simulation period. At $t = 10^6$ years, R is 0.98, 0.86, and 0.42 for the three infiltration rates, respectively (Figure 3.11-5).

Table 3.11-3. Breakthrough Time of Radionuclides at the Water Table (Years) (CRWMS M&O 2000, U0060, Table 6.15)

		Present-Day Infiltration		
		Lower Bound	Mean	Upper Bound
⁹⁹ Tc	t ₁₀	10,000	300	45
	t ₅₀	45,000	4,000	1,000
²³⁷ Np	t ₁₀	220,000	10,000	1,700
	t ₅₀	>1,000,000	120,000	22,000
²³⁹ Pu + ²³⁵ U + ²³¹ Pa	t ₁₀	600,000	40,000	12,000
	t ₅₀	>1,000,000	250,000	90,000

Important members in the ²³⁷Np decay chain are shown in Equation 2. The relative flux fraction M_R of each member of the chain, defined as the fraction of each radionuclide in the sum of the mass fluxes at the water table, shows that the daughter contribution only reaches a maximum of 2% at 10^6 years (CRWMS M&O 2000, U0060, Section 6.13.1.2). As such, daughter contributions to the ²³⁷Np transport are rather insignificant and could be safely ignored.



3.11.6.4 Transport Simulations of ²³⁹Pu and its Daughters

The value of R for ²³⁹Pu never reaches the 0.1 level even after 10^6 years of continuous release because of the strong sorption of ²³⁹Pu (Figure 3.11-5). The picture changes dramatically, however, if the daughter contributions to the release rate at the water table are accounted for in the computations. Given the half-life of ²³⁹Pu and the much longer one of ²³⁵U, the daughter contributions can become significant under the upper bound infiltration regime (Table 3.11-3).

The relative flux fractions M_R are also shown in Figure 3.11-5. The Pu contribution to the release rate starts declining rapidly after 100 years, and ²³⁵U is by far the dominant species after $t = 20,000$ years. Earlier emergence of ²³⁵U is associated with the lower bound infiltration rates because less ²³⁹Pu reaches the water table owing to strong sorption. Thus, after 1,000 years, the release at the water table consists mostly (over 95%) of ²³⁵U under lower bound present-day infiltration conditions. The ²³¹Pa contribution is negligible because of the very long half-life of ²³⁵U.

3.11.6.5 Transport-Controlling Features

The simulation results reveal that transport is controlled by the faults, especially at the early times. Splay G of the Solitario Canyon fault is the main transport-facilitating feature, as shown from the ^{99}Tc distribution of the fracture mass fraction (normalized to that at the point of release in the potential repository) at the bottom of the TSw at $t = 100$ years (Figure 3.11-6). Once contaminants reach the TSw-CHn interface, they move in an easterly direction, moving with the draining water that hugs the downward sloping low-permeability interface (CRWMS M&O 2000, U0060, Section 6.12).

The Ghost Dance fault splay is the next most important transport-facilitating feature (Figure 3.11-6). Though it facilitates downward migration, this fault appears to act as a barrier to the lateral migration of radionuclides, as evidenced both at the bottom of the TSw and at the water table. The Sundance fault and the Drill Hole Wash fault are also important. The Drill Hole Wash fault appears to act as a barrier to radionuclide migration laterally across it, while providing pathways for relatively fast transport to the water table (Figure 3.11-6). The main Ghost Dance fault does not play an important role in transport at the bottom of the TSw, as the ^{99}Tc does not reach the fault at this level even after 10^5 years (CRWMS M&O 2000, U0060, Section 6.12.2.2). This fault is more important at the water table, where it acts as a barrier to lateral transport while facilitating downward migration into the groundwater (Figure 3.11-6).

As time progresses, contributions of fractures and matrix become important. Fractures act as the important pathways of transport, and diffusion from the fractures into the matrix is the main retardation process in radionuclide transport. By sorbing onto the matrix into which they diffuse, the migration of radionuclides is retarded (CRWMS M&O 2000, U0060, Section 7.2).

The emerging transport pattern indicates that radionuclide transport to the groundwater is faster in the southern part of the potential repository block, where it is also areally concentrated. There are several reasons for this transport pattern (CRWMS M&O 2000, U0060, Section 6.12.2.3). First, the water flow pattern dictates the advective transport pattern, and the maximum water flow within the footprint of the potential repository is in its southern part in the Perched water model #1 (see Section 3.7.3.3). Second, the presence of the highly conductive faults (e.g., Splay G of the Solitario Canyon fault and the Ghost Dance fault splay) act as the venue for fast transport, despite the fact that the vitric CHn behaves as a porous medium (with relatively lower water velocities). This may be facilitated by flow focusing in the vitric CHn, whose vertical distribution shows a funnel-type structure in the south. Third, the low-permeability zones at the TSw-CHn interface in the northern part of the potential repository act as barriers to water drainage, and lead to low water velocities and presence of perched water bodies. Radionuclides move slowly through the perched water before reaching the underlying conductive zeolitic CHn, hence the delay in transport.

3.11.7 3-D Site-Scale Transport of Pu True Colloids

EOS9nT V1.0 is used for colloidal transport simulations, and the flow field and 3-D grid are identical to the ones discussed in Section 3.11.6.

3.11.7.1 Colloidal Forms, Properties, and Filtration Model

As concluded in CRWMS M&O 2000 (U0070, Section 7), the waste-form colloids (i.e., true colloids) will play a more significant role than natural colloids. True colloids are taken to have the properties of PuO_2 and are subject to radioactive decay. Four colloids of different sizes (450 nm, 200 nm, 100 nm, and 6 nm) are considered, with their accessibility factors into the geological units taken from CRWMS M&O (2000, U0070, Table 1). As reported by CRWMS M&O (2000, U0060, Section 6.16), the linear kinetic model of colloid filtration was used, with the forward kinetic coefficient, κ^+ , directly computed. There is no information on the kinetic declogging (reverse) coefficient, κ^- , which was entered as a fraction of κ^+ to examine the sensitivity of this parameter on colloidal transport.

3.11.7.2 Colloid Transport Simulations

For a given κ^+ , the transport of radioactive true colloids is strongly influenced by the κ^- . When no declogging is allowed, no colloids reach the groundwater (CRWMS M&O 2000, U0060, Section 6.16). Smaller values of κ^- (i.e., slow declogging) lead to significant retardation of colloids and longer times to reach the water table. In this case, t_{10} is more than 10^4 years, and t_{50} cannot be reached because the maximum attainable R at the water table never exceeds 0.3 (Figure 3.11-7). Larger values of κ^- (i.e., fast declogging) lead to dramatically different behavior, with very fast transport for the radioactive colloids to the water table. In this case, t_{10} can be as low as 15 years (Figure 3.11-7). The extreme sensitivity of colloid filtration on κ^- and the dearth of any representative information on this value in the various UZ geologic units underline the need for attention to this subject.

For a given κ^- , the colloid size has a significant effect on transport (Figure 3.11-7). Given the fact that fractures are the main transport conduit at Yucca Mountain, the inability of larger colloids to diffuse into the matrix, because of smaller diffusion coefficient values and size exclusion, result in fast transport to the groundwater. Smaller colloidal particles can diffuse more easily into the matrix, and their transport is thus more retarded. Size exclusion at the interfaces of different geologic units leads to colloid concentrations that can be significantly higher than that in the water released from the potential repository. These high concentrations are observed behind (i.e., they do not penetrate) the straining interfaces and are due to colloid accumulation because of their inability to move across these interfaces. This phenomenon is more pronounced for larger colloids (CRWMS M&O 2000, U0060, Section 6.16).

3.11.8 Estimates of Mass Breakthrough

This section summarizes the studies of tracer (conservative and reactive) transport using more than 20 3-D UZ flow fields and the T2R3D code V1.4 (see Section 1.3.2). The results provide insight to flow and transport processes from the repository to the water table (saturated zone) or from the land surface to the repository level and consider the potential effects of the major faults, different perched water conceptual models, infiltration scenarios, and sorption onto rocks.

Estimates of breakthrough are based on calculations of a conservative (nonsorbing) tracer, using the properties of ^{99}Tc and chloride-36 (^{36}Cl), and a reactive (adsorbing) tracer, using the properties of ^{237}Np (CRWMS M&O 2000, U0050, Section 6.7). Except for ^{36}Cl , the mechanical

dispersion effects through the fracture-matrix system are ignored, because sensitivity analyses show little effects of mechanical dispersion on cumulative tracer breakthrough curves at the water table. All transport simulations are run to 1 million years under steady-state flow and an initial, constant source concentration or constant mass flux conditions at the repository or surface fracture blocks. This assumes that all of the tracer is released instantaneously from the starting time of a simulation at the repository or land surface, while the radionuclides and/or colloids are released continuously at the potential repository for transport simulations discussed in Sections 3.11.6 and 3.11.7.

The fractional mass breakthrough is shown in Figures 3.11-8 and 3.11-9 and is defined as the cumulative mass of a tracer arrived at the water table or at the repository level over the entire bottom model boundary or the entire repository layer at the time, normalized by the total initial mass of the component at the source. Fifty percent mass breakthrough times for transport from the repository to the water table, estimated using 36 simulations are summarized in Figure 3.11-8. The figure correlates average infiltration rates with 50% cumulative mass-breakthrough, including all the infiltration scenarios and two perched water conceptual models discussed in Section 3.7. As shown in Figure 3.11-8, the predominant factors are (1) infiltration rates or net water recharge and (2) adsorption effects. In addition, perched water conceptual models also affect transport. However, the overall impact of the perched water conceptual models on tracer breakthrough at the water table is insignificant compared to infiltration and adsorption effects.

Analyses of mass breakthrough estimates at the water table indicate that:

- Times for 50% mass breakthrough are inversely proportional to the average infiltration (net water recharge) rate over the model domain. When an average infiltration rate increases from 5 to 35 mm/yr, the time for 50% mass breakthrough decreases by one to two orders of magnitude.
- Nonsorbing tracers migrate about one to two orders of magnitude faster than sorbing tracer when travelling from the repository to the water table under the same infiltration condition.

The transport of ^{36}Cl from the ground surface to the potential repository is also estimated using a fractional breakthrough curve, as shown in Figure 3.11-9, under the present-day, mean infiltration scenario. The figure shows a similar range of tracer transport times from the simulations with different surface source conditions (CRWMS M&O 2000, U0050, Section 6.7). Simulations 3 and 4 apply the ^{36}Cl source over the entire upper boundary while simulations 1 and 2 apply the source over the central area only to avoid lateral boundary effects. Simulations 1 and 3 apply all the ^{36}Cl at time = 0 while simulations 2 and 4 apply it as a constant mass fraction of the infiltrating water. There is about 1% or less total mass breakthrough during 10 to 100 years after tracer release on the ground. This indicates the existence of possible fast flow pathways with a transport time of 50 years, travelling from the ground surface to the repository level, under the steady-state UZ flow condition. However, the cumulative mass breakthrough is small (~1% of the total mass released on the ground) for the early breakthrough at 50 years. The average transport time from the surface to the repository level is estimated between 5,000 to 20,000 years using the 50% mass breakthrough curves of Figure 3.11-9 from the four simulation results.

Simulated tracer concentration distributions along vertical cross sections, and the ESF and ECRB tunnels show that earlier breakthrough of the tracer at the repository level is associated only with high-permeability faults.

3.11.9 Alternative Models

As discussed above in Sections 3.11.6 and 3.11.7, the main mechanism of radionuclide retardation in the UZ is diffusion from the fractures into the matrix. This process transfers radionuclides from the fast pathways to the matrix, where their transport is retarded because of the much slower water velocities and matrix sorption for sorbing radionuclides. An alternative conceptual model that does not allow diffusion (but still allows advection) into the matrix was investigated by CRWMS M&O 2000 (U0060, Section 6.17); the results of the investigation are discussed below.

3.11.9.1 Effects of Matrix Diffusion on Radionuclide Transport

For the no-diffusion alternative model using mean present-day infiltration, the nonsorbing ^{99}Tc and the moderately sorbing ^{237}Np move unhindered in the fractures, with their t_{10} and t_{50} about 5 and 30 years, respectively. A characteristic plateau at $t = 50$ years marks their arrival at the water table from fracture flow (Figure 3.11-10). The effects of the matrix flow become evident for $t > 100$ years, when matrix flow and contaminant transport begin to arrive at the water table. The nonsorbing ^{99}Tc arrives at the water table earlier than the moderately sorbing ^{237}Np . The phase of ^{237}Np release from fracture flow lasts from 50 to about 2,000 years, after which time the matrix flow (and the ^{237}Np it transports) arrives at the water table (Figure 3.11-10).

The limited sorption on the fracture walls is, however, sufficiently important to retard transport of strongly sorbing ^{239}Pu in the fractures (CRWMS M&O 2000, U0060, Section 6.17). If only ^{239}Pu is considered, the fracture release rate reaches a plateau at about 300 years, i.e., a very short time considering its half-life. There is no matrix flow contribution to the groundwater release of ^{239}Pu in the first 10^6 years. Accounting for the daughter products leads to matrix contributions to the water table after 10^4 years. These result (almost) exclusively from the release of the ^{235}U daughter, which sorbs less strongly than ^{239}Pu (Figure 3.11-10).

3.11.9.2 Colloidal Transport Simulation

Analysis of the alternative model indicates that diffusion is less significant in colloid transport than in solute transport, because (a) colloid diffusion is smaller than solute molecular diffusion because of the larger colloid size, and (b) size-exclusion effects at the interfaces of different geologic units further limit entry through diffusion into the matrix (especially for larger colloids) (CRWMS M&O 2000, U0060, Section 6.17). Its effect, however, becomes increasingly important for a decreasing colloid size (Figure 3.11-10).

The colloid breakthrough curves do not exhibit the plateaus (denoting pure fracture transport with no matrix contribution) of the solute curves, but rather a section of milder slope (Figure 3.11-10). This is attributed to the slower transport in the fractures (as a result of straining at the geologic unit interfaces) and the resulting evolution of concentrations larger than the one in the water released from the potential repository. Hence, the colloid concentration gradients across

straining interfaces keep increasing over time (because of colloid accumulation behind them), and they do not reach a steady state as in solutes (CRWMS M&O 2000, U0060, Section 6.17.2).

3.11.10 Uncertainty and Limitations

This section discusses the uncertainties and limitations related to radionuclide transport analysis in the UZ.

3.11.10.1 Assumptions

The soundness of radionuclide transport analysis depends upon the validity of the assumptions discussed in Section 3.11.1.3.

3.11.10.2 Sorption

Experimentally determined K_d values in Yucca Mountain studies have been predominantly derived from batch experiments using crushed tuff (with the sample size of 75–500 μm) under saturated conditions. There are concerns that this experimental approach may overestimate the K_d values (CRWMS M&O 2000, U0060, Section 6.1.3.1). This is because:

1. Batch experiment conditions may not be representative of the unsaturated conditions in the UZ. Little work has been reported for radionuclide sorption and transport in unsaturated rocks. Values of K_d may be invariant with respect to the water content, *if* similar experimental conditions (e.g., sample size, water chemistry, contact time) are employed. Experimental measurement of radionuclide sorption in unsaturated tuffs, however, deserves more attention. Laboratory studies of tracer penetration were presented to generate K_d values for core-sized samples under unsaturated conditions (CRWMS M&O 2000, U0015, Section 6.4). This approach could be adopted to generate K_d values of radionuclides in unsaturated solid tuff samples.
2. Crushing of tuff may create new surfaces and also increase the accessibility of pores that may not be contributing to radionuclide sorption in the intact rocks. Using smaller-sized samples could likely generate larger K_d values. Some studies have compared the K_d values obtained from batch sorption with diffusion-sorption experiments that use multimillimeter scale samples. The results consistently show little agreement between K_d values from these two methods, which could be largely attributable to the difference in sample sizes used (CRWMS M&O 2000, U0060, Section 6.1.3.1). Removal of fines (particle sizes less than 75 μm) is a routine step used in the standard batch-sorption procedures of the YMP; however, this could serve as a compensating factor for this issue.

Rate-limited sorption could be important, especially for fluid-radionuclide-rock systems with large sorption potential. Breakthrough curves for ^{237}Np transport in tuffs from the column experiments cannot be analyzed without considering rate-limited sorption (Viswanathan et al. 1998, p. 267). This result indicates the existence of rate-limited sorption under flowing conditions, possibly resulting from the slow diffusion of radionuclides into tuff pores. Rate-limited sorption may have a substantial effect on transport in fast fracture flow because it reduces

the extent of sorption in the matrix, thus allowing larger radionuclide concentrations and longer migration in the fractures. Nonlinear and irreversible sorption are also evident from the diffusion and transport studies by CRWMS M&O (2000 U0100, Sections 6.5 and 6.6). Overall, rate-limited and nonlinear sorption can insert an element of uncertainty into the validity of the linear equilibrium isotherm assumed in UZ transport studies.

There is limited information on sorption onto the fracture surfaces, which will retard migration of sorbing radionuclides. However, sorption in the fractures is not considered in the TSPA transport evaluations because of the limited data and conservative nature of this assumption.

3.11.10.3 Matrix Diffusion

Very limited experimental data exist on the tortuosity distribution in the various Yucca Mountain geologic units. In CRWMS M&O (2000, U0060), tortuosity is approximated by the value of porosity, an approach validated by the available, yet limited, experimental data (Section 3.11.2.5). Even less information exists on the effect of water content on effective diffusion coefficient, and the dependence could be much stronger than what could be expected from a linear relationship. This subject deserves more attention, because it could significantly affect transport estimates.

No information exists on whether the UZ media support surface diffusion (a possibility in zeolites). Surface diffusion can be important in radionuclides that exhibit strong sorption (e.g., Pu). A larger K_d clearly indicates stronger sorption, but this does not mean immobilization of the dissolved species when the fractured porous medium supports surface diffusion (Moridis 1999, pp. 1729–1740).

Different approaches to represent matrix diffusion could yield different transport behavior. Comparisons between FEHM V2.10 (see Section 1.3.2) particle-tracker and DCPT (see Section 1.3.2) were performed by CRWMS M&O (2000, U0155, Section 6.4.3). The two particle-tracking routines agree only if diffusion and dispersion are neglected. For the cases that include diffusion and dispersion, the median breakthrough for FEHM V2.10 occurs at times more than one or two orders of magnitude earlier. The difference is more pronounced for radionuclides undergoing sorption in the matrix. These differences stem from different implementations of the diffusive mass flow between fractures and the matrix in the two codes (CRWMS M&O, 2000, U0155, Section 7).

3.11.10.4 Radioactive Decay and Daughter Products

The ζ factor defines the fraction of the mass of the decayed sorbed parent that remains sorbed as a daughter ($0 \leq \zeta \leq 1$). The term ζ is introduced to account for the different sorption behavior of parents and daughters, and the fact that daughters can be ejected from grain surfaces because of recoil (CRWMS M&O 2000, U0060, Section 6.2.8.1). The ζ factor is a function of the decay type as well as of the chemical form of the sorbed cation. In alpha decay (e.g., ^{237}Np , ^{239}Pu), $\zeta = 0$ (CRWMS M&O 2000, U0060, Section 6.2.8.2). There is no information on the behavior of ζ for other types of decay. This issue can have significant implications for the transport behavior of daughters if (a) the large sorbed masses of strongly sorbing parents are ejected back

into the aqueous phase after decay, (b) the daughter is a much weaker sorber, or (c) its sorption follows a kinetic isotherm (CRWMS M&O 2000, U0060, Section 6.2.8.2).

3.11.10.5 Radionuclide Transport Simulations

The importance of faults and perched water bodies in transport depends directly upon the underlying geologic and perched water conceptual models. In the simulations discussed in Section 3.11.6, the geological model discussed in Section 3.2 and implemented in Section 3.4.2 and Perched water model #1 (see Section 3.7.3.3) were assumed. Changing geologic and perched water models may very well lead to different results (CRWMS M&O 2000, U0060, Section 6.11).

3.11.10.6 Colloidal Transport

Caution should be exercised in the interpretation of the colloid simulation results of Figure 3.11-7 because substantial knowledge gaps exist. The tremendous variation in behavior with the change in the kinetic declogging coefficient should only serve as an indication of the sensitivity of this parameter and to underline the need for more reliable information on this subject. The limits of the equations for the prediction of the forward kinetic filtration (clogging coefficient) have not been tested under the UZ conditions, and the subject of kinetic declogging coefficient has barely been raised (let alone studied). Additionally, it is unclear how representative the current size exclusion models are, because they are not based on laboratory measurements of filtered colloid suspension through rock samples but rather on predicted values obtained from retention curves and theoretical soil physics equations. The affinity of colloids for air-water interfaces could also have a potential effect on their transport (CRWMS M&O 2000, U0060, Section 6.15.8). The TSPA model only uses simple size exclusion filtering at fracture-matrix interfaces (Section 3.11.3.5).

3.11.11 Model Validation

This subsection discusses the validation of the Transport Model utilizing the results from Alcove 1 and Busted Butte tracer tests, and it shows that the model can be considered valid for its intended use.

3.11.11.1 Alcove Tracer Test

This section is based on Section 6.8.1 of CRWMS M&O (2000, U0050), which includes more detailed discussions and references for data sources. An infiltration and tracer transport test was performed in Alcove 1, located near the North Portal of the ESF in the upper lithophysal zone of the Tiva Canyon Tuff (Tpcpul). The crown of Alcove 1 is approximately 30 m below the ground surface. The infiltration test at Alcove 1 involved applying water at the ground surface. At a late stage of the test, a conservative tracer, bromide, was introduced into the infiltrating water. The seepage into the alcove and the tracer arrival time were recorded. The tracer test was carried out over a 51-day period, beginning on May 18, 1999. First detection of the tracer within the seepage occurred after 28 days.

Hydrological properties calibrated to earlier seepage data were used in the tracer simulation. The simulated breakthrough curve closely matches the tracer concentration data for a tortuosity value

of 0.75, which is close to the value of 0.7 given by Francis (1997, p. 5). This relatively high tortuosity value (see Section 3.11.2.5) is possibly related to the nearly saturated conditions in the test. The results indicate that the continuum approach is valid for modeling flow and transport in unsaturated fractured rock. The use of an active fracture model can capture the major features of fingering flow and transport in fractures. The matrix diffusion has a significant effect on the overall transport behavior in unsaturated fractured rock, while the dispersion in fractures does not.

3.11.11.2 Busted Butte Tracer Test

3.11.11.2.1 Laboratory K_d Measurements

The Busted Butte test facility was chosen based on the presence of a readily accessible exposure of the TSw and CHn and the similarity of these units at this location to their occurrence beneath the potential repository horizon (CRWMS M&O 2000, U0100, Section 6.8.1). Table 3.11-4 presents the K_d results obtained on rock samples collected from the TSw and CHn at Busted Butte. Values of K_d for Np and Am in Table 3.11-4 are similar to these in Table 3.11-1. However, the sorption values for Pu are significantly larger.

Table 3.11-4. Summary of Radionuclide Sorption Results from Busted Butte Tests (adapted from CRWMS M&O 2000, U0100, Tables 27-28)

Sample Source	Geologic Unit (Model Layer)	Approximate Average K_d (mL g ⁻¹)		
		Np	Am	Pu
Phase 1A, BH 3	Ttpv1 (ch1v)	0.3	380	19
Phase 1A, BH 4	Tac (ch2v)	1.4	470	2500
Phase 1B, BH 7	Ttpv2 (tsw39)	1.1	460	1100

3.11.11.2.2 Field Tracer Tests

The Busted Butte Unsaturated Zone Transport Test is a long-term experiment conducted by the YMP. Numerical simulations were conducted for two components of the first phase (Phases 1A and 1B) by CRWMS M&O (2000, U0060, Section 6.10). The field work of the first phase has been completed, but the analysis of the experimental results is not yet complete.

3.11.11.2.2.1 Phase 1A Test

The location of Phase 1A test was the vitric CHn (i.e., layers ch1v and ch2v; CRWMS M&O 2000, U0060, Figure VI.1). It involved injection rates of 10 mL/hr into boreholes 1 and 3, with borehole 3 located above and near the ch1v-ch2v interface and borehole 1 farther away from the interface. Injections were conducted continuously for 285 days, starting from April 2, 1998. At the end of the test, digital photographs were taken to evaluate tracer distribution, and rock samples were collected for moisture and tracer analysis. A 3-D modeling study, using the Calibrated Properties Model (Section 3.6) and hydraulic property measurements from field-collected samples, was conducted to predict the concentration of a nonreactive tracer and water saturation distributions (CRWMS M&O 2000, U0060, Section 6.10).

The simulated Br distribution in borehole 1 exhibits symmetric, near-circular patterns, and indicates the dominance of capillary over gravitational forces in the vitric CHn. This is consistent with the experimental results and the expected flow and transport behavior in the vitric CHv discussed in Section 3.11.4. Borehole 3 simulations using the Calibrated Properties Model show that the flattening of tracer distribution occurs as the tracer moves preferentially laterally along the chl_v-ch_{2v} interface. Experimental results also show the flattening behavior for borehole 3. When the hydraulic property measurements from field-collected samples are used, the Br distribution follows a more uniform pattern, which exhibits little flattening. This indicates that the permeability contrast from the limited number of core measurements is smaller than that suggested from the Calibrated Properties Model.

3.11.11.2.2.2 Phase 1B Test

In the Phase 1B field test, the tracers were injected into the lower portion of the TSw basal vitrophyre, which is a relatively low-permeability fractured rock. The tracer solution was injected at a rate of 10 mL/hr at the location $x = 1.30$ m from the rock surface into borehole 5. Injections began on May 12, 1998, and ceased on November 9, 1998. Liquid samples from collection borehole 6 were regularly collected and analyzed. For the 3-D numerical studies, the geologic model treated the domain as a homogeneous, unfractured rock matrix. Although this geologic layer is known to have fractures, the use of unfractured rock matrix as the domain model in the simulation was made possible by the system behavior during the injections, which did not show evidence of fracture flow.

Experimental breakthrough data for both the nonsorbing and sorbing tracers can be found in CRWMS M&O (2000, U0100, Section 6.8.5.3.2). Peak concentrations are observed directly beneath the injection point of borehole 5. The measured concentrations indicate transport consistent with flow in the matrix (rather than in the fractures), which appears to quickly imbibe the injected solution.

Visual inspection of the predicted breakthrough curves for nonsorbing tracer at several sampling locations indicates that the predictions are in good agreement with the measured data (CRWMS M&O 2000, U0060, Section 6.10). The breakthrough curves of sorbing tracer Li⁺ (lithium) follow a distinctively different pattern. Sorption of Li⁺ results in maximum relative concentrations significantly lower than the ones observed in the nonsorbing tracers. Predictions based on the laboratory-derived $K_d = 1$ mL/g are higher than the measured concentrations in CRWMS M&O (2000, U0100, Section 6.8.5.3.2). When K_d is increased to 2 mL/g, predictions are consistent with the measured Li⁺ concentrations (CRWMS M&O 2000, U0060, Section 6.10).

3.11.12 Analogs to Radionuclide Transport in the UZ

This section is based on Section 6.5.2.1 of CRWMS M&O (2000, U0135), which includes more detailed discussions and references for data sources. Three UZ analogs are considered: (1) the Nopal I uranium deposit at Peña Blanca, Chihuahua, Mexico, (2) the collective northwestern Nevada-Southeastern Oregon uranium deposits, and (3) the trace metal migration study at Santorini, Greece.

3.11.12.1 Natural Analog Studies at Peña Blanca, Mexico

From the 1980s, the Nopal I uranium deposit at Peña Blanca has been recognized as a natural analog for the potential repository at Yucca Mountain. Transport of U-series nuclides at Peña Blanca has occurred over a range of time scales. From the U-Th (thorium) age data, it appears that the primary transport of U to the fractures occurred more than 300 ka (thousand years) ago. Subsequently, there has not been significant ^{238}U or ^{235}U redistribution. The 300 ka stability of uranium (235, 238), thorium, and protactinium in the fracture-filling minerals has apparently survived even recent hydrological disturbances from surface water infiltration of the fractures, as well as the infiltration of rainwater.

Recent data obtained from U-series thermal ionization mass spectrometry indicate that the geochemical system at Nopal I restricts actinide mobility in the unsaturated environment. By analog, the tuffs at Yucca Mountain should have similar retentive properties to impede oxidized uranium mobility. The accumulation of natural analog data from Peña Blanca and similar sites would be of particular importance if such data demonstrated the general validity (or lack thereof) of low actinide mobility in unsaturated silicious tuffs under semi-arid climate conditions.

3.11.12.2 Uranium Deposits in Northwestern Nevada/Southeastern Oregon

The McDermitt Caldera uranium deposits and other uranium deposits in northwestern Nevada and southeastern Oregon have also been mentioned as possible analogs. Some of the uranium mineralization at these sites may constitute good analogs to aspects of radionuclide transport at Yucca Mountain, but this is questionable for several reasons. One reason is that the host volcanic rocks for these deposits are somewhat different. Another is that the uranium mineralization is fine-grained and low in concentration in these deposits. Also, age of deposition is poorly constrained for most of the deposits, and source-term information needed for models is lacking. Furthermore, hydrological data are sparse. Hence, in spite of their appealing proximity to Yucca Mountain for ease of study, these uranium deposits would require extensive additional characterization to build confidence in flow and transport process models.

3.11.12.3 Akrotiri Archeological Site, Santorini, Greece

Akrotiri is similar to Yucca Mountain in its silicic volcanic rocks, dry climate, and oxidizing, hydrologically unsaturated subsurface conditions. Bronze and lead artifacts were buried under 1.5 to 2.0 meters of volcanic ash 3,600 years ago. Evidence for a plume of Cu (copper), Sn (tin), and Pb (lead) was investigated through selective leaching of packed earth and bedrock samples collected directly beneath the site where bronze and lead artifacts were excavated. Field data indicated that little of the bronze material had been transported away from its primary location. The total amount of Cu predicted to have been removed from the artifacts is roughly three orders of magnitude smaller than the volume of the artifacts. Neither Cu nor Pb was detected below a depth of 45 cm. The Akrotiri study shows preservation of artifacts for a long period of time in an oxidizing environment, indicating that unsaturated systems in arid environments may provide favorable sites for geologic disposal of radioactive waste.

3.11.13 Abstraction of Transport Model

3.11.13.1 Introduction

An abstraction of Transport Model in the UZ is used for calculations of radionuclide transport in performance assessment. In this case, the abstraction is also a process model in which simplified mathematical representations of the physical processes are used. The reason for using a model abstraction for performance assessment is that computational requirements for the process model are too demanding for performance assessment calculations that require a large number of calculations to address different scenarios and encompass the desired parameter ranges. Therefore, the transport model abstraction is computationally streamlined to allow for more rapid calculations. As a more streamlined computational tool, the transport model abstraction can be run concurrently with the TSPA model. Changes in radionuclide releases from the engineered barrier system over time are directly input to the transport model abstraction, which then determines the spatial and temporal distributions of the radionuclides at the water table.

The transport model abstraction is a 3-D, dual-permeability, particle-tracking method (CRWMS M&O 2000, U0065). Flow fields derived using the 3-D site-scale flow model are input directly to the particle-tracking method and are used to compute transport velocities. The method explicitly accounts for transport in both the fracture and matrix continua, with exchange between continua resulting from advective or diffusive processes. The velocity fields from the flow model are also used for advective transport exchange between the fracture and matrix continua. The various aspects of the transport process—advection, diffusion, dispersion, sorption, radionuclide decay, and colloid-facilitated transport—are all explicitly modeled.

3.11.13.2 Assumptions

As for any mathematical model of a physical process, there are assumptions associated with the model. These assumptions represent simplifications or idealizations that allow a specific mathematical treatment.

Assumption 1: Sorption can be adequately represented by a linear model.

Basis: The basis for this assumption is discussed in Section 3.11.3.2.

Assumption 2: The effects of flow in the matrix are negligible with respect to radionuclide exchange between fractures and matrix through matrix diffusion.

Basis: This is a simplifying assumption that allows for rapid computation of the effects of matrix diffusion on transport while including the specific effects of the radionuclide concentration gradients in the matrix (normal to the fracture planes). The details of this fracture to matrix concentration gradient are difficult to capture in a numerical model because of the fine spatial resolution of the grid required. This assumption allows for the treatment of this process with an analytical or semi-analytical model that captures the effects of this gradient without requiring the numerical gridding. Results from comparison calculations between the model abstraction and the process-level model suggest that this assumption is conservative for predictions of radionuclide transport (CRWMS M&O 2000, U0065, Section 6.3; CRWMS M&O 2000, U0160, Section 6.2.5).

Assumption 3: Colloid-facilitated radionuclide transport can be approximated by two end-member representations for colloid-radionuclide associations: equilibrium, reversible exchange of radionuclides between colloids and the aqueous-phase radionuclides, and irreversible association of radionuclides with colloids.

Basis: Any radionuclide/colloid association would lie somewhere between the bounds established by this assumption. Because transport behavior is expected to be conservatively bounded by radionuclides irreversibly attached to colloids, the effects of colloid transport can be conservatively bounded with a mixture of these end-member models.

Assumption 4: Colloid filtration/resuspension processes can be represented as an equilibrium process in which colloids are partitioned between mobile and immobile conditions.

Basis: Any opposing first-order rate reactions can be expressed in terms of an equivalent, equilibrium partitioning coefficient that is proportional to the ratio of the forward and reverse rate constants — if the process can be averaged over a sufficiently long time. The rate constants identified by CRWMS M&O (2000, U0070, Section 6.2.3) indicate that filtration/resuspension time scales are on the order of tens of days. Given typical UZ transport times of years to thousands of years, the use of an equilibrium-partitioning coefficient is reasonable.

Assumption 5: Dispersive transport is small in comparison with advective transport.

Basis: The criterion for applicability is based on the grid Peclet number $Pe_g = \Delta x / \alpha$, where Δx is the characteristic length scale of the computational cell and α is the dispersivity, or dispersion length scale, associated with transport across the cell (Fetter 1993, pp. 49–52). Dispersive transport over a computational cell in the numerical model is expected to be scale dependent, i.e., the appropriate value of dispersivity is proportional to the size of the computational cell. This Pe_g ratio is expected to be greater than 10 for a scale-dependent dispersivity, indicating advection-dominated transport.

3.11.13.3 Approach

The particle-tracking abstraction model follows particles through an interconnected network of computational cells that constitutes the computational domain. Particle locations are identified by the computational cell coordinates, which is the lower limit of spatial resolution in the model. This cell-to-cell particle tracking method is similar to that described by Desbarats (1990, pp. 153–163). The basis for the method is described by CRWMS M&O (2000, U0065, Section 6.1.1). Briefly, particles are assigned a residence time randomly from a residence time distribution that is computed from the processes that affect residence time (e.g., advection, sorption, and matrix diffusion). For a cumulative probability distribution function of particle residence times, we compute the residence time of a particle in a cell by generating a random number between 0 and 1 to determine the corresponding residence time from the distribution function in Figure 3.11-11. The advection-dispersion equation was used to generate the schematic residence time transfer function (RTTF) curve, but other transport mechanisms can be incorporated as well. The particle moves from the resident cell to an adjoining cell randomly, with the probability of entering an adjoining cell set according to the proportion of efflux from the resident cell into each of the adjoining cells.

This same methodology is extended to a dual-permeability grid with residence time distributions in a single cell determined through mathematical models for advection, sorption, matrix diffusion, dispersion, radionuclide decay, and colloid-facilitated transport. The dual-permeability transport model includes advective and diffusive transfers between the fracture and matrix continua.

Colloid transport is included in the abstraction through two end-member representations of radionuclide/colloid associations (Assumption 3 in Section 3.11.13.2). Radionuclides that reversibly exchange between the aqueous phase and a sorbed phase on colloids are included in the transport abstraction as a separate aqueous "species". It is shown in CRWMS M&O 2000 (U0065, Section 6.1.4) that this type of colloid-facilitated radionuclide transport is mathematically equivalent to aqueous transport with appropriately modified transport coefficients. This approach assumes a linear partition coefficient between the mass concentration of radionuclide in the aqueous phase and the mass concentration of radionuclide attached to any given type of colloid. Colloids may be temporarily "detained" at the fracture/matrix interfaces, and this interaction is captured in the colloid transport model as a retardation factor for colloid transport in the fracture system. Finally, colloids are subject to size exclusion for entering the matrix from the fractures. This is represented by a size exclusion factor that multiplies the probability for a colloid to enter the matrix from the fractures. The size exclusion factor is computed based on the colloid sizes and matrix pore size distribution.

Colloids that have a fixed radionuclide content represent the other end-member representation for colloid-facilitated radionuclide transport. In this case, the radionuclides may be considered permanently fixed in the colloid structure and do not partition with the aqueous phase. Radionuclides permanently attached to colloids are also tracked as separate species in the particle-tracking model. This colloid type is subject to retardation in the fracture system and size exclusion, as described above. In addition, this colloid type is subject to permanent filtration for cases in which the colloids are making a transition from one matrix unit to another. Permanent filtration is computed in a manner similar to the way colloid size exclusion is computed for movement between fractures and matrix. The colloid filtration is expressed as a factor that multiplies the probability for colloid movement between matrix units, which is again a function of the colloid size and matrix pore size distribution. It should be noted that this filtration mechanism is not applied to colloids with radionuclides that reversibly exchange with the aqueous phase because a permanently filtered colloid in this case will not remove the radionuclide from subsequent transport.

3.11.13.4 Results

The particle-tracking method has been compared to alternate solution methods for a variety of problems. Results for 1-D transport with diffusion and sorption are found to agree with well-established analytical solutions (CRWMS M&O 2000, U0065, Section 6.2.1). A good match is also obtained for transport in a dual-porosity system including matrix diffusion (CRWMS M&O 2000, U0065, Section 6.2.2).

Comparisons with numerical models for transport in a 1-D, dual-permeability model have also been performed (CRWMS M&O 2000, U0065, Section 6.3). The comparisons shown here are for a simplified, 1-D, dual-permeability flow model for the UZ of Yucca Mountain. The flow

system consists of three significant hydrological units between the solute release point (the potential repository elevation) and the water table. Figure 3.11-12 shows the ability of the particle-tracking abstraction to match the full numerical solution for a dual-permeability model. The Y-axis is labeled the Cumulative RTD, which stands for Cumulative Residence Time Distribution. This is the fraction of particles that have traversed the UZ (between the potential repository and the water table) at any given time. This case, without matrix diffusion, shows how the model is able to capture advection and dispersion (the solid black line is the full dual-permeability numerical solution and the dashed red line is for dispersion with no diffusion using the particle-tracking algorithm). The dashed black line in Figure 3.11-12 shows that the particle-tracking algorithm is also able to produce sharp breakthrough curves when dispersion is zero, something that is difficult to do in a conventional numerical solution.

Figure 3.11-13 shows comparisons for a 1-D dual-permeability solution when matrix diffusion is included. Here there is a discrepancy at early time, in which the conventional numerical simulation predicts an early breakthrough in the case where the matrix diffusion is nonzero. The conventional solution uses a single cell to represent the matrix adjacent to a fracture cell. Thus the concentration gradient in the matrix (in a direction normal to the fracture plane) is only roughly represented in the conventional model. This discrepancy results in an early breakthrough because the exact representation of this gradient can represent a steep but narrow gradient in the matrix near the fracture plane and therefore gives a larger fracture to matrix diffusive flux. This reduced diffusive flux into the matrix leads to an earlier breakthrough.

Matrix diffusion in the particle-tracking algorithm is only exact if matrix advection is zero (see Assumption 2). To test this assumption, we performed calculations (CRWMS M&O 2000, U0160) using a particle-tracking method that does not use this assumption. The results shown in Figures 3.11-14 and 3.11-15 are for a 3-D simulation using the dual-permeability site-scale flow model. Transport is calculated for the 3-D, dual-permeability system using the model abstraction (FEHM V2.10) and a second particle-tracking routine, DCPT V1.0. The DCPT V1.0 code uses a Lagrangian approach that interpolates the velocity field onto a continuous space in which particles can travel. This routine simultaneously accounts for the effects of matrix diffusion and matrix advection. The breakthrough for the nonsorbing Tc is shown in Figure 3.11-14. The reason for the delayed breakthrough curve for DCPT V1.0 is thought to be a result of the inclusion of matrix advection in the treatment of matrix diffusion. Advective flow from the fractures to the matrix will reduce the flux of radionuclides from matrix to fractures through diffusion. Thus, radionuclides will tend to be retained for longer times in the matrix, leading to slower breakthrough.

A similar comparison is also made for the sorbing Np in Figure 3.11-16. The differences in the two solution methods found in Figure 3.11-14 are accentuated for sorbing radionuclides. In these comparisons, we find that in the model abstraction solution FEHM V2.10 predicts radionuclide movement to the water table that is significantly faster than that predicted by the DCPT V1.0 solution. Although the differences can be large, the model abstraction solution is found to be conservative. These two particle tracking methodologies and the advective-dispersive approach utilized in T2R3D V1.4 are further compared in CRWMS M&O (2000, U0155).

3.11.14 Summary and Conclusions

Figure 3.11-16 corresponds to Figure 3.11-1, which shows key issues related to radionuclide transport in the UZ. The following conclusions can be drawn from this section:

1. Two-dimensional simulations show that transport in the CHn is strongly dependent on the distribution of the vitric and zeolitic tuffs at the different locations. Occurrence of the zeolitic CHn leads to fast transport; on the other hand, the vitric CHn acts as an effective barrier to radionuclide transport, and its effectiveness increases with the sorptive tendencies of the radionuclides.
2. Three-dimensional site-scale simulations indicate that radionuclide transport is both dominated and controlled by the faults (especially at early times). Faults provide fast pathways to downward migration to the water table, but also limit lateral transport across them.
3. Fractures are also the main pathway of transport. Diffusion from the fractures into the matrix is the main retardation mechanism in radionuclide transport. By sorbing onto the matrix into which they diffuse, the migration of radionuclides is retarded.
4. Three-dimensional site-scale simulations show that radionuclide breakthrough at the water table occurs early and over a large area in the southern part of the potential repository block. The maximum water flow within the footprint of the potential repository in the southern part in the Perched water model #1 contributes to this transport pattern. Also the low-permeability zones at the TSw-CHn interface in the northern part of the potential repository are barriers to water drainage and lead to low water velocities and formation of perched water bodies. The presence of the highly conductive Solitario Canyon fault Splay G and Ghost Dance fault splay also contributes to the dominance of the southern part as the main pathway.
5. The members of the decay chain (^{239}Pu , ^{235}U , and ^{231}Pa) must be considered in the transport of ^{239}Pu . Uranium-235 will become the main contributor in the release at the water table after 10,000 years (at most) because of its weaker sorption onto the matrix and longer half-life. The contributions of ^{231}Pa are not important.
6. Colloidal transport is very sensitive to filtration parameters, and for the given parameters, the colloid size has a significant effect on transport.
7. More than 40 tracer transport simulations indicate a wide range of time for mass breakthrough depending on infiltration rates, type of tracers/radionuclides, and perched water conceptual models. The most important of these factors for transport times are (1) surface infiltration rates and (2) adsorption effects in the CHn. Compared with the effects of infiltration and adsorption, perched water conceptual models are of secondary importance to the overall impact on transport,

but have primary impact on determining breakthrough areas of tracers/radionuclides at the water table.

8. The modeling results of tracer (^{36}Cl) transport from the land surface to the repository level indicate the existence of possible fast flow pathways with transport times of 50 years. However, the cumulative mass breakthrough carried by the fast flow is relative small (about 1%) for the early times of 50 to 100 years. The 50% mass breakthrough times to the repository level since release from the surface is estimated between 5,000 to 20,000 years under the present-day, mean infiltration scenario. The fast flow breakthrough at the earlier time occurs mainly along faults.
9. Available tracer transport results of the ESF Alcove 1 and Busted Butte tests are analyzed for model validation as a confidence-building process. The Alcove 1 analyses indicate that the continuum approach is valid for modeling flow and transport in unsaturated fractured rock, an active fracture model can capture the major features of fingering flow and transport in fractures, and matrix diffusion has a significant effect on the overall transport behavior. Busted Butte tracer tests and simulations of the vitric CHn show that the unit behaves as a porous medium, which is consistent with the expected behavior.
10. Known analog sites for UZ transport are reviewed as additional corroborative analyses with respect to radionuclide transport at Yucca Mountain. Analyses of the Nopal I uranium deposit in Mexico and the trace metal migration study in Greece indicate that unsaturated systems in arid environments may provide favorable sites for geologic disposal of radioactive waste.
11. An efficient particle-tracking model abstraction for 3-D site-scale simulations of radionuclide transport in the UZ has been developed for TSPA analysis. This model abstraction utilizes simplified mathematical representations of advection, dispersion, sorption, matrix diffusion, colloid transport, and radionuclide chain decay in a dual-permeability system. Comparisons show that the TSPA particle-tracker will yield conservative transport calculations.

INTENTIONALLY LEFT BLANK

3.12 MOUNTAIN-SCALE TH MODEL

3.12.1 Introduction

Unsaturated zone (UZ) flow and transport will be affected by the heat released from the decay of radioactive waste in emplacement drifts of the potential repository at Yucca Mountain. The Analysis/Model Report for mountain-scale coupled processes (CRWMS M&O 2000, U0105), documents the development of the Mountain-Scale Thermal-Hydrological (TH) Model. This model evaluates the effects of heat on UZ flow and the distribution of liquid and temperature over a period of 100,000 years and provides the necessary framework to test conceptual hypotheses of coupled heat and fluid flow in the UZ. This model can then be used to predict future behavior in the UZ under thermal loading. This section summarizes the results of the TH Model, identifies the performance issues addressed and provides resolutions of the issues in terms of input for Performance Assessment (PA).

The Mountain-Scale UZ TH model complements the EBS MultiScale TH (MSTH) (CRWMS M&O 2000, E0120) model in the evaluation of the impact of thermal loading on the NFE TH conditions and the EBS system, at the potential repository. The MSTH model samples TH conditions at several locations at the potential repository and includes influence of alternative waste package configurations. The model is a localized alternative to a fully coupled 3-D drift-scale and Mountain-Scale TH model, that provides detailed drift-scale processes at the repository under thermal loading, from a sampling of mountain-scale locations. The Mountain-Scale UZ TH model on the other hand provides an estimate of mountain-scale evolution of the flow field coupled to a simplified representation of the drift-scale processes. Detailed drift-scale TH and THC processes are modeled and discussed in CRWMS M&O (2000, N0120/U0110).

Figure 3.12-1 presents design issues modeled by heating the volume of UZ rock surrounding the potential repository. The issues provide for qualitative and quantitative evaluation of the impact of potential repository heat on the UZ and include the following:

- Extent of the two-phase zone
- Liquid and gas flux in near field and far field
- Moisture redistribution in the UZ
- Temperature at drift walls and in pillars in between drifts
- Potential for flow and transport property changes in the PTn and CHn
- TH effects on water table and perched water bodies
- Influence of climate and ventilation.

The thermal load and the resulting temperature changes have a large influence on many related processes, which directly impact the performance of the potential repository. The emplacement of heat-generating high-level waste will elevate temperatures and cause the redistribution of the *in situ* moisture in the unsaturated zone. For example, if the temperature of the rocks near the emplacement drifts approaches or exceeds the boiling point of water (97°C at ambient pressure), boiling of formation water will take place, with the associated increase in vapor pressure and overall gas-phase pressure. This will result in forced convection of the gas phase, that is accompanied by large latent heat effects. Phase transformation and gas-phase flow will perturb the *in situ* fluid distribution in the fractures and matrix, thereby changing capillary pressure gradients, relative

permeability and liquid-phase flow rates. The impact of heat on the TH processes will depend on the thermal load as well as its distribution in the emplacement drifts.

The Mountain-Scale TH Model numerically simulates the potential impact of the heat that is released by radioactive decay on the natural hydrogeological system, including a representation of heat-driven processes occurring in regions far away from the potential repository (the far field). The simulations provide predictions for thermally affected liquid saturation, gas- and liquid-phase flux (together referred to as flow fields), and the distribution of temperature and saturation in the UZ. Of particular interest is the impact of thermal loading imposed by waste emplacement on water percolation at and near the potential repository host rock and the flow barrier effects in the basal vitrophyre of the Topopah Springs and the Calico Hills zeolites underlying the potential repository horizon. These rock units impede the transport of radionuclides from the potential repository to the water table due to their low permeability and high sorptivity. When heated for long periods of time at temperatures exceeding 90°C, the flow and transport properties of these rocks can be altered, thus directly impacting their ability to impede transport of radionuclides.

The Mountain-Scale TH Model is developed based on the UZ Flow Model. This model uses input parameters based on the calibrated property set (CRWMS M&O 2000, U0035), a spatially varying mean infiltration rate, with varying climates during the thermal-loading period. The simulations were performed using the average initial thermal load of 72.7 kW/acre, scaled down by the natural decay curve over a total simulation period of 100,000 years. To account for ventilation, only 30% of this heat is used during the first 50 years.

Prediction of the thermal-loading effect in such models in turn requires establishment and acceptance of mathematical models that accurately represent the physics of coupled heat and fluid flow in the UZ. The TH Model uses the mathematical formulation employed in the TOUGH2 family of codes (Pruess 1987, pp. 2–11; Pruess 1991), the dual-continua approach (Section 3.4) and the van Genuchten capillary pressure and relative permeability parameter values obtained from the calibrated properties data (CRWMS M&O 2000, U0035) to describe the behavior of the UZ under thermal-loading conditions. This formulation is based on the traditional energy- and mass-conservation relationships.

During the development of the TH Model (CRWMS M&O 2000, U0105), the accuracy and validity of the model results were evaluated based on current understanding of fracture-matrix interactions, heat transfer, and two-phase flow in unsaturated subsurface systems. Calibration of modeled temperature against the measured temperature profiles in boreholes (CRWMS M&O 2000, U0050, Section 6.3) provides a basis for assessing the effectiveness of the model to capture the ambient, mountain-scale temperature distribution, which is used as the initial temperature for TH modeling.

3.12.2 Modeling Approach

The TH Model is used to model the nonisothermal TH processes due to heat generated by the emplaced heat source. Figure 3.12-2 shows the relationship between the TH Model, the input data, and the models supporting its development. This section presents a brief discussion of the

development of the TH conceptual model and numerical grids, as well as the selection of input data and the model boundary and initial conditions.

3.12.2.1 Conceptual Model

The conceptual model for describing the TH processes at Yucca Mountain is based on the conceptual model used for the UZ Flow Model, as discussed in Sections 3.3 and 3.7. In this hydrogeological conceptual model, the UZ system consists of multi-layered hydrogeologic units, with flow behavior determined primarily by the degree of welding of the Yucca Mountain tuffs (Sections 3.2 and 3.4). The heat transfer within the UZ system is fully coupled with other processes, such as liquid percolation and air circulation.

The numerical approaches (Section 3.4) involve volume averaging and the continuum concept for modeling coupled fluid and heat flow and fracture-matrix interaction. The dual-permeability formulation described in Section 3.4 and CRWMS M&O (2000, U0000, Section 6.7) with a single fracture element and single matrix element representing each continuum is used in all the TH simulations. This dual-continua method allows for global flow through both the fracture and matrix continua. The fracture-matrix interaction is modeled using the active fracture concept (Liu et al. 1998, pp. 2633–2646) for liquid flow in dual-continua.

The TH simulations were conducted using TOUGH2 V1.4 (Section 1.3), with the equation-of-state module EOS3 (water, air and heat). The EOS3 module contains the constitutive relationships that describe the thermodynamic properties of water (enthalpy, density, viscosity) as functions of temperature and pressure. In all simulated cases the relationships between relative permeability and capillary pressure for unsaturated rock are estimated using documented relations of Brooks and Corey (1966, pp. 61–88) and van Genuchten (1980, pp. 892–898).

3.12.2.2 Numerical Grids

Several numerical grids were used for TH simulations, including (1) a 3-D submodel grid of the UZ 3-D grid and (2) two 2-D cross-section grids (NS#1 and NS#2). All the numerical grids are based on the Geologic Framework Model (GFM 3.1). Figure 3.12-3 shows a plan view of the UZ 3-D grid and the location of the potential repository submodel grid and the 2-D cross-section grids NS#1 and NS#2. The numerical grid resolution and layers along the NS#2 cross section are shown in Figure 3.12-4. Most of the results presented in this section utilize this cross section, with the lateral grid spacing equal to 1/4 of the drift spacing. A detailed discussion of numerical grids is presented in Section 3.4 and in CRWMS M&O (2000, U0000) and CRWMS M&O (2000, U0105, Section 6.2).

The design of the lateral grid spacing within the potential repository domain includes the proposed spacing and orientation of the drifts. For the 3-D grid, the lateral spacing over the potential repository domain is equal to the spacing between the drifts (81 meters). The vertical grid design uses a 5 m thick grid layer to represent the potential repository horizon, at the elevation of the proposed repository. This layer is bounded above and below by 5 m thick layers CRWMS M&O (2000, U0000, Section 6.6.2). This type of grid, although sufficient to resolve mountain-scale processes, does not provide sufficient resolution for detailed evaluation of TH conditions around and between drifts.

In the 3-D grids discussed above and in CRWMS M&O (2000, U0000 and 2000, U0105), each potential repository drift is represented by elements aligned along the direction of drifts. For the 2-D cross-section grids, each drift is represented by a single element (with both matrix and fracture continua). In the design for the potential repository, the heat-generating radioactive waste will be stored in widely spaced drifts (up to 81 m spacing) at the repository horizon. This physical separation of the drifts in the real world can be lost in numerical grids if large grid spacing is used. If the grid spacing within the potential repository is equal to the drift spacing, then although the drifts are physically separated, they are in fact numerically adjacent. This results in a laterally continuous (smeared) heat source across the potential repository. Such a numerical grid (although sufficient for resolution of UZ Mountain-Scale ambient flow processes) cannot provide adequate resolution to study TH processes in terms of temperature, saturation, and flux between the drifts. The discrete (drift-by-drift) grid provides a model in which such phenomena can be investigated and the effect on the mountain-scale TH processes to be documented. In the 3-D grids this requires development of a new, locally refined grid, with a large number of elements, which greatly increases numerical computation time. In the cross-section grids, locally refined drift elements can be added at the potential repository horizon, without a substantial increase in the total number of elements.

To develop TH models that provide a detailed resolution of the ambient flux and resolve the TH conditions near and between the drifts, the locally refined grid NS#2 described in CRWMS M&O (2000, U0105, Section 6.2.2) was used. This grid incorporates individual drifts, and provides several nodes between the drifts so that evolution of TH conditions at the drifts and within the pillars can be modeled. Detailed discussion of the development of this numerical grid that provides a physically more accurate representation of the heat distribution at the potential repository is presented in CRWMS M&O (2000, U0105 Sections 6.2 and 6.3).

3.12.2.3 Potential Repository Thermal Load

Mountain-scale thermal-loading data, which include the initial thermal load and the natural radioactive decay rate, were used in all the TH models. The total initial thermal load for the base-case scenario is 72.7 kW/acre (18.0 W/m²), based on a potential repository area of 1,050 acres (4.25×10⁶ m²). In the cross-section grids, the amount of heat to be applied to individual drifts was computed based on this initial thermal load, the decay curve, and the lateral spacing between the drifts. This thermal load was then applied as a heat source to the matrix continuum of the discrete drift elements at the potential repository, beginning with the maximum thermal load at time zero and scaling it down according to the tabulated decay curve at subsequent times. This thermal load is included in the TOUGH2 input as a tabulated lookup of time versus heat for matrix elements representing the potential repository drifts. To include the effects of a 50 year pre closure period of ventilation, this heat load is further scaled down. In the ventilated drift thermal-loading scenario, 70% of the heat generated by the radioactive is removed by the ventilation system. Therefore, only 30% of the computed heat is included in the input during this period. After 50 years, the “no-ventilation” heat input is used. Since the practical and logistical details of ventilation and its efficiency have not been ascertained both the “no-ventilation” and “ventilation” scenarios were modeled in order to quantify the impact of ventilation.

3.12.2.4 Boundary and Initial Conditions

The UZ numerical grids (Section 3.4 and CRWMS M&O 2000, U0000) consider the top of Tiva Canyon (TCw) hydrogeological unit as the top boundary. This coincides with the ground surface in most areas, except in areas with thick alluvium cover, where the top of the model is at the alluvium-TCw contact. All TH numerical grids also use this surface as the reference top boundary. Fixed temperature, gas saturation and gas pressure corresponding to the near surface conditions are assigned along this boundary.

The water table is used as the bottom boundary for fluid flow with a fixed liquid saturation and gas pressure prescribed. These conditions represent estimated gas pressure and capillary fringe saturation at the water table. Temperature changes at the water table are modeled by extending the bottom temperature boundary to 1,000 meters below the water table. The temperature at the extended boundary is then fixed at 65°C. A simulation of nonisothermal UZ flow under the fixed top temperature and saturation conditions, and fixed bottom temperature, pressure, and saturation boundary conditions, was conducted to obtain mountain-scale ambient conditions using the present-day mean infiltration. This simulation shows that the average temperature at the water table (730 masl) is between 30 to 33°C over the potential repository domain, which is in agreement with the calibrated temperature distribution at the water table (CRWMS M&O 2000, U0050, Section 6.3). The average temperature at the repository horizon is about 23°C. These mountain-scale ambient conditions are the initial conditions for the TH simulations.

3.12.2.5 Input Data and Parameters

Key input data used in the TH model development are summarized in CRWMS M&O (2000, U0105, Section 4) and include the following:

- Fracture properties (frequency, permeability, van Genuchten α and m , and aperture, porosity, and surface area) for each UZ model layer.
- Matrix properties (porosity, permeability, van Genuchten α and m) for each UZ model layer.
- Thermal properties (grain density, wet and dry thermal conductivity, grain specific heat, and tortuosity coefficients) for each UZ model layer.
- Fault properties (matrix and fracture) for each hydrogeologic unit.
- Repository thermal-load and ventilation scenarios.
- Present-day infiltration and temporal changes in infiltration due to long-term climate changes.

In the TH models, three infiltration rates based on three climate scenarios were used over the thermal loading period. These are discussed in detail in Sections 3.3 and 3.5, and in USGS (2000, U0010, Section 5.1). Net infiltration maps corresponding to the following climates were used for TH modeling:

Present Day: The mean present-day climate was used. In the 3-D models and the 2-D model NS#1, this climate was used for the entire simulation period. For the refined 2-D cross-section NS#2 model, this climate was used for the period from 0 to 600 years.

Monsoon: The mean monsoon climate was used for the 2-D NS#2 model and was applied for the period 600 to 2,000 years.

Glacial Transition: The mean glacial transition climate was used for the rest of the simulation period beyond 2,000 years in the 2-D NS#2 models. Although models of climate only cover a period of 10,000 years, the glacial-transition climate is assumed to extend up to the total modeled period of 100,000 years.

The average net infiltration rate along the NS#2 cross-section is 4.8 mm/yr for the mean present-day infiltration rate, 11.3 mm/yr for the mean monsoon climate average infiltration, and 16.9 mm/yr for the mean glacial transition climate. These rates compare well with the net infiltration rates over the entire UZ model domain, as presented in Section 3.5, Table 3.5-4.

3.12.3 Results of TH Simulations

Table 3.12-1 summarizes the cases simulated to characterize the TH processes on the Mountain-Scale under thermal loading. The simulations of the non-isothermal fluid and heat flow were conducted for a thermal-loading period of 100,000 years. The simulations start at time zero using the ambient conditions of the UZ Flow Model as initial conditions. The simulations were stopped at 600 years and at 2,000 years to change the infiltration to that of the corresponding climate.

The main purpose of the Mountain-Scale TH Model is to predict the extent of the thermally disturbed zone, i.e., the mountain-scale changes in temperature, saturation, and liquid and gas flux. In particular, attention is given the TH Model results that directly impact performance issues, as outlined in the introduction. This section presents a detailed discussion of the results only for the fine grid simulations (Cases 5 and 6). The reader is referred to CRWMS M&O (2000, U0105, Sections 6.10 and 6.11) for detailed discussions of the other cases.

Table 3.12-1. Summary of Numerical Model Cases for Mountain-Scale TH.

Case No.	Numerical Grid	Infiltration	Thermal Load	Temperature Boundary
1	3-D Submodel, no drifts	Mean present day	72.7 kW/acre; no ventilation	1,000 m below the water table
2	3-D Submodel, no drifts	Mean present day	72.7 kW/acre; no ventilation	At the water table
3	2-D Cross-Section (NS#1), no drifts	Mean present day	72.7 kW/acre; no ventilation	1,000 m below water table
4	2-D Cross-Section (NS#1) with locally refined drifts	Mean present day	72.7 kW/acre; no ventilation	1,000 m below water table
5	2-D Cross-Section (NS#2) with locally refined drifts	0-600 years, mean present day; 600-2,000 years, mean monsoon; 2,000+ years, glacial transition	72.7 kW/acre; no ventilation	1,000 m below water table
6	2-D Cross-Section (NS#2) with locally refined drifts	0-600 years, mean present day; 600-2,000 years, mean monsoon; 2,000+ years, glacial transition	72.7 kW/acre; with ventilation: use 30% of the total heat for 50 years	1,000 m below water table

SOURCE: Adapted from CRWMS M&O 2000, U0105, Table 5)

3.12.3.1 Temperature

The evolution of the temperature distribution provides an estimate of the volume and lateral extent the UZ that is affected by the heat at the potential repository, as well as the temperature in the drifts and in the pillars. The numerical model can provide the predicted distribution at any desired time during the thermal loading period. The average ambient temperature at the potential repository horizon is about 23 °C (CRWMS M&O 2000, U0105, Section 6.9). Figure 3.12-5 shows the distribution of temperature along the cross-section NS#2 after 1,000 years of thermal load (a) without ventilation, and (b) with ventilation (for the first 50 years). The variations in net infiltration across the model strongly influence the evolution of temperature in both cases. Higher temperatures are predicted in the low infiltration areas. The plots show extensive boiling only in the area immediately above and at the potential repository horizon. At a lateral distance of 100 meters or more from the potential repository, no substantial increases in temperature are predicted. For example, the predicted maximum temperature is 37°C at 100 meters north of the potential repository and about 40°C at 100 meters south. The temperatures at 200 meters away from the potential repository remain near ambient conditions throughout the simulation. This response suggests that the convection mode of heat transfer, driven by extensive boiling and rapid fracture flow, is dominant near the potential repository. The ambient infiltration flux (predominantly vertical) controls the temperature changes outside the potential repository boundaries.

A detailed evaluation of temperature changes can be obtained by plotting the evolution of temperature profiles in a column within the potential repository domain. The plots of vertical temperature profiles in a column at the center of the potential repository (location #1, see Figure 3.12-4) are shown in Figure 3.12-6. The figure shows that TH processes at and near the potential repository are controlled by convection. Without ventilation (Figure 3.12-6a), the model predicts that temperature at the drift wall could rise to 250°C after both the matrix and the fracture elements of the drifts become completely dry. In this case, a two-phase boiling zone at 97°C develops above the potential repository and extends out to 50 meters after 500 years. This zone expands to 200 meters after 1,000 years. With ventilation (Figure 3.12-6b) the two-phase boiling zone is small and is confined to within 20 meters above the potential repository drifts. In this case the average temperature within the drifts rises to boiling conditions (97°C), although in a few locations, temperatures rise to about 110°C (CRWMS M&O 2000, U0105, Section 6.11).

A plot of the evolution of temperature along the middle section of the potential repository horizon is presented in Figure 3.12-7 (a) without ventilation, and (b) with ventilation. The peaks correspond to the individual drifts that are spaced about 21.4 m along this cross section. The maximum temperatures occur in the drifts and minimum temperatures occur in the pillars. Without ventilation, the temperatures at the potential repository horizon rise to above boiling conditions (97°C) between 5 and 10 years. At ten years, most of the drifts are at a temperature of 100°C as shown in Figure 3.12-7a. However, at this time the temperatures rise to 260–300°C in the completely dried out zone at the northern end of the potential repository, where the surface infiltration rate is nearly zero (CRWM M&O 2000, U0105, Section 6.11). At 50 years, the temperatures in most drifts decline to 210–235°C. After 50 years, the temperatures in the drifts decline rapidly due to re-wetting, driven by strong capillary suction in the near-field environment. At 100 years, temperature within the drifts is 160–180°C but continues to decline. After 500 years, the temperature range of the drifts is 120–135°C and after 1,000 years the average temperature is about 97°C at the center of the pillars with peaks of 100°C to 110°C within the drifts. After 10,000 years the average is about 65°C between the pillars, but rises to about 70°C at the drifts. Therefore, even without ventilation, the predicted maximum temperatures at the center of the pillars between the drifts do not exceed boiling temperature.

Figure 3.12-7b shows the temperatures in the middle section of the potential repository horizon with ventilation. Even with ventilation, the models predict the development of a small zone of two-phase counter-current flow of liquid towards the drifts and vapor away from the drifts (heat-pipe) at the potential repository horizon. The model predicts much lower elevated temperatures within the drifts due to ventilation cooling. When the ventilation system is shut-off after 50 years, the temperatures at the drift wall are predicted to rise. The models predict that maximum temperatures at most locations along the potential repository horizon will not exceed boiling temperature (Figure 3.12-7b), although at localized areas with low ambient infiltration the temperature may rise to 110°C after these zones dry out (CRWM M&O 2000, U0105, Section 6.11). In this case, the temperatures in the central pillars rise to a maximum of 85°C after 1,000 years. After 10,000 years this temperature drops to about 65°C at the center of the pillars and to about 70°C at the drifts. Similar temperature conditions are predicted at 10,000 years without ventilation (Figure 3.12-7a), showing that the long-term temperature response is not affected by the 50 years of ventilation.

At the top of the Calico Hills nonwelded hydrogeological unit (CHn), at an elevation of 907 masl (at location #1), the models predict a maximum temperature of 70–75°C between 2,000 and 7,000 years. This temperature range suggests minimal potential for temperature-induced mineralogical changes to occur within the zeolites of nonwelded hydrogeological Calico Hills unit. Therefore, the sorptive properties of these zeolites will not be altered significantly as a result of thermal load at the potential repository. At the water table the models predict a maximum temperature of 65–70°C compared to the average ambient temperature of 30°C. Without ventilation, temperatures at the base of the PTn may rise to boiling conditions at an elevation of 1,250–1,270 masl (Figure 3.12-5) and induce property changes within the low infiltration areas. Temperatures within the PTn are predicted to rise to a maximum of 70–75°C. With ventilation, temperatures in the PTn are predicted to rise by 20–25°C from the ambient condition to an average of 40–45°C. The numerical simulations show that there is minimal potential for temperature induced property changes within the PTn.

The elevated temperature at the drift wall during thermal loading may lead to significant changes in thermal-mechanical stresses that may alter permeability and other properties of the host rock in the vicinity of the drifts. The extent of permeability changes as a result of thermally induced stresses are not addressed in the Mountain-Scale TH Model, because the thermal-mechanical effects are expected to occur on smaller scale. In addition, there are few site-specific studies or data available for describing thermal-hydrological-mechanical processes at Yucca Mountain.

3.12.3.2 Saturation

Changes in liquid saturation are important for several reasons. First, they indicate how long the dryout period at the potential repository will be. Secondly, they are used to assess the potential desaturation-induced changes in porosity and hydraulic conductivity (for example, in the zeolitic units). Finally, they help identify the onset of re-wetting processes and the subsequent potential for corrosion at the potential repository horizon. The TH simulations begin with the ambient liquid saturation obtained by a steady-state simulation using the present day mean infiltration and the boundary conditions discussed in Section 3.12.2.4. The heat leads to mobilization of liquid and gas in both the matrix and fracture continua.

Figure 3.12-8 shows contour plots of matrix liquid saturation at 1,000 years (a) without ventilation, and (b) with ventilation. The plots show large decreases in matrix liquid saturation only near the drifts. In both models all fractures in the drifts at the potential repository horizon are completely dry within the first few years of thermal loading and do not rewet until 1,000 years after thermal loading begins. Figure 3.12-9 shows the matrix liquid saturation at location #1 whereas Figure 3.12-10 shows the corresponding matrix saturation along the entire repository horizon. Without ventilation, the models predict completely dry matrix conditions (Figures 3.12-9a and 3.12-10a) for all the drifts between 10 and 50 years, and an area of reduced matrix liquid saturation below and above the potential repository. This area of reduced matrix liquid saturation extends up to 100 m below and above the potential repository horizon without ventilation. In this case, the matrix liquid saturation in the pillars drops to a minimum of 0.4 after 500 years. The fracture liquid saturation in pillars adjacent to drifts rises above ambient saturation at 10 years (CRWMS M&O 2000, U0105, Section 6.11) due to condensing of water vapor. After 10 years the fracture liquid saturation reduces to and remains at near ambient saturation controlled by the climate.

With ventilation (Figures 3.12-9b and 3.12-10b), completely dry matrix conditions are predicted only at a few isolated locations having low percolation flux. Vertically (Figure 3.12-9b) the zone of reduced matrix saturation extends to about 50 m above and below the drifts. The matrix saturation in several drifts with high percolation flux recovers to above 0.9 at 1,000 years (Figure 3.12-10b). After 5,000 years the matrix liquid saturation is almost fully recovered to the liquid saturation controlled primarily by the prevailing climate. In this case the fracture and matrix liquid saturation within the pillars remains at near-ambient conditions and is controlled primarily by the changes in climate throughout the simulated period. With and without ventilation the simulations predict that the liquid saturation at a lateral distance more than 50 meters away from the repository remains at near-ambient conditions.

3.12.3.3 Water Flux

Analysis of the liquid flux gives an estimate of the quantity and duration of enhanced liquid flux that may potentially contact the waste canisters (near-field environment) under thermal load. Flow at the potential horizon can be enhanced by a decrease in saturation, which leads to an increase the capillary suction. The liquid flux can also be enhanced by an increase in saturation due to drainage of condensate that leads to an increased liquid relative permeability. The suction-induced increase in liquid flux is due to the intense boiling and vaporization of both fracture and matrix liquid at the potential repository drifts because the temperatures reach or exceed boiling conditions (about 97°C) even with ventilation. The liquid vaporization results in increased gas flow at the potential repository, which dries up the fractures first and reduces matrix liquid saturation at the potential repository horizon. The dry-out of fractures and lower matrix saturation at the potential repository drifts creates a large capillary pressure gradient between the continua at the potential repository horizon and the adjacent formations. This promotes liquid flow toward the potential repository, i.e., enhances percolation flux. This liquid flux is directed toward the repository drifts, but there is ample heat to vaporize all the liquid, particularly at early times. The vaporization leads to increased gas flux, which may cause localized condensation and drainage through the fractures in the pillars and the drifts. Details of such processes are better resolved by the refined NS#2 grid, which is described Section 3.12.2.2 and used for the TH simulations described here.

Figure 3.12-11 shows the evolution of predicted liquid flux through the fractures at location #1 at the center of the potential repository with and without ventilation. Because of an extensive low-saturation zone within the drifts, both models predict high percolation fluxes near the drifts. Figure 3.12-11a, shows a plot the vertical liquid flux at this location without ventilation (the plots here show liquid flux scale of up to 200 mm/yr for clarity). The predicted maximum liquid flux rises 360 mm/yr at 10 years (CRWMS M&O 2000, U0105, Section 6.11), but declines to less than 30 mm/yr at 500 years. With ventilation (Figure 3.12-11b) the average vertical flux near the potential repository rises to only 60 mm/yr at 10 year. When ventilation is turned off at 50 years, the increase in the available heat within the drifts leads to further decrease in matrix liquid saturation and increase in capillary pressure gradients. This in turn increases liquid flow toward the drier drifts. After 500 years the liquid flux is has only declined about 40 mm/yr.

Figure 3.12-12a (the figures here show liquid flux scale of up to 100 mm/yr for clarity) shows the liquid flux through the fractures at the potential repository horizon, without ventilation. Note that vertical liquid flux at location #1 (Figure 3.12-11) is calculated based on the entire column

area. In the locally refined NS#2 grid, 5 m drifts plus two equal elements represent the columns at the potential repository horizon in which drifts are located (CRWMS M&O 2000, U0105, Section 6.3.3.2). The liquid flux through an entire column above the drift is thus funneled toward the narrower drift by the high capillary gradients, because heat is applied only to the drift element. The figure shows that without ventilation, the liquid flux through the fractures toward the drifts, calculated based on this smaller drift area, rises to between 1,250–1,600 mm/yr (CRWMS M&O 2000, U0105, Section 6.11) after 10 years. This liquid flux drops to zero, as the fractures in the drifts become completely dry (between 10 and 50 years). As the fractures begin to rewet between 500 and 1,000 years (see Figure 3.12-10a), the fracture liquid flux recovers (Figure 3.12-12a). Around 1,000 years, fracture liquid flux at several locations increases to 20–50 mm/yr (2 to 5 times mean infiltration rate for the monsoon climate), controlled by the infiltration rate, capillary-pressure and the liquid-saturation gradients. This is the liquid flux that can potentially contact the canisters. The simulations also show increased fracture liquid flux in the pillars between the drifts. At around 500 years the average fracture flux between drifts is about 20 mm/yr, about 5 times higher than the infiltration rate. This is because the predicted boiling within the pillars in the no-ventilation case leads to a decrease in saturation and increased capillary suction.

Although ventilation lasts only 50 years, it results in changes in flux patterns that last for several hundred years. This is because the heat removed by ventilation results in a delay in the dry-out of the matrix, and decreased gas flux at the potential repository horizon. Ventilation leads to much lower induced liquid and gas flux because the effective thermal load is only 30% of the total load during the period in which the heat yield of the emplaced waste is highest. With ventilation (Figure 3.12-12b, plot shows scale of up to 100 mm/yr for clarity) the predicted fracture flux at the potential repository horizon rises to maximum of 270–300 mm/yr at 10 years, but subsequently declines due to decreased vaporization. When ventilation is shut off at 50 years, the retained heat leads to increased drying of the matrix and an increase liquid flux. However, this process is delayed because first the temperature of the rock-mass at the potential repository must rise to boiling conditions before liquid can be vaporized to create the large capillary pressure gradients. At 100 years (50 years after end of ventilation) the liquid flux is 10 mm/yr. However, flux recovers to over 150 mm/yr at 500 years (Figure 3.12-12b) as a result of increased heating, drying of matrix and re-wetting of the fractures. Because of the general decline in the heat released from the emplaced nuclear waste and the increased infiltration due to climate change, the fracture continuum at the potential repository horizon is almost completely re-wetted after 5,000 years, and the fracture liquid flux recovers to the ambient percolation flux. With ventilation, the fracture flux through the pillars between the drifts remains at or above ambient conditions throughout the thermal-loading period. This is because temperatures do not rise to boiling conditions and condensation of liquid vapor gives rise to localized increase in fracture liquid saturation and a corresponding increase in liquid relative permeability. For example, the liquid flux between the drifts is 15 to 20 mm/yr, (about 2 to 3 times the ambient infiltration rate), at 500 years. Beyond 500 years the fracture liquid flux in the pillars is controlled primarily by the changes in ambient infiltration due to changes in the ambient climate, monsoon climate at 600 to 2,000 years and glacial transition climate thereafter.

Analysis of the liquid flux through the matrix gives an indication of the liquid that flows toward the potential repository primarily through the matrix during thermal loading. Figure 3.12-13 shows the matrix liquid flux at the potential repository (a) without ventilation, and (b) with

ventilation. Without ventilation (Figure 3.12-13a, plot shows scale of up to 100 mm/yr for clarity) the matrix liquid flux rises to a maximum of 400–450 mm/yr after 500 years at the drifts, but stays at ambient conditions between the drifts. As the matrix continuum of the drifts becomes completely dry, this flux also drops to near zero between 500 to 1,000 years. With ventilation (Figure 3.12-13b) the matrix liquid flux rises to a maximum of 20 to 30 mm/yr at the drifts after 500 years but remains at ambient conditions (about 0.25 mm/yr which is less than 6% of total liquid flux) between the drifts throughout the thermal-loading period.

3.12.4 Model Validation

Model validation here is discussed in terms of confidence building for the validity of the numerical and mathematical approaches used to model TH processes. There is no data for direct validation of the Mountain-Scale response to thermal loading. Validation data for a Mountain-Scale TH Model can only be obtained by monitoring the response of a fully operational repository. Numerical modeling of Mountain-Scale TH processes can provide a prediction of the performance of the potential repository under thermal loading. Such a model can then provide quantitative and qualitative evaluation of the issues discussed in Section 3.12.1, which are used to evaluate alternative designs for the potential repository. The validation process then becomes one of assuring that the numerical model adequately represents the physical processes, and that the results of such a model provide reliable data for decisions on the design of the potential repository.

The problem to be modeled here is essentially that of coupled two-phase fluid and heat flow in a fractured geological medium. Approaches for the development of the numerical models for the simulation of the two-phase processes in such systems are generally based on geothermal and petroleum reservoir simulation methods. Numerical models of geothermal and petroleum systems can be validated from a wealth of field-scale tests and production data. The validity of model predictions based on this modeling approach is demonstrated using corroborative results from the modeling of these natural analog systems (Table 3.2-1), from the previously published UZ numerical modeling studies, and from small-scale underground thermal tests in the ESF discussed in Section 2.2.4.

Validation of the TH Model, although incorporating results of the small-scale TH tests, relies mainly on the conceptual and mathematical validity of the models, the validity of flow and thermal properties, and the associated numerical grids. Performance Assessment of the effect of heat on the UZ flow, based on numerical simulation of fluid and heat flow, can include the physical processes affecting repository and host-rock behavior. The TH models explicitly represent the relevant thermal-hydrological conditions at the potential repository over the applicable time and space scale. These TH numerical models can then provide model predictions of the mountain-scale responses to thermal loading under the proposed design conditions. For example, the numerical models can be used to determine the effect of thermal loading on mountain-scale liquid and gas flux, temperature, and moisture distribution in the UZ. This coupled flow of heat and fluid in the UZ is modeled using TOUGH2 V1.4 (STN: 10007-1.4-0). Previous versions of this code have been used in the modeling of several natural analogs discussed in CRWMS M&O (2000, U0105, Section 6.12) and presented in Table 2.3-1 of this PMR. The table also documents the similarity between these natural analog systems and the UZ at Yucca Mountain that is modeled here. Applications include detailed studies, production

history and future performance of geothermal fields. The justification for the modeling approaches employed in the TH Model and the validity of the TH predictions rely upon the successful modeling of fluid and heat transport in large natural sub-surface systems (for example geothermal systems) for which an extensive volume of field data is available for model validation. These natural analog models are validated by field measurements in several operating geothermal fields as discussed in Section 2.2.4.

The predicted heat-pipe mode of heat transfer near the drifts in the Mountain-Scale TH Model, and its influence on temperature distribution agrees with the observations from the SHT results and the interim results of the thermal DST, discussed in Section 2.4 and documented in CRWMS M&O (2000, N0000). In addition, the modeled drift-scale THC response discussed in Section 3.10 shows similar heat-pipe signatures and condensation in fractures. This response is validated by comparison to measured temperature at several observation points, by repeat air-injection tests, neutron logs and electrical-conductivity logs, which measure changes in liquid in liquid saturation. Both the results of the heater tests and the TH Model suggest no major adverse conditions in terms of temperature changes, moisture redistribution near the drifts, as well as liquid drainage towards the drifts and within the pillars. The TH Model shows no major moisture redistribution in the UZ except near the heated drifts. The simulations also show only moderate temperature increase within the zeolites and at the water table. We consider the TH Model developed here validated for the intended use because of this good agreement with the heater test models, the validity of the geothermal analog models, and the documented theoretical and physical validity of similar unsaturated flow studies with and without heat.

3.12.5 Summary and Conclusions

The TH modeling study investigates the effects of thermal loading on the UZ of Yucca Mountain. This study uses both 3-D and 2-D dual-permeability submodels of the 3-D UZ Flow Model and incorporates the calibrated model properties. Detailed investigation of the UZ response to thermal loading discussed in this PMR is conducted using refined 2-D cross-section models that include explicit representation of the drifts at the potential repository.

These models simulate the mountain-scale TH response under the design base-case thermal load scenario. The models include expected future climatic changes in infiltration rate and the effects of drift ventilation. The numerical grids are sufficiently refined to determine Mountain-Scale, long-term TH behavior resulting from thermal load within the drifts, but do not explicitly include detailed heat transfer processes within the drifts. This is because such processes affect only small distances around the drift (a few meters) and at early times (less than 500 years) relative to the Mountain-Scale model spatial domain and the modeled temporal scale. Figure 3.12-14 summarizes the results of the TH modeling in terms of the issues discussed in Section 3.12.1. The figure provides qualitative and quantitative data primarily based on the results of the detailed NS#2 cross-section UZ model. This study indicates that the available heat source and its distribution as well as the infiltration rates are the determining factors for boiling and re-wetting TH processes at the potential repository.

With or without ventilation, heat-pipe conditions are developed in a region above the potential repository in the period of 10 to 100 years after thermal loading starts. Without ventilation, the TH models predict drift temperatures exceeding 100°C for hundreds of years. The results show

that temperatures may be elevated to more than 250°C within the completely dry drift zone, when no ventilation is implemented. In this case, temperature within the pillars may rise to boiling temperature (about 97°C) after 1,000 years of heating. With ventilation, temperatures only rise to boiling conditions in the immediate vicinity of the drifts, but may reach 110°C at drifts with low ambient liquid flux. In this case the temperatures in the pillars are predicted to rise to an average of 80–85°C. In both cases the models predict a nearly 30–35°C temperature increase at the water table to an average of 60–65°C. At the top of the CHn stratigraphic unit, the predicted maximum temperature rises to 70–75°C and occurs between 2,000 and 7,000 years. This suggests that temperature-induced property changes will be insignificant in the CHn because such changes are expected to occur if CHn zeolite temperatures remain above 90°C for prolonged periods of time. Without ventilation, temperatures within the PTn are predicted to rise to a maximum of 70–75°C. With ventilation, temperatures within the PTn are predicted to rise by 20–25°C from the ambient condition to an average of 40–45°C, indicating minimal potential for temperature-induced property changes within the PTn. In both cases, temperatures at a lateral distance of more than 100 m outside the potential repository are expected to remain at near ambient conditions.

Therefore, thermal loading at the potential repository results in significant changes in the temperature conditions particularly near the drifts. The models predict that heating of the potential repository drifts will result in hot and dry conditions within the drifts that last for hundreds of years in the fractures with and without ventilation. Two-phase heat-pipe conditions will develop in a region above the potential repository. In areas with low surface infiltration this region may extend to the base of the PTn stratigraphic unit if no ventilation is implemented.

Without ventilation most of the rock mass surrounding the drifts is predicted to become completely dry and remain so for over 1,000 years. With ventilation, although the TH Model does not predict completely dry conditions near all the drifts, the walls of the drifts are expected to remain dry for hundreds of years. In both cases the fractures at the potential repository drifts are predicted to completely dry and remain so for hundreds of years. With and without ventilation the matrix and fracture liquid saturation within the pillars remains high, and at several locations increases to above the ambient liquid saturation because of vapor condensation. Vertically, the zone of substantially reduced matrix liquid saturation extends to 50 m directly above and below the drifts with ventilation, and up to 100 m without ventilation, except in areas of high ambient liquid infiltration.

With and without ventilation, large liquid and gas flow rates are predicted, primarily through the fractures. These flow rates are two to three orders of magnitude higher than the ambient flux at the repository drifts and are primarily driven by capillary pressure gradients due to drying of both the matrix and the fractures at the drifts. However, these large fluxes are confined to a period of less than 100 years. The liquid flux through the fractures towards the drifts may exceed 1,250–1,600 mm/yr without ventilation, and 270–300 mm/yr with ventilation, particularly in the low infiltration areas due to these high capillary pressure gradients. However, in both cases there is ample heat within the potential repository drifts that immediately vaporizes this liquid flux, at this early period. Therefore, this liquid does not directly seep into the drifts and has little impact on the waste canisters in the drifts. The liquid flow through matrix towards the drifts rises to maximum of 400–450 mm/yr without ventilation but is only 20–30 mm/yr with ventilation. This liquid flux is also vaporized by the repository heat. The TH Model predicts continued liquid

flow through the pillars, at a rate close to the ambient percolation flux for most of the thermal-loading period. In some locations the flow may be enhanced by condensate drainage for several hundred years. The models predict little impact on liquid and gas flux outside the potential repository domain.

INTENTIONALLY LEFT BLANK

3.13 OVERVIEW OF UNCERTAINTIES IN UZ FLOW AND TRANSPORT MODELS

The models and components that comprise the UZ Flow and Transport Model contain inherent uncertainties. The identification and propagation of these uncertainties is important for the appropriate treatment of the models used in TSPA-SR calculations. Table 3.13-1 lists the major model components described in the UZ PMR and the uncertainties in the model inputs and outputs. Uncertainties in conceptual models are also identified. It is important to note that input and output parameters have both variability and uncertainty. For example, infiltration is spatially variable at the surface of Yucca Mountain, and there is also uncertainty in the rates that are simulated because of uncertainty in the input parameters such as precipitation, soil depth, and evapotranspiration. Spatial and temporal variability and uncertainty are included in the models where they are important and could potentially have a significant effect on TSPA calculations for repository performance.

Table 3.13-1. Uncertainty in Major Model Components of the UZ Flow and Transport Model

Model Component	Input Parameter Uncertainty & Variability	Conceptual and Numerical Model Uncertainty	Output Parameter Uncertainty & Variability
Climate (USGS, 2000, U0005; Section 3.5 this PMR)	Uncertainty in Owens Lake sediment-accumulation rate, Devils Hole age data, time when Devils Hole record implies climate has changed, exact location of the past/present point in the Owens Lake record (analog climate proxy record)	Uncertainty in use of orbital cycles, interpretation of climate analogs	Upper and lower bounds for precipitation and temperature using different meteorological stations as analogs; duration of climate periods
Infiltration (USGS 2000, U0010; CRWMS M&O 2000, U0095; Section 3.5 this PMR)	Uncertainty in precipitation, bedrock permeability, soil depth, evapotranspiration, etc.; variability in precipitation, temperature, etc. at surface	Deterministic use of surface mass balance model	Spatial and temporal variability of infiltration (USGS 2000, U0010); uncertainty in infiltration rates based on input parameters (CRWMS M&O 2000, U0095)
UZ Properties (CRWMS M&O 2000, U0035; CRWMS M&O 2000, U0090; Section 3.6 this PMR)	Uncertainty in measured core data parameters and cross-correlation; spatial variability in properties	Uncertainty in calibration method (non-uniqueness); initial estimates; upscaling	Spatial variability in calibrated parameters; parameter calibration for different infiltration cases
UZ Flow (CRWMS M&O 2000, U0050; CRWMS M&O 2000, U0125; CRWMS M&O 2000, U0000; Section 3.7 this PMR)	Uncertainty and variability in hydrologic parameters (CRWMS M&O 2000, U0035); infiltration uncertainty (CRWMS M&O 2000, U0095)	Uncertainty in dual-permeability model (Doughty, 1999); active fracture model (Liu et al. 1998); perched water models, fault models (CRWMS M&O 2000, U0030; CRWMS M&O 2000, U0050); water table rise (CRWMS M&O 2000, U0125); refinement of mesh (CRWMS M&O (2000, U0000)	Spatial and temporal variability and uncertainty in flow fields

Model Component	Input Parameter Uncertainty & Variability	Conceptual and Numerical Model Uncertainty	Output Parameter Uncertainty & Variability
Ambient Geochemistry (CRWMS M&O 2000, U0085; Section 3.8 this PMR)	Uncertainty and spatial variability in precipitation (chloride concentrations); reactive surface area; kinetic and thermodynamic parameters	Uncertainty in thermodynamic and kinetic relationships; same conceptual uncertainties as UZ Flow Model	Spatial prediction of percolation; uncertainty in estimate of infiltration rates
Drift Seepage (CRWMS M&O 2000, U0075; CRWMS M&O 2000, U0080; CRWMS M&O 2000, U0120; Section 3.9 this PMR)	Spatial variability of fracture permeability (CRWMS M&O 2000, U0080); spatial variability and uncertainty in fracture permeability and van Genuchten α (CRWMS M&O 2000, U0075; CRWMS M&O 2000, U0080)	Uncertainty in heterogeneous fracture continuum model (CRWMS M&O 2000, U0080); effects of drift degradation (CRWMS M&O 2000, U0075); episodic flow (CRWMS M&O 2000, U0075); refinement of mesh; correlation of k and α	Variability and uncertainty in seepage distributions (seepage fraction, mean seep flow rate, standard deviation of seep flow rate, flow focusing factor) (CRWMS M&O 2000, U0120)
Drift-Scale THC (CRWMS M&O 2000, N0120/U0110; Section 3.10 this PMR)	Variability in hydrologic parameters—use of calibrated parameters (CRWMS M&O 2000, U0035); uncertainty in chemistry data (thermodynamic and kinetic data, chemistry of infiltrating water) (CRWMS M&O 2000, U0085)	Uncertainty in dual-permeability model to capture THC changes in matrix at fracture wall; use of middle-nonlithophysal parameters instead of lower-lithophysal parameters; refinement of mesh to capture THC changes in matrix at fracture wall	Temporal and spatial variability of water and gas composition, as well as uncertainty from different infiltration cases (CRWMS M&O 2000, N0120/U0110); temporal variability in water and gas composition for TSPA-SR
UZ Transport (CRWMS M&O 2000, U0060; CRWMS M&O 2000, U0065; CRWMS M&O 2000, U0160; Section 3.11 this PMR)	Uncertainty and variability in transport parameters (CRWMS M&O 2000, U0100); spatial and temporal variability and uncertainty in flow fields (CRWMS M&O 2000, U0050; CRWMS M&O 2000, U0125)	Uncertainty in matrix-diffusion model and particle tracking model (CRWMS M&O 2000, U0060; CRWMS M&O 2000, U0065; CRWMS M&O 2000, U0155; CRWMS M&O 2000, U0160); colloidal transport model (CRWMS M&O 2000, U0070); discretization of gradient for matrix diffusion (CRWMS M&O 2000, U0065); number of particles (CRWMS M&O 2000, U0160)	Spatial and temporal radionuclide mass flux at water table (CRWMS M&O 2000, U0065)
Mountain-Scale Thermal Hydrology (CRWMS M&O 2000, U0105; Section 3.12 this PMR)	Variability in hydrologic and thermal properties for different units (CRWMS M&O 2000, U0105)	Uncertainty in dual-permeability model for transient TH simulations (Doughty, 1999); active fracture model (Liu et al., 1998); perched water models, fault models (CRWMS M&O 2000, U0030; CRWMS M&O 2000, U0050); water table rise (CRWMS M&O 2000, U0125); Refinement of mesh (CRWMS M&O (2000, U0000)	Spatial and temporal variations in temperature and hydrologic conditions (CRWMS M&O 2000, U0105)

Table 3.13-2 provides a distilled list of uncertainties that are carried forward to TSPA calculations. The uncertainty in the parameters and models is included in TSPA calculations through the use of multiple realizations (statistically equivalent simulations) and stochastic sampling of parameters (i.e., a Monte Carlo approach). Each realization samples a set of parameters and/or models from given distributions for use in the TSPA calculation. The simulation of multiple realizations produces a range of performance results, with each outcome having a probability corresponding to its likelihood of occurrence. Thus, the uncertainty of the parameters and models leads to uncertainty in system performance. In the TSPA, the uncertainty in performance is analyzed, both in terms of its importance (i.e., is the uncertainty so great that it casts doubt on the safety of the repository?) and in terms of sensitivities (i.e., which parameter and submodel uncertainties have the greatest impact on the uncertainty in performance?).

In addition, uncertainties in the process-model outputs can also be addressed in abstracted TSPA models and analyses that use conservative assumptions. If insufficient evidence exists to provide a defensible range of values for a given parameter, values that bound the physical behavior or provide conservative estimates of the range of physical behavior are used. For example, a conservative factor that increases the seep flow rate by over 50% is used in the TSPA seepage-abstraction model to account for the uncertain impacts of drift degradation and rock bolts. For future climates, the water table is assumed to rise by a conservative amount in the abstracted UZ Flow Model, which will reduce travel times in the UZ. These conservative assumptions are intended to increase the defensibility of the models used in TSPA calculations given the inherent uncertainties in the actual system.

The uncertainty and variability in the model parameters are due, in part, to the natural variability and heterogeneity in the geological, hydrological, chemical, and mechanical systems that are difficult to characterize in situ, such as the precise fracture network in the UZ. Uncertainties in models may also be due to conditions that are difficult to predict, such as future climate states. Nevertheless, the previous sections in this PMR have provided the basis and confidence (through data collection, field tests, and calibration exercises) for using these parameters and models. In addition, the models and analyses that are used in TSPA calculations address remaining uncertainties through probabilistic simulations or appropriate conservative bounding assumptions.

Table 3.13-2. Uncertainties in UZ Flow and Transport Products for TSPA-SR

Model Component	Treatment of Uncertainty in Abstracted Product for TSPA-SR
Climate	<ul style="list-style-type: none"> • Future climates: three climates are assumed with uncertainty in precipitation and temperature (Section 3.5), which provide ranges of infiltration. • Duration of climates: Duration of the three climate states is assumed to be fixed and transitions are assumed to be instantaneous. Sensitivity studies of different climate durations are required.
Infiltration	<ul style="list-style-type: none"> • Three spatially variable infiltration maps (low, mean, and high) are used for each of the three climates (Section 3.5). • Monte Carlo simulations produced weightings for three infiltration cases used in each climate (Section 3.5).
UZ Flow	<ul style="list-style-type: none"> • Nine flow fields are used that correspond to low, mean, and high infiltration cases for each of the three climates (Section 3.7). • Assessment of uncertainty in the two perched water models revealed that both are similar. Only perched water model #1 is used for TSPA (Section 3.7). • Conservative estimate for water-table rise is used for future climates (Section 3.5 and CRWMS M&O 2000, U0125). • Weightings for three infiltration cases are used for each corresponding flow field.
Drift Seepage	<ul style="list-style-type: none"> • Distributions are developed for seepage fraction, mean seep flow rate, standard deviation of seep flow rate, and flow focusing factor based on process model results (Section 3.9). • A conservative factor is applied to increase seepage due to drift degradation and rock-bolt effects. • A conservative factor is applied to increase seepage to account for potential parameter correlations not included in process models.
Drift-Scale THC	<ul style="list-style-type: none"> • Water and gas compositions are abstracted and prescribed at four discrete time periods following emplacement based on drift-scale THC process model results (Section 3.10). Sensitivity studies may be required.
UZ Transport	<ul style="list-style-type: none"> • Distributions of K_d and K_c (for reversible colloids), colloid filtration parameter, aperture parameter, and diffusion coefficient are used to capture uncertainty (CRWMS M&O 2000, U0100; CRWMS M&O 2000, U0065). • Weightings for three infiltration cases are used for each corresponding flow field during transport simulations. • Uncertainty in location of source term is implemented through random nodal release within bins in the repository region that are consistent with bins used in the near-field environment. • Uncertainty in dispersion of radionuclides within the UZ is treated conservatively by collecting mass flux at the water table in the UZ and releasing it at "point locations" at the water table in the SZ model.
Mountain-Scale TH	<ul style="list-style-type: none"> • Based on results of the process model (Section 3.12 and CRWMS M&O 2000, U0105), TH effects on far-field flow and transport are not considered. Sensitivity studies may be required. Note that thermal impacts on the near-field environment are considered in the Near-Field Environment PMR.

4. RELATIONSHIP TO NRC ISSUE RESOLUTION STATUS REPORTS

4.1 SUMMARY OF THE KEY TECHNICAL ISSUES

As part of the review of site characterization activities, the Nuclear Regulatory Commission (NRC) has undertaken an ongoing review of information on Yucca Mountain site characterization activities to allow early identification and resolution of potential licensing issues. The principal means of achieving this goal is through informal, prelicensing consultation with the DOE. This approach attempts to reduce the number of, and to better define, issues that may be in dispute during the NRC licensing review, by obtaining input and striving for consensus from the technical community, interested parties, and other groups on such issues.

The NRC has focused prelicensing issue resolution on those topics most critical to the post-closure performance of the potential geologic repository. These topics are called Key Technical Issues (KTIs). Each KTI is subdivided into a number of subissues. The KTIs are:

- Activities Related to Development of the EPA Standard
- Container Lifetime and Source Term
- Evolution of the Near-field Environment
- Igneous Activity
- Radionuclide Transport
- Repository Design and Thermal Mechanical Effects
- Structural Deformation and Seismicity
- Thermal Effects on Flow (TEF)
- Total System Performance Assessment (TSPA) and Integration
- Unsaturated Zone (UZ) and Saturated Zone (SZ) Flow under Isothermal Conditions

Identifying KTIs, integrating their activities into a risk informed approach, and evaluating their significance for postclosure performance helps ensure that NRC's attention is focused on technical uncertainties that will have the greatest affect on the assessment of repository safety.

Early feedback among all parties is essential to define what is known, what is not known, and where additional information is likely to make a significant difference in the understanding of future repository safety. The Issue Resolution Status Reports (IRSRs) are the primary mechanism that the NRC staff uses to provide feedback to the DOE on the status of the KTI subissues. IRSRs focus on NRC acceptance criteria for issue resolution and the status of issue resolution, including areas of agreement or when the staff has comments or questions. Open meetings and technical exchanges between NRC and DOE provide additional opportunities to discuss issue resolution, identify areas of agreement and disagreement, and develop plans to resolve any disagreements.

KTIs are subdivided into a number of subissues. For most subissues, the NRC staff has identified technical acceptance criteria that the NRC may use to evaluate the adequacy of information related to the KTIs. The NRC has also identified two cross-cutting programmatic criteria that apply to all IRSRs related to the implementation of the Quality Assurance Program and the use of

expert elicitation. The following sections provide a summary level discussion of the KTIs by subissues (Section 4.2) and a discussion of the specific NRC acceptance criteria (Section 4.3).

4.2 RELATIONSHIP OF THE UZ FLOW AND TRANSPORT PMR TO THE KTIS

The UZ PMR provides technical analyses that relate to six of the KTIs and their associated IRSRs. Table 4.2-1 shows these KTIs and their subissues; subissues that relate directly to this PMR, hereafter referred to as the UZ PMR, are shown in italics. The KTIs and subissues that relate directly to the UZ PMR are discussed in the following sections.

4.2.1 Evolution of the Near-Field Environment

The near field is considered to be the part of the site for which changes in the physical and chemical properties (that result from construction of the underground facility or from heat generated by the emplaced radioactive waste) affect performance of the repository (NRC 1999a). Evolution of the near field is expected to include coupling of thermal, hydrological, and chemical (THC) processes that could affect parts of the mountain. These coupled processes could affect components of the natural and engineered barrier system (EBS) and thereby affect repository system performance. The introduction of repository construction material and waste package materials may also perturb the near-field environment.

The resolution of each of the subissues of this KTI (see Table 4.2-1) must adequately address four aspects of coupled processes:

- Identify the potential effects of coupled processes on performance
- Determine how the natural system will influence, and be influenced by, coupled processes
- Evaluate how the engineered materials will influence, and be influenced by, coupled processes
- Determine the adequacy of any representation of the effects of coupled processes in performance assessment.

Two of the subissues for the near-field environment KTI relate to the UZ PMR (see Table 4.2-1), as described in the following subsections. PMRs on the EBS, the near-field environment, and waste-form degradation also provide information relevant to the evolution of the near-field environment.

4.2.1.1 Effects of Coupled THC Processes on Seepage and Flow

The NRC notes that previous performance assessments have included limited analyses of the effects of coupled processes for the representation of seepage and groundwater flow (NRC 1999a, p. 15). For example, coupled THC processes that affect seepage and flow were not explicitly addressed in the Total System Performance Assessment (TSPA) that was completed

for the Viability Assessment (VA) (DOE 1998). There was no abstraction of the effect of coupled THC on seepage and flow and no corresponding sensitivity and uncertainty analysis to evaluate the need for additional data (NRC 1999a, p. 107). The NRC also notes that use of homogeneous hydrological properties in modeling coupled processes did not account for the spatial and temporal variability in fracture flow.

Table 4.2-1. Issue Resolution Status Report/Key Technical Issues (IRSR/KTI) Related to the UZ PMR

NRC Key Technical Issues	Subissues
Evolution of the Near-field Environment	<i>Coupled thermal-hydrological-chemical (THC) processes effects on seepage and flow</i> Coupled THC effects on the waste package chemical environment Coupled THC effects on the chemical environment for radionuclide release <i>Coupled THC processes effects on radionuclide transport</i> Coupled THC processes effects on potential nuclear criticality in the near field
Radionuclide Transport	<i>Radionuclide transport through porous rock</i> Radionuclide transport through alluvium <i>Radionuclide transport through fractured rock</i> Nuclear criticality
Structural Deformation and Seismicity	Faulting Seismic hazard <i>Fracturing and structural framework of the geologic setting</i> Tectonics and crustal conditions
Thermal Effects on Flow (TEF)	Is DOE's thermal testing program, including performance confirmation, sufficient to evaluate the potential for thermal reflux to occur in the near field? <i>Is DOE's thermal modeling approach sufficient to predict the nature and bounds of TEF in the near field?</i> <i>Does DOE's total system performance assessment (TSPA) adequately account for TEF?</i>
Total System Performance Assessment (TSPA) and Integration	System Description and demonstration of multiple barriers <i>Scenario analysis</i> <i>Model abstraction</i> Demonstration of the Overall Performance Objection
UZ and SZ Flow Under Isothermal Conditions	<i>Future climates</i> <i>Hydrological effects of climate change</i> <i>Shallow infiltration</i> <i>Deep percolation</i> Saturated zone <i>Matrix diffusion UZ/SZ</i>

NOTE: Italicized subissues are addressed in the UZ PMR

Analyses have been completed to evaluate the effects of various coupled processes on seepage into drifts, including coupled THC processes (see Section 3.10). A fully coupled drift-scale THC model has been developed. Simulations using this model show only very small changes in hydrological properties, suggesting that thermal-chemical effects on seepage do not need to be represented in the abstraction of seepage.

4.2.1.2 Effects of Coupled THC Processes on Radionuclide Transport

The evolution of the near-field environment influences two abstractions of UZ flow and transport processes that are important to this subissue. These are (1) the distribution of mass flux between fracture and matrix and (2) radionuclide retardation in fractures in the UZ. The NRC staff has no major concerns with DOE's analyses of the distribution of mass flux between fracture and matrix and retardation in fractures in the UZ (NRC 1999a, p. 140).

Section 3.13 summarizes modeling studies of transport in the UZ (see Section 4.2.2). Note that current transport models do not take credit for retardation in fractures because of relatively rapid travel times and limited data on the details of fracture mineralogy. This approach is conservative.

4.2.2 Radionuclide Transport

The primary objective of the Radionuclide Transport KTI is to evaluate the processes that may affect radionuclide transport from the repository to the biosphere (NRC 1999b). Transport in the near-field environment is considered in the IRSR/KTI for evolution of the near-field environment (Section 4.2.1). The key elements of the Radionuclide Transport KTI are retardation of radionuclides in fractures and the matrix in the UZ and retardation in the saturated zone (NRC 1999b, p. 5). The IRSR focuses on sorption and other chemical processes that affect transport and colloid-facilitated transport. Two mechanisms that can reduce radionuclide concentrations along flow paths, matrix diffusion and dilution, are evaluated separately in the IRSR/KTI for UZ and SZ Flow under Isothermal Conditions (Section 4.2.6). Resolution of the KTI for radionuclide transport requires adequate characterization of the physical and chemical processes that affect radionuclide transport (NRC 1999b, p. 3).

Two of the subissues for this KTI relate to the UZ PMR, as described in the following subsections. The PMR on SZ flow and transport also provides information relevant to radionuclide transport.

4.2.2.1 Radionuclide Transport through Porous Rock

This subissue focuses on the extent to which radionuclides can sorb onto minerals in the porous matrix and filtration of colloidal and particulate contaminants (NRC 1999b, p. 3). It addresses physical transport processes, chemical processes, and heterogeneities (NRC 1999b, p. 12). Issues related to physical transport processes include the appropriate conceptual models for fracture-matrix interaction, the range and dependencies of parameters associated with fracture-matrix interactions, the effects of both long and short term transient flow conditions, and the expected magnitude of lateral and longitudinal dispersion. Chemical issues include the appropriateness of the minimum K_d approach, the amount of sorption expected in fractures, and the contribution of

colloids to radionuclide flux. Issues related to heterogeneities in the UZ include the spatial distribution of infiltration, areal variations in amounts and compositions of zeolites, and the appropriate scale of heterogeneities.

The NRC indicates that methods proposed to treat sorption are generally acceptable (NRC 1999b, p. 80). In some cases, particularly for neptunium, adequate investigations have been completed. Additional work may be needed, such as batch sorption experiments for a few radionuclides, crushed tuff and intact rock column experiments for some radionuclides, and analyses using theoretical models and experimental data to demonstrate that sorption coefficients are compatible with the range of geochemical conditions expected in the postclosure time-frame.

This PMR documents the current representation of UZ transport (see Section 3.11). It includes the following improvements to the UZ Transport Model:

- Enhancement of the UZ/EBS transport interface and refinement of the UZ grid between the repository and the water table
- A matrix diffusion algorithm that recognizes finite fracture spacing effects and an improved model for colloid transport
- Improved justification for the treatment of sorption, chain decay, radionuclide screening, and gas-phase radionuclide transport.

Current modeling provides better justification for coupling with the EBS transport at the potential repository and SZ transport at the water table, with releases spread over a more realistic area compared to the VA analysis. The effects of repository heating have also been considered in the UZ transport model. The improved colloid transport model was developed in conjunction with modeling conducted for the Nevada Test Site (NTS) (Section 3.11), using data from the NTS to calibrate the colloid model.

The issue of heterogeneity requires proper scaling from laboratory-derived parameters; this has been evaluated with respect to the Calico Hills vitric unit (Section 3.8).

4.2.2.2 Radionuclide Transport through Fractured Rock

This subissue evaluates radionuclide transport in fractured rock where there is a potential for preferential pathways for transport and limited radionuclide-rock interactions. For the UZ, important factors include percolation rate, partitioning of flow between fractures and matrix, and sorption coefficients (NRC 1999b, p. 11). Many of the process parameters considered in this subissue are the same as those identified for the subissue on radionuclide transport through porous rock (Section 4.2.2.1). The NRC notes that preliminary experiments suggest that some sorption does occur in fractures (NRC 1999b, p. 94).

Current transport models (Section 3.11) do not take credit for retardation in fractures because of relatively rapid travel times and limited data on the details of fracture mineralogy. This is a conservative assumption.

4.2.3 Structural Deformation and Seismicity

The objective of this KTI is to evaluate the tectonic features, events, and processes (FEPs) that may affect performance of the potential repository (NRC 1999c). One of the subissues for this KTI relates to the UZ PMR. The PMR on disruptive events provides information relevant to the remaining subissues.

4.2.3.1 Fracturing and Structural Framework of the Geologic Setting

The NRC will evaluate alternative modeling approaches for distribution and properties of fractures that are consistent with current data and geologic understanding. They will review representations of fracture data and properties in the UZ models and their abstractions to evaluate the degree to which data on fracture variability are honored, the justification for excluding data, and the degree to which there is adequate integration of fracture data into the UZ models (NRC 1999c, p. 51).

The NRC did not consider the values assigned to fracture-continuum hydraulic properties in the TSPA-VA (DOE 1998) parameter sets justified by the distribution of apertures in the model-grid scale. They were concerned with the limited fracture characterization in key stratigraphic units in the UZ, the potential bias in ESF fracture measurements by the one-meter cut-off, and low-angle fractures not being properly represented (NRC 1999c, pp. 113–114). Thus, uncertainties in the representation of fractures and their properties were not reasonably bounded. Data used in the abstractions were not representative, and alternative modeling approaches were not adequately considered (NRC 1999c, p. 117). The NRC also states that the assumption of spatial homogeneity in fracture distribution in the UZ is not supported by sufficient field evidence (NRC 1999c, p. 107).

Section 2.2 of the UZ PMR documents current data and analyses from ambient field testing in the ESF. These data and analyses provide an enhanced framework in which to refine the conceptual model of matrix and fracture processes in the UZ. Fracture property estimates are based on permeability data from *in situ* air-injection tests conducted in four surface boreholes and boreholes in alcoves of the ESF, porosity data from gas-tracer tests in boreholes in Alcove 5, and fracture mapping from the ESF, the ECRB, and surface boreholes. The YMP is considering reevaluating the decision to exclude small-scale data, although the impact on the mountain-scale and the drift-scale calibrated properties is not likely to be large.

4.2.4 Thermal Effects on Flow (TEF)

This KTI focuses on the estimation of temperature, moisture content, and humidity at the waste package surface and estimation of temperature and thermally driven water flux with respect to transport of radionuclides away from failed waste packages (NRC 1999d, p. 3). This includes evaluating the redistribution of moisture driven by heat that may result in periods of dryness in the potential repository and in channeling of moisture towards waste packages. The UZ PMR evaluates parameters and processes that are key to understanding the TH behavior of the potential repository, such as percolation flux, seepage into drifts, and the effect of coupled TH processes

on seepage. Other technical concerns related to this KTI are addressed in the Near-Field Environment and EBS PMRs.

Two of the KTI subissues apply to this PMR, as discussed in the following subsections. The PMRs on the near-field environment and the EBS provide additional information related to these subissues and the remaining subissues.

4.2.4.1 Is DOE's Thermal Modeling Approach Sufficient to Predict the Nature and Bounds of TEF in the Near Field?

This subissue addresses the ability of the DOE's TH process models to represent thermally driven flow in the near field. For example, these models should adequately account for the effects of heterogeneities in the models (including focused recharge) and discrete geologic features (NRC 1999d, pp. 66–67). The models do not adequately account for the effects of spatially variable infiltration coupled with the effect of variable heat load at the repository edge, seepage into drifts, and capillary diversion (NRC 1999d, pp. 68–70).

As discussed in Section 4.2.1.1, analyses have been completed to evaluate the effects of various coupled processes on seepage into drifts, including coupled THC processes (see Section 3.10). Current analyses consider the effects of mineral dissolution and precipitation, CO₂ exsolution and transport in the region surrounding the drift, the potential for forming zones of calcite, silica, or other minerals, the resulting changes to porosity, and permeability, and the potential effects on seepage.

4.2.4.2 Does DOE's TSPA Adequately Account for TEF?

This subissue addresses adequate representation of TH processes in the TSPA. Model abstraction should conservatively bound the predictions from the process models. Process models in TSPA-VA do not adequately incorporate processes such as seepage into drifts under ambient conditions and refluxing into drifts during and after the thermal period (NRC 1999d, p. 77). When these processes have been adequately represented in the process models and abstraction, sensitivity analyses should be completed to assess the need for additional data with respect to TEF (NRC 1999d, p. 78).

The UZ PMR summarizes a systematic modeling study that evaluates the effects of TH processes in the UZ (Section 3.12). The model provides mountain-scale thermal response (based on infiltration rate), thermal load, numerical discretization, and the effects of ventilation. It simulates the potential impact of thermal perturbations from emplaced waste on the natural hydrological system, including a representation of heat-driven processes in the far field.

The seepage abstraction has been enhanced to include additional effects, such as changes in drift shape, preferential pathways resulting from degraded rock bolts, and focusing of flow. THC processes have been found to have little effect on seepage (Section 3.10.12).

4.2.5 TSPA and Integration

The objective of this KTI is to describe an acceptable methodology for conducting performance assessments of repository performance and using these assessments to demonstrate compliance with the overall performance objective and requirements for multiple barriers (NRC 2000, p.3). Three of the subissues for this KTI relate to the UZ PMR, as described in the following subsections.

4.2.5.1 System Description and Demonstration of Multiple Barriers

This subissue addresses the demonstration of multiple barriers. This includes the identification of natural and engineered barriers important to isolation, the capability of these barriers to isolate waste, and the identification of processes that may degrade the engineered barriers and thus adversely affect performance of the natural barriers (NRC 2000, p. 4). DOE's TSPA, including scenario analysis (Section 4.2.5.2), model abstractions (Section 4.2.5.3) and transparency and traceability (this section) will support the demonstration of multiple barriers (NRC 2000, p. 17). Specific technical acceptance criteria have not yet been developed for the demonstration of multiple barriers.

This subissue also addresses the NRC's staff expectation on the contents of DOE's TSPA and supporting documents (NRC 2000, p. 4). It provides criteria to evaluate the transparency and traceability of the DOE's TSPA, of the identification and classification of features, events, and processes (FEPs), and of the abstractions for TSPA. Finally, this subissue focuses on the transparency, traceability and validity of data used to support TSPA and of code design and the flow of data in the TSPA (NRC 2000, pp. 10-17).

With respect to transparency and traceability, the YMP is committed to improving the documentation of the technical analyses that support the TSPA. The development of this PMR, and the associated AMRs, focused on improving the transparency and traceability from initial data collection through the analysis and incorporation of data and analyses into the process model for UZ flow and transport to the abstraction of the process models for use in the TSPA. Attachment 1 to the UZ PMR summarizes the data used in the UZ PMR, including the major inputs and outputs with specific references to the technical data bases that store the data. Section 1.3 summarizes the quality assurance status of data and software.

4.2.5.2 Scenario Analysis

This subissue focuses on the process of identifying, screening, and selecting FEPs for inclusion in the TSPA. FEPs that could affect future system performance are used to formulate scenarios. This includes construction of scenario classes, assignment of probabilities to scenario classes, and their incorporation into the TSPA. This is a key factor in ensuring the completeness of the TSPA (NRC 2000, p. 4).

A systematic method was applied to identify and screen FEPs for UZ flow and transport phenomena. One hundred and fifteen FEPs have been identified and grouped into two broad categories of primary and secondary FEPs. The primary FEPs capture the issues associated with

the secondary FEPs. The FEPs are further divided into “included” and “excluded” FEPs. Included FEPs are those directly represented in TSPA models and process models that support the TSPA. Analyses have focused on the identification and screening of FEPs; this work partially addresses this subissue (see Section 1.2.3). The construction and evaluation of scenario classes will be documented in TSPA-SR.

4.2.5.3 Model Abstraction

This subissue focuses on the information and technical approaches needed to develop defensible model abstractions and their integration into TSPA. The following aspects of model abstraction are addressed under this subissue: data used in the development of conceptual approaches or process models, the abstracted models, and estimates of system performance (NRC 2000, p. 4). Specifically, this subissue requires documentation of data used to develop conceptual or process models for model abstractions, verification of the consistency of the abstractions, and explanation of their integration (such as coupling and dependencies) into the TSPA.

For each model abstraction for unsaturated zone flow and transport models, this PMR addresses the NRC’s five general principles underlying the technical acceptance criteria: data and model justification, data uncertainty and verification, model uncertainty, model verification, and integration (NRC 2000, p. 32). The PMR summarizes: 1) data available to support the conceptual basis of process models and abstractions, 2) the basis for bounding assumptions and representations of uncertainties and parameter variabilities, 3) alternative conceptual models, 4) abstractions based on and consistent with the underlying process models, and 5) incorporation of design features, physical phenomena, and couplings and use of consistent assumptions throughout the abstraction process. To address consistency in assumptions, the AMRs that document assumptions have been subjected to interdisciplinary review to help ensure that assumptions are applied consistently to the extent practicable. In addition, the PMRs have been reviewed by a single team whose main objective was to identify inconsistencies among the PMRs. These measures provide confidence that consistent assumptions are used in the abstraction process, as appropriate.

4.2.6 UZ and SZ Flow under Isothermal Conditions

The main objective of this KTI is to evaluate all aspects of the ambient hydrological regime at Yucca Mountain that may adversely impact the performance of a potential repository (NRC 1999e). Another objective is to assess the adequacy of the characterization of key hydrological processes and features at the site and in the region that may adversely affect performance.

Four of the subissues for this KTI relate to the UZ PMR, as described in the following subsections. The PMR on SZ flow and transport provides information on the subissue for the SZ.

4.2.6.1 Future Climates and Hydrological Effects on Climate Change: What Is the Likely Range of Future Climates at Yucca Mountain and What Are the Likely Hydrological Effects of Climate Change?

The NRC considers all acceptance criteria for these subissues (NRC 1999e, pp. 170–174) closed with the exception of the programmatic criterion on adequacy of the quality assurance program. This PMR summarizes improvements to the representation of future climate for the Yucca Mountain site since the VA. Section 3.5 provides a more defensible climate model that is focused on 10,000 years and includes upper- and lower-bound climate analogs as compared to TSPA-VA.

4.2.6.2 Present-Day Shallow Infiltration: What Is the Estimated Amount and Spatial Distribution of Present-Day Shallow Infiltration?

The NRC staff agrees with the use of multipliers of the mean annual infiltration (MAI) to incorporate the uncertainty of MAI estimates into the abstraction of the infiltration model (NRC 1999e, p. 176). They note that the infiltration model does not account for surface runoff and shallow lateral flow, potentially impacting calculations of MAI. The NRC is also concerned that the methodology used to assign probabilities to the MAI multipliers is biased towards producing low values for the MAI. All other technical acceptance criteria are considered closed.

The Infiltration Model (Section 3.5) has been refined to provide an improved surface water model and to enhance the ability to model future climate states by considering temperature dependence, vegetation dependence, and snow pack. These improvements provide a better representation of infiltration under future climates and a more defensible basis for the uncertainty in the Infiltration Model to address the NRC concerns. The methodology for assigning probabilities to the MAI multipliers has been enhanced to address the bias towards producing low values for the MAI.

4.2.6.3 Deep Percolation: What Is the Estimated Amount and Spatial Distribution of Percolation through the Proposed Repository Horizon (Present Day and through the Period of Repository Performance)?

The NRC has several concerns with respect to the representation of deep percolation in the UZ. The analyses do not provide a reasonable bound on the uncertainty in the distribution of UZ flow between fractures and the rock matrix (NRC 1999e, p. 181). In addition, fast-path contributions to flow are not adequately represented in the UZ Flow Model (NRC 1999e, p. 179). The effects of climate-induced change (temperature, soil, and vegetation) have not been addressed in defining the bounds on percolation flux and seepage. Uncertainty in flow paths below the repository needs to be addressed and incorporated into the TSPA.

A new active fracture model for fracture-matrix interaction has been used to provide an improved theoretical basis for fracture-matrix interaction as compared to TSPA-VA (DOE 1998). The model describes gravity-dominated, nonequilibrium, preferential liquid-water flow through fractures, including a reduction factor for the interface area that conducts flow between fractures and matrix. As noted in Section 4.2.6.1, improvements have been made to the representation of climate states to address NRC concerns.

The NRC is also concerned that the drift-scale seepage model in the VA did not incorporate several potentially important processes, such as multiple scales of heterogeneity in the hydraulic properties around the drift, modifications to drift geometry from rock fall, thermally induced geochemical changes, and episodic percolation flux (NRC 1999e, p. 180). This PMR summarizes the current seepage model (Section 3.9). This model has been enhanced to incorporate data from niche testing, establish a range of flux values for the upper boundary of the model, and provide a simplified representation of partial collapse of a drift. The model evaluates drift seepage under long-term, steady-state, and episodic conditions for a range of parameters and conditions. Alternative models of flow and transport around and through the perched water beneath the repository have been analyzed (Section 3.7).

4.2.6.4 Matrix Diffusion: To what Degree Does Matrix Diffusion Occur in the UZ and SZ?

If the DOE takes credit for matrix diffusion in the UZ, then the NRC will expect predictions of transport to be consistent with geochemical and isotopic data for the site (NRC 1999e, p. 191). The NRC is concerned about the application of matrix diffusion in the residence-time transfer function (RTTF) approach to modeling transport. This approach has a bias towards predicting faster diffusion from fractures into the matrix. If matrix diffusion is incorporated into UZ transport models, the DOE should (NRC 1999e, p. 192):

- Implement small-scale discrete-fracture models to verify the RTTF approach
- Scale the assumed value for the matrix diffusion coefficient for radionuclide diffusion to account for diminished transport resulting from reduced matrix saturation and reduced fracture-matrix interface area.

The UZ PMR summarizes the current approach to modeling matrix diffusion in the UZ. The former model for matrix diffusion was based on the assumption that fracture spacing is large relative to the average diffusion penetration depth from fractures into the matrix. The matrix-diffusion model has been enhanced to account for the effects of finite fracture spacing. UZ transport modeling assumes that the active fracture model appropriately accounts for reduced fracture-matrix interaction. The current model also assumes that effects of flow in the matrix are negligible with respect to exchange between fractures and matrix through matrix diffusion.

4.3 NRC ACCEPTANCE CRITERIA

Specific technical acceptance criteria for each subissue that relates to this PMR are summarized in Table 4.3-1, along with the approach to addressing the criteria and sections of the PMR that describe these approaches.

The UZ PMR also addresses the NRC's programmatic criteria for quality assurance and the use of expert elicitation. These programmatic criteria apply to all subissues and are not repeated under each subissue in Table 4.3-1.

The acceptance criteria for quality assurance addresses DOE's implementation of an adequate quality assurance program. The UZ PMR was developed in accordance with project procedures

for documenting data, analyses, models, and/or computer codes and preparing and reviewing technical reports (see Section 1.3). The programmatic criterion for expert elicitation specifies that expert elicitation should be conducted in accordance with NUREG-1563 (Kotra et al. 1996) or other acceptable approaches. An expert elicitation on the UZ flow model was completed in 1997 (see Section 1.2). This elicitation was conducted and documented following the NRC guidance on the use of expert elicitation (Kotra et al. 1996). No additional expert elicitations have been completed for the UZ PMR.

Table 4.3-1. Issue Resolution Status Reports, Subissues, Technical Acceptance Criteria, and PMR Approach (NRC 1997, 1999a-e, 2000)

NRC Technical Acceptance Criteria	PMR Approach and Section Reference
IRSR: Evolution of the Near-field Environment	
Subissue 1 - Effects of coupled THC processes on seepage and flow	
Data and model justification acceptance criteria for Subissue 1	
1 - Available data relevant to both temporal and spatial variations in conditions affecting coupled THC effects on seepage and flow were considered.	The TSPA-VA did not explicitly consider the effects of coupled THC processes; the evaluation of coupled THC effects is documented in this PMR. Attachment I summarizes available site data. Section 3.10 documents the abstraction of coupled THC effects for TSPA, based on the process modeling results presented in the same section.
2 - DOE's evaluation of coupled THC processes properly considered site characteristics in establishing initial and boundary conditions for conceptual models and simulations of coupled processes that may affect seepage and flow.	Attachment I summarizes available data. These data on the site characteristics were used to establish initial and boundary conditions for the evaluation of THC effects on seepage and flow in the near field (Section 3.10).
3 - Sufficient data were collected on the characteristics of the natural system and engineered materials, such as the type, quantity, and reactivity of material, to establish initial and boundary conditions for conceptual models and simulations of THC coupled processes that affect seepage and flow.	Attachment I summarizes available data. The THC model incorporates site data to establish initial and boundary conditions and incorporates specific aspects of the design, including in-drift geometry, drift spacing, and the TH properties of the components of the EBS, such as waste packages and invert (Section 3.10). The current design does not include concrete liners in the emplacement drifts limiting the potential effects of interactions between concrete and tuff on seepage and flow.
4 - Sensitivity and uncertainty analyses (including consideration of alternative conceptual models) were used to determine whether additional new data are needed to better define ranges of input parameters.	Sensitivity and uncertainty analyses will be included in TSPA-SR.
5 - If the testing program for coupled THC processes on seepage and flow is not complete at the time of license application, or if sensitivity and uncertainty analyses indicate additional data are needed, DOE will identify specific plans to acquire the necessary information as part of the performance confirmation program.	The performance confirmation plan addresses coupled THC effects on seepage and flow. Rock mass cooling response, coupled process testing, and seepage testing under heated environments are planned for the pre-emplacement period. Longer term testing for seepage and near-field THC testing and monitoring around selected emplacement drifts and under simulated postclosure conditions is also addressed (CRWMS M&O 2000c, Appendix G).
Data uncertainty and verification acceptance criteria for Subissue 1	
1 - Reasonable or conservative ranges of parameters or functional relations were used to determine effects of coupled THC processes on seepage and flow. Parameter values, assumed ranges, probability distributions, and bounding assumptions are technically defensible and reasonably account for uncertainties.	The TSPA-VA did not explicitly consider the effects of coupled THC processes; the evaluation of the effects of coupled THC processes is documented in this PMR. Section 3.10.3 discusses ranges in the characteristics of the natural system that were used to evaluate the effects of THC processes on seepage and flow and the rationale for these ranges.

NRC Technical Acceptance Criteria	PMR Approach and Section Reference
Data uncertainty and verification acceptance criterion for Subissue 1, continued	
2 - Uncertainty in data due to both temporal and spatial variations in conditions affecting coupled THC effects on seepage and flow were considered.	Section 3.10.6 discusses the uncertainty in data affecting THC coupled processes on seepage and flow.
3 - DOE's evaluation of coupled THC processes properly considered the uncertainties in the characteristics of the natural system and engineered materials, such as type, quantity, and reactivity of material, in establishing initial and boundary conditions for conceptual models and simulations of THC coupled processes that affect seepage and flow.	Section 3.10.6 discusses uncertainties in the characteristics of the natural system. Engineered materials are discussed in the PMR on the engineered barrier system.
4 - The initial conditions, boundary conditions, and computational domain used in sensitivity analyses involving coupled THC effects on seepage and flow were consistent with available data.	Sensitivity analyses will be included in TSPA-SR.
5 - DOE's performance confirmation program should assess whether the natural system and engineered materials are functioning as intended and anticipated with regard to coupled THC effects on seepage and flow.	The performance confirmation plan addresses coupled THC effects on seepage and flow. Rock mass cooling response, coupled process testing, and seepage testing under heated environments are planned for the pre-emplacment period. Longer term testing for seepage and near-field THC testing and monitoring around selected emplacement drifts and under simulated postclosure conditions is also addressed (CRWMS M&O 2000c, Appendix G).
Model uncertainty acceptance criteria for Subissue 1	
1 - Appropriate models, tests, and analyses were used that are sensitive to the THC couplings under consideration for both natural and engineered systems, as described in the following examples. The natural setting data indicate processes that should be evaluated include: (i) zeolitization of volcanic glass, which could affect flow pathways; (ii) precipitation of calcite and opal on the footwall of fracture surfaces and the bottoms of lithophysal cavities, which indicates gravity-driven flow in open fractures that could affect permeability and porosity; and (iii) potential dehydration of zeolites and vitrophyre glass, which could release water affecting heat and fluid flow. The effects of THC coupled processes that may occur due to interactions with engineered materials or their alteration products include: (i) changes in water chemistry that may result from interactions between cementitious materials and groundwater, which, in turn, may affect seepage and flow; (ii) dissolution of the geologic barrier (e.g. tuff) by a hyperalkaline fluid that could lead to changes in the hydraulic properties of the geologic barrier; and (iii) precipitation of calcite or calcium-silica-hydrate phases along fracture surfaces as a result of migration of a hyperalkaline fluid that could affect hydraulic properties.	Attachment I summarizes available site data. Section 3.10 summarizes data, analyses, and models that were used to evaluate THC processes on the natural system. The purpose of the THC seepage model is to evaluate the effects of THC processes in the rock around the emplacement drift on seepage water chemistry, gas-phase composition, and the potential effects of THC processes on UZ flow and transport. This model evaluates the effects of mineral dissolution and precipitation, the effects of CO ₂ exsolution and transport in the region surrounding the drift, the potential for forming zones of calcite, silica or other minerals, the resulting changes in porosity and permeability, and the potential effects on seepage. See also the PMR on the near field environment.

NRC Technical Acceptance Criteria	PMR Approach and Section Reference
2 - Given the current design of the repository, it will be acceptable to ignore the potential effects of microbial processes on seepage and flow.	The DOE agrees that the potential effects of microbial processes on seepage and flow are not significant, given the current design (Section 1.2.3, Assumption 3) (CRWMS M&O 2000, EBS PMR; CRWMS M&O 2000, WFD PMR).
Model uncertainty acceptance criteria for Subissue 1, continued	
3 - Alternative modeling approaches consistent with available data and current scientific understanding were investigated, and their results and limitations were appropriately considered.	Section 3.10.7 addresses the alternative conceptual model proposed by Matyskiela (1997).
4 - DOE provided a reasonable description of the mathematical models included in its analyses of coupled effects on seepage and flow. The description should include a discussion of alternative modeling approaches not considered its final analysis and the limitations and uncertainties of the chosen model.	Section 3.10 summarizes the mathematical models used; an alternative conceptual model is discussed in Section 3.10.7.
Model verification acceptance criteria for Subissue 1	
1 - The mathematical models for coupled THC effects on seepage and flow are consistent with conceptual models based on inferences about near-field environment, field data and natural alteration observed at the site, and expected engineered materials.	Section 3.10 summarizes the mathematical models used to evaluate coupled THC effects on seepage and flow.
2 - DOE appropriately adopted accepted and well-documented procedures to construct and test the numerical models used to simulate coupled THC effects on seepage and flow.	Procedures were followed, consistent with the governing quality assurance requirements (see Chapter 1).
3 - Abstracted models for coupled THC effects on seepage and flow were based on the same assumptions and approximations shown to be appropriate for closely analogous natural or experimental systems. Abstracted model results were verified through comparison to outputs of detailed process models and empirical observations. Abstracted model results are compared with different mathematical models to judge robustness of results.	Abstractions in Section 3.10 were derived from the underlying process models described in the UZ PMR.
Integration acceptance criteria for Subissue 1	
1 - DOE has considered all the relevant features, events, and processes. The abstracted models adequately incorporated design features, physical phenomena, and couplings, and used consistent and appropriate assumptions throughout.	Section 1.2.3 discusses the relevant features, processes and events. Included FEPS are directly represented in the process models and abstractions that support TSPA and discussed in other sections of the PMR corresponding to the specific models.
2 - Models reasonably accounted for known temporal and spatial variations in conditions affecting coupled THC effects on seepage and flow.	Section 3.10 summarizes the parameter ranges used in the THC model and provides a rationale for these ranges. Section 3.10.4 describes the process of validating the THC model with results from the drift scale test.

NRC Technical Acceptance Criteria	PMR Approach and Section Reference
Integration acceptance criteria for Subissue 1, continued	
3 - Not all THC couplings may be determined to be important to performance, and DOE may adopt assumptions to simplify PA analyses. If potentially important couplings are neglected, DOE should provide a technical basis for doing so. The technical basis could include activities, such as independent modeling, laboratory or field data, or sensitivity studies.	The DOE agrees that simplifying assumptions may be appropriate if not all the THC couplings are determined to be important to performance and will provide the technical basis for the simplifying assumptions.
4 - Where simplifications for modeling coupled THC effects on seepage and flow were used for PA analyses instead of detailed process models, the bases used for modeling assumptions and approximations were documents and justified.	Section 3.10 11 documents the basis for the abstraction of coupled THC effects on seepage and flow.
Subissue 2 - Waste package chemical environment (Waste Package Degradation PMR)	
Subissue 3 - Effects of THC processes on the chemical environment for radionuclide release (Waste Form /Engineered Barrier System PMRs)	
Subissue 4 - Effects of coupled THC processes on the radionuclide transport through engineered and natural barriers	
Data and model justification acceptance criteria for Subissue 4	
1 - Available data relevant to both temporal and spatial variations in conditions affecting coupled THC effects on transport of radionuclides in the near field were considered.	The TSPA-VA did not explicitly consider the effects of coupled THC processes; the evaluation of coupled THC effects are documented in this PMR. Attachment I summarizes available data; Section 3.10 describes how relevant data were incorporated into the modeling.
2 - DOE's evaluation of coupled THC processes properly considered site characteristics in establishing initial and boundary conditions for conceptual models and simulations of coupled processes that may affect radionuclide transport in the near field.	The evaluation of coupled THC processes in Section 3.10 considered site characteristics in establishing initial and boundary conditions for conceptual models and simulation of coupled processes. See also the PMRs on near field environment and EBS.
3 - Sufficient data were collected on the characteristics of natural system and engineered materials, such as the type, quantity, and reactivity of material, in establishing initial and boundary conditions for conceptual models and simulations of THC coupled processes that affect transport of radionuclides in the near field.	Attachment I summarizes available site data. The THC model incorporates site data to establish initial and boundary conditions and incorporates specific aspects of the design, including in-drift geometry, drift spacing, and the TH properties of the components of the EBS, such as waste packages and invert (Section 3.10). The current design does not include concrete liners in the emplacement drifts limiting the potential effects of interactions between concrete and tuff on seepage and flow (CRWMS M&O 2000, EBS PMR; CRWMS M&O 2000, WFD PMR).
4 - A nutrient and energy inventory calculation should be used to determine the potential for microbial activity that could adversely affect radionuclide transport through engineered and natural barriers.	The potential effects of microbial processes on transport away from a drift are not considered significant, given the current design (Section 1.2.3, Assumption 3). See the PMRs on the engineered barrier system and waste form.

NRC Technical Acceptance Criteria	PMR Approach and Section Reference
Data and model justification acceptance criteria for Subissue 4, continued	
5 - Should microbial activity be sufficient to allow microbial effects on transport of radionuclides through engineered and natural barriers, then the time-history of temperature, humidity, and water saturation in engineered and natural materials should be used to constrain the probability for these effects.	See the PMRs on the engineered barrier system and waste form.
6 - Sensitivity and uncertainty analyses (including consideration of alternative conceptual models) were used to determine whether additional new data are needed to better define ranges of input parameters.	Sensitivity and uncertainty analyses will be included in TSPA-SR.
7 - If the testing program for coupled THC processes on the chemical environment for radionuclide release from the engineered barrier system is not complete at the time of license application, or if sensitivity and uncertainty analyses indicate additional data are needed, DOE has identified specific plans to acquire the necessary information as part of the performance confirmation program.	Although THC effects on radionuclide transport have been determined not to be important to performance, the performance confirmation plan contains testing during the pre-emplacement period to confirm this assumption (CRWMS M&O 2000c, Appendix G).
Data uncertainty and verification acceptance criteria for Subissue 4	
1 - Reasonable or conservative ranges of parameters or functional relations were used to determine effects of coupled THC processes on transport of radionuclides in the near field. Parameter values, assumed ranges, probability distributions, and bounding assumptions are technically defensible and reasonably account for uncertainties.	The TSPA-VA did not explicitly consider the effects of THC processes; the evaluation of coupled THC effects is documented in this PMR. Attachment 1 summarizes available site data. Section 3.10 discusses the range of parameters in the characteristics of the natural system that were used to evaluate the effects of coupled processes along with the rationale for the range of parameters.
2 - Uncertainty in data due to both temporal and spatial variations in conditions affecting coupled THC effects on radionuclide transport in the near field were considered.	Section 3.10.6 discusses uncertainties in data due to temporal and spatial variations in conditions affecting THC processes.
3 - DOE's evaluation of coupled THC processes properly considered the uncertainties in the characteristics of the natural system and engineered materials, such as type, quantity, and reactivity of material, in establishing initial and boundary conditions for conceptual models and simulations of THC coupled processes that affect transport of radionuclides in the near field.	Section 3.10.6 discusses uncertainties in the characteristics of the natural system. See also the PMR on the engineered barrier system.
4 - The initial conditions, boundary conditions, and computational domain used in sensitivity analyses involving coupled THC effects on radionuclide transport in the near field were consistent with available data.	Sensitivity analyses will be included in the TSPA-SR.
5 - DOE's performance confirmation program should assess whether the natural system and engineered materials are functioning as intended and anticipated with regard to coupled THC effects on transport of radionuclides in the near field.	Although THC effects on radionuclide transport have been determined not to be important to performance, the performance confirmation plan contains testing during the pre-emplacement period to confirm this assumption (CRWMS M&O 2000c, Appendix G).

NRC Technical Acceptance Criteria	PMR Approach and Section Reference
Model uncertainty acceptance criteria for Subissue 4	
<p>1 - Appropriate models, tests, and analyses were used that are sensitive to the THC couplings under consideration for both natural and engineered systems, as described in the following examples. The effects of THC coupled processes that may occur in the natural setting or due to interactions with engineered materials or their alteration products include: (i) TH effects on gas and water chemistry in the unsaturated zone and saturated zone; (ii) precipitation of calcite and opal on the footwall of fracture surfaces and the bottoms of lithophysal cavities, which indicates gravity-driven flow in open fractures, and isolation of transport pathways from sorption sites in the rock matrix; (iii) zeolitization of volcanic glass, that could affect transport pathways; (iv) precipitation and dissolution of oxides and hydroxides on fracture surfaces, illitization of smectite, and recrystallization of zeolites to analcime, which could affect sorption characteristics; (v) effects of microbial processes; (vi) effects of corrosion products of container materials and waste forms on transport of radionuclides in the near field; and (vii) changes in hydraulic and sorptive properties of the natural system resulting from interactions between cementitious materials and groundwater.</p>	<p>Attachment I summarizes available site data. Section 3.10 summarizes data, analyses, and models that were used to evaluate THC processes on the natural system. The purpose of the THC seepage model is to evaluate the effects of THC processes in the rock around the emplacement drift on seepage water chemistry, gas-phase composition, and the potential effects of THC processes on UZ flow and transport. This model evaluates the effects of mineral dissolution and precipitation, the effects of CO₂ exsolution and transport in the region surrounding the drift, the potential for forming zones of calcite, silica or other minerals, the resulting changes in porosity and permeability, and the potential effects on seepage. See also the PMR on the near field environment.</p>
<p>2 - Alternative modeling approaches consistent with available data and current scientific understanding were investigated, and their results and limitations were appropriately considered.</p>	<p>Section 3.10.7 addresses the alternative conceptual model proposed by Matyskiela (1997).</p>
<p>3 - DOE provided a reasonable description of the mathematical models included in its analyses of coupled effects on radionuclide transport in the near field. The description should include a discussion of alternative modeling approaches not considered its final analysis and the limitations and uncertainties of the chosen model.</p>	<p>Section 3.10 summarizes the relevant mathematical models.</p>
Model verification acceptance criteria for Subissue 4	
<p>1 - The mathematical models for coupled THC effects on radionuclide transport in the near field are consistent with conceptual models based on inferences about near-field environment, field data and natural alteration observed at the site, and expected engineered materials.</p>	<p>Section 3.10 summarizes the basis for the mathematical models used to evaluate coupled THC effects.</p>
<p>2 - DOE appropriately adopted accepted and well-documented procedures to construct and test the numerical models used to simulate coupled THC effects on transport of radionuclides in the near field.</p>	<p>Procedures were followed, consistent with the governing quality assurance requirements (See Section 1).</p>

NRC Technical Acceptance Criteria	PMR Approach and Section Reference
Model verification acceptance criteria for Subissue 4, continued	
<p>3 - Abstracted models for coupled THC effects on radionuclide transport in the near field were based on the same assumptions and approximations shown to be appropriate for closely analogous natural or experimental systems. Abstracted model results were verified through comparison to outputs of detailed process models and empirical observations. Abstracted model results are compared with different mathematical models to judge robustness of results.</p>	<p>Thermal effects on flow were not found to be significant and will not be included in UZ transport simulations for TSPA-SR (Sections 3.11.1.3, 3.11.2, and 5.2.4).</p>
Integration acceptance criteria for Subissue 4	
<p>1 - DOE has considered all the relevant features, events, and processes. The abstracted models adequately incorporated design features, physical phenomena, and couplings, and used consistent and appropriate assumptions throughout.</p>	<p>Section 1.2.3 discusses the relevant features, processes and events. Included FEPs are directly represented in the process models and abstractions that support TSPA and are discussed in sections of the PMR corresponding to the specific models.</p>
<p>2 - Models reasonably accounted for known temporal and spatial variations in conditions affecting coupled THC effects on transport of radionuclides in the near field.</p>	<p>Section 3.10 discusses temporal and spatial variations in conditions affecting THC effects.</p>
<p>3 - Not all THC couplings may be determined to be important to performance, and DOE may adopt assumptions to simplify PA analyses. If potentially important couplings are neglected, DOE should provide a technical basis for doing so. The technical bases could include activities, such as independent modeling, laboratory or field data, or sensitivity studies.</p>	<p>The DOE agrees that simplifying assumptions may be appropriate if not all the THC couplings are determined to be important to performance and will provide the technical basis for the simplifying assumptions.</p>
<p>4 - The bases used for modeling assumptions and approximations were documented and justified, where simplifications for modeling coupled THC effects on radionuclide transport in the near field were used for performance assessment analyses instead of detailed process models.</p>	<p>In general, the PMR documents the basis for modeling assumptions and approximations in the specific sections addressing the UZ flow and transport models. Also see Assumption 4 in Section 1.2.3.</p>
<p align="center">Subissue 5 - Coupled THC processes affecting potential nuclear criticality in the near field (covered in a topical report and supporting documents)</p>	
<p align="center">IRSR: Radionuclide Transport</p>	
<p align="center">Subissue 1 - Estimation of radionuclide transport through porous rock</p>	
<p>1 - For the estimation of radionuclide transport through porous rock DOE has:</p>	
<p>1.a - Determined, through PA calculations, whether radionuclide attenuation process such as sorption, precipitation, radioactive decay, and colloidal filtration are important to performance.</p>	<p>Section 3.11.2 evaluates the effect of processes such as hydrodynamic dispersion, matrix diffusion, sorption (solutes), filtration (colloids), and radioactive decay. These processes are considered important to performance and are all explicitly modeled in the transport model abstraction (3.11.12).</p>

NRC Technical Acceptance Criteria	PMR Approach and Section Reference
Subissue 1 - Estimation of radionuclide transport through porous rock, continued	
1.b - (i) Assumed K_d is zero and radionuclides travel at the rate of groundwater flow, if it has been found that radionuclide attenuation is unimportant to performance and it can be demonstrated that this assumption is conservative, in which case Acceptance Criteria 2 and 3 do not have to be met, or (ii) demonstrated that Criterion 2 or 3 has been met, if radionuclide attenuation in porous rock is important to performance, or if an assumption that K is zero in porous rock is not conservative	This PMR uses an assumed K_d of zero, therefore acceptance criteria 2 and 3 need to be evaluated.
2 - For the valid application of the constant K_d approach, using equation (1) $R_t = 1 + \rho_b K_d/n$, DOE has:	
2.a - Demonstrated that the flow path acts as a single continuum porous medium. If the flow can not be shown to be a single continuum porous medium, then the Acceptance Criteria for radionuclide transport in fractured rock apply.	Section 3.4 summarizes numerical approaches for modeling UZ hydrology; transport modeling is based on the UZ flow model summarized in Section 3.7.2.
2.b - Demonstrated that appropriate values for the parameters. K_d , n or θ , and ρ_b have been adequately considered (e.g., experimentally determined or measured).	Details of the experimental program are provided in the Yucca Mountain Site Description.
2.c - Demonstrated that the three implicit assumptions (i.e. linear isotherm, fast reversible sorption reaction, and constant bulk chemistry) are valid.	Section 3.11 discusses these assumptions; the AMR on radionuclide transport models under ambient conditions provides the supporting rationale.
3 - For the valid application of process models affecting radionuclide transport such as surface complexation, ion exchange, precipitation/dissolution, and processes involving colloidal material	
3.a - Demonstrated that the flow path acts as a single-continuum porous medium. See Subissue 4, page 312 of this PMR.	Transport modeling is based on the UZ flow models discussed in Section 3.7.
3.b - Demonstrated that values for the parameters used in process models are appropriate and sufficient.	Transport parameters are summarized in Section 3.11.2.
3.c - (i) Demonstrated that the three implicit assumptions (see 2c) are valid, if process models are intended to yield a constant K_d for use in the retardation equation (equation 1); or (ii) determined transport in a dynamic reactive transport system mode (e.g., PHREEQC, MULTIFLO, HYDROGEOCHEM, etc.).	See 2 c) above.
Subissue 2 - For the estimation of radionuclide transport through alluvium (covered in Saturated Zone Flow and Transport PMR)	
Subissue 3 - Radionuclide transport through fractured rock	
1 - For estimation of radionuclide transport through fractured rock, DOE has continued	

NRC Technical Acceptance Criteria	PMR Approach and Section Reference
1a - Determined, through PA calculations, whether radionuclide attenuation processes such as sorption, precipitation, and radioactive decay, and colloidal transport are important to performance.	Section 3.11 summarizes attenuation processes, such as sorption, precipitation, radioactive decay, and colloidal transport. These processes are considered important to performance.
1b - Assumed K_d (or K_a) is zero and that radionuclides travel at the velocity of groundwater flow through fractures, if it has been found that radionuclide attenuation in fractures is unimportant to performance, and it can be demonstrated that this assumption is conservative. In this case, Acceptance Criterion 2 does not have to be met.	There is limited information on sorption onto the fracture surfaces, which will retard migration of sorbing radionuclides. However, sorption in the fractures is neglected in the PA transport evaluations because of limited data and the conservative nature of the assumption.
1c - Justified the length of flow path to which these fracture transport conditions apply	There is limited information on sorption onto the fracture surfaces, which will retard migration of sorbing radionuclides. However, sorption in the fractures is neglected in the PA transport evaluations because of limited data and the conservative nature of the assumption (Section 3.11.10.2.).
2 - If credit is taken for radionuclide attenuation in fractured rock, DOE has:	There is limited information on sorption onto the fracture surfaces, which will retard migration of sorbing radionuclides. However, sorption in the fractures is neglected in the PA transport evaluations because of limited data and the conservative nature of the assumption (Section 3.11.10.2.).
2a - Demonstrated capability to predict breakthrough curves or reactive, nonreactive, and colloidal tracers in field tests.	There is limited information on sorption onto the fracture surfaces, which will retard migration of sorbing radionuclides. However, sorption in the fractures is neglected in the PA transport evaluations because of limited data and the conservative nature of the assumption (Section 3.11.10.2.).
2b - Demonstrated nonradioactive tracers used in field tests are appropriate homologues for radioelements.	There is limited information on sorption onto the fracture surfaces, which will retard migration of sorbing radionuclides. However, sorption in the fractures is neglected in the PA transport evaluations because of limited data and the conservative nature of the assumption (Section 3.11.10.2.).
2c - Justified the length of flowpath to which these fracture transport conditions apply.	There is limited information on sorption onto the fracture surfaces, which will retard migration of sorbing radionuclides. However, sorption in the fractures is neglected in the PA transport evaluations because of limited data and the conservative nature of the assumption (Section 3.11.10.2.).
Subissue 4 - Nuclear criticality in the far field (covered in a topical report and supporting documents)	
IRSR: Structural Deformation and Seismicity	
Subissue 1 - Fault displacement hazard (covered in Disruptive Events PMR)	
Subissue 2 - Seismic hazard (covered in Disruptive Events PMR)	

NRC Technical Acceptance Criteria	PMR Approach and Section Reference
Subissue 3 - Fracturing and structural framework of the geologic setting	
1 - Data and model justification: Adequate field, borehole, and underground excavation data are acquired to sufficiently support conceptual models, assumptions, and boundary conditions of numerical abstractions of fracture data and fracture models of ambient and perturbed conditions.	This information is provided in the Yucca Mountain Site Description. Attachment I summarizes data on the properties of fractures. Fracture property estimates are based on permeability data from <i>in situ</i> air injection tests conducted in four surface boreholes and boreholes in alcoves in the ESF, porosity data from gas tracer tests in boreholes in Alcove 5, and fracture mapping from the ESF, ECRB, and surface based boreholes (Section 3.6.3.2).
2 - Data and uncertainty verification: Parameter values, assumed ranges, probability distributions, and bounding assumptions used to determine fracture distributions and properties reasonably account for uncertainties and variabilities.	See above. Small-scale fracture data from detailed line surveys have become available since the analysis in this PMR was performed. Although the impact of small-scale fracture data on mountain-scale and drift-scale calibrated properties is not likely to be large, the impact will be evaluated in the future (Section 3.6.3.2).
3 - Model uncertainty: Alternative modeling approaches for fracture distribution and properties of fractures consistent with available data and current geologic understanding are investigated and results and limitations are appropriately considered in process, TSPA, or both models of ambient and perturbed repository conditions	Physical processes, including a discussion of the fracture and matrix flow component for each major unit, are discussed in Section 3.3. Alternative numerical approaches for modeling are summarized in section 3.4. The representation of fractures in the UZ model is discussed in Section 3.7. Section 3.7.3.2 analyzes the effects of major faults on UZ flow. The results indicate that faults serve as major focusing conduits for downward liquid flow in the UZ. For the seepage model (Section 3.9.) model calibration is used to determine the effective parameters, including potential effects of individual fractures and microfractures on seepage. Simulations with multiple realizations of a heterogeneous property field are completed to account for the random nature of the fracture field.
4 - Model verification: Results of fracture data analyses and fracture models are verified by comparison with output of sensitivity studies, detailed process level models, natural analogs, and empirical observations, as appropriate.	Physical processes, including a discussion of fracture and matrix flow component for each major unit, are discussed in Section 3.3. The representation of fractures in the UZ model is discussed in Section 3.7.
5 - Integration: Results of abstractions of fracture data are consistent with physical and geological phenomena and coupled processes.	Abstractions are based on available site fracture characteristics (Section 3.7).
Subissue 4 - Tectonic framework of the geologic setting (covered in Disruptive Events PMR and the Yucca Mountain Site Description)	
IRSR: Thermal Effects on flow	
Subissue 1 - Is the U.S. Department of Energy TH testing program, including performance confirmation testing, sufficient to evaluate the potential for thermal reflux to occur in the near field? (covered in Near Field Environment PMR)	

NRC Technical Acceptance Criteria	PMR Approach and Section Reference
Subissue 2 - Is the thermohydrologic modeling approach sufficient to predict the nature and bounds of thermal effects on flow in the near field?	
1 - Sufficient data are available to adequately define relevant parameters, parameter values, and conceptual models. Demonstrate that:	
1.1 - Uncertainties and variabilities in parameter values are accounted for using defensible methods. The technical bases for parameter ranges, probability distributions or bounding values used are provided. Parameter values (single values, ranges, probability distributions, or bounding values) are derived from site-specific data or an analysis is included to show the assumed parameter values lead to a conservative effect on performance.	Section 3.10 summarizes the parameter ranges and the technical basis for these ranges. Parameter values derived from site data are specified.
1.1.- Analyses are consistent with site characteristics in establishing initial conditions, boundary conditions, and computational domains for conceptual models evaluated.	Analyses in Section 3.10 considered site characteristics in establishing initial conditions, boundary conditions, and computational domains. In addition to the required UZ hydrologic properties, the model includes initial and boundary water and gas chemistry, initial mineralogy, mineral volume fractions, reactive surface areas, equilibrium thermodynamic data for minerals, aqueous and gaseous species, kinetic data for mineral-water reactions, and diffusion coefficients for aqueous and gaseous species (Section 3.10.2).
2 - Descriptions of process-level conceptual and mathematical models used in the analyses are reasonably complete. Demonstrate that:	
2.1 - Models are based on well-accepted principles of heat and mass transfer applicable to unsaturated geologic media.	Sections 3.10 and 3.12 summarize TH models that are based on accepted principles of heat and mass transfer.
2.2 - Models include, at a minimum, the processes of evaporation and condensation and the effects of discrete geologic features.	Current models (Section 3.10.2) include processes of evaporation and condensation. Figure 3.10-2 shows schematically the relationships between TH and geochemical processes in zones of boiling, condensation, and drainage in the rock mass outside of the drift and above the heat source. Seepage models (Section 3.9) now include an active fracture model to describe fracture-matrix interactions.

NRC Technical Acceptance Criteria	PMR Approach and Section Reference
Subissue 2 - Is the thermohydrologic modeling approach sufficient to predict the nature and bounds of thermal effects on flow in the near field?, continued	
2.3 - Models include, at a minimum, an evaluation of important thermohydrological phenomena, such as: (i) multidrift dry-out zone coalescence, (ii) lateral movement of condensate, (iii) cold-trap effect, (iv) repository edge effects, and (v) condensate drainage through fractures.	The current design has a lower thermal load than the VA design to eliminate dryout zone coalescence. Section 3.10 evaluates the extent of the dryout zone and time of rewetting for different calibrated property sets and climate scenarios. Section 3.12 summarizes TH mountain scale models of the effects of temperature changes over the mountain, including effects on flow around the drift.
2.4 - Models include all significant repository design features.	Sections 3.10 and 3.12 summarize the design features included in the TH model. For example, the THC model uses in-drift geometry and drift spacing, and the thermal and hydrologic properties of the EBS components, such as waste package and invert, from the current design.
2.5 - Models are capable of accommodating variation in infiltration.	The TH model incorporates variation in infiltration (Sections 3.10 and 3.12).
2.6 - Conceptual model uncertainties have been defined and documented and effects on conclusions regarding performance assessed.	Sections 3.10 and 3.12 summarize conceptual uncertainties.
2.7 - Mathematical models are consistent with conceptual models, based on consideration of site characteristics.	Sections 3.10 and 3.12 discuss mathematical models used to represent conceptual models and are based on site characteristics.
2.8 - Alternative models and modeling approaches, which are consistent with available data and current scientific understanding, have been investigated, limitations defined, and results appropriately considered.	Sections 3.10.7 discusses an alternative model proposed by Matyskiela (1997).
2.9 - Results from different mathematical models have been compared to judge robustness of results.	Numerical approaches that can be used for unsaturated, fractured rock have been reviewed in the AMR on conceptual and numerical models for UZ flow and transport.
2.10 - Models used to predict shedding around emplacement drifts are shown to contain an adequate level of heterogeneity in media properties.	Sections 3.10 and 3.12 summarize the approach to evaluating heterogeneities in TH models.
2.11 - TH models have been demonstrated to be appropriate for the temperature regime expected at the repository.	TH models incorporated the anticipated thermal load for the current design (Sections 3.10 and 3.12).
2.12 - Models include radiative heat transport unless it is shown that radioactive heat loss by a WP is not significant.	TH models include radiative heat transfer at the drift scale (Section 3.10.5.1).
2.13 - Models include the effect of ventilation particularly if ventilation could result in deposition or condensation of moisture on a WP surface.	Effects of ventilation are included (Sections 3.10.5.1 and 3.12.1).

NRC Technical Acceptance Criteria	PMR Approach and Section Reference
Subissue 2 - Is the thermohydrologic modeling approach sufficient to predict the nature and bounds of thermal effects on flow in the near field?, continued	
2.14 - The media properties of a model contain an adequate level of heterogeneity so that mechanisms such as dripping are not neglected or misrepresented.	The drift seepage model has been enhanced to account for heterogeneities (Section 3.9.3).
2.15 - Drift wall representations in models contain sufficient physical detail so that processes predicted using a continuum model, such as capillary diversion, are appropriate for the geologic media at the proposed repository horizon.	Models predicting seepage include partial drift collapse and multiple realizations of heterogeneous rock properties (Sections 3.9.3.4 and 3.9.4.5). See also the PMR on near field environment.
2.16 - Physical mechanisms such as penetration of the boiling isotherm by flow down a fracture are not omitted from model predictions due to over simplification or the physical medium or the conceptual model.	Section 3.9 summarizes the drift seepage models, including enhancements such as the evaluation of partial drift collapse and episodic percolation flux. Section 3.10 describes the seepage THC models.
3 - Coupling of processes has been evaluated using a methodology in accordance with NUREG-1466 (Nataraja and Brandshaug, 1992) or other acceptable methodology. Coupled processes may be uncoupled, if it is shown that the uncoupled model results bound the predictions of the fully coupled model results.	NUREG-1466 provides logical steps for the development of predictive models and their numerical representation of thermally induced TMHC behavior of the host rock. Models of coupled processes in Sections 3.10 and 3.12 present the current approach to modeling drift scale and mountain scale TH effects. The DOE agrees that coupled processes may be uncoupled if the models bound the effects of fully coupled processes.
4 - The dimensionality of models, which include heterogeneity at appropriate scales and significant process couplings, may be reduced, if shown that the reduced dimension model bounds the predictions of the full dimension model.	The DOE agrees with this approach, and has implemented a modeling approach with models of different dimensions and scales. See for example Section 3.10, Drift-Scale THC Processes and Models, and Section 3.12, Mountain-Scale TH Model.
5 - Equivalent continuum models are acceptable for the rock matrix and small discrete features, if it can be demonstrated that water in small discrete features is in continuous hydraulic equilibrium with matrix water. Significant discrete features, such as fault zones, should be represented separately unless it can be shown that inclusion in the equivalent continuum model (ECM) produces a conservative effect on calculated overall performance.	Section 3.10.3 summarizes the approach to modeling thermal-hydrologic processes.
6 - Accepted and well-documented procedures have been adopted to construct and calibrate numerical models used.	Procedures were followed, consistent with the governing quality assurance requirements (see Section 1).
7 - Results of process-level models have been verified by demonstrated consistency with results/observations from field-scale, thermohydrologic tests. In particular, sufficient physical evidence should exist to support the conceptual models used to predict thermally driven flow in the near field.	Process level models have been calibrated against field data and observations (Sections 3.9.4.5, 3.10.4, 3.12.4).

NRC Technical Acceptance Criteria	PMR Approach and Section Reference
Subissue 3: Does the DOE's TSPA adequately account for thermal effects on flow?	
1 - Abstractions of process-level models may be used if predictions from the abstracted model are shown to conservatively bound process-level predictions. In particular, DOE may use an abstracted model to predict water influx into an emplacement drift if the abstracted model is shown to bound process-level model predictions of the influx of water as liquid or vapor into an emplacement drift.	Section 3.9 summarizes the abstraction of seepage into drifts. As noted in Section 3.9.6.3, distributions for the amount of seepage as a function of percolation flux are derived directly from process-model results and constrained by measurements of permeability around three niches in the ESF and calibration of seepage tests conducted in one niche in the ESF.
2 - Sufficient data are available to adequately define relevant parameter values and conceptual models. Demonstrate that:	
2.1 - Uncertainties and variabilities in parameter values are accounted for using defensible methods. The technical bases for parameter ranges, probability distributions or bounding values used are provided. Parameter values (single values, ranges, probability distributions, or bounding values) are derived from site-specific data or an analysis is included to show the assumed parameter values lead to conservative effect on performance.	The THC abstraction of the mean infiltration rate (with climate changes) includes both geochemical systems (full and calcite-silica-gypsum) considered in the THC process model (Section 3.10.11).
2.2 - Analysis are consistent with site characteristics in establishing initial conditions, boundary conditions, and computational domains for conceptual models evaluated.	Site characteristics have been considered in establishing initial conditions, boundary conditions, and computational domains (Sections 3.10 and 3.12).
3 - Descriptions of conceptual and mathematical models used in DOE's TSPA are reasonably complete.	
3.1 - Performance affecting heat and mass transfer mechanisms, including processes observed in available thermohydrologic tests and experiments, have been identified and incorporated into the TSPA. Specifically, it is necessary to either demonstrate that liquid water will not reflux into the underground facility or incorporate refluxing water into the TSPA and bound the potential adverse effects of: (i) corrosion of the WP; (ii) accelerated transport of radionuclides; and (iii) alteration of hydraulic and transport pathways that result from refluxing water.	Section 3.12 summarizes the evaluation of flow changes close to drifts and drainage in the pillars.
3.2 - Significant Geologic Repository Operations Area underground facility design features, such as the addition of backfill of drip shields, that can result in changes in TSP have been identified and incorporated in to the TSPA.	See the PMR for the engineered barrier system.
3.3 - Conceptual model uncertainties have been defined and documented, and their effects on conclusions regarding TSP have been assessed.	Section 3.12 summarizes the evaluation of flux into drifts during and after the thermal period.
3.4 - Mathematical models are consistent with conceptual models, based on consideration of site characteristics.	Modeling approaches for thermal effects are summarized in Sections 3.10 and 3.12.

NRC Technical Acceptance Criteria	PMR Approach and Section Reference
Subissue 3: Does the DOE's TSPA adequately account for thermal effects on flow?, continued	
3.5 - Alternative models and modeling approaches, consistent with available data and current scientific understanding, are investigated; limitations defined; and results appropriately considered.	Alternative modeling approaches are discussed in Section 3.10.7.
3.6 - Results from different mathematical models have been compared to judge robustness of results.	Sensitivity analyses will be included in TSPA-SR.
4 - Coupling of thermal processes has been evaluated using a methodology in accordance with NUREG-1466 (Nataraja and Brandshaug, 1992) or other acceptable methodology. Coupled processes may be uncoupled, if it is shown that the uncoupled model results bound the predictions of the fully-coupled model results.	NUREG-1466 provides logical steps for the development of predictive models and their numerical representation of thermally induced THMC behavior of the host rock. Sections 3.10 and 3.12 summarize the approach to evaluating coupled processes at the drift-scale and mountain-scale. The DOE agrees that coupled processes may be uncoupled if the models bound the effects of fully coupled processes.
5 - The dimensionality of models used to assess the importance of refluxing water on repository performance may be reduced if it is shown that the reduced dimension model bounds the predictions of the full dimension model in performance.	The DOE agrees with this approach. Section 3.4.2.4 summarizes studies of grid refinement; Section 3.12.2.2 summarizes numerical grids for TH simulations.
6 - Results of the TSPA related to TEF have been verified by demonstrating consistency with results of process-level models.	TSPA analyses related to TEF were based on the process level models.
7 - Sensitivity and importance analyses were conducted to assess the need for additional data or information with respect to TEF.	Sensitivity analyses will be included in TSPA-SR.
IRSR: Total System Performance Assessment and Integration	
Subissue 1 – System description and demonstration of multiple barriers	
Total system performance assessment documentation style, structure, and organization	
Doe's approach to document structure and organization will be acceptable if:	
1 - Documents and reports are complete, clear, and consistent.	The UZ PMR was carefully structured to be complete, clear, and consistent. The review of the draft document included checks for completeness, clarity and consistency.
2 - Information is amply cross-referenced	The UZ PMR contains ample references to data sources, codes, assumptions, and conclusions.
Features, Events, and Processes Identification and Screening	
1 - The screening process by which FEPs were included or excluded from the TSPA is fully described.	Section 1.2.3 summarizes excluded and included FEPs along with the rationale for these decisions.
2. Relationships between relevant FEPs are fully documented.	Section 1.2.3 describes the relationship between primary and secondary FEPs based on the overlap that exists among the FEPs for UZ flow and transport.

NRC Technical Acceptance Criteria	PMR Approach and Section Reference
Abstraction Methodology	
1- The levels and method(s) of abstraction are described starting from assumptions defining the scope of the assessment down to assumptions concerning specific processes and the validity of given data.	For each model in the UZ PMR, the relevant chapter summarizes the data used to construction the process model, the process model, and the abstraction of that model, if the model is abstracted for TSPA.
2 - A mapping (e.g., a road map diagram, a traceability matrix, a cross-reference matrix) is provided to show what conceptual features (e.g., patterns of volcanic events) and processes are represented in the abstracted models, and by what algorithms.	The UZ PMR provides a sufficient basis for the decisions and assumptions that were made during the abstraction process.
3 - An explicit discussion of uncertainty is provided to identify which issues and factors are of most concern or are key sources of disagreement among experts.	The UZ PRM provides a discussion of uncertainties and limitations for the major process models included in the report.
Data Use and Validity	
1 - The pedigree of data from laboratory tests, natural analogs, and the site is clearly identified.	Section 1.3 summarizes the quality assurance status of the data and software used in the component models.
2 - Input parameter development and basis for their selection is described.	The UZ PMR discusses input parameter development and the basis for using the parameters. For example, Section 3.6 summarizes the development of UZ properties, model calibration, and the results.
3 - A thorough description of the methods used to identify performance confirmation program parameters.	The DOE is developing a plan that will define the performance confirmation program. Performance confirmation testing is not covered in this PMR.
Assessment results	
1 - PA results (i.e., the peak expected annual dose within the compliance period) can be traced back to applicable analyses that identify the FEPs, assumptions, input parameters, and models in the PA.	The TSPA-SR will summarize UZ flow and transport features, processes and the conceptual model, and their implementation into the TSPA. This discussion will be based on the UZ PMR.
2 - The PA results include a presentation of intermediate results that provide insight into the assessment (e.g., results of intermediate calculations of the behavior of individual barriers).	Intermediate results for PA are not discussed in the UZ PMR. The TSPA-SR is planned to include sensitivity analysis, including uncertainty importance analyses, one-off analyses, and robustness analyses.
Code design and data flow	
1 - The flow of information (input and output) between the various modules is clearly described.	The flow of information (input and output) is documented in accordance with QA procedures to ensure traceability.
2 - Supporting documentation (e.g., user's manuals, design documents) clearly describes code structure and relations between modules.	The codes used in the UZ PMR were documented in accordance with software QA procedures that include requirements for appropriate documentation.
Demonstration of multiple barriers (acceptance criteria have not been included in this revision of the IRSR).	

NRC Technical Acceptance Criteria	PMR Approach and Section Reference
Subissue 2 – Scenario Analysis	
Identification of an initial set of processes and events	
1 - DOE has identified a comprehensive list of processes and events that: (i) are present or might occur in the Yucca Mountain region and (ii) includes those processes and events that have the potential to influence repository performance.	Section 1.2.3 discusses the relevant FEPs for unsaturated zone flow and transport. Included FEPs are directly represented in the process models and abstractions that support TSPA, and discussed in sections of the PMR corresponding to the specific models.
Classification of Processes and events	
1 - DOE has provided adequate documentation identifying how its initial list of processes and events has been grouped into categories.	Section 1.2.3 discusses the identification and categories of relevant FEPs for unsaturated zone flow and transport.
2 - Categorization of processes and events is compatible with the use of categories during the screening of processes and events.	Section 1.2.3 discusses categories of relevant FEPs for unsaturated zone flow and transport and their use.
Subissue 2 – Scenario Analysis, continued	
Screening of processes and events	
1 - Categories of processes and events that are not credible for the Yucca Mountain repository because of waste characteristics, repository design, or site characteristics are identified and sufficient justification is provided for DOE's conclusions.	Sections 1.2.3 discusses excluded FEPs and the rationale for exclusion. The exclusion of FEPs from TSPA is based on arguments of low probability or low consequence.
2 - The probability assigned to each category of processes and events not screened based on criterion T1 or criterion T2 is consistent with site information, well documented, and appropriately considers uncertainty.	Section 1.2.3 provides the rationale for excluding FEPs.
3 - DOE has demonstrated that processes and events screened from the PA on the basis of their probability of occurrence, have a probability of less than one chance in 10,000 years of occurring over 10,000 years.	Section 1.2.3 provides the rationale for excluding FEPs.
4 - DOE has demonstrated that categories of processes and events omitted from the PA on the basis that their omission would not significantly change the calculated expected annual dose, do not significantly change the calculated annual dose.	Section 1.2.3 summarizes information on FEPs that are directly and the rationale for their exclusion.
Formation of scenarios (covered in TSPA-SR)	
Screening of scenario classes (covered in TSPA-SR)	
Subissue 3 - Model abstraction	
Engineered barrier system	
Engineered barrier degradation (to be covered in the Waste Package Degradation PMR)	
Mechanical disruption of engineered barriers (to be covered in the Disruptive Events PMR)	
Quantity and quality of water contacting waste packages and waste forms	

NRC Technical Acceptance Criteria	PMR Approach and Section Reference
1 - Sufficient data (field, laboratory, and/or natural analog data) are available to adequately define relevant parameters and conceptual models necessary for developing the quantity and chemistry of water contacting WPs and waste forms abstraction in TSPA. Where adequate data do not exist, other information sources such as expert elicitation have been appropriately incorporated into the TSPA.	Section 3.9 summarizes the available data and conceptual models for seepage into drifts.
2 - Parameter values, assumed ranges, probability distributions, and bounding assumptions used in the quantity and chemistry of water contacting WPs and waste forms abstraction, such as pH, chloride concentration, and amount of water flowing in and out of the breached WP, are technically defensible and reasonably account for uncertainties and variability.	See the PMRs on waste package degradation and waste form.
3 - Alternative modeling approaches consistent with available data and current scientific understanding are investigated and results and limitations appropriately factored into the quantity and chemistry of water contacting WPs and waste forms abstraction.	See the PMRs on waste package degradation and waste form.
4 - Output of quantity and chemistry of water contacting WPs and waste forms abstraction are verified through comparison to output of detailed process models and/or empirical observations (laboratory testing or natural analogs, or both).	See the PMRs on waste package degradation and waste form.
5 - Important design features, physical phenomena and couplings, and consistent and appropriate assumptions are incorporated into the mechanical disruption of WPs abstraction.	See the PMR for waste package degradation.
Radionuclide release rates and solubility limits (to be covered in Waste Form PMR)	
Geosphere	
Unsaturated zone flow and transport	
Spatial and temporal distribution of flow	
1 - Sufficient data (field, laboratory, and/or natural analog data) are available to adequately define relevant parameters and conceptual models necessary for developing the spatial and temporal distribution of flow abstraction in TSPA. Where adequate data do not exist, other information sources such as expert elicitation have been appropriately incorporated into the TSPA.	Attachment I summarizes available data used to define relevant parameters and conceptual models. Section 3.7.5 summarizes the abstraction of flow fields for TSPA-SR. The UZ flow model forms the basis for the model that is abstracted for TSPA-SR.

NRC Technical Acceptance Criteria	PMR Approach and Section Reference
2 - Parameter values, assumed ranges, probability distributions, and/or bounding assumptions used in the spatial and temporal distribution of flow abstraction, such as the effects of climate change on infiltration, near surface influences (e.g., evapotranspiration and runoff) on infiltration, structural controls on the spatial distribution of deep percolation, and thermal reflux owing to repository heat load, are technically defensible and reasonably account for uncertainties and variabilities.	Sections 3.7.2 through 3.7.4 summarize UZ flow models and Section 3.7.5 summarizes the results of abstractions of UZ flow. The abstraction considers three infiltration cases (low, mean, and high) within each of the three climate states (present-day, monsoon, and glacial transition). For the abstraction of TH processes, only the mean infiltration cases were selected since the results of the low and high infiltration cases showed similar behavior in general.
3 - Alternative modeling approaches consistent with available data and current scientific understanding are investigated and results and limitations appropriately factored into the spatial and temporal distribution of flow abstraction.	Section 3.7.4 summarizes alternative conceptual models.
4 - Spatial and temporal distribution of flow abstraction output is justified through comparison to output of detailed process models, and/or empirical observations (laboratory testing or natural analogs, or both).	The abstraction of flow was based on detailed process models (Section 3.7.5).
5 - Important design features, physical phenomena and couplings, and consistent and appropriate assumptions are incorporated into the spatial and temporal distribution of flow abstraction.	The abstraction of UZ flow is summarized in Section 3.7.5.
Flow paths in the unsaturated zone	
1 - Sufficient data (field, laboratory and/or natural analog data) are available to adequately define relevant parameters and conceptual models necessary for developing the distribution of mass flux between fracture and matrix in the abstraction in TSPA. Where adequate data cannot be readily obtained, other information such as expert elicitation or bounding values have been appropriately incorporated in the TSPA.	Attachment I describes available data used to define relevant parameters and conceptual models. The abstraction in Section 3.7.5. was based on available data and conceptual models.
2 - Parameter values, assumed ranges, probability distributions, and bounding assumptions used in the flow paths in the UZ in the abstraction, such as hydrologic properties, stratigraphy, and infiltration rate, are technically defensible and reasonably account for uncertainties and variability.	Abstraction results are summarized in Section 3.7.5. The abstraction considers three infiltration cases (low, mean, and high) within each of the three climate states (present-day, monsoon, and glacial transition), based on the process-model results.
3 - Alternative modeling approaches consistent with available data and current scientific understanding are investigated and results and limitations appropriately factored into the distribution of mass flux between fracture and matrix in the abstraction.	Abstraction results are summarized in Section 3.7.5.

NRC Technical Acceptance Criteria	PMR Approach and Section Reference
4 - Flow paths in the UZ abstraction output is verified through comparison to output of detailed flow process models, or empirical observations (laboratory testing or natural analogs, or both).	The abstraction was based on detailed process models (Sections 3.7.2 through 3.7.4).
5 - Important design features, physical phenomena and couplings, and consistent and appropriate assumptions are incorporated into the flow paths in the UZ abstraction.	The results of the abstraction are summarized in Section 3.7.5.
Radionuclide transport in the unsaturated zone	
1 - Sufficient data (field, laboratory and/or natural analog data) are available to adequately define relevant parameters and conceptual models necessary for developing the RT in the UZ abstraction in TSPA. Where adequate data do not exist, other information sources such as expert elicitation have been appropriately incorporated in the TSPA. Alternatively, The parameters or models lacking sufficient data have been replaced by bounding parameter values.	Section 3.11.3 summarizes the transport properties that are used for the abstraction of radionuclide transport in the UZ. The AMR on UZ and SZ transport properties provides additional detail on transport properties for the UZ.
2 - Parameter values, assumed ranges, probability distributions, and bounding assumptions used in the RT in the UZ in the abstraction, such as sorption on fracture surfaces, and K_d for the matrix, are technically defensible and reasonably account for uncertainties and variability.	Section 3.11.3 summarizes parameter values, ranges, distributions, and bounding assumptions for the abstraction of radionuclide transport, as applicable.
3 - Alternative modeling approaches consistent with available data and current scientific understanding are investigated and results and limitations appropriately factored into the RT in the UZ abstraction.	Section 3.11.9 summarizes an alternative conceptual model for transport in the UZ.
4 - RT in the UZ abstraction output is justified through comparison to output of detailed process models, or empirical observations (laboratory testing or natural analogs, or both).	The abstraction of radionuclide transport is based on process models and compared to alternate solutions methods.
5 - Important physical phenomena and couplings and consistent and appropriate assumptions are incorporated into the consideration of radionuclide transport in the UZ abstraction.	Section 3.11.13 discusses the abstraction of radionuclide transport, including physical phenomena, couplings, and assumptions.
Saturated zone flow and transport (to be covered in Saturated Zone Flow and Transport PMR)	
Radionuclide transport in the saturated zone (to be covered in Saturated Zone Flow and Transport PMR)	
Direct release and transport (to be covered in Disruptive Events PMR)	
Biosphere (to be covered in the Biosphere PMR)	

NRC Technical Acceptance Criteria	PMR Approach and Section Reference
Subissue 4 – Demonstration of the overall performance objective (acceptance criteria not included in the IRSR)	
IRSR: Unsaturated and Saturated Zone Flow Under Isothermal Conditions	
Subissue 1 - Climate change	
1 - Climate projections used in performance assessments of the YM region are based on paleoclimate data, considering, at a minimum, information contained in Forester et al. (1996); Winograd et al. (1992); Szabo et al. (1994)	Climate projections are based on paleoclimate data (Section 3.5.1). The Yucca Mountain Site Description provides contains a detailed discussion of the paleoclimate data, including references to Forester, et al. (1996) and Szabo, et al. (1994) in Section 4 (Climatology and Meteorology). Winograd et al. (1992) is referenced in Section 5 (Hydrologic System).
2 - DOE has evaluated long-term climate change based on known patterns of climatic cycles during the Quaternary, especially the last 500 k.y.	Long term climate change is based on an analogous climate cycle that occurred approximately 400,000 years ago (Section 3.5.1).
3 - If used, numerical climate models are calibrated with paleoclimate data and their use suitably simulates the historical record, before being used for projection of future climate.	Numerical models of climate are not used in this PMR.
4 - Climate-affected parameters (e.g., onset times for climate change, MAP, and MAT) used in YM performance assessment models include, as bounding condition, a return to full pluvial climate (higher precipitation and lower temperatures) for at least a part of the first 10-k.y. period, using parameter values that are supported by scientific data and analyses.	The future climate at Yucca Mountain is treated as a sequence of three climate states, including a glacial transition at 1400 years (Section 3.5.1). Analog climate sites are used define the three climate states, including low, mean, and upper bound annual precipitation and temperature.
Subissue 2 - Hydrologic effects of climate change	
1 - If bounding analyses are used to predict climate-induced effects (water table rise, for example), the analysis are based on a reasonably complete search of paleoclimate data pertinent to water-table rise and other effects (for example, changes in precipitation and geochemistry), including, at a minimum, information contained in Paces et al. (1996), Szabo et al. (1994), Forester et al. (1996).	A comprehensive literature search of the paleoclimate data has been completed and documented in the Yucca Mountain Site Description. This description references Paces et al. (1996) in Section 5 (Hydrologic System). Szabo et al. (1994) and Forester et al. (1996) are referenced in Section 4 (Climatology and Meteorology).
2 - Regional and sub-regional models for the SZ that are used to predict climate-induced consequences are calibrated with the paleohydrology data, and are consistent with evidence that the water-table rise during the late Pleistocene was up to 120 m.	This acceptance criterion is addressed in the Saturated Zone PMR.

NRC Technical Acceptance Criteria	PMR Approach and Section Reference
3 - DOE has incorporated future climate changes and associated effects in its performance assessments. For example, available information does not support an assumption that present-day climate will persist unchanged for 10 k.y. or more.	Future climate changes and associated effects have been incorporated into TSPA (Section 3.5). Three climate states are expected to occur over the next 10,000 years: the current modern climate, a monsoon climate, and a glacial transition climate.
Subissue 3 - Present day shallow infiltration	
1 - DOE has estimated present-day shallow infiltration at YM for use in TSPA using mathematical models that are reasonably verified with site-specific climatic, surface, and subsurface information, and the fundamental effects of heterogeneities, time-varying boundary conditions, evapotranspiration, depth of soil cover, and surface-water runoff have been considered in ways that do not underestimate infiltration.	Section 3.5.2 summarizes models of present day infiltration and the site-specific parameters that are incorporated into the model. Important processes considered include precipitation, runoff and run-on, evapotranspiration, transpiration, and moisture redistribution in the shallow subsurface.
2- DOE has analyzed infiltration at appropriate time and space scales for performance assessment, and has tested the abstracted model against more detailed models to assure that it produces reasonable results.	The infiltration model in Section 3.5.2 evaluates time and space scales for infiltration.
3 - DOE has characterized shallow infiltration in the form of either probability distributions or deterministic upper-bound values for performance assessment, and provided sufficient data and analyses to justify the chosen probability distribution or bounding value.	The methodology for assigning probabilities to the mean annual infiltration multipliers has been enhanced to address the NRC concern that the method used to assign probabilities to the mean annual infiltration multipliers is biased toward lower values of mean annual infiltration (Section 3.5.1).
4 - If DOE can show through TSPA and associated sensitivity analyses that refinements of shallow infiltration estimates will not significantly alter performance predictions, no further refinement will be necessary.	Sensitivity studies will be included in TSPA-SR.
Subissue 4 - Deep percolation	
1 - Estimates of deep percolation flux rates and the fraction of flux that occurs in fractures will be acceptable provided that they are: (i) shown to constitute a conservative upper bound, or (ii) based on a technically defensible UZ flow model that reasonably represents the physical system, including flow in fracture systems and matrix-fracture interaction. The flow model has been calibrated using site-specific hydrologic, geologic, and geochemical data.	The UZ flow model has been calibrated with available site data (Section 3.6). The representation of flow in the UZ is summarized in Section 3.7, including a discussion of fracture-matrix interaction.
2 - To estimate deep-percolation flux, spatial and temporal variability of model parameters and boundary conditions must be considered. Model parameters must be averaged over appropriate time and space scales. DOE must also consider climate-induced change in soil depth and vegetation.	Section 3.7 summarizes the UZ flow model, including the treatment of spatial and temporal variability of model parameters and boundary conditions. The infiltration model has been enhanced to include an improved surface-water model.

NRC Technical Acceptance Criteria	PMR Approach and Section Reference
Subissue 4 - Deep percolation, continued	
<p>3 - For estimates of the amount of water that may contact waste packages DOE must (i) demonstrate that coupled thermal-mechanical-chemical changes in rock mass properties will not focus deep percolation into the drifts; and (ii) rigorously justify estimated diversion of deep percolation away from the waste package footprints. This must include direct observations of dripping in test drifts or tunnels under ambient (unventilated) conditions in the repository horizon, or in an analog horizon with similar characteristics. Also needed are model calculations that account for the effects of backfill (if used), drift collapse, and coupled thermal-mechanical-chemical changes to rock properties. The models have been calibrated to niche studies and tracer tests in the ESF, or using an analog with characteristics similar to the repository horizon.</p>	<p>Seepage models (Sections 3.9 and 3.10) evaluate partial drift collapse and coupled THM changes. These models have been calibrated to available data from the ESF and the cross drift. Direct observation of an unventilated segment of the ECRB is ongoing and dripping has not been observed.</p>
<p>4 - In predicting likely flow and transport pathways beneath the proposed repository horizon, DOE must either (i) conservatively assume that all deep percolation below the repository level bypasses the bulk of the non-welded units, either by lateral movement above the units or through vertical flow through fractures and faults; or (ii) demonstrate that the estimated fraction of deep percolation that flows vertically through the matrix of the non-welded units is supported by (a) characterization data and (b) two-dimensional or three-dimensional modeling that accounts for spatial and temporal variability that may result in lateral diversion of flow, and uses model parameter values appropriate for the scale of model discretization.</p>	<p>Section 3.7 summarizes the approach to modeling flow through each of the major units below the repository horizon. Modeling results show that fracture flow is dominant both at the potential repository horizon and at the water table. The model uses input from perched water and matrix properties, calibrated properties model, the geologic and numerical grid model, the climate/infiltration model, and the geochemistry model.</p>
Subissue 5 - Saturated zone ambient flow (covered in Saturated Zone PMR)	
Subissue 6 - Matrix diffusion	
<p>1 - If credit for matrix diffusion in the UZ is taken, then transport predictions must be consistent with site geochemical and isotopic data.</p>	<p>The matrix diffusion model has been enhanced to account for the effects of finite fracture spacing (Section 3.11.3).</p>
<p>2 - If credit for matrix diffusion in the SZ is taken, rock matrix and solute diffusion parameters must be (i) based on a SZ transport model that reasonably matches the results of the field tracer tests that are conducted over different distance scales and flow rates with multiple tracers of different diffusive properties, and (ii) consistent with laboratory data.</p>	<p>This acceptance criterion is addressed in the Saturated Zone PMR.</p>

INTENTIONALLY LEFT BLANK

5. SUMMARY AND CONCLUSIONS

The Unsaturated Zone Flow and Transport Process Model Report (UZ PMR) documents the approach, development, and basis for the models and analyses that are used to understand and predict flow and transport processes in the unsaturated zone at Yucca Mountain. The models and analyses are supported by data collection, experiments, field tests, and calibration efforts that have been performed by project scientists for many years. The extensive studies provide confidence in the models and tools that will be used in Total System Performance Assessments for Site Recommendation and License Application. The following two sections provide a general summary of the contents of this PMR (Section 5.1), as well as a more detailed summary of the models and abstractions that will be used in TSPA-SR calculations (Section 5.2).

5.1 SUMMARY OF THE UZ FLOW AND TRANSPORT PMR

This section provides a concise summary and review of the contents of this PMR. More detailed summaries and conclusions can be found at the end of each chapter, as well as at the end of major subsections describing the process models.

Chapter 1 provides an introduction to the scope and objectives of this PMR. Identification of key issues and FEPs (features, events, and processes) are presented to provide the motivation and requirements for this document. A summary of the quality assurance (QA) requirements for the data, software, models, and analyses in this PMR are also presented, and relationships to other relevant PMRs are discussed.

Chapter 2 presents historical background on the evolution of site characterization and data collection at Yucca Mountain that support this PMR. This includes early surface-based testing and more recent underground testing and monitoring activities in the Exploratory Studies Facility (ESF). These characterization studies provide the basis for the geological, hydrological, geochemical, and thermal models presented in this PMR. Natural analogs to the processes and events at Yucca Mountain are also presented in Chapter 2, and an overview of the evolution of the conceptual and mathematical UZ Flow and Transport Model is given.

Chapter 3 includes a description of the relevant process models and their underlying basis. Applicable abstractions for TSPA-SR are also presented. Section 3.2 begins with geological considerations for flow and transport. Geological issues important to repository performance (e.g., fracture characterization, mineralogy, and location of major faults) are listed and discussed. The hydrogeologic units at Yucca Mountain are identified, and their major features and impact to hydrology are presented. Mineralogy and locations of altered rock that may be important for UZ transport are also presented.

Section 3.3 provides a summary of the physical processes and conceptual models relevant to UZ flow and transport. The components and processes that are described include climate, infiltration, flow through fractures and matrix in various hydrogeologic units, fracture-matrix interaction, effects of major faults, transient flow, focusing of flow, perched water, seepage into drifts, gas flow processes, radionuclide transport processes, and the effects of coupled processes. These process and component conceptualizations comprise the UZ Flow and Transport Model

described in this PMR. Alternative conceptual models that are not used in this PMR are also presented.

Section 3.4 documents the development of the numerical approaches and grids that are used in the development of the UZ Flow and Transport Model. Numerical modeling approaches that are discussed include continuum vs. discrete fracture-network modeling for flow through fractured rock, and a description of the current numerical approach is presented. Other numerical approaches that are discussed include the active fracture model, particle tracking, and methods for modeling dispersion and heterogeneities. The development of the numerical grids is then presented, starting with the required inputs and data for grid generation. The outputs are described, which include one-, two-, and three-dimensional grids for various aspects of the development of the UZ Flow and Transport Model. Grid-refinement studies were also performed that showed the refinement of the current grid used in the UZ Flow and Transport Model was adequate.

Section 3.5 summarizes the development of the Climate and Infiltration Models, which provide the upper boundary condition (net infiltration) for the UZ Flow and Transport Model. The results and abstraction of the Climate Model reveal that a modern-like climate will persist for approximately 600 years, followed by a warmer and wetter monsoon climate for another ~1,400 years. A cooler and wetter glacial-transition climate follows the monsoon climate for the remaining duration of the 10,000-year period analyzed in TSPA-SR. For each of these climates, three infiltration scenarios ranging from low to high are generated using different values for precipitation and temperature, as well as surface infiltration parameters such as soil depth, and evapotranspiration. The three infiltration cases are denoted as low, mean, and high (or upper); Section 3.5 provides a summary of how weightings are assigned to each case for TSPA-SR calculations.

Section 3.6 documents the available hydrologic parameter data and the development of the calibrated hydrologic property sets for the UZ Flow and Transport Model. The data that were evaluated and used for property calibrations include information on measured matrix, fracture, and fault parameters. The calibration process is then presented to obtain calibrated parameter sets for mountain-scale and drift-scale applications. One- and two-dimensional numerical inversions were performed to estimate parameters that optimize the match between predicted results and measured data. Results and uncertainties of the calibration process are presented, and comparisons to additional data and alternative models are discussed.

Section 3.7 provides a description of the site-scale UZ Flow Model, which simulates three-dimensional flow fields that are used in transport calculations. This section begins with a summary of the inputs that are subsequently used in the Flow Model, which include the infiltration boundary conditions, the numerical grids, calibrated properties, and conceptual models of flow and fracture-matrix interaction. A description of the Flow Model and its submodels is provided, which include flow through the PTn, effects of major faults, flow through the Calico Hills, and the effects of perched water. Results of the site-scale Flow Model are then presented, which describe the flow fields for the nine infiltration scenarios (three infiltration cases for each of the three climates) and different perched water models. Flow predominantly occurs in the fractures in the welded units and in the matrix in the nonwelded units. Significant lateral diversion exists, especially in the northern portion of the potential repository, where

perched water is simulated over zeolitized units. Abstractions include assessment of perched water models and water-table rise.

Section 3.8 presents an analysis of the Ambient Geochemistry Model and its use in testing various components of the site-scale UZ Flow Model. The features and processes that can be analyzed using the Ambient Geochemistry Model include infiltration rate, percolation flux, partitioning between matrix and fracture flow, flow pathways, and travel times in the UZ. This section summarizes the geochemical data that are available for the analyses, and it describes the development of the model, which uses the calibrated properties (see Section 3.6) and available geochemical data as input. Results indicate that chloride concentrations in the ESF and ECRB can be qualitatively predicted by the model using the mean present-day infiltration rates. Modeling studies that investigated the relationship of calcite deposition to infiltration rate, water and gas compositions, and reactive surface area also revealed that the range of net infiltration rates used in the model could capture the calcite abundance in the TSw.

Section 3.9 documents the development of the drift seepage models that are used to estimate the fraction of waste packages contacted by water and the amount of water that enters the drift as a function of several hydrologic parameters and boundary conditions. The relevant processes that impact drift seepage are detailed along with the inputs required for the model. Then, a sequence of seepage models is presented, beginning with the Seepage Calibration Model that provides seepage-related calibrated parameters. The Seepage Model for Performance Assessment is used to perform a wide range of seepage simulations using a combination of input parameters. Finally, seepage abstraction creates distributions for four seepage parameters that are sampled in TSPA-SR. Results indicate that seepage fluxes are likely to be significantly lower than percolation fluxes even under conservative assumptions, and that only a fraction of the waste packages will encounter seepage.

Section 3.10 describes the thermal-hydrological-chemical drift-scale model, which is used to simulate the composition of the water and gas in the vicinity of the heated repository as well as any mineralogical alterations that result from precipitation and dissolution processes. A description of the conceptual model for coupled processes is provided, along with a complete description of the numerical approach, which is consistent with the approach taken by the Flow Model. The results of the drift-scale THC Model reveal that the water seeping into the drifts is likely to be neutral, and the concentration of chloride in the water will not be more than four times the concentration in ambient pore water. The fracture porosity decreases by less than 1% (e.g., from 0.01 to 0.0099) in the vicinity of the drifts, which suggests that the impacts of THC effects on fracture and matrix properties (and subsequently on UZ flow) are negligible. In the abstraction for TSPA-SR calculations, the transient water and gas compositions are averaged over four discrete time periods from 0 to 100,000 years. These results are used to determine the in-drift environment and the corrosion of the drip shields and waste packages over time.

Section 3.11 presents the UZ Transport Model that is used to investigate radionuclide transport between the potential repository and the water table. This section presents two distinct transport models. The first is a process-oriented model used to investigate the importance of several features and processes that include advection, matrix diffusion, sorption, flow through faults, radioactive decay, colloidal transport, and perched water. Results of the process modeling indicate that (1) fast transport is controlled by faults at early times; (2) matrix diffusion and

sorption can be effective retardation mechanisms; (3) the vitric Calico Hills layers can provide effective retardation via flow through the matrix; (4) decay products may be important for radionuclide transport; and (5) colloidal transport is very sensitive to filtration. The second model is the particle-tracking method that is used in TSPA-SR to simulate radionuclide transport, which also includes the same processes considered in the first model. The benefit of the particle-tracking method is its computationally efficiency, which is essential for TSPA calculations.

Section 3.12 presents the mountain-scale Thermal-Hydrological (TH) Model, which is used to assess the importance of TH effects on far-field flow and transport. A description of the mountain-scale TH Model is presented, which consists of the conceptual model, input parameters, design configuration for heat load, and boundary conditions. The numerical approach for flow is consistent with that used in the Flow Model. Results are provided regarding the hydrologic and thermal behavior throughout the simulated two- and three-dimensional domains. The refined 2-D model predicts that vertical liquid flow crossing the interval between the drifts continues at a rate close to the ambient percolation flow for most of the thermal-loading period, although at some locations enhanced flow may occur as a result of condensate drainage for early times (less than a few hundred years). Based on these results, the effects of TH on far-field flow and transport are assumed negligible for TSPA-SR calculations, which simulate performance over a 10,000-year period.

Section 3.13 summarizes the uncertainties associated with the UZ flow and transport models and components. A brief description of the uncertainties in the model inputs and outputs is presented, along with the uncertainties that are carried forward to TSPA-SR. A description of how uncertainties are treated in TSPA calculations is also summarized.

Finally, Chapter 4 presents a detailed summary of the Key Technical Issues (KTIs) issued by the Nuclear Regulatory Commission that are relevant to this PMR. The six KTIs relevant to UZ flow and transport are the following: (1) Evolution of the Near-Field Environment; (2) Radionuclide Transport; (3) Structural Deformation and Seismicity; (4) Thermal Effects on Flow; (5) Total System Performance Assessment and Integration; and (6) Unsaturated Zone and Saturated Zone Flow Under Isothermal Conditions. Chapter 4 provides pointers to sections in this PMR that address each of these KTIs.

5.2 SUMMARY OF MODELS AND ABSTRACTIONS FOR TSPA-SR

This section summarizes the major components that comprise the UZ Flow and Transport Model for TSPA-SR. An overview of the process models is presented that highlights the primary inputs, outputs, and basis for each model. The subset of products that are actually used in TSPA-SR are also discussed along with a summary of the abstraction methodology. The reader is referred to the model sections (Section 3.5–3.12) for a more thorough discussion of the major conclusions from each process model component.

The integrated UZ Flow and Transport Model for TSPA-SR is comprised of four major components: (1) UZ flow, (2) drift seepage, (3) drift-scale coupled thermal-hydrologic-chemical (THC) processes, and (4) UZ transport. Figure 5.2-1 shows the icons that represent these components along with a conceptual sketch of the UZ at Yucca Mountain. Additional sub-

components (e.g., infiltration, thermal-hydrology) are described within the four major components.

5.2.1 UZ Flow

The UZ Flow Model is a three-dimensional, site-scale numerical model that simulates groundwater flow from the surface of the mountain to the water table using a dual-permeability formulation to capture flow through fracture and matrix materials (see Section 3.7). The model is generated based on information from the Geologic Framework Model, Rock Properties Model, and Mineralogical Model. It is calibrated and tested against relevant data that include perched-water data, matrix saturation, moisture potential, pneumatic data, air-permeability data, temperature data, and ambient geochemistry data. The 3-D Flow Model is also validated through percolation tests performed in Alcove 1 and comparisons to data from the ECRB, SD-6 and WT-24.

Additional submodels that provide input to the Flow Model include climate and Infiltration Models (see Section 3.5). The Climate Model provides upper and lower bounds for precipitation and temperature for modern and future climates. The temperature and precipitation records are obtained through selected meteorological stations that are chosen based on interpretation of climate analogs and orbital cycles. In the TSPA-SR base-case calculations, the timing of the climate states following post-closure are deterministically prescribed and assumed to be as follows: (1) a modern climate lasting for 600 years; (2) a monsoon climate from 600 years to 2,000 years; and (3) a glacial-transition climate for the remainder of the simulated 10,000-year period. Planned sensitivity studies using a different duration of the climate states are not expected to reveal a significant impact on performance.

The Infiltration Model uses the precipitation and temperature data from the Climate Model, along with other inputs such as hydraulic permeability and soil depth, to determine the amount of net infiltration that penetrates beneath the surface of the mountain. The Infiltration Model implements a mass balance among flow processes at the surface such as precipitation, evapotranspiration, run-on, run-off, and net infiltration. The resulting products are maps of spatially variable infiltration rates that serve as the upper boundary condition for the 3-D Flow Model. Three infiltration maps, representing low, mean, and high infiltration cases, are produced for each of the three climates to capture the uncertainty in the infiltration parameters. Therefore, a total of nine infiltration maps are used in the Flow Model.

The nine infiltration maps are used in the simulation of steady-state flow fields that are used in TSPA-SR calculations. Additional flow fields are generated for an alternative conceptual model of perched water. The alternative is a flow-through model (perched water model #1; Section 3.7) that allowed more water to percolate downward through the northern portion of the repository rather than being diverted above the basal vitrophyre. A comparison of the different perched water models revealed that the models produced similar results, although the flow-through model was slightly more conservative. As a result, only the flow-through perched water model was carried through to TSPA-SR, and the final product consisted of nine three-dimensional flow fields in the UZ (i.e., three infiltration cases for each of the three climate states).

The flow fields are used directly in TSPA-SR calculations of transport. As part of the post-processing of the flow fields, the water-table elevation is increased for the two future climate states, which are wetter than the modern climate. A conservative water-table elevation of 850 m is implemented by changing the liquid saturation of all elements (nodes) below 850 m to a value of one and adding a large sink to those nodes, effectively removing particles from the UZ. The cumulative mass of these particles leaving the UZ system are used as the source term for SZ modeling.

To weight the three infiltration cases (low, mean, and high) within each climate for TSPA-SR calculations, a Monte Carlo analysis was performed using distributions for the input parameters (e.g., hydraulic permeability, soil depth, precipitation). The results of the uncertainty analysis yielded statistical weightings of 0.17, 0.48, and 0.35 for the low, mean, and high infiltration cases, respectively (see Section 3.5.3). The weightings are used to select a flow field (corresponding to one of the three infiltration cases) within each realization of the TSPA-SR calculation. In other words, for each realization, there is a 17% chance that the low infiltration case will be selected, a 48% chance that the mean infiltration case will be selected, and a 35% chance that the high infiltration case will be selected. A given realization uses the same infiltration case for all climate states (e.g., if a realization uses a high infiltration case for the modern climate, then a high infiltration case is used for the monsoon and glacial-transition climates as well).

A final submodel that complements the ambient, steady-state flow simulations is the mountain-scale Thermal-Hydrological Model (see Section 3.12). This model consists of two- and three-dimensional submodels of the UZ Flow Model that include refinement around the repository to accommodate thermal loading. Temperatures and hydrologic conditions are simulated to determine the impact of repository heating on far-field flow. Currently, the impact of thermal effects on far-field transport remains to be rigorously tested, but based on results of the TH Model regarding increased flow through fractures due to condensate drainage, the changes to the far-field flow during the 10,000 period are not expected to be significant.

A schematic of major inputs to and outputs from the UZ Flow Model and its submodels is shown in Figure 5.2-2.

5.2.2 Drift Seepage

The drift-scale seepage models consist of a sequence of models that are used to estimate the amount of water that can enter the waste emplacement drifts under a variety of conditions (see Section 3.9). The first model in the sequence of seepage models is the Seepage Calibration Model (SCM). The SCM is a three-dimensional heterogeneous fracture-continuum numerical model that contains small-scale variability and correlation structure in the hydrologic properties. The input parameters include permeabilities from air-injection tests and other hydrologic parameters from the Calibrated Properties Model. The SCM is calibrated to seepage data obtained from liquid-release tests in the ESF to produce model-related, seepage-relevant flow parameters. The calibrated model is then used to predict the behavior of additional liquid-release tests to validate the model. Results of the SCM include a conceptual seepage process model and calibrated parameters that are relevant to the seepage processes.

The second model in the sequence of seepage models is the Seepage Model for Performance Assessment (SMPA). The SMPA is a three-dimensional, heterogeneous fracture-continuum numerical model that uses the conceptual model from the SCM as its basis. It implements a broader range of parameters from available data as well as drift-degradation scenarios. The SMPA considers variations in percolation flux, permeability, and capillarity (van Genuchten α). Results from the SMPA indicate that seepage decreases with increasing capillary strength and increasing permeability, which are conducive to greater capillary diversion around the drifts. The results also show that seepage increases with increasing permeability correlation length and drift degradation.

The wide range of seepage rates calculated from the SMPA are then used in a PA abstraction model that creates distributions for seepage fraction, mean seep flow rate, standard deviation of seep flow rate, and a flow-focusing factor. The flow-focusing factor is based on estimates of discrete "weep" spacings implied by the active fracture model and percolation fluxes calculated by the Flow Model. It is used to scale the percolation flux and the seepage fraction. Greater amounts of flow focusing yield increased seep flow rates (where seepage exists) but lower seepage fractions. Additional effects of drift degradation, rock bolts, and possible correlation between hydrologic parameters are accounted for in the abstracted model by increasing the seep flow rates. The PA seepage abstraction also has provisions for episodicity, but because the PTn overlies the entire potential repository, transient effects of precipitation and infiltration are effectively dampened at the potential repository horizon.

A schematic of major inputs to and outputs from the drift seepage models is shown in Figure 5.2-3.

5.2.3 Drift-Scale THC

The Drift-Scale THC Model is a two-dimensional dual-permeability "chimney" model that extends from the surface to the water table. It includes geologic layering consistent with the Flow Model. The model is more refined in and around the drift region, where it captures the features of the waste package, invert, and backfill (after 50 years; note that a design change was made in January 2000 that removed backfill from the reference design). It predicts transient water and gas chemistry, mineralogy, porosity, and permeability for 100,000 years (see Section 3.10). A 50-year ventilation period is simulated, as well as three infiltration scenarios corresponding to the three climate states. The model is validated through predictions and comparisons to the measured gas and water chemistry from the Drift Scale Test.

The results of the drift-scale THC process model reveal that the water seeping into the drifts is likely to be neutral (pH between 7 and 9), and the concentration of chloride in the water will not be more than a factor of four times the concentration in ambient pore water. The carbon dioxide concentrations increase with time in the drift, and the aqueous carbonate concentrations increase up to a few thousand mg/l. However, the fracture porosity decreases by less than 1% (e.g., from 0.01 to 0.0099) in the vicinity of the drifts, which suggests that the impacts of THC effects on fracture and matrix properties (and subsequently on UZ flow) are negligible.

In the abstraction for TSPA-SR calculations, the transient water and gas compositions are averaged over four discrete time periods from 0 to 100,000 years. Only the mean infiltration

cases are selected since the results of the low and high infiltration cases showed similar behavior in general. The results that are passed to the in-drift geochemical models in TSPA are aqueous concentrations for five cations and six anions, pH, and partial pressure of carbon dioxide during the four discrete periods. These results are used to determine the in-drift environment and the corrosion of the drip shields and waste packages over time.

A schematic of major inputs to and outputs from the drift-scale THC Model is shown in Figure 5.2-4.

5.2.4 UZ Transport

There are two distinct UZ transport modeling approaches: (1) a process model that tests and evaluates various transport processes and mechanisms, and (2) a TSPA particle-tracking model that incorporates the tested transport processes and mechanisms (see Section 3.11). The process model is used to gain confidence in understanding the impacts of various processes such as matrix diffusion, sorption, colloid filtration, and decay. It also serves as a basis for comparison to the TSPA model, which incorporates the same features and processes, but which uses an efficient particle-tracking algorithm that can be run in a few minutes for each TSPA realization.

The UZ transport process model includes advection, dispersion, sorption, matrix diffusion, radioactive decay and daughter products, and colloid transport. The model uses geologic and hydrologic parameters from the Flow Model and transport parameters from CRWMS M&O (2000, U0100) and CRWMS M&O (2000, U0070). The model consists of 2-D and 3-D numerical simulations that can efficiently simulate radionuclide transport. Results of the process modeling indicate that (1) fast transport is controlled by faults at early times; (2) matrix diffusion and sorption can be effective retardation mechanisms; (3) the vitric Calico Hills layers can provide effective retardation via flow through the matrix; (4) the ^{239}Pu daughter products are important to transport (at least for this subsystem analysis; full TSPA calculations must be performed to determine the overall importance to performance); and (5) colloidal transport is very sensitive to filtration.

The TSPA transport model uses the FEHM particle-tracking algorithm. It also considers advection, dispersion, matrix diffusion, sorption, and colloidal transport. It uses the flow fields generated from the Flow Model, so the dual-permeability nature of flow through fractures and matrix is preserved. The individual components and processes of the FEHM particle-tracking algorithm have been compared to other process models and analytical solutions, and the basis for the particle-tracking method is substantiated. A notable discrepancy has been identified in the conceptualization for matrix diffusion. The FEHM particle-tracking method uses a dual-porosity semi-analytical solution for retardation due to matrix diffusion (i.e., no flow occurs in the matrix in the matrix diffusion model). Studies evaluating the use of a dual-permeability matrix diffusion model have shown that significantly longer travel times can result when particles that diffuse into the matrix are allowed to subsequently transport through the matrix. Thus, the dual-porosity matrix diffusion model is considered to be a conservative choice.

As presented earlier, the thermal effects on flow are not expected to be significant, so thermal effects are neglected in the UZ transport simulations for TSPA-SR. The influence of increased temperatures on transport parameters such as distribution coefficients are also neglected.

Uncertainty in the radionuclide source-term location is implemented by using discretized zones in the repository region. The zones are currently based on ranges of infiltration (0–3, 3–10, 10–20, 20–60, and > 60 mm/yr). The release of radionuclides occurs at a random location within one of these five zones depending on the zone in which the release occurs in the engineered barrier system (EBS) models. Four zones are also defined at the water table, where radionuclide mass is collected for release at a random point in the SZ model.

A schematic of major inputs to and outputs from the UZ transport models is shown in Figure 5.2-5.

5.2.5 Treatment of Uncertainties

As discussed in Section 3.13, the models that comprise the UZ Flow and Transport Model for TSPA-SR contain inherent uncertainty and variability. The uncertainty and variability in the parameters are due, in part, to the natural variability and heterogeneity in the geological, hydrological, chemical, and mechanical systems that are difficult to characterize *in situ*, such as the precise fracture network in the UZ. Uncertainties in models may also be due to conditions that are difficult to predict, such as future climate states.

This PMR presented the bases (data collection, field tests, and calibration exercises) for using these parameters and process models. In addition, the models and analyses that are used in TSPA calculations address remaining uncertainties through probabilistic simulations or appropriate conservative assumptions.

The probabilistic simulations used in TSPA calculations consist of multiple realizations (statistically equivalent simulations) and stochastic sampling of parameters (i.e., a Monte Carlo approach). Each realization samples a set of parameters and/or models from given distributions for use in the TSPA calculation. The simulation of multiple realizations produces a range of performance results, with each outcome having a probability corresponding to its likelihood of occurrence. Thus, the uncertainty of the parameters and models leads to uncertainty in system performance. In the TSPA, the uncertainty in performance is analyzed, both in terms of its importance (i.e., is the uncertainty so great that it casts doubt on the safety of the potential repository?) and in terms of sensitivities (i.e., which parameter and submodel uncertainties have the greatest impact on the uncertainty in performance?). The probability distributions used in the TSPA uncertainty analyses reflect the degree of confidence in the input parameters and model assumptions. The resulting output distributions show whether input uncertainties have an acceptable or unacceptable impact on the calculated repository performance. The actual results of the TSPA calculations and uncertainty analyses will be included in the documentation for TSPA-SR.

In addition to probabilistic analyses, uncertainties in the process-model outputs can be addressed in abstracted TSPA models and analyses that use conservative assumptions. If insufficient evidence exists to provide a defensible range of values for a given parameter, values that bound the physical behavior or provide conservative estimates are used. These conservative assumptions are intended to increase the defensibility of the models used in TSPA calculations given the inherent uncertainties in the actual system.

In summary, as detailed in this report, the confidence in the models and parameters is built on rigorous experimental and numerical studies; remaining uncertainties are addressed in the TSPA models and analyses through probabilistic simulations or appropriate conservative assumptions.

6. REFERENCES AND INPUTS

6.1 CITED DOCUMENTS

- Abdel-Salam, A. and Chrysikopoulos, C.V. 1996. "Unsaturated Flow in a Quasi-Three-Dimensional Fractured Medium with Spatially Variable Aperture." *Water Resources Research*, 32, (6), 1531-1540. Washington, D.C.: American Geophysical Union. TIC: 239861.
- Ahlers, C.F.; Finsterle, S.; and Bodvarsson, G.S. 1999. "Characterization and Prediction of Subsurface Pneumatic Response at Yucca Mountain, Nevada." *Journal of Contaminant Hydrology*, 38, (1-3), 47-68. New York, New York: Elsevier. TIC: 244160.
- Airey, P.L. 1986. "Radionuclide Migration Around Uranium Ore Bodies in the Alligator Rivers Region of the Northern Territory of Australia: Analogue of Radioactive Waste Repositories - A Review." *Chemical Geology*, 55, (3/4), 255-268. Amsterdam, The Netherlands: Elsevier. TIC: 246691.
- Albin, A.L.; Singleton, W.L.; Moyer, T.C.; Lee, A.C.; Lung, R.C.; Eatman, G.L.W.; and Barr, D.L. 1997. *Geology of the Main Drift—Station 28+00 to 55+00, Exploratory Studies Facility, Yucca Mountain Project, Yucca Mountain, Nevada*. Denver, Colorado: Bureau of Reclamation and U.S. Geological Survey. ACC: MOL.19970625.0096.
- Anderson, R.E.; Hanks, T.C.; Reilly, T.E.; Weeks, E.P.; and Winograd, I.J. 1998. *Viability Assessment of a Repository at Yucca Mountain*. A Report to the Director, U.S. Geological Survey. Reston, Virginia: U.S. Geological Survey. ACC: HQO.19990205.0013.
- Aydan, O.; Ulusay, R.; Yuzer, E.; and Erdogan, M. 1999. "Man-made Rock Structures in Cappadocia, Turkey and Their Implications in Rock Mechanics and Rock Engineering." *International Society for Rock Mechanics News Journal*, 6, (1), 63-73. Orebro, Sweden: International Society for Rock Mechanics. TIC: 247253.
- Baker, A.; Genty, D.; Dreybrodt, W.; Barnes, W.L.; Mockler, N.J.; and Grapes, J. 1998. "Testing Theoretically Predicted Stalagmite Growth Rate with Recent Annually Laminated Samples: Implications for Past Stalagmite Deposition." *Geochimica et Cosmochimica Acta*, 62, (3), 393-404. Amsterdam, The Netherlands: Elsevier Science. TIC: 247408.
- Bandurraga, T.M. and Bodvarsson, G.S. 1999. "Calibrating Hydrogeologic Parameters for the 3-D Site-Scale Unsaturated Zone Model of Yucca Mountain, Nevada." *Journal of Contaminant Hydrology*, 38, (1-3), 25-46. New York, New York: Elsevier. TIC: 244160.
- Barnard, R.W.; Wilson, M.L.; Dockery, H.A.; Gauthier, J.H.; Kaplan, P.G.; Eaton, R.R.; Bingham, F.W.; and Robey, T.H. 1992. *TSPA 1991: An Initial Total-System Performance Assessment for Yucca Mountain*. SAND91-2795. Albuquerque, New Mexico: Sandia National Laboratories. ACC: NNA.19920630.0033.
- Barnett, D.B.; Bergeron, M.P.; Cole, C.R.; Freshley, M.D.; and Wurstner, S.K. 1997. *Tritium Monitoring in Groundwater and Evaluation of Model Predictions for the Hanford Site 200 Area*

Effluent Treatment Facility. PNNL-11665. Richland, Washington: Pacific Northwest National Laboratory. TIC: 246769.

Barr, D.L.; Moyer, T.C.; Singleton, W.L.; Albin, A.L.; Lung, R.C.; Lee, A.C.; Beason, S.C.; and Eatman, G.L.W. 1996. *Geology of the North Ramp — Stations 4+00 to 28+00, Exploratory Studies Facility, Yucca Mountain Project, Yucca Mountain, Nevada*. Denver, Colorado: U.S. Geological Survey. ACC: MOL.19970106.0496.

Bates, J.K.; Bradley, J.P.; Teetsov, A.; Bradley, C.R.; and Buchholtz ten Brink, M. 1992. "Colloid Formation During Waste Form Reaction: Implications for Nuclear Waste Disposal." *Science*, 256, 649-651. Washington, D.C.: American Association for the Advancement of Science. TIC: 239138.

Bear, J. 1988. *Dynamics of Fluids in Porous Media*. New York, New York: Dover Publications. TIC: 217568.

Bear, J.; Tsang, C.F.; and de Marsily, G., eds. 1993. *Flow and Contaminant Transport in Fractured Rock*. San Diego, California: Academic Press. TIC: 235461.

Belyaev, B.N.; Gavrilov, V.N.; Domkin, V.D.; Ivanova, V.P.; Tishkov, V.P.; Tishkova, N.A.; and Tsvetkov, O.S. 1997. "Isotope Composition of Plutonium in Soil and Possibilities of Contamination Source Identification." *Atomnaya Energiya*, 83, (4), 298-304. New York, New York: Consultants Bureau. TIC: 246731.

Bidaux, P. and Tsang, C.-F. 1991. "Fluid Flow Patterns Around a Well Bore or an Underground Drift with Complex Skin Effects." *Water Resources Research*, 27, (11), 2993-3008. Washington, D.C.: American Geophysical Union. TIC: 247407.

Birkholzer, J. and Tsang, C.F. 1997. "Solute Channeling in Unsaturated Heterogeneous Porous Media." *Water Resources Research*, 33, (10), 2221-2238. Washington, D.C.: American Geophysical Union. TIC: 235675.

Birkholzer, J.; Li, G.; Tsang, C.-F.; and Tsang, Y. 1999. "Modeling Studies and Analysis of Seepage into Drifts at Yucca Mountain." *Journal of Contaminant Hydrology*, 38, (1-3), 349-384. New York, New York: Elsevier. TIC: 244160.

Bish, D.L. and Aronson, J.L. 1993. "Paleogeothermal and Paleohydrologic Conditions in Silicic Tuff from Yucca Mountain, Nevada." *Clays and Clay Minerals*, 41, (2), 148-161. Long Island City, New York: Pergamon Press. TIC: 224613.

Bish, D.L. and Chipera, S.J. 1989. *Revised Mineralogic Summary of Yucca Mountain, Nevada*. LA-11497-MS. Los Alamos, New Mexico: Los Alamos National Laboratory. ACC: NNA.19891019.0029.

Bodvarsson, G.S.; Benson, S.M.; Sigurdsson, O.; Stefansson, V.; and Eliasson, E.T. 1984. "The Krafla Geothermal Field, Iceland, 1. Analysis of Well Test Data." *Water Resources Research*, 20, (11), 1515-1530. Washington, D.C.: American Geophysical Union. TIC: 247406.

- Bodvarsson, G.S.; Boyle, W.; Patterson, R.; and Williams, D. 1999. "Overview of Scientific Investigations at Yucca Mountain—The Potential Repository for High-Level Nuclear Waste." *Journal of Contaminant Hydrology*, 38, (1-3), 3-24. New York, New York: Elsevier. TIC: 244160.
- Bodvarsson, G.S.; Pruess, K.; Stefansson, V.; Bjornsson, S.; and Ojiambo, S.B. 1987. "East Olkaria Geothermal Field, Kenya, 1. History Match With Production and Pressure Decline Data." *Journal of Geophysical Research*, 92, (B1), 521-539. Washington, D.C.: American Geophysical Union. TIC: 236629.
- Bradshaw, L.W. 1999. "Nye County Comments on the Department of Energy (DOE) Viability Assessment (VA)." Letter from L.W. Bradshaw (Nye County Department of Natural Resources & Federal Facilities) to L.H. Barrett (DOE/OCRWM), April 13, 1999, 99-020-LB, with enclosure. ACC: MOL.19990609.0149; HQO.19990812.0019.
- Brodsky, N.S.; Riggins, M.; Connolly, J.; and Ricci, P. 1997. *Thermal Expansion, Thermal Conductivity, and Heat Capacity Measurements for Boreholes UE25 NRG-4, UE25 NRG-5, USW NRG-6, and USW NRG-7/7A*. SAND95-1955. Albuquerque, New Mexico: Sandia National Laboratories. ACC: MOL.19980311.0316.
- Brookins, D.G. 1986. "Natural Analogues for Radwaste Disposal: Elemental Migration in Igneous Contact Zones." *Chemical Geology*, 55, 337-344. Amsterdam, The Netherlands: Elsevier. TIC: 246170.
- Brooks, R.H. and Corey, A.T. 1966. "Properties of Porous Media Affecting Fluid Flow." *Journal of the American Society of Civil Engineers, Irrigation and Drainage Division*, 92, (IR2), 61-89. New York, New York: American Society of Civil Engineers. TIC: 216867.
- Broxton, D.E.; Bish, D.L.; and Warren, R.G. 1987. "Distribution and Chemistry of Diagenetic Minerals at Yucca Mountain, Nye County, Nevada." *Clays and Clay Minerals*, 35, (2), 89-110. Long Island City, New York: Pergamon Press. TIC: 203900.
- Bruton, C.J.; Glassley, W.E.; and Bourcier, W.L. 1993. "Testing Geochemical Modeling Codes Using New Zealand Hydrothermal Systems." *Proceedings of the Topical Meeting on Site Characterization and Model Validation, Focus '93, September 26-29, 1993, Las Vegas, Nevada*. Pages 240-245. La Grange Park, Illinois: American Nuclear Society. TIC: 102245.
- Buddemeier, R.W. and Hunt, J.R. 1988. "Transport of Colloidal Contaminants in Groundwater: Radionuclide Migration at the Nevada Test Site." *Applied Geochemistry*, 3, 535-548. Oxford, England: Pergamon Press. TIC: 224116.
- Budnitz, B.; Ewing, R.C.; Moeller, D.W.; Payer, J.; Whipple, C.; and Witherspoon, P.A. 1999. *Peer Review of the Total System Performance Assessment-Viability Assessment Final Report*. Las Vegas, Nevada: Total System Performance Assessment Peer Review Panel. ACC: MOL.19990317.0328.
- Buesch, D.C. and Spengler, R.W. 1998. "Character of the Middle Nonlithophysal Zone of the Topopah Spring Tuff at Yucca Mountain." *High-Level Radioactive Waste Management*,

Proceedings of the Eighth International Conference, Las Vegas, Nevada, May 11-14, 1998. Pages 16-23. La Grange Park, Illinois: American Nuclear Society. TIC: 237082.

Buesch, D.C.; Spengler, R.W.; Moyer, T.C.; and Geslin, J.K. 1996. *Proposed Stratigraphic Nomenclature and Macroscopic Identification of Lithostratigraphic Units of the Paintbrush Group Exposed at Yucca Mountain, Nevada.* Open-File Report 94-469. Denver, Colorado: U.S. Geological Survey. ACC: MOL.19970205.0061.

Buesch, D.C.; Spengler, R.W.; Nelson, P.H.; Vaniman, D.T.; Chipera, S.J.; and Bish, D.L. 1995. "Geometry of the Vitric-Zeolitic Transition in Tuffs and the Relation to Fault Zones at Yucca Mountain, Nevada." *International Union of Geodesy and Geophysics, XXI General Assembly, July 2-14, 1995*, A426. Boulder, Colorado: Geological Society of America. TIC: 237709.

Bullivant, D.P. and O'Sullivan, M.J. 1998. "Inverse Modelling of the Wairakei Geothermal Field." *Proceedings of the TOUGH Workshop '98, Lawrence Berkeley National Laboratory, Berkeley, California, May 4-6, 1998.* Preuss, K., ed. LBNL-41995. Pages 53-58. Berkeley, California: Lawrence Berkeley National Laboratory. TIC: 247159.

Buscheck, T.A. and Nitao, J.J. 1992. "Impact of Thermal Loading on Repository Performance at Yucca Mountain." *High Level Radioactive Waste Management, Proceedings of the Third International Conference, Las Vegas, Nevada, April 12-16, 1992.* 1, 1003-1017. La Grange Park, Illinois: American Nuclear Society. TIC: 204231.

Buscheck, T.A. and Nitao, J.J. 1993. "Repository-Heat-Driven Hydrothermal Flow at Yucca Mountain, Part I: Modeling and Analysis." *Nuclear Technology*, 104, (3), 418-448. La Grange Park, Illinois: American Nuclear Society. TIC: 224039.

Carrera, J. and Neuman, S.P. 1986. "Estimation of Aquifer Parameters Under Transient and Steady State Conditions: 1. Maximum Likelihood Method Incorporating Prior Information." *Water Resources Research*, 22, (2), 199-210. Washington, D.C.: American Geophysical Union. TIC: 245915.

Castor, S.B.; Henry, C.D.; and Shevenell, L.A. 1996. *Volcanic Rock-Hosted Uranium Deposits in Northwestern Nevada and Southeastern Oregon - Possible Sites for Studies of Natural Analogues for the Potential High-Level Nuclear Waste Repository at Yucca Mountain, Nevada.* Reno, Nevada: Nevada Bureau of Mines and Geology. ACC: MOL.19960927.0026.

Chandler, N.; Davidson, C.C.; Gee, G.; LaPointe, P.; and Newman, P. 1999. *A Consensus Peer Review of Predictions of Seepage into Drifts of a Proposed Repository at Yucca Mountain.* Las Vegas, Nevada: Drift Seepage Peer Review Panel. Submit to RPC URN-0078

Clemo, T. and Smith, L. 1997. "A Hierarchical Model for Solute Transport in Fractured Media." *Water Resources Research*, 33, (8), 1763-1783. Washington, D.C.: American Geophysical Union. TIC: 239864.

Crowe, B.; Self, S.; Vaniman, D.; Amos, R.; and Perry, F. 1983. "Aspects of Potential Magmatic Disruption of a High-Level Radioactive Waste Repository in Southern Nevada."

Journal of Geology, 91, (3), 259-276. Chicago, Illinois: University of Chicago Press. TIC: 216959.

CRWMS M&O (Civilian Radioactive Waste Management System Management and Operating Contractor) 1995. *Total System Performance Assessment - 1995: An Evaluation of the Potential Yucca Mountain Repository*. B00000000-01717-2200-00136 REV 01. Las Vegas, Nevada: CRWMS M&O. ACC: MOL.19960724.0188.

CRWMS M&O 1997a. *ISM2.0: A 3D Geologic Framework and Integrated Site Model of Yucca Mountain*. B00000000-01717-5700-00004 REV 00. Las Vegas, Nevada: CRWMS M&O. ACC: MOL.19970625.0119.

CRWMS M&O 1997b. *Unsaturated Zone Flow Model Expert Elicitation Project*. Las Vegas, Nevada: CRWMS M&O. ACC: MOL.19971009.0582.

CRWMS M&O 1997c. *Unsaturated Zone Radionuclide Transport Abstraction/Testing Workshop Results*. B00000000-01717-2200-00185 REV 00. Las Vegas, Nevada: CRWMS M&O. ACC: MOL.19980528.0035.

CRWMS M&O 1998a. "Climatology and Meteorology." Book 2 - Section 4 of *Yucca Mountain Site Description*. B00000000-01717-5700-00019 REV 00. Las Vegas, Nevada: CRWMS M&O. ACC: MOL.19980729.0050.

CRWMS M&O 1998b. "Geochemistry." Book 3 - Section 6 of *Yucca Mountain Site Description*. B00000000-01717-5700-00019 REV 00. Las Vegas, Nevada: CRWMS M&O. ACC: MOL.19980729.0052.

CRWMS M&O 1998c. "Geography and Demography." Book 1 - Section 1 of *Yucca Mountain Site Description*. B00000000-01717-5700-00019 REV 00. Las Vegas, Nevada: CRWMS M&O. ACC: MOL.19980729.0047.

CRWMS M&O 1998d. "Geology." Book 1 - Section 3 of *Yucca Mountain Site Description*. B00000000-01717-5700-00019 REV 00. Las Vegas, Nevada: CRWMS M&O. ACC: MOL.19980729.0049.

CRWMS M&O 1998e. "Hydrologic System." Book 2 - Section 5 of *Yucca Mountain Site Description*. B00000000-01717-5700-00019 REV 00. Las Vegas, Nevada: CRWMS M&O. ACC: MOL.19980729.0051.

CRWMS M&O 1998f. "Nearby Industrial, Transportation, and Military Facilities." Book 1 - Section 2 of *Yucca Mountain Site Description*. B00000000-01717-5700-00019 REV 00. Las Vegas, Nevada: CRWMS M&O. ACC: MOL.19980729.0048.

CRWMS M&O 1998g. "Unsaturated Zone Hydrology Model." Chapter 2 of *Total System Performance Assessment-Viability Assessment (TSPA-VA) Analyses Technical Basis Document*. B00000000-01717-4301-00002 REV 01. Las Vegas, Nevada: CRWMS M&O. ACC: MOL.19981008.0002.

CRWMS M&O 1998h. *Ex-Container System Description Document*. BCA000000-01717-1705-00019 REV 00. Two volumes. Las Vegas, Nevada: CRWMS M&O. ACC: MOL.19981211.0159.

CRWMS M&O 1998i. "Near-Field Geochemical Environment." Chapter 4 of *Total System Performance Assessment-Viability Assessment (TSPA-VA) Analyses Technical Basis Document*. B00000000-01717-4301-00004 REV 01. Las Vegas, Nevada: CRWMS M&O. ACC: MOL.19981008.0004.

CRWMS M&O 1999a. *M&O Site Investigations -- (Q)*. Activity Evaluation, September 28, 1999. Las Vegas, Nevada: CRWMS M&O. ACC: MOL.19990928.0224.

CRWMS M&O 1999b. *M&O Site Investigations*. Activity Evaluation, January 23, 1999. Las Vegas, Nevada: CRWMS M&O. ACC: MOL.19990317.0330.

CRWMS M&O 1999c. *Work Package Planning Summary, UZ Flow and Transport Process Model Report FY00*. Work Package 1401213UM1, Rev. 00. WPP-NBS-HS-000002. Las Vegas, Nevada: CRWMS M&O. ACC: MOL.19991020.0177.

CRWMS M&O 1999d. Machine Readable Media Forms; Compact Disk YMP FEP Database Rev. 00C. Las Vegas, Nevada: CRWMS M&O. ACC: MOL.19991214.0518.

CRWMS M&O 1999e. Request for Repository Subsurface Design Information to Support TSPA-SR. Input Transmittal PA-SSR-99218.Ta. Las Vegas, Nevada: CRWMS M&O. ACC: MOL.19990901.0312.

CRWMS M&O 1999f. Subsurface Design for Enhanced Design Alternative (EDA) II. Design Input Transmittal SEI-SSR-99172.T. Las Vegas, Nevada: CRWMS M&O. ACC: MOL.19990409.0100.

CRWMS M&O 2000a. *Unsaturated Zone Flow and Transport Model PMR*. Development Plan TDP-NBS-HS-000091 REV 01. Las Vegas, Nevada: CRWMS M&O. ACC: MOL.20000510.0174.

CRWMS M&O 2000b. *Repository Safety Strategy: Plan to Prepare the Postclosure Safety Case to Support Yucca Mountain Site Recommendation and Licensing Considerations*. TDR-WIS-RL-000001 REV 03. Las Vegas, Nevada: CRWMS M&O. ACC: MOL.20000119.0189.

CRWMS M&O 2000c. *Performance Confirmation Plan*. TDR-PCS-SE-000001 REV 01. Las Vegas, Nevada: CRWMS M&O. ACC: MOL.20000302.0312.

CRWMS M&O 2000 (E0040). *In Drift Microbial Communities*. ANL-EBS-MD-000038 REV 00. Las Vegas, Nevada: CRWMS M&O. ACC: MOL.20000331.0661.

CRWMS M&O 2000 (E0120). *Multiscale Thermohydrologic Model*. ANL-EBS-MD-000049 REV 00. Las Vegas, Nevada: CRWMS M&O. Submit to RPC URN-0019

CRWMS M&O 2000 (EBS PMR). *Engineered Barrier System Degradation, Flow, and Transport Process Model Report*. TDR-EBS-MD-000006 REV 00. Las Vegas, Nevada: CRWMS M&O. ACC: MOL.20000324.0558.

CRWMS M&O 2000 (I0035). *Geologic Framework Model (GFM3.1)*. MDL-NBS-GS-000002 REV 00 ICN 01. Las Vegas, Nevada: CRWMS M&O. ACC: MOL.20000121.0115.

CRWMS M&O 2000 (I0040). *Rock Properties Model (RPM3.1)*. MDL-NBS-GS-000004 REV 00 ICN 01. Las Vegas, Nevada: CRWMS M&O. ACC: MOL.20000121.0117.

CRWMS M&O 2000 (I0045). *Mineralogical Model (MM3.0) Analysis Model Report*. MDL-NBS-GS-000003 REV 00 ICN 01. Las Vegas, Nevada: CRWMS M&O. ACC: MOL.20000120.0477.

CRWMS M&O 2000. (ISM PMR) *Integrated Site Model Process Model Report*. TDR-NBS-GS-000002 REV 00 ICN 01. Las Vegas, Nevada: CRWMS M&O. ACC: MOL.20000121.0116.

CRWMS M&O 2000 (N0120/U0110). *Drift-Scale Coupled Processes (DST and THC Seepage) Models*. MDL-NBS-HS-000001 REV 00. Las Vegas, Nevada: CRWMS M&O. ACC: MOL.19990721.0523.

CRWMS M&O 2000 (N0125). *Abstraction of Drift-Scale Coupled Processes*. ANL-NBS-HS-000029 REV 00. Las Vegas, Nevada: CRWMS M&O. ACC: MOL.20000525.0371.

CRWMS M&O 2000 (U0000). *Development of Numerical Grids for UZ Flow and Transport Modeling*. ANL-NBS-HS-000015 REV 00. Las Vegas, Nevada: CRWMS M&O. ACC: MOL.19990721.0517.

CRWMS M&O 2000 (U0015). *In-Situ Field Testing of Processes*. ANL-NBS-HS-000005 REV 00. Las Vegas, Nevada: CRWMS M&O. ACC: MOL.20000504.0304.

CRWMS M&O 2000 (U0030). *Conceptual and Numerical Models for Unsaturated Zone Flow and Transport*. MDL-NBS-HS-000005 REV 00. Las Vegas, Nevada: CRWMS M&O. Submit to RPC URN-0036

CRWMS M&O 2000 (U0035). *Calibrated Properties Model*. MDL-NBS-HS-000003 REV 00. Las Vegas, Nevada: CRWMS M&O. ACC: MOL.19990721.0520.

CRWMS M&O 2000 (U0050). *UZ Flow Models and Submodels*. MDL-NBS-HS-000006 REV 00. Las Vegas, Nevada: CRWMS M&O. ACC: MOL.19990721.0527.

CRWMS M&O 2000 (U0060). *Radionuclide Transport Models under Ambient Conditions*. MDL-NBS-HS-000008 REV 00. Las Vegas, Nevada: CRWMS M&O. Submit to RPC URN-0064

CRWMS M&O 2000 (U0065). *Particle Tracking Model and Abstraction of Transport Processes*. ANL-NBS-HS-000026 REV 00. Las Vegas, Nevada: CRWMS M&O. ACC: MOL.20000502.0237

CRWMS M&O 2000 (U0070). *Unsaturated Zone Colloid Transport Model*. ANL-NBS-HS-000028 REV 00. Las Vegas, Nevada: CRWMS M&O. Submit to RPC URN-0031

CRWMS M&O 2000 (U0075). *Seepage Model for PA Including Drift Collapse*. MDL-NBS-HS-000002 REV 00. Las Vegas, Nevada: CRWMS M&O. Submit to RPC URN-0023

CRWMS M&O 2000 (U0080). *Seepage Calibration Model and Seepage Testing Data*. MDL-NBS-HS-000004 REV 00. Las Vegas, Nevada: CRWMS M&O. ACC: MOL.19990721.0521.

CRWMS M&O 2000 (U0085). *Analysis of Geochemical Data for the Unsaturated Zone*. ANL-NBS-HS-000017 REV 00. Las Vegas, Nevada: CRWMS M&O. Submit to RPC URN-0048

CRWMS M&O 2000 (U0090). *Analysis of Hydrologic Properties*. ANL-NBS-HS-000002 REV 00. Las Vegas, Nevada: CRWMS M&O. Submit to RPC URN-0055

CRWMS M&O 2000 (U0095). *Analysis of Infiltration Uncertainty*. ANL-NBS-HS-000027 REV 00. Las Vegas, Nevada: CRWMS M&O. ACC: MOL.20000525.0377.

CRWMS M&O 2000 (U0100). *Unsaturated Zone and Saturated Zone Transport Properties*. ANL-NBS-HS-000019 REV 00. Las Vegas, Nevada: CRWMS M&O. Submit to RPC URN-0038.

CRWMS M&O 2000 (U0105). *Mountain-Scale Coupled Processes (TH) Models*. MDL-NBS-HS-000007 REV 00. Las Vegas, Nevada: CRWMS M&O. ACC: MOL.19990721.0528.

CRWMS M&O 2000 (U0120). *Abstraction of Drift Seepage*. ANL-NBS-MD-000005 REV 00. Las Vegas, Nevada: CRWMS M&O. ACC: MOL.20000322.0671.

CRWMS M&O 2000 (U0125). *Abstraction of Flow Fields for RIP (ID:U0125)*. ANL-NBS-HS-000023 REV 00. Las Vegas, Nevada: CRWMS M&O. ACC: MOL.20000127.0089.

CRWMS M&O 2000 (U0135). *Natural Analogs for the Unsaturated Zone*. ANL-NBS-HS-000007 REV 00. Las Vegas, Nevada: CRWMS M&O. ACC: MOL.19990721.0524.

CRWMS M&O 2000 (U0155). *Analysis Comparing Advective-Dispersive Transport Solution to Particle Tracking*. ANL-NBS-HS-000001 REV 00. Las Vegas, Nevada: CRWMS M&O. ACC: MOL.19990721.0518.

CRWMS M&O 2000 (U0160). *Analysis of Base-Case Particle Tracking Results of the Base-Case Flow Fields*. ANL-NBS-HS-000024 REV 00. Las Vegas, Nevada: CRWMS M&O. ACC: MOL.20000207.0690.

CRWMS M&O 2000 (U0170). *Features, Events, and Processes in UZ Flow and Transport*. ANL-NBS-MD-000001 REV 00. Las Vegas, Nevada: CRWMS M&O. ACC: MOL.20000502.0240.

CRWMS M&O 2000 (WFD PMR). *Waste Form Degradation Process Model Report*. TDR-WIS-MD-000001 REV 00. Las Vegas, Nevada: CRWMS M&O. ACC: MOL.20000403.0495.

Cushey, M. and Liu, H.H. 1999. Summary of the UZ Model Workshop, Draft C, held on March 15-16, 1999, Berkeley, California: Lawrence Berkeley National Laboratory. ACC: MOL.20000510.0180.

Czarnecki, J.B.; Nelson, P.H.; O'Brien, G.M.; Sass, J.H.; Thapa, B.; Matsumoto, Y.; and Murakami, O. 1995. "Testing in Borehole USW G-2 at Yucca Mountain: The Saga Continues." *Eos*, 76, (46), 191-192. Washington, D.C.: American Geophysical Union. TIC: 240933.

Czarnecki, J.B.; O'Brien, G.M.; Nelson, P.H.; Sass, J.H.; Bullard, J.W.; and Flint, A.L. 1994. "Is There Perched Water Under Yucca Mountain in Borehole USW G-2?" *1994 Fall Meeting, Supplement to Eos, November 1, 1994*, 75, (44), 249-250. Washington, D.C.: American Geophysical Union. TIC: 226992.

Davis, O.K. 1990. "Caves as Sources of Biotic Remains in Arid Western North America." *Palaeogeography, Palaeoclimatology, Palaeoecology*, 76, (3-4), 331-348. Amsterdam, The Netherlands: Elsevier Science. TIC: 247413.

Day, W.C.; Potter, C.J.; Sweetkind, D.S.; Dickerson, R.P.; and San Juan, C.A. 1998. *Bedrock Geologic Map of the Central Block Area, Yucca Mountain, Nye County, Nevada*. Map I-2601. Washington, D.C.: U.S. Geological Survey. TIC: 237019.

de Marsily, G. 1986. *Quantitative Hydrogeology: Groundwater Hydrology for Engineers*. San Diego, California: Academic Press. TIC: 208450.

Desbarats, A.J. 1990. "Macrodispersion in Sand-Shale Sequences." *Water Resources Research*, 26, (1), 153-163. Washington, D.C.: American Geophysical Union. TIC: 236576.

DOE (U.S. Department of Energy) 1988. *Site Characterization Plan Yucca Mountain Site, Nevada Research and Development Area, Nevada*. DOE/RW-0199. Nine volumes. Washington, D.C.: U.S. Department of Energy, Office of Civilian Radioactive Waste Management. ACC: HQO.19881201.0002.

DOE 1998. *Total System Performance Assessment*. Volume 3 of *Viability Assessment of a Repository at Yucca Mountain*. DOE/RW-0508. Washington, D.C.: U.S. Department of Energy, Office of Civilian Radioactive Waste Management. ACC: MOL.19981007.0030.

DOE 1999. *Draft Environmental Impact Statement for a Geologic Repository for the Disposal of Spent Nuclear Fuel and High-Level Radioactive Waste at Yucca Mountain, Nye County, Nevada*. DOE/EIS-0250D. Summary, Volumes I and II. Washington, D.C.: U.S. Department of Energy, Office of Civilian Radioactive Waste Management. ACC: MOL.19990816.0240.

Domenico, P.A. and Schwartz, F.W. 1990. *Physical and Chemical Hydrogeology*. New York, New York: John Wiley & Sons. TIC: 234782.

Doughty, C. 1999. "Investigation of Conceptual and Numerical Approaches for Evaluating Moisture, Gas, Chemical, and Heat Transport in Fractured Unsaturated Rock." *Journal of Contaminant Hydrology*, 38, (1-3), 69-106. New York, New York: Elsevier Science Publishers. TIC: 244160.

Drozhko, E.G.; Glagolenko, Y.U.; Mokrov, Y.G.; Postovalova, G.A.; Samsonova, L.M.; Glagolev, A.V.; Ter-Saakian, S.A.; Glinsky, M.L.; Vasil'kova, N.A.; Skokov, A.V.; Wollenberg, H.A.; Tsang, C-F.; Frangos, W.; Solbau, R.D.; Stevenson, K.A.; Lowder, W.M.; and Foley, M.G. 1997. "Joint Russian-American Hydrogeological-Geochemical Studies of the Karachai-Mishelyak System." *Environmental Geology*, 29, (3/4), 216-227. Berlin, Germany: Springer-Verlag. TIC: 246744.

Ehlers, E.G. 1972. *The Interpretation of Geological Phase Diagrams*. San Francisco, California: W.H. Freeman and Company. TIC: 247331.

Ehrlich, R.; Etris, E.L.; Brumfield, D.; Yuan, L.P.; and Crabtree, S.J. 1991. "Petrography and Reservoir Physics III: Physical Models for Permeability and Formation Factor." *AAPG Bulletin*, 75, (10), 1579-1592. Tulsa, Oklahoma: American Association of Petroleum Geologists. TIC: 246294.

Ervin, E.M.; Luckey, R.R.; and Burkhardt, D.J. 1994. *Revised Potentiometric-Surface Map, Yucca Mountain and Vicinity, Nevada*. Water-Resources Investigations Report 93-4000. Denver, Colorado: U.S. Geological Survey. ACC: NNA.19930212.0018.

Fabryka-Martin, J.T.; Wightman, S.J.; Murphy, W.J.; Wickham, M.P.; Caffee, M.W.; Nimz, G.J.; Southon, J.R.; and Sharma, P. 1993. "Distribution of Chlorine-36 in the Unsaturated Zone at Yucca Mountain: An Indicator of Fast Transport Paths." *Proceedings of the Topical Meeting on Site Characterization and Model Validation, Focus '93, September 26-29, 1993, Las Vegas, Nevada*. Pages 58-68. La Grange Park, Illinois: American Nuclear Society. TIC: 102245.

Farrell, J. and Reinhard, M. 1994. "Desorption of Halogenated Organics from Model Solids, Sediments, and Soil Under Unsaturated Conditions. 2. Kinetics." *Environmental Science and Technology*, 28, (1), 63-72. Washington, D.C.: American Chemical Society. TIC: 246770.

Faybishenko, B.; Salve, R.; Zawislanski, P.; Doughty, C.; Lee, K.H.; Cook, P.; Freifeld, B.; Jacobsen, J.; Sisson, B.; Hubbell, J.; and Dooley, K. 1998. *Ponded Infiltration Test at the Box Canyon Site, Data Report and Preliminary Analysis*. LBNL-40183. Berkeley, California: Lawrence Berkeley National Laboratory. ACC: MOL.19981002.0035.

Fetter, C.W. 1993. *Contaminant Hydrogeology*. New York, New York: Macmillan Publishing. TIC: 240691.

Finch, R.J. and Ewing, R.C. 1991. "Alteration of Natural UO₂ Under Oxidizing Conditions from Shinkolobwe, Katanga, Zaire: A Natural Analogue for the Corrosion of Spent Fuel."

Radiochimica Acta, 52/53, 395-401. München, Germany: R. Oldenbourg Verlag. TIC: 237035.

Finsterle, S. 1999. *ITOUGH2 User's Guide*. LBNL-40040. Berkeley, California: Lawrence Berkeley National Laboratory. TIC: 243018.

Flint, L.E. 1998. *Characterization of Hydrogeologic Units Using Matrix Properties, Yucca Mountain, Nevada*. Water-Resources Investigations Report 97-4243. Denver, Colorado: U.S. Geological Survey. ACC: MOL.19980429.0512.

Flint, L.E. and Flint, A.L. 1995. *Shallow Infiltration Processes at Yucca Mountain, Nevada—Neutron Logging Data 1984-93*. Water-Resources Investigations Report 95-4035. Denver, Colorado: U.S. Geological Survey. ACC: MOL.19960924.0577.

Flury, M.; Flühler, H.; Jury, W.A.; and Leuenberger, J. 1994. "Susceptibility of Soils to Preferential Flow of Water: A Field Study." *Water Resources Research*, 30, (7), 1945-1954. Washington, D.C.: American Geophysical Union. TIC: 247441.

Forester, R.M.; Bradbury, J.P.; Carter, C.; Elvidge, A.B.; Hemphill, M.L.; Lundstrom, S.C.; Mahan, S.A.; Marshall, B.D.; Neymark, L.A.; Paces, J.B.; Sharpe, S.E.; Whelan, J.F.; and Wigand, P.E. 1996. *Synthesis of Quaternary Response of the Yucca Mountain Unsaturated and Saturated Zone Hydrology to Climate Change*. Milestone 3GCA102M. Las Vegas, Nevada: U.S. Geological Survey. ACC: MOL.19970211.0026.

Forester, R.M.; Bradbury, J.P.; Carter, C.; Elvidge-Tuma, A.B.; Hemphill, M.L.; Lundstrom, S.C.; Mahan, S.A.; Marshall, B.D.; Neymark, L.A.; Paces, J.B.; Sharpe, S.E.; Whelan, J.F.; and Wigand, P.E. 1999. *The Climatic and Hydrologic History of Southern Nevada During the Late Quaternary*. Open-File Report 98-635. Denver, Colorado: U.S. Geological Survey. TIC: 245717.

Francis, N.D. 1997. "The Base-Case Thermal Properties for TSPA-VA Modeling." Memorandum from N.D. Francis (SNL) to Distribution, April 16, 1997. ACC: MOL.19980518.0229.

Freeze, R.A. and Cherry, J.A. 1979. *Groundwater*. Englewood Cliffs, New Jersey: Prentice-Hall. TIC: 217571.

Frind, E.O.; Gillham, R.W.; and Pickens, J.F. 1977. "Application of Unsaturated Flow Properties in the Design of Geologic Environments for Radioactive Waste Storage Facilities." *Finite Elements in Water Resources*, 3133-3163. London, United Kingdom: Pentech Press. TIC: 239854.

Gauthier, J.H.; Wilson, M.L.; and Lauffer, F.C. 1992. "Estimating the Consequences of Significant Fracture Flow at Yucca Mountain." *High-Level Radioactive Waste Management, Proceedings of the Third Annual International Conference, Las Vegas, Nevada, April 12-16, 1992*. Pages 891-898. La Grange Park, Illinois: American Nuclear Society. TIC: 204231.

Gauthier-Lafaye F.; Weber F.; and Ohmoto, H. 1989. "Natural Fission Reactors of Oklo." *Economic Geology*, 84, (8), 2286-2295. El Paso, Texas: Economic Geology Publishing Company. TIC: 246605.

Gelhar, L.W.; Welty, C.; and Rehfeldt, K.R. 1992. "A Critical Review of Data on Field-Scale Dispersion in Aquifers." *Water Resources Research*, 28, (7), 1955-1974. Washington, D.C.: American Geophysical Union. TIC: 235780.

Ginn, T.R. and Murphy, E.M. 1997. "A Transient Flux Model for Convective Infiltration: Forward and Inverse Solutions for Chloride Mass Balance Studies." *Water Resources Research*, 33, (9), 2065-2079. Washington, D.C.: American Geophysical Union. TIC: 247422.

Glass, R.J.; Nicholl, M.J.; and Tidwell, V.C. 1996. *Challenging and Improving Conceptual Models for Isothermal Flow in Unsaturated, Fractured Rock through Exploration of Small-Scale Processes*. SAND95-1824. Albuquerque, New Mexico: Sandia National Laboratories. ACC: MOL.19970520.0082.

Glass, R.J.; Parlange, J.Y.; and Steenhuis, R.S. 1991. "Immiscible Displacement in Porous Media: Stability Analysis of Three-Dimensional, Axisymmetric Disturbances with Application to Gravity-Driven Wetting Front Instability." *Water Resources Research*, 27, (8), 1947-1956. Washington, D.C.: American Geophysical Union. TIC: 239458.

Glassley, W.E. and Christensen, B.W. 1992. "Water-Rock Interaction in New Zealand Hydrothermal Systems: Comparison of Some Simulated and Observed Geochemical Processes." *High Level Radioactive Waste Management, Proceedings of the Third International Conference, Las Vegas, Nevada, April 12-16, 1992*. 1, 352-356. La Grange Park, Illinois: American Nuclear Society. TIC: 204231.

Grathwohl, P. 1998. *Diffusion in Natural Porous Media: Contaminant Transport, Sorption/Desorption and Dissolution Kinetics*. Boston, Massachusetts: Kluwer Academic Publishers. On Order Library Tracking Number-247983.

Haukwa, C.B.; Wu, Y.S.; and Bodvarsson, G.S. 1999. "Thermal Loading Studies Using the Yucca Mountain Unsaturated Zone Model." *Journal Of Contaminant Hydrology*, 38, (1-3), 217-255. New York, New York: Elsevier Science Publishers. TIC: 244160.

Hevesi, J.A.; Ambos, D.S.; and Flint, A.L. 1994. "A Preliminary Characterization of the Spatial Variability of Precipitation at Yucca Mountain, Nevada." *High-Level Radioactive Waste Management, Proceedings of the Fifth Annual International Conference, Las Vegas, Nevada, May 22-26, 1994*. 4, 2520-2529. La Grange Park, Illinois: American Nuclear Society. TIC: 210984.

Ho, C.K. 1997a. "Evaporation of Pendant Water Droplets in Fractures." *Water Resources Research*, 33, (12), 2665-2671. Washington, D.C.: American Geophysical Union. TIC: 246969.

Ho, C.K. 1997b. "Models of Fracture-Matrix Interactions During Multiphase Heat and Mass Flow in Unsaturated Fractured Porous Media." *ASME International Mechanical Engineering*

- Congress and Exposition, Dallas, Texas, November 16-21, 1997. *FED-Vol. 244*, 401-412. New York, New York: American Society of Mechanical Engineers. TIC: 241082.
- Hoffman, D.C. and Daniels, W.R. 1981. "Assessment of the Potential for Radionuclide Migration from a Nuclear Explosion Cavity." *Groundwater Contamination Symposium*. LA-UR-81-3181. Los Alamos, New Mexico: Los Alamos Scientific Laboratory. TIC: 204725.
- Houseworth, J. and Ho, C. 1999. *Unsaturated Zone Flow and Transport Workshop Summary*. Milestone SL948M4. Las Vegas, Nevada: CRWMS M&O. ACC: MOL.19990329.0388.
- Isobe, H.; Murakami, T.; and Ewing, R.C. 1992. "Alteration of Uranium Minerals in the Koongarra Deposit, Australia: Unweathered Zone." *Journal of Nuclear Materials*, 190, 174-187. Amsterdam, The Netherlands: Elsevier Science Publishers. TIC: 246371.
- Jackson, C.P.; Hoch, A.R.; and Todman, S. 2000. "Self-Consistency of a Heterogeneous Continuum Porous Medium Representation of a Fractured Medium." *Water Resources Research*, 36, (1), 189-202. Washington, D.C.: American Geophysical Union. TIC: 247466.
- James, S.C. and Chrysikopoulos, C.V. 1999. "Transport of Polydisperse Colloid Suspensions in a Single Fracture." *Water Resources Research*, 35, (3), 707-718. Washington, D.C.: American Geophysical Union. TIC: 245938.
- Jercinovic, M.J. and Ewing, R.C. 1987. *Basaltic Glasses from Iceland and the Deep Sea: Natural Analogues to Borosilicate Nuclear Waste-Form Glass*. JSS Project Technical Report 88-01. Stockholm, Sweden: Swedish Nuclear Fuel and Waste Management Company. TIC: 205668.
- Jercinovic, M.J.; Ewing, R.C.; and Byers, C.D. 1986. "Alteration Products of Basalt Glass from Frenchman Springs Flow, Wanapum Basalts, Hanford, Washington." *Advances in Ceramics, Third Annual Symposium on Ceramics in Nuclear Waste Management, April 28-30, 1986, Chicago, Illinois*. Clark, D.E.; White, W.B.; and Machiels, A.J., eds. 20, 671-679. Westerville, Ohio: The American Ceramic Society. TIC: 210019.
- Kaplan, M.F. and Mendel, J.E. 1982. "Ancient Glass and the Safe Disposal of Nuclear Waste." *Archaeology*, 35, (4), 22-29. New York, New York: Archeological Institute of America. TIC: 247471.
- Karasaki, K.; Segan, S.; Pruess, K.; and Vomvoris, S. 1994. "A Study of Two Phase Flow in Fracture Networks." *High-Level Radioactive Waste Management, Proceedings of the Fifth Annual International Conference, Las Vegas, Nevada, May 22-26, 1994*. 4, 2633-2638. La Grange Park, Illinois: American Nuclear Society. TIC: 210984.
- Kersting, A.B.; Efurud, D.W.; Finnegan, D.L.; Rokop, D.J.; Smith, D.K.; and Thompson, J.L. 1999. "Migration of Plutonium in Ground Water at the Nevada Test Site." *Nature*, 397, 56-59. London, England: Macmillan Publishers. TIC: 243597.
- Khoury, H.N.; Salameh, E.; Clark, I.D.; Fritz, P.; Milodowski, A.E.; Cave, M.R.; Bajjali, W.; and Alexander, W.R. 1992. "A Natural Analogue of High pH Cement Pore Waters from the

Maqarin Area of Northern Jordan. I: Introduction to the Site." *Journal of Geochemical Exploration*, 46, (1), 117-132. New York, New York: Elsevier Science. TIC: 247469.

Klavetter, E.A. and Peters, R.R. 1986. *Estimation of Hydrologic Properties of an Unsaturated, Fractured Rock Mass*. SAND-84-2642. Albuquerque, New Mexico: Sandia National Laboratories. TIC: 202727.

Kneafsey, T.J. and Pruess, K. 1998. "Laboratory Experiments on Heat-Driven Two-Phase Flows in Natural and Artificial Rock Fractures." *Water Resources Research*, 34, (12), 3349-3367. Washington, D.C.: American Geophysical Union. TIC: 247468.

Koltermann, C.E. and Gorelick, S.M. 1996. "Heterogeneity in Sedimentary Deposits: A Review of Structure-Imitating, Process-Imitating, and Descriptive Approaches." *Water Resources Research*, 32, (9), 2617-2658. Washington, D.C.: American Geophysical Union. TIC: 239856.

Kotra, J.P.; Lee, M.P.; Eisenberg, N.A.; and DeWispelare, A.R. 1996. *Branch Technical Position on the Use of Expert Elicitation in the High-Level Radioactive Waste Program*. NUREG-1563. Washington, D.C.: U.S. Nuclear Regulatory Commission. TIC: 226832.

Kwicklis, E.M. and Healey, R.W. 1993. "Numerical Investigation of Steady Liquid Water Flow in a Variably Saturated Fracture Network." *Water Resources Research*, 29, (12), 4091-4102. Washington, D.C.: American Geophysical Union. TIC: 226993.

LaBolle, E.M.; Fogg, G.E.; and Tompson, A.F.B. 1996. "Random-Walk Simulation of Transport in Heterogeneous Porous Media: Local Mass-Conservation Problem and Implementation Methods." *Water Resources Research*, 32, (3), 583-593. Washington, D.C.: American Geophysical Union. TIC: 245563.

Lasaga, A.C. 1998. *Kinetic Theory in the Earth Sciences*. Princeton, New Jersey: Princeton University Press. TIC: 246279.

LeCain, G.D. 1997. *Air-Injection Testing in Vertical Boreholes in Welded and Nonwelded Tuff, Yucca Mountain, Nevada*. Water-Resources Investigations Report 96-4262. Denver, Colorado: U.S. Geological Survey. ACC: MOL.19980310.0148.

LeCain, G.D. 1998. *Results from Air-Injection and Tracer Testing in the Upper Tiva Canyon, Bow Ridge Fault, and Upper Paintbrush Contact Alcoves of the Exploratory Studies Facility, August 1994 through July 1996, Yucca Mountain, Nevada*. Water-Resources Investigations Report 98-4058. Denver, Colorado: U.S. Geological Survey. ACC: MOL.19980625.0344.

Leverett, M.C. 1941. "Capillary Behavior in Porous Solids." *AIME Transactions, Tulsa Meeting, October 1940*. 142, 152-169. New York, New York: American Institute of Mining, Metallurgical, and Petroleum Engineers. TIC: 240680.

Levy, S.S.; Fabryka-Martin, J.T.; Dixon, P.R.; Liu, B.; Turin, H.J.; and Wolfsberg, A.V. 1997. "Chlorine-36 Investigations of Groundwater Infiltration in the Exploratory Studies Facility at Yucca Mountain, Nevada." *Scientific Basis for Nuclear Waste Management XX, Symposium*

held December 2-6, 1996, Boston, Massachusetts. Gray, W.J. and Triay, I.R., eds. 465, 901-908. Pittsburgh, Pennsylvania: Materials Research Society. TIC: 238884.

Lichtner, P.C.; Keating, G.; and Carey, B. 1999. *A Natural Analogue for Thermal-Hydrological-Chemical Coupled Processes at the Proposed Nuclear Waste Repository at Yucca Mountain, Nevada*. LA-13610-MS. Los Alamos, New Mexico: Los Alamos National Laboratory. TIC: 246032.

Lin, W.; Wilder, D.; Blair, S.; Daily, W.; Gdowski, G.; Glassley, W.; Lee, K.; Meike, A.; Ramirez, A.; Roberts, J.; Ruddle, D.; Wagoner, J.; Watwood, D.; Williams, T.; and Carlson, R. 1998. "The Large Block Test of the Exploratory Studies Facility Thermal Tests." *High-Level Radioactive Waste Management, Proceedings of the Eighth International Conference, Las Vegas, Nevada, May 11-14, 1998*. Pages 49-51. La Grange Park, Illinois: American Nuclear Society. TIC: 237082.

Lippmann, M.J. and Bodvarsson, G.S. 1985. "The Heber Geothermal Field, California: Natural State and Exploitation Modeling Studies." *Journal of Geophysical Research*, 90, (B1), 745-758. Washington, D.C.: American Geophysical Union. TIC: 247477.

Liu, H.H. and Dane, J.H. 1996. "An Interpolation-Corrected Modified Method of Characteristics to Solve Advection-Dispersion Equations." *Advances in Water Resources*, 19, (6), 359-368. Amsterdam, The Netherlands: Elsevier Science. TIC: 247478.

Liu, H.H.; Doughty, C.; and Bodvarsson, G.S. 1998. "An Active Fracture Model for Unsaturated Flow and Transport in Fractured Rocks." *Water Resources Research*, 34, (10), 2633-2646. Washington, D.C.: American Geophysical Union. TIC: 243012.

Loeven, C. 1993. *A Summary and Discussion of Hydrologic Data from the Calico Hills Nonwelded Hydrogeologic Unit at Yucca Mountain, Nevada*. LA-12376-MS. Los Alamos, New Mexico: Los Alamos National Laboratory. ACC: NNA.19921116.0001.

Luckey, R.R.; Tucci, P.; Faunt, C.C.; Ervin, E.M.; Steinkampf, W.C.; D'Agnese, F.A.; and Patterson, G.L. 1996. *Status of Understanding of the Saturated-Zone Ground-Water Flow System at Yucca Mountain, Nevada, as of 1995*. Water-Resources Investigations Report 96-4077. Denver, Colorado: U.S. Geological Survey. ACC: MOL.19970513.0209.

Luckner, L.; van Genuchten, M.T.; and Nielsen, D.R. 1989. "A Consistent Set of Parametric Models for the Two-Phase Flow of Immiscible Fluids in the Subsurface." *Water Resources Research*, 25, (10), 2187-2193. Washington, D.C.: American Geophysical Union. TIC: 224845.

Matyskiela, W. 1997. "Silica Redistribution and Hydrologic Changes in Heated Fractured Tuff." *Geology*, 25, (12), 1115-1118. Boulder, Colorado: Geological Society of America. TIC: 236809.

McCarthy, J.F. and Zachara, J.M. 1989. "Subsurface Transport of Contaminants." *Environmental Science & Technology*, 23, (5), 496-502. Easton, Pennsylvania: American Chemical Society. TIC: 224876.

- McKelvey, V. 1976. Major Assets and Liabilities of the Nevada Test Site as a High-Level Radioactive Waste Repository. Letter from Dr. V. McKelvey (USGS) to R.W. Roberts (U.S. Energy Research and Development Administration), July 9, 1976, with enclosure, "Table 1. Assets and Liabilities of Nevada Test Site as Potential High-Level Radioactive Waste Repository." ACC: MOL.19990119.0314.
- McKinley, I.G.; Bath, A.H.; Berner, U.; Cave, M.; and Neal, C. 1988. "Results of the Oman Analogue Study." *Radiochimica Acta*, 44/45, (2), 311-316. Munich, Germany: R. Oldenbourg Verlag. TIC: 247492.
- Mercer, J.W. and Faust, C.R. 1979. "Geothermal Reservoir Simulation: 3. Application of Liquid- and Vapor-Dominated Hydrothermal Modeling Techniques to Wairakei, New Zealand." *Water Resources Research*, 15, (3), 653-671. Washington, D.C.: American Geophysical Union. TIC: 247493.
- Montazer, P. 1987. "Monitoring Hydrologic Conditions in the Vadose Zone in Fractured Rocks, Yucca Mountain, Nevada." Flow and Transport through Unsaturated Fractured Rock. Evans, D.D. and Nicholson, T.J., eds. Geophysical Monograph No. 42, 31-42. Washington, D.C.: American Geophysical Union. TIC: 225379.
- Montazer, P. and Wilson, W.E. 1984. *Conceptual Hydrologic Model of Flow in the Unsaturated Zone, Yucca Mountain, Nevada*. Water-Resources Investigations Report 84-4345. Lakewood, Colorado: U.S. Geological Survey. ACC: NNA.19890327.0051.
- Moridis, G.J. 1999. "Semianalytical Solutions for Parameter Estimation in Diffusion Cell Experiments." *Water Resources Research*, 35, (6), 1729-1740. Washington, D.C.: American Geophysical Union. TIC: 246266.
- Moyer, T.C.; Geslin, J.K.; and Flint, L.E. 1996. *Stratigraphic Relations and Hydrologic Properties of the Paintbrush Tuff Nonwelded (PTn) Hydrologic Unit, Yucca Mountain, Nevada*. Open-File Report 95-397. Denver, Colorado: U.S. Geological Survey. ACC: MOL.19970204.0216.
- Murakami, T.; Ohnuki, T.; Isobe, H.; and Sato, T. 1997. "Mobility of Uranium During Weathering." *American Mineralogist*, 82, 888-899. Washington, D.C.: Mineralogical Society of America. TIC: 246053.
- Murphy, W.M.; Percy, E.C.; Green, R.T.; Prikryl, J.D.; Mohanty, S.; Leslie, B.W.; and Nedungadi, A. 1998. "A Test of Long-Term, Predictive, Geochemical Transport Modeling at the Akrotiri Archaeological Site." *Journal of Contaminant Hydrology*, 29, 245-279. Amsterdam, The Netherlands: Elsevier Science B.V. TIC: 247211.
- Nataraja, M.S. and Brandshaug, T. 1992. Staff Technical Position on Geologic Repository Operations Area Underground Facility Design - Thermal Loads. NUREG-1466. Washington, D.C.: U.S. Nuclear Regulatory Commission. ACC: NNA.19921030.0049.
- National Research Council 1996. *Rock Fractures and Fluid Flow, Contemporary Understanding and Applications*. Washington, D.C.: National Academy Press. TIC: 235913.

- Nativ, R.; Adar, E.; Dahan, O.; and Geyh, M. 1995. "Water Recharge and Solute Transport through the Vadose Zone of Fractured Chalk Under Desert Conditions." *Water Resources Research*, 31, (2), 253-261. Washington, D.C.: American Geophysical Union. TIC: 233563.
- Neretnieks, I. 1993. "Solute Transport in Fractured Rock - Applications to Radionuclide Waste Repositories." Chapter 2 of *Flow and Contaminant Transport in Fractured Rock*. Bear, J.; Tsang, C.F.; and de Marsily, G., eds. 39-127. San Diego, California: Academic Press. TIC: 235461.
- Neuman, S.P. 1990. "Universal Scaling of Hydraulic Conductivities and Dispersivities in Geologic Media." *Water Resources Research*, 26, (8), 1749-1758. Washington, D.C.: American Geophysical Union. TIC: 237977.
- Nicholl, M.J.; Glass, R.J.; and Wheatcraft, S.W. 1994. "Gravity-Driven Infiltration Instability in Initially Dry Nonhorizontal Fractures." *Water Resources Research*, 30, (9), 2533-2546. Washington, D.C.: American Geophysical Union. TIC: 243493.
- Nitao, J. and Buscheck, T. 1991. "Infiltration of a Liquid Front in an Unsaturated, Fractured Porous Medium." *Water Resources Research*, 27, (8), 2099-2112. Washington, D.C.: American Geophysical Union. TIC: 224848.
- Nitao, J.J. 1998. "Thermohydrochemical Alteration of Flow Pathways Above and Below the Repository." Chapter 5.6 of *Near-Field/Altered-Zone Models Report*. Hardin, E.L. UCRL-ID-129179 DR. Livermore, California: Lawrence Livermore National Laboratory. ACC: MOL.19980504.0577.
- NRC (U.S. Nuclear Regulatory Commission) 1997. *Issue Resolution Status Report on Methods to Evaluate Climate Change and Associated Effects at Yucca Mountain (Key Technical Issue: Unsaturated and Saturated Flow Under Isothermal Conditions)*. Washington, D.C.: U.S. Nuclear Regulatory Commission. ACC: MOL.19980219.0880.
- NRC 1999a. *Issue Resolution Status Report Key Technical Issue: Radionuclide Transport*. Rev. 1. Washington, D.C.: U.S. Nuclear Regulatory Commission. ACC: MOL.19991214.0621.
- NRC 1999b. *Issue Resolution Status Report Key Technical Issue: Evolution of the Near-Field Environment*. Rev. 2. Washington, D.C.: U.S. Nuclear Regulatory Commission. ACC: MOL.19990810.0640.
- NRC 1999c. *Issue Resolution Status Report Key Technical Issue: Structural Deformation and Seismicity*. Rev. 2. Washington, D.C.: U.S. Nuclear Regulatory Commission. ACC: MOL.19991214.0623.
- NRC 1999d. *Issue Resolution Status Report Key Technical Issue: Thermal Effects on Flow*. Rev. 2. Washington, D.C.: U.S. Nuclear Regulatory Commission. ACC: MOL.19991021.0156.

- NRC 1999e. *Issue Resolution Status Report Key Technical Issue: Unsaturated and Saturated Flow Under Isothermal Conditions*. Rev. 2. Washington, D.C.: U.S. Nuclear Regulatory Commission. ACC: MOL.19990810.0641.
- NRC 2000. *Issue Resolution Status Report Key Technical Issue: Total System Performance Assessment and Integration*. Rev. 2. Washington, D.C.: U.S. Nuclear Regulatory Commission. TIC: 247614.
- NWTRB (Nuclear Waste Technical Review Board) 1999. *Report to the U.S. Congress and The Secretary of Energy, January to December 1998*. Arlington, Virginia: U.S. Nuclear Waste Technical Review Board. ACC: HQO.19990706.0007.
- NWTRB 2000. *Report to the U.S. Congress and the Secretary of Energy, January to December 1999*. Arlington, Virginia: U.S. Nuclear Waste Technical Review Board. TIC: 247806.
- Oldenburg, C.M. and Pruess, K. 1993. "On Numerical Modeling of Capillary Barriers." *Water Resources Research*, 29, (4), 1045-1056. Washington, D.C.: American Geophysical Union. TIC: 238834.
- Paces, J.B.; Forester, R.M.; Whelan, J.F.; Mahan, S.A.; Bradbury, J.P.; Quade, J.; Neymark, L.A.; and Kwak, L.M. 1996. *Synthesis of Ground-Water Discharge Deposits Near Yucca Mountain*. Milestone 3GQH671M. Las Vegas, Nevada: U.S. Geological Survey. ACC: MOL.19970205.0007.
- Paces, J.B.; Ludwig, K.R.; Peterman, Z.E.; Neymark, L.A.; and Kenneally, J.M. 1998a. "Anomalous Groundwater ²³⁴U/²³⁸U Beneath Yucca Mountain: Evidence of Local Recharge?" *High-Level Radioactive Waste Management, Proceedings of the Eighth International Conference, Las Vegas, Nevada, May 11-14, 1998*. Pages 185-188. La Grange Park, Illinois: American Nuclear Society. TIC: 237082.
- Paces, J.B.; Newmark, L.A.; Marshall, B.D.; Whelan, J.F.; and Peterman, Z.E. 1998b. "Inferences for Yucca Mountain Unsaturated-Zone Hydrology from Secondary Minerals." *High-Level Radioactive Waste Management, Proceedings of the Eighth International Conference, Las Vegas, Nevada, May 11-14, 1998*. Pages 36-39. La Grange Park, Illinois: American Nuclear Society. TIC: 237082.
- Paleologos, E.K.; Neuman, S.P.; and Tartakovsky, D. 1996. "Effective Hydraulic Conductivity of Bounded, Strongly Heterogeneous Porous Media." *Water Resources Research*, 32, (5), 1333-1341. Washington, D.C.: American Geophysical Union. TIC: 245760.
- Pearcy, E.C.; Prikryl, J.D.; and Leslie, B.W. 1995. "Uranium Transport Through Fractured Silicic Tuff and Relative Retention in Areas with Distinct Fracture Characteristics." *Applied Geochemistry*, 10, 685-704. Oxford, United Kingdom: Elsevier Science. TIC: 246848.
- Pearcy, E.C.; Prikryl, J.D.; Murphy, W.M.; and Leslie, B.W. 1994. "Alteration of Uraninite from the Nopal I Deposit, Pena Blanca District, Chihuahua, Mexico, Compared to Degradation of Spent Nuclear Fuel in the Proposed U.S. High-Level Nuclear Waste Repository at Yucca

Mountain, Nevada." *Applied Geochemistry*, 9, 713-732. New York, New York: Elsevier. TIC: 236934.

Peters, R.R. and Klavetter, E.A. 1988. "A Continuum Model for Water Movement in an Unsaturated Fractured Rock Mass." *Water Resources Research*, 24, (3), 416-430. Washington, D.C.: American Geophysical Union. TIC: 223603.

Philip, J.R.; Knight, J.H.; and Waechter, R.T. 1989. "Unsaturated Seepage and Subterranean Holes: Conspectus, and Exclusion Problem for Circular Cylindrical Cavities." *Water Resources Research*, 25, (1), 16-28. Washington, D.C.: American Geophysical Union. TIC: 239117.

Phillips, F.M. 1994. "Environmental Tracers for Water Movement in Desert Soils of the American Southwest." *Soil Science Society of America Journal*, 58, 15-24. Madison, Wisconsin: Soil Science Society of America. TIC: 240651.

Pickett, D.A. and Murphy, W.M. 1997. "Isotopic Constraints on Radionuclide Transport at Pena Blanca." *Seventh EC Natural Analogue Working Group Meeting: Proceedings of an International Workshop held in Stein am Rhein, Switzerland from 28 to 30 October 1996.* von Maravic, H. and Smellie, J., eds. EUR 17851EN, 113-122. Luxembourg, Luxembourg: European Communities. TIC: 247461.

Pickett, D.A. and Murphy, W.M. 1999. "Unsaturated Zone Waters from the Nopal I Natural Analog, Chihuahua, Mexico - Implications for Radionuclide Mobility at Yucca Mountain." *Scientific Basis for Nuclear Waste Management XXII, Materials Research Society Symposium held November 30-December 4, 1998, Boston, Massachusetts, U.S.A.* Wronkiewicz, D.J. and Lee, J.H., eds. 556, 809-816. Warrendale, Pennsylvania: Materials Research Society. TIC: 246426.

Plummer, M.A.; Phillips, F.M.; Fabryka-Martin, J.; Turin, H.J.; Wigand, P.E.; and Sharma, P. 1997. "Chlorine-36 in Fossil Rat Urine: An Archive of Cosmogenic Nuclide Deposition During the Past 40,000 Years." *Science*, 277, 538-541. Washington, D.C.: American Association for the Advancement of Science. TIC: 237425.

Potter, C.J.; Dickerson, R.P.; and Day, W.C. 1999. *Nature and Continuity of the Sundance Fault.* Open-File Report 98-266. Denver, Colorado: U.S. Geological Survey. TIC: 246609.

Pruess, K. 1987. *TOUGH User's Guide.* NUREG/CR-4645. Washington, D.C.: U.S. Nuclear Regulatory Commission. TIC: 217275.

Pruess, K. 1991. *TOUGH2-A General-Purpose Numerical Simulator for Multiphase Fluid and Heat Flow.* LBL-29400. Berkeley, California: Lawrence Berkeley Laboratory. ACC: NNA.19940202.0088.

Pruess, K. 1997. "On Vaporizing Water Flow in Hot Sub-Vertical Rock Fractures." *Transport in Porous Media*, 28, 335-372. Amsterdam, The Netherlands: Kluwer Academic Publishers. TIC: 238922.

- Pruess, K. 1999. "A Mechanistic Model for Water Seepage through Thick Unsaturated Zones in Fractured Rocks of Low Matrix." *Water Resources Research*, 35, (4), 1039-1051. Washington, D.C.: American Geophysical Union. TIC: 244913.
- Pruess, K. and Narasimhan, T.N. 1985. "A Practical Method for Modeling Fluid and Heat Flow in Fractured Porous Media." *Society of Petroleum Engineers Journal*, 25, (1), 14-26. Richardson, Texas: Society of Petroleum Engineers. TIC: 221917.
- Pruess, K.; Faybishenko, B.; and Bodvarsson, G.S. 1999. "Alternative Concepts and Approaches for Modeling Flow and Transport in Thick Unsaturated Zones of Fractured Rocks." *Journal of Contaminant Hydrology*, 38, (1-3), 281-322. New York, New York: Elsevier. TIC: 244160.
- Pruess, K.; Tsang, Y.W.; and Wang, J.S.Y. 1984. *Numerical Studies of Fluid and Heat Flow Near High-Level Nuclear Waste Packages Emplaced in Partially Saturated Fractured Tuff*. LBL-18552. Berkeley, California: Lawrence Berkeley Laboratory. TIC: 211033.
- Pruess, K.; Wang, J.S.Y.; and Tsang, Y.W. 1990a. "On Thermohydrologic Conditions Near High-Level Nuclear Wastes Emplaced in Partially Saturated Fractured Tuff: 1. Simulation Studies with Explicit Consideration of Fracture Effects." *Water Resources Research*, 26, (6), 1235-1248. Washington, D.C.: American Geophysical Union. TIC: 221923.
- Pruess, K.; Wang, J.S.Y.; and Tsang, Y.W. 1990b. "On Thermohydrologic Conditions Near High-Level Nuclear Wastes Emplaced in Partially Saturated Fractured Tuff: 2. Effective Continuum Approximation." *Water Resources Research*, 26, (6), 1249-1261. Washington, D.C.: American Geophysical Union. TIC: 224854.
- Ramirez, A.L.; Carlson, R.C.; and Buscheck, T.A. 1991. *In Situ Changes in the Moisture Content of Heated, Welded Tuff Based on Thermal Neutron Measurements*. UCRL-ID-104715. Livermore, California: Lawrence Livermore National Laboratory. ACC: NNA.19910701.0097.
- Rasmussen, T.C. 1991. "Steady Fluid Flow and Travel Times in Partially Saturated Fractures Using a Discrete Air-Water Interface." *Water Resources Research*, 27, (1), 67-76. Washington, D.C.: American Geophysical Union. TIC: 247498.
- Rautman, C.A. and McKenna, S.A. 1997. *Three-Dimensional Hydrological and Thermal Property Models of Yucca Mountain, Nevada*. SAND97-1730. Albuquerque, New Mexico: Sandia National Laboratories. ACC: MOL.19980311.0317.
- Reed, M.H. 1982. "Calculation of Multicomponent Chemical Equilibria and Reaction Processes in Systems Involving Minerals, Gases, and an Aqueous Phase." *Geochimica et Cosmochimica Acta*, 46, 513-528. New York, New York: Pergamon Press. TIC: 224159.
- Richards, L.A. 1931. "Capillary Conduction of Liquids Through Porous Media." *Physics*, 1, 318-333. Washington, D.C.: American Physical Society. TIC: 225383.
- Ritcey, A.C. and Wu, Y.S. 1999. "Evaluation of the Effect of Future Climate Change on the Distribution and Movement of Moisture in the Unsaturated Zone at Yucca Mountain, NV."

Journal of Contaminant Hydrology, 38, (1-3), 257-279. New York, New York: Elsevier. TIC: 244160.

Robinson, B.A.; Wolfsberg, A.V.; Viswanathan, H.S.; Bussod, G.Y.; Gable, C.W.; and Meijer, A. 1997. *The Site-Scale Unsaturated Zone Transport Model of Yucca Mountain*. Milestone Report SP25BM3. Los Alamos, New Mexico: Los Alamos National Laboratory. ACC: MOL.19980203.0570.

Robinson, B.A.; Wolfsberg, A.V.; Viswanathan, H.S.; Gable, C.W.; Zyvoloski, G.A.; and Turin, H.J. 1996. *Site Scale Unsaturated Zone Flow and Transport Model, Modeling of Flow, Radionuclide Migration, and Environmental Isotope Distributions at Yucca Mountain*. Milestone 3672. Draft. Los Alamos, New Mexico: Los Alamos National Laboratory. ACC: MOL.19971111.0625.

Robinson, B.A.; Wolfsberg, A.V.; Zyvoloski, G.A.; and Gable, C.W. 1995. *An Unsaturated Zone Flow and Transport Model of Yucca Mountain*. Milestone 3468. Draft. Los Alamos, New Mexico: Los Alamos National Laboratory. ACC: MOL.19960415.0218.

Robison, J.H. 1984. *Ground-Water Level Data and Preliminary Potentiometric-Surface Maps, Yucca Mountain and Vicinity, Nye County Nevada*. Water-Resources Investigations Report 84-4197. Lakewood, Colorado: U.S. Geological Survey. ACC: NNA.19930629.0013.

Roseboom, E.H., Jr. 1983. *Disposal of High-Level Nuclear Waste above the Water Table in Arid Regions*. Geological Survey Circular 903. Denver, Colorado: U.S. Geological Survey. TIC: 216597.

Ross, B. 1990. "The Diversion Capacity of Capillary Barriers." *Water Resources Research*, 26, (10), 2625-2629. Washington, D.C.: American Geophysical Union. TIC: 225235.

Rousseau, J.P.; Kwicklis, E.M.; and Gillies, D.C. 1999. *Hydrogeology of the Unsaturated Zone, North Ramp Area of the Exploratory Studies Facility, Yucca Mountain, Nevada*. Water-Resources Investigations Report 98-4050. Denver, Colorado: U.S. Geological Survey. ACC: MOL.19990419.0335.

Rousseau, J.P.; Loskot, C.L.; Thamir, F.; and Lu, N. 1997. *Results of Borehole Monitoring in the Unsaturated Zone Within the Main Drift Area of the Exploratory Studies Facility, Yucca Mountain, Nevada*. Milestone SPH22M3. Denver, Colorado: U.S. Geological Survey. ACC: MOL.19970626.0351.

Rulon, J.; Bodvarsson, G.S.; and Montazer, P. 1986. *Preliminary Numerical Simulations of Groundwater Flow in the Unsaturated Zone, Yucca Mountain, Nevada*. LBL-20553. Berkeley, California: Lawrence Berkeley Laboratory. ACC: NNA.19870908.0027.

Rumynin, V.G.; Mironenko, V.A.; Sindalovsky, L.N.; Boronina, A.V.; Konosavsky, P.K.; and Pozdniakov, S.P. 1998. *Evaluation of Conceptual, Mathematical and Physical-and-Chemical Models for Describing Subsurface Radionuclide Transport at the Lake Karachai Waste Disposal Site*. LBNL-41974. Berkeley, California: Lawrence Berkeley National Laboratory. TIC: 246562.

Russell, C.E.; Hess, J.W.; and Tyler, S.W. 1987. "Hydrogeologic Investigations of Flow in Fractured Tuffs, Rainier Mesa, Nevada Test Site." *Flow and Transport Through Unsaturated Fractured Rock*. AGU Geophysical Monograph 42. Washington, D.C.: American Geophysical Union. TIC: 247649.

Rybal'chenko, A.I.; Pimenov, M.K.; Kostin, P.P.; Balukova, V.D.; Nosukhin, A.V.; Mikerin, E.I.; Egorov, N.N.; Kaimin, E.P.; Kosareva, I.M.; and Kurochkin, V.M. 1998. *Deep Injection Disposal of Liquid Radioactive Waste in Russia*. Foley, M.G. and Ballou, L.M.G., eds. Columbus, Ohio: Battelle Press. TIC: 247062.

Sammel, E.A.; Ingebritsen, S.E.; and Mariner, R.H. 1988. "The Hydrothermal System at Newberry Volcano, Oregon." *Journal of Geophysical Research*, 93, (B9), 10147-10162. Washington, D.C.: American Geophysical Union. TIC: 247523.

Sass, J.H.; Lachenbruch, A.H.; Dudley, W.W., Jr.; Priest, S.S.; and Munroe, R.J. 1988. *Temperature, Thermal Conductivity, and Heat Flow Near Yucca Mountain, Nevada: Some Tectonic and Hydrologic Implications*. Open-File Report 87-649. Denver, Colorado: U.S. Geological Survey. ACC: MOL.19971027.0303.

Sawyer, D.A.; Fleck, R.J.; Lanphere, M.A.; Warren, R.G.; Broxton, D.E.; and Hudson, M.R. 1994. "Episodic Caldera Volcanism in the Miocene Southwestern Nevada Volcanic Field: Revised Stratigraphic Framework, $^{40}\text{Ar}/^{39}\text{Ar}$ Geochronology, and Implications for Magmatism and Extension." *Geological Society of America Bulletin*, 106, (10), 1304-1318. Boulder, Colorado: Geological Society of America. TIC: 222523.

Scott, R.B. and Bonk, J. 1984. *Preliminary Geologic Map of Yucca Mountain, Nye County, Nevada, with Geologic Sections*. Open-File Report 84-494. Denver, Colorado: U.S. Geological Survey. TIC: 203162.

Selker, J.S.; Steenhuis, R.T.; and Parlange, J.-Y. 1992. "Wetting Front Instability in Homogeneous Sandy Soils Under Continuous Infiltration." *Soil Science Society of America Journal*, 56, (5), 1346-1350. Madison, Wisconsin: Soil Science Society of America. TIC: 247522.

Sharp J.M.; Kreisel, J.I.; and Milliken K.L. 1996. "Fracture Skin Properties and Effects on Solute Transport: Geotechnical and Environmental Implications." *Rock Mechanics, Tools and Techniques, Proceedings of the 2nd North American Rock Mechanics Symposium, NARMS '96, A Regional Conference of ISRM, Montreal, Quebec, Canada, 19-21 June 1996*. 1329-1335. Rotterdam, The Netherlands: A.A. Balkema. TIC: 239941.

Sinnock, S.; Lin, Y.T.; and Brannen, J.P. 1987. "Preliminary Bounds on the Expected Postclosure Performance of the Yucca Mountain Repository Site, Southern Nevada." *Journal of Geophysical Research*, 92, (B8), 7820-7842. Washington, D.C.: American Geophysical Union. TIC: 222650.

Slider, H.C. 1976. *Practical Petroleum Reservoir Engineering Methods, An Energy Conservation Science*. Tulsa, Oklahoma: Petroleum Publishing Company. TIC: 247798.

Sonnenthal, E.L. and Bodvarsson, G.S. 1999. "Constraints on the Hydrology of the Unsaturated Zone at Yucca Mountain, NV from Three-Dimensional Models of Chloride and Strontium Geochemistry." *Journal of Contaminant Hydrology*, 38, (1-3), 107-156. New York, New York: Elsevier. TIC: 244160.

Spaulding, W.G. 1985. *Vegetation and Climates of the Last 45,000 Years in the Vicinity of the Nevada Test Site, South-Central Nevada*. Professional Paper 1329. Washington, D.C.: U.S. Geological Survey. TIC: 203210.

Spengler, R.W.; Braun, C.A.; Martin, L.G.; and Weisenberg, C.W. 1994. *The Sundance Fault: A Newly Recognized Shear Zone at Yucca Mountain, Nevada*. Open-File Report 94-49. Denver, Colorado: U.S. Geological Survey. ACC: NNA.19940128.0119.

Steefel, C.I. and Lasaga, A.C. 1994. "A Coupled Model for Transport of Multiple Chemical Species and Kinetic Precipitation/Dissolution Reactions with Application to Reactive Flow in Single Phase Hydrothermal Systems." *American Journal of Science*, 294, (5), 529-592. New Haven, Connecticut: Kline Geology Laboratory, Yale University. TIC: 235372.

Steefel, C.I. and Lichtner, P.C. 1998. "Multicomponent Reactive Transport in Discrete Fractures: I. Controls on Reaction Front Geometry." *Journal of Hydrology*, 209, 186-199. Amsterdam, The Netherlands: Elsevier Science B.V. TIC: 247524.

Stockman, H.; Krumhansl, J.; Ho, C.; and McConnell, V. 1994. *The Valles Natural Analogue Project*. NUREG/CR-6221. Washington, D.C.: U.S. Nuclear Regulatory Commission. TIC: 246123.

Stroupe, E.P. 2000. "Approach to Implementing the Site Recommendation Design Baseline." Interoffice correspondence from E.P. Stroupe (CRWMS M&O) to D.R. Wilkins, January 26, 2000, LV.RSO.EPS.1/00-004, with attachment. ACC: MOL.20000214.0480.

Stuckless, J.S.; Peterman, Z.E.; and Muhs, D.R. 1991. "U and Sr Isotopes in Ground Water and Calcite, Yucca Mountain, Nevada: Evidence Against Upwelling Water." *Science*, 254, 551-554. Washington, D.C.: American Association for the Advancement of Science. TIC: 224423.

Szabo, B.J.; Kolesar, P.T.; Riggs, A.C.; Winograd, I.J.; and Ludwig, K.R. 1994. "Paleoclimatic Inferences from a 120,000-Yr Calcite Record of Water Table Fluctuation in Browns Room of Devils Hole, Nevada." *Quaternary Research*, 41, 59-69. New York, New York: Academic Press. TIC: 234642.

Thoma, S.G.; Gallegos, D.P.; and Smith, D.M. 1992. "Impact of Fracture Coatings on Fracture/Matrix Flow Interactions in Unsaturated, Porous Media." *Water Resources Research*, 28, (5), 1357-1367. Washington, D.C.: American Geophysical Union. TIC: 237509.

Thordarson, W. 1965. *Perched Ground Water in Zeolitized-Bedded Tuff, Rainier Mesa and Vicinity, Nevada Test Site, Nevada*. TEI-862. Washington, D.C.: U.S. Geological Survey. ACC: NN1.19881021.0066.

- Tompson, A.F.B. and Gelhar, L.W. 1990. "Numerical Simulation of Solute Transport in Three-Dimensional, Randomly Heterogeneous Porous Media." *Water Resources Research*, 26, (10), 2541-2562. Washington, D.C.: American Geophysical Union. TIC: 224902.
- Tsang, Y.W. and Birkholzer, J.T. 1999. "Predictions and Observations of the Thermal-Hydrological Conditions in the Single Heater Test." *Journal of Contaminant Hydrology*, 38, (1-3), 385-425. New York, New York: Elsevier. TIC: 244160.
- Tucci, P. and Burkhardt, D.J. 1995. *Potentiometric-Surface Map, 1993, Yucca Mountain and Vicinity, Nevada*. Water-Resources Investigations Report 95-4149. Denver, Colorado: U.S. Geological Survey. ACC: MOL.19960924.0517.
- Tyler, S.W.; Chapman, J.B.; Conrad, S.H.; Hammermeister, D.P.; Blout, D.O.; Miller, J.J.; Sully, M.J.; and Ginanni, J.M. 1996. "Soil-Water Flux in the Southern Great Basin, United States: Temporal and Spatial Variations Over the Last 120,000 Years." *Water Resources Research*, 32, (6), 1481-1499. Washington, D.C.: American Geophysical Union. TIC: 235938.
- USGS (U.S. Geological Survey) 2000 (U0005). *Future Climate Analysis*. ANL-NBS-GS-000008 REV 00. Denver, Colorado: U.S. Geological Survey. Submit to RPC URN-0004
- USGS 2000 (U0010). *Simulation of Net Infiltration for Modern and Potential Future Climate*. ANL-NBS-HS-000032 REV 00. Denver, Colorado: U.S. Geological Survey. Submit to RPC URN-0006.
- van Genuchten, M.T. 1980. "A Closed-Form Equation for Predicting the Hydraulic Conductivity of Unsaturated Soils." *Soil Science Society American Journal*, 44, (5), 892-898. Madison, Wisconsin: Soil Science Society of America. TIC: 217327.
- Villar, E.; Bonet, A.; Diaz-Caneja, B.; Fernandez, P.L.; Gutierrez, I.; Quindos, L.S.; Solana, J.R.; and Soto, J. 1985. "Natural Evolution of Percolation Water in Altamira Cave." *Cave Science*, 12, (1), 21-24. Bridgewater, United Kingdom: British Cave Research Association. TIC: 247713.
- Viswanathan, H.S.; Robinson, B.A.; Valocchi, A.J.; and Triay, I.R. 1998. "A Reactive Transport Model of Neptunium Migration from the Potential Repository at Yucca Mountain." *Journal of Hydrology*, 209, 251-280. Amsterdam, The Netherlands: Elsevier. TIC: 243441.
- Wallace, A.B. and Roper, M.W. 1981. *Geology and Uranium Deposits Along the Northeastern Margin, McDermitt Caldera Complex, Oregon*. Uranium in Volcanic and Volcaniclastic Rocks. AAPG Studies in Geology No. 13, 73-80. Tulsa, Oklahoma: American Association of Petroleum Geologists. TIC: 245898.
- Wang, J.S.Y. and Elsworth, D. 1999. "Permeability Changes Induced by Excavation in Fractured Tuff." *Rock Mechanics for Industry, Proceedings of the 37th U.S. Rock Mechanics Symposium, Vail, Colorado, June 6-9, 1999*. Amadei, B., ed. 2, 751-757. Rotterdam, The Netherlands: A.A. Balkema. TIC: 245246.

- Wang, J.S.Y. and Narasimhan, T.N. 1985. "Hydrologic Mechanisms Governing Fluid Flow in a Partially Saturated, Fractured, Porous Medium." *Water Resources Research*, 21, (12), 1861-1874. Washington, D.C.: American Geophysical Union. TIC: 225290.
- Wang, J.S.Y. and Narasimhan, T.N. 1988. *Hydrologic Modeling of Vertical and Lateral Movement of Partially Saturated Fluid Flow Near a Fault Zone at Yucca Mountain*. SAND87-7070. Albuquerque, New Mexico: Sandia National Laboratories. TIC: 202856.
- Wang, J.S.Y. and Narasimhan, T.N. 1993. "Unsaturated Flow in Fractured Porous Media." Chapter 7 of *Flow and Contaminant Transport in Fractured Rocks*. Bear, J., Tsang, C.F., and de Marsily, G., eds. San Diego, California: Academic Press. TIC: 235461.
- Wang, J.S.Y.; Cook, N.G.W.; Wollenberg, H.A.; Carnahan, C.L.; Javandel, I.; and Tsang, C.F. 1993. "Geohydrologic Data and Models of Rainier Mesa and Their Implications to Yucca Mountain." *High Level Radioactive Waste Management, Proceedings of the Fourth Annual International Conference, Las Vegas, Nevada, April 26-30, 1993*. 1, 675-681. La Grange Park, Illinois: American Nuclear Society. TIC: 208542.
- Wang, J.S.Y.; Trautz, R.C.; Cook, P.J.; Finsterle, S.; James, A.L.; and Birkholzer, J. 1999. "Field Tests and Model Analyses of Seepage into Drift." *Journal of Contaminant Hydrology*, 38, (1-3), 323-347. New York, New York: Elsevier. TIC: 244160.
- Warren, J.E. and Root, P.J. 1963. "The Behavior of Naturally Fractured Reservoirs." *Society of Petroleum Engineers Journal*, 3, (3), 245-255. Dallas, Texas: Society of Petroleum Engineers. TIC: 233671.
- Watson, P.; Sinclair, P.; and Waggoner, R. 1976. "Quantitative Evaluation of a Method for Estimating Recharge to the Desert Basins of Nevada." *Journal of Hydrology*, 31, (3/4), 335-357. Amsterdam, Netherlands: Elsevier Scientific. TIC: 234481.
- Weeks, E.P. 1987. "Effect of Topography on Gas Flow in Unsaturated Fractured Rock: Concepts and Observations." *Flow and Transport Through Unsaturated Fractured Rock*. Evans, D.D. and Nicholson, T.J., eds. Geophysical Monograph 42, 165-170. Washington, D.C.: American Geophysical Union. TIC: 223605.
- Weeks, E.P. and Wilson, W.E. 1984. *Preliminary Evaluation of Hydrologic Properties of Cores of Unsaturated Tuff, Test Well USW H-1, Yucca Mountain, Nevada*. Water-Resources Investigations Report 84-4193. Denver, Colorado: U.S. Geological Survey. ACC: NNA.19870407.0037.
- Wemheuer, R.F. 1999. "First Issue of FY00 NEPO QAP-2-0 Activity Evaluations." Interoffice correspondence from R.F. Wemheuer (CRWMS M&O) to R.A. Morgan, October 1, 1999, LV.NEPO.RTPS.TAG.10/99-155, with enclosures. ACC: MOL.19991028.0162.
- Wilkins, D.R. and Heath, C.A. 1999. "Direction to Transition to Enhanced Design Alternative II." Letter from Dr. D.R. Wilkins (CRWMS M&O) and Dr. C.A. Heath (CRWMS M&O) to Distribution, June 15, 1999, LV.NS.JLY.06/99-026, with enclosures, "Strategy for Baselineing

EDA II Requirements" and "Guidelines for Implementation of EDA II." ACC: MOL.19990622.0126; MOL.19990622.0127; MOL.19990622.0128.

Wilson, M.L.; Gauthier, J.H.; Barnard, R.W.; Barr, G.E.; Dockery, H.A.; Dunn, E.; Eaton, R.R.; Guerin, D.C.; Lu, N.; Martinez, M.J.; Nilson, R.; Rautman, C.A.; Robey, T.H.; Ross, B.; Ryder, E.E.; Schenker, A.R.; Shannon, S.A.; Skinner, L.H.; Halsey, W.G.; Gansemer, J.D.; Lewis, L.C.; Lamont, A.D.; Triay, I.R.; Meijer, A.; and Morris, D.E. 1994. *Total-System Performance Assessment for Yucca Mountain – SNL Second Iteration (TSPA-1993)*. SAND93-2675. Executive Summary and two volumes. Albuquerque, New Mexico: Sandia National Laboratories. ACC: NNA.19940112.0123.

Winograd, I.J. 1981. "Radioactive Waste Disposal in Thick Unsaturated Zones." *Science*, 212, (4502), 1457-1464. Washington, D.C.: American Association for the Advancement of Science. TIC: 217258.

Winograd, I.J. 1986. *Archaeology and Public Perception of a Transscientific Problem – Disposal of Toxic Wastes in the Unsaturated Zone*. Circular 990. Denver, Colorado: U.S. Geological Survey. TIC: 237946.

Winograd, I.J. and Thordarson, W. 1975. *Hydrogeologic and Hydrochemical Framework, South-Central Great Basin, Nevada-California, with Special Reference to the Nevada Test Site*. Professional Paper 712-C. Washington, D.C.: U.S. Geological Survey. TIC: 206787.

Winograd, I.J.; Coplen, T.B.; Landwehr, J.M.; Riggs, A.C.; Ludwig, K.R.; Szabo, B.J.; Kolesar, P.T.; and Revesz, K.M. 1992. "Continuous 500,000-Year Climate Record from Vein Calcite in Devils Hole, Nevada." *Science*, 258, 255-260. Washington, D.C.: American Association for the Advancement of Science. TIC: 237563.

Wittwer, C.; Chen, G.; Bodvarsson, G.S.; Chornack, M.; Flint, A.; Flint, L.; Kwicklis, E.; and Spengler, R. 1995. *Preliminary Development of the LBL/USGS Three-Dimensional Site-Scale Model of Yucca Mountain, Nevada*. LBL-37356. Berkeley, California: Lawrence Berkeley Laboratory. ACC: MOL.19960924.0538.

Wittwer, C.S.; Bodvarsson, G.S.; Chornack, M.P.; Flint, A.L.; Flint, L.E.; Lewis, B.D.; Spengler, R.W.; and Rautman, C.A. 1992. "Design of a Three-Dimensional Site-Scale Model for the Unsaturated Zone at Yucca Mountain, Nevada." *High Level Radioactive Waste Management, Proceedings of the Third International Conference, Las Vegas, Nevada, April 12-16, 1992*. 1, 263-271. La Grange Park, Illinois: American Nuclear Society. TIC: 204231.

WoldeGabriel, G.; Keating, G.N.; and Valentine, G.A. 1999. "Effects of Shallow Basaltic Intrusion into Pyroclastic Deposits, Grants Ridge, New Mexico, USA." *Journal of Volcanology and Geothermal Research*, 92, 389-411. Amsterdam, The Netherlands: Elsevier Science. TIC: 246037.

Wollenberg, H.A. and Flexser, S. 1986. "Contact Zones and Hydrothermal Systems as Analogues to Repository Conditions." *Chemical Geology*, 55, 345-359. Amsterdam, The Netherlands: Elsevier Science B.V. TIC: 246171.

- Wu, Y.S.; Chen, G.; and Bodvarsson, G. 1995. *Preliminary Analysis of Effects of Thermal Loading on Gas and Heat Flow Within the Framework of the LBNL/USGS Site-Scale Model*. LBNL- 37729. Berkeley, California: Lawrence Berkeley National Laboratory. TIC: 222270.
- Wu, Y-S.; Haukwa, C.; and Bodvarsson, G.S. 1999a. "A Site-Scale Model for Fluid and Heat Flow in the Unsaturated Zone of Yucca Mountain, Nevada." *Journal of Contaminant Hydrology*, 38, (1-3), 185-215. New York, New York: Elsevier. TIC: 244160.
- Wu, Y.S.; Ritcey, A.C.; and Bodvarsson, G.S. 1999b. "A Modeling Study of Perched Water Phenomena in the Unsaturated Zone at Yucca Mountain." *Journal of Contaminant Hydrology*, 38, (1-3), 157-184. New York, New York: Elsevier. TIC: 244160.
- Xu, T. and Pruess, K. 1998. *Coupled Modeling of Non-Isothermal Multi-Phase Flow, Solute Transport and Reactive Chemistry in Porous and Fractured Media: 1. Model Development and Validation*. LBNL-42050. Berkeley, California: Lawrence Berkeley National Laboratory. TIC: 243735.
- Xu, T.; Pruess, K.; and Brimhall, G. 1998. *An Improved Equilibrium-Kinetics Speciation Algorithm for Redox Reactions in Variably Saturated Subsurface Flow Systems*. LBNL-41789. Berkeley, California: Lawrence Berkeley National Laboratory. TIC: 240019.
- Yang, I.C.; Rattray, G.W.; and Yu, P. 1996. *Interpretation of Chemical and Isotopic Data from Boreholes in the Unsaturated Zone at Yucca Mountain, Nevada*. Water-Resources Investigations Report 96-4058. Denver, Colorado: U.S. Geological Survey. ACC: MOL.19980528.0216.
- Yang, I.C.; Yu, P.; Rattray, G.W.; Ferarese, J.S.; and Ryan, J.N. 1998. *Hydrochemical Investigations in Characterizing the Unsaturated Zone at Yucca Mountain, Nevada*. Water-Resources Investigations Report 98-4132. Denver, Colorado: U.S. Geological Survey. ACC: MOL.19981012.0790.
- Yao, T-M and Hendrickx, J.M.H. 1996. "Stability of Wetting Fronts in Dry Homogeneous Soils Under Low Infiltration Rates." *Soil Science Society of America Journal*, 60, (1), 20-28. Madison, Wisconsin: Soil Science Society of America. TIC: 246692.
- YMP (Yucca Mountain Project) 1999. *Unsaturated Zone Flow and Transport Model Independent Evaluation Panel Preliminary Report*. Las Vegas, Nevada: Yucca Mountain Site Characterization Office. ACC: MOL.20000111.0135.
- Zhou, W. and Apted, M.J. 1995. "Flow and Transport Simulation in Yucca Mountain Using Dual-Porosity Model." *High Level Radioactive Waste Management, Proceedings of the Sixth Annual International Conference, Las Vegas, Nevada, April 30-May 5, 1995*. Pages 160-162. La Grange Park, Illinois: American Nuclear Society. TIC: 215781.
- Zimmerman, R.M.; Blanford, M.L.; Holland, J.F.; Schuch, R.L.; and Barrett, W.H. 1986. *Nevada Nuclear Waste Storage Investigations Project, Final Report: G-Tunnel Small-Diameter Heater Experiments*. SAND84-2621. Albuquerque, New Mexico: Sandia National Laboratories. ACC: HQS.19880517.2365.

Zimmerman, R.W. and Bodvarsson, G.S. 1996. "Effective Transmissivity of Two-Dimensional Fracture Networks." *International Journal of Rock Mechanics and Mining Sciences & Geomechanics Abstracts*, 33, (4), 433-438. Oxford, United Kingdom: Pergamon Press. TIC: 245649.

6.2 CODES, STANDARDS, REGULATIONS, AND PROCEDURES

64 FR (Federal Register) 8640. Disposal of High-Level Radioactive Waste in a Proposed Geologic Repository at Yucca Mountain. Proposed rule 10 CFR 63. Readily available.

AP-2.14Q, Rev. 0, ICN 1. *Review of Technical Products*. Washington, D.C.: U.S. Department of Energy, Office of Civilian Radioactive Waste Management. ACC: MOL.20000405.0477.

AP-2.16Q, Rev. 0, ICN 0. *Activity Evaluation*. Washington, D.C.: U.S. Department of Energy, Office of Civilian Radioactive Waste Management. ACC: MOL.20000207.0716.

AP-3.10Q, Rev. 2, ICN 1. *Analyses and Models*. Washington, D.C.: U.S. Department of Energy, Office of Civilian Radioactive Waste Management. ACC: MOL.20000512.0066.

AP-3.10Q, Rev. 2, ICN 2. *Analyses and Models*. Washington, D.C.: U.S. Department of Energy, Office of Civilian Radioactive Waste Management. ACC: MOL.20000619.0576.

AP-3.11Q, Rev. 1, ICN 1. *Technical Reports*. Washington, D.C.: U.S. Department of Energy, Office of Civilian Radioactive Waste Management. ACC: MOL.20000726.0216.

AP-3.15Q, Rev. 1, ICN 1. *Managing Technical Product Inputs*. Washington, D.C.: U.S. Department of Energy, Office of Civilian Radioactive Waste Management. ACC: MOL.20000218.0069.

AP-7.5Q, Rev. 0, ICN 1. *Submittal, Review, and Acceptance of Deliverables*. Washington, D.C.: U.S. Department of Energy, Office of Civilian Radioactive Waste Management. TIC: MOL.20000518.0343.

AP-SI.1Q, Rev. 2, ICN 4. *Software Management*. Washington, D.C.: U.S. Department of Energy, Office of Civilian Radioactive Waste Management. ACC: MOL.20000223.0508.

DOE 2000. *Quality Assurance Requirements and Description*. DOE/RW-0333P, Rev. 10. Washington, D.C.: U.S. Department of Energy, Office of Civilian Radioactive Waste Management. ACC: MOL.20000427.0422.

QAP-2-0, Rev. 5. *Conduct of Activities*. Las Vegas, Nevada: CRWMS M&O. ACC: MOL.19980826.0209.

YMP-LBNL-QIP-6.1, Rev. 5, Mod. 0. *Document Review*. Berkeley, California: Lawrence Berkeley National Laboratory. ACC: MOL.19991210.0091.

6.3 SOURCE DATA, LISTED BY DATA TRACKING NUMBER

GS990708312242.008. Physical and Hydraulic Properties of Core Samples from Busted Butte Boreholes. Submittal date: 07/01/1999.

GS990908314224.009. Detailed Line Survey Data for Horizontal and Vertical Traverses, ECRB. Submittal date: 09/16/1999.

LB002181233124.001. Air Permeability and Pneumatic Pressure Data Collected Between October 27, 1999 through November 7, 1999 from Niche 5 (ECRB Niche 1620) of the ESF. Submittal date: 02/18/2000.

LB990501233129.004. 3-D UZ Model Calibration Grids for AMR U0000, "Development of Numerical Grids of UZ Flow and Transport Modeling". Submittal date: 09/24/1999.

LB990701233129.001. 3-D UZ Model Grids for Calculation of Flow Fields for PA for AMR U0000, "Development of Numerical Grids For UZ Flow and Transport Modeling". Submittal date: 09/24/1999.

MO9901MWDISMMM.000. ISM3.0 Mineralogic Models. Submittal date: 01/22/1999. Submit to RPC URN-0074.

MO9901MWDISMRP.000. ISM3.0 Rock Properties Models. Submittal date: 01/22/1999. Submit to RPC URN-0075.

MO9910MWDISMMM.003. ISM3.1 Mineralogic Models. Submittal date: 10/01/1999. Submit to RPC URN-0076.

MO9910MWDISMRP.002. Rock Properties Model (RPM3.1). Submittal date: 10/06/1999. Submit to RPC URN-0080.

6.3.1 Data Tracking Numbers Listed for Tables and Figures in Attachment II

GS000399991221.002. Rainfall/Runoff/Run-on 1999 Simulations. Submittal date: 03/10/2000.

GS000399991221.003. Preliminary Alcove 1 Infiltration Experiment Data. Submittal date: 03/10/2000.

GS000399991221.004. Preliminary Developed Matrix Properties. Submittal date: 03/10/2000.

GS960308312232.001. Deep Unsaturated Zone Surface-Based Borehole Instrumentation Program Data from Boreholes USW NRG-7A, USW NRG-6, UE-25 UZ#4, UE-25 UZ#5, USW UZ-7A, and USW SD-12 for the Time Period 10/01/95 through 3/31/96. Submittal date: 04/04/1996.

GS960908315215.014. Uranium and Thorium Isotope Data for ESF Secondary Minerals Collected Between March 1996 and July 1996. Submittal date: 09/25/1996.

GS980908312242.036. Water Potentials Measured With Heat Dissipation Probes in ECRB Holes from 4/23/98 to 7/31/98. Submittal date: 09/22/1998.

GS980908315215.015. Uranium and Thorium Isotope Data Including Calculated $^{230}\text{Th}/\text{U}$ Ages and Initial $^{234}\text{U}/^{238}\text{U}$ Activity Ratios for in Situ Microdigestions of Outermost Opal-Rich Mineral Coatings from the Exploratory Studies Facility Analyzed Between 12/01/97 and 09/15/98. Submittal date: 09/23/1998.

GS991299992271.001. Preliminary Unsaturated Zone Borehole Hydrochemistry Data. Submittal date: 12/23/1999.

LA0003AM831341.001. Preliminary Revision of Probability Distributions for Sorption Coefficients (K_{DS}). Submittal date: 03/29/2000. Submit to RPC URN-0267

LA0003JC831362.001. Preliminary Matrix Diffusion Coefficients for Yucca Mountain Tuffs. Submittal date: 4/10/2000. Submit to RPC URN-0305

LA0004WS831372.002. Sorption of Np, Pu, and Am on Rock Samples From Busted Butte, NV. Submittal date: 04/19/2000. Submit to RPC URN-0304

LA9909JF831222.005. Chlorine-36 Analyses of ESF and Busted Butte Porewaters in FY99. Submittal date: 09/29/1999.

LA9909JF831222.010. Chloride, Bromide, Sulfate, and Chlorine-36 Analyses of ESF Porewaters. Submittal date: 09/29/1999.

LAJF831222AQ98.004. Chloride, Bromide, Sulfate, and Chlorine-36 Analyses of Salts Leached from ESF Rock Samples. Submittal date: 09/10/1998.

LAJF831222AQ98.011. Chloride, Bromide, Sulfate and Chlorine-36 Analyses of Springs, Groundwater, Porewater, Perched Water and Surface Runoff. Submittal date: 09/10/1998.

LB980001233124.003. Liquid Release Tests Performed to Determine if a Capillary Barrier Exists in Niches 3566 and 3650. Submittal date: 04/23/1998.

LB00032412213U.001. Busted Butte Ground Penetrating Radar Data Collected June 1998 through February 2000 at the Unsaturated Zone Transport Test (UZTT): GPR Velocity Data. Submittal date: 03/24/2000. Submit to RPC URN-0303

LB980901123142.006. Laboratory Test Results of Hydrological Properties from Post-Test Dry-Drilled Cores in the Single Heater Test Area for the Final TDIF Submittal for the Single Heater Test. Submittal date: 08/31/1998.

LB980930123112.001. Surface to ESF Seismic Tomography. Submittal date: 09/30/1998.

LB990051233129.001. Extent of Vitric Region Used to Assign Material Properties in FY 99 UZ Model Layers; Figure 5 From AMR U0000, "Development of Numerical Grids for UZ Flow and Transport Modeling." Submittal date: 09/24/99.

LB990501233129.004. 3-D UZ Model Calibration Grids for AMR U0000, "Development of Numerical Grids of UZ Flow and Transport Modeling." Submittal date: 09/24/1999.

LB990701233129.001. 3-D UZ Model Grids for Calculation of Flow Fields for PA for AMR U0000, "Development of Numerical Grids for UZ Flow and Transport Modeling." Submittal date: 09/24/1999.

LB990801233129.001. TSPA Grid Flow Simulations for AMR U0050, "UZ Flow Models and Submodels" (Flow Field #1). Submittal date: 11/29/1999.

LB990801233129.003. TSPA Grid Flow Simulations for AMR U0050, "UZ Flow Models and Submodels" (Flow Field #3). Submittal date: 11/29/1999.

LB990801233129.004. TSPA Grid Flow Simulations for AMR U0050, "UZ Flow Models and Submodels" (Flow Field #4). Submittal date: 11/29/1999.

LB990801233129.005. TSPA Grid Flow Simulations for AMR U0050, "UZ Flow Models and Submodels" (Flow Field #5). Submittal date: 11/29/1999.

LB990801233129.007. TSPA Grid Flow Simulations for AMR U0050, "UZ Flow Models and Submodels" (Flow Field #7). Submittal date: 11/29/1999.

LB990801233129.009. TSPA Grid Flow Simulations for AMR U0050, "UZ Flow Models and Submodels" (Flow Field #9). Submittal date: 11/29/1999.

LB990801233129.011. TSPA Grid Flow Simulations for AMR U0050, "UZ Flow Models and Submodels" (Flow Field #11). Submittal date: 11/29/1999.

LB990801233129.013. TSPA Grid Flow Simulations for AMR U0050, "UZ Flow Models and Submodels" (Flow Field #13). Submittal date: 11/29/1999.

LB990801233129.015. TSPA Grid Flow Simulations for AMR U0050, "UZ Flow Models and Submodels" (Flow Field #15). Submittal date: 11/29/1999.

LB990801233129.017. TSPA Grid Flow Simulations for AMR U0050, "UZ Flow Models and Submodels" (Flow Field #17). Submittal date: 11/29/1999.

LB990801233129.025. TSPA Grid Flow Simulations for AMR U0050, "UZ Flow Models and Submodels" Flow Field #25: Present Day Mean Infiltration for Flow-Through Perched-Water Conceptual Model. Submittal date: 3/11/2000.

LB990831012027.001. Input to Seepage Calibration Model AMR U0080. Submittal date: 08/31/1999.

LB9908T1233129.001. Transport Simulations for the Low, Mean, and Upper Infiltration Scenarios of the Present-Day, Monsoon, and Glacial Transition Climates for AMR U0050, "UZ Models and Submodels." Submittal date: 3/11/2000.

LB990901233124.002. Alcove 6 Flow Data for AMR U0015, "In Situ Field Testing of Processes." Submittal date: 11/01/1999.

LB990901233124.005. Alcove 4 Flow Data for AMR U0015, "In Situ Field Testing of Processes." Submittal date: 11/01/1999.

LB990901233129.001. Input and Output Data for Verification of Dual-Continua Particle Tracker (DCPT) for AMR U0155, "Analysis Comparing Advect-Dispersion Transport Solution to Particle Tracking." Submittal date: 10/26/1999.

LB991091233129.001. One-Dimensional, Mountain-Scale Calibration for AMR U0035, "Calibrated Properties Model." Submittal date: 10/22/1999.

LB991091233129.003. Two-Dimensional Fault Calibration for AMR U0035, "Calibrated Properties Model." Submittal date: 10/22/1999.

LB991101233129.001. Model Input/Output Files Supporting Seepage Model for PA in AMR U0075, "Seepage Model for PA Including Drift Collapse." Submittal date: 11/30/1999.

LB991121233129.007. Calibrated Parameters for the Present-Day, Mean Infiltration Scenario, Used for Simulations with Perched Water Conceptual Model #3 for the Mean Infiltration Scenarios of the Present-Day, Monsoon and Glacial Transition Climates. Submittal date: 3/1/2000.

LB991131233129.001. Modeling Calcite Deposition and Percolation. AMR U0050, "UZ Flow Models and Submodels". Submittal date: 03/11/2000.

LB991131233129.002. Modeling Seepage and Tracer Tests at Alcove 1. AMR U0050, "UZ Flow Models and Submodels". Submittal date: 03/11/2000.

LB991131233129.003. Analytical and Simulation Results of Chloride and Chlorine-36 Analysis. AMR U0050, "UZ Flow Models and Submodels". Submittal date: 3/11/2000.

LB991200DSTTHC.001. Pore Water Composition and CO2 Partial Pressure Input into Thermal-Hydrological-Chemical (THC) Simulations: Table 3 of AMR N0120/U0110, "Drift-Scale Coupled Processes (Drift-Scale and THC Seepage) Models". Submittal date: 03/11/2000.

LB991200DSTTHC.002. Model Input and Output Files, Excel Spreadsheets and Resultant Figures Which are Presented in AMR N0120/U0110, "Drift-Scale Coupled Processes (Drift-Scale Test and THC Seepage) Models." Submittal date: 3/11/2000.

LB991201233129.001. The Mountain-Scale Thermal-Hydrologic Model Simulations for AMR U0105, "Mountain-Scale Coupled Processes (TH) Models." Submittal date: 3/11/2000.

LB991220140160.012. Model Prediction of 3-D Transport, Present-Day Infiltration, #1 Perched Water Model, Using EOS9nT Input and Output files. AMR U0060, "Radionuclide Transport Models under Ambient Conditions". Submittal date: 3/11/2000.

LB991220140160.017. Model Prediction of 3-D Colloid Transport, Present-Day Infiltration, #1 Perched Water Model, using EOS9nT Input and Output files. AMR U0060, "Radionuclide Transport Models under Ambient Conditions". Submittal date: 3/11/2000.

LB997141233129.001. Calibrated Basecase Infiltration 1-D Parameter Set for the UZ Flow and Transport Model, FY99. Submittal date: 07/21/1999.

MO9804MWDGFM03.001. An Update to GFM 3.0; Corrected Horizon Grids for Four Fault Blocks. Submittal date: 04/14/1998.

MO9901MWDGFM31.000. Geologic Framework Model. Submittal date: 01/06/1999.

MO9901MWDISMMM.000. ISM 3.0 Mineralogic Models. Submittal date: 01/22/1999. Submit to RPC URN-0074.

MO9910MWDISMMM.003. ISM3.1 Mineralogic Models. Submittal date: 10/01/1999. Submit to RPC URN-0076.

MO9901MWDISMRP.000. ISM3.0 Rock Properties Models. Submittal date: 01/22/1999. Submit to RPC URN-0075.

MO9910MWDISMRP.002. Rock Properties Model (RPM3.1). Submittal date: 10/06/1999. Submit to RPC URN-0080.

MO9912SPAPAI29.002. PA Initial Abstraction of THC Model Chemical Boundary Conditions. Submittal date: 01/11/2000. Submit to RPC URN-0282.

SN0001T0581699.004. Supplemental Files to Support Base-Case Particle-Tracking Analysis for TSPA-SR (Total System Performance Assessment-Site Recommendation) (In Analysis/Model Report U0160, ANL-NBS-HS-000024). Submittal date: 01/06/2000.

SN0003T0503100.001. Weighting Factors for Low, Middle and High Climate Infiltration Rate Maps. Submittal date: 03/20/2000.

SN9908T0581699.001. Files to Support 1-D Comparison Between FEHM Particle Tracking and T2R3D Advective-Dispersive Transport Simulations Along SD-9. Submittal date: 08/16/1999.

SN9912T0511599.002. Revised Seepage Abstraction Results for TSPA-SR (Total System Performance Assessment-Site Recommendation). Submittal date: 12/15/1999.

SN9912T0581699.003. Files to Support Base-Case Particle-Tracking Analyses (AMR U0160) for TSPA-SR. Submittal date: 12/13/1999.

INTENTIONALLY LEFT BLANK

7. ATTACHMENTS

Attachment I – UZ Data and Associated Data Tracking Numbers (DTNs)

Attachment II – List of DTNs for Figures and Tables

Attachment III – Figures

INTENTIONALLY LEFT BLANK

ATTACHMENT I – UZ Data and Associated Data Tracking Numbers (DTNs)

I.1 Available Site Data

This section summarizes the data used in the AMRs supporting the UZ Flow and Transport PMR. The input data represent the current understanding of UZ flow and transport processes. Tables are presented to summarize the different data reviewed, analyzed, and developed in associated Analysis/Model Reports (AMRs). Some data sets are used in multiple analyses. The discussions associated with the tables cross-reference the relationships among data sets and AMRs. The details of analysis and modeling are given in individual AMRs and in Section 3. The Q-status of these data is provided in the DIRS database for the associated AMR. It should be noted that this Attachment is only intended to give the main data sets and the associated DTNs for the unsaturated zone, and is therefore not necessarily complete.

I.2 Geologic Data

The major inputs and outputs of the CRWMS M&O (2000, U0000), *Development of Numerical Grids for UZ Flow and Modeling*, are summarized in Table I-1 (with outputs presented in *italic*).

Table I-1. Geologic Data for the UZ Model

Data Description	DTN or ACC
Geologic Framework Model, GFM3.1	MO9901MWDGFM31.000
Integrated Site Model, components	MO9901MWDISMRP.000 MO9804MWDGFM03.001
Repository layout configuration	MOL.19990409.001
<i>Mesh files for model calibrations, CRWMS M&O 2000, U0000</i>	
<i>Tables supporting UZ Model grid development</i>	<i>LB990501233129.001</i>
<i>1-D hydrogeologic property set inversions and model calibration</i>	<i>LB990501233129.002</i>
<i>2-D fault hydrogeologic property calibration</i>	<i>LB990501233129.003</i>
<i>3-D UZ Model calibration</i>	<i>LB990501233129.004</i>
<i>3-D UZ Model calibration grid for non-water-perching mode</i>	<i>LB990701233129.002</i>
<i>Mesh file for generating 3-D UZ flow fields, CRWMS M&O 2000, U0000</i>	<i>LB990701233129.001</i>

The primary data input for UZ Flow and Transport Model grids is GFM3.1 (Geological Framework Model) for lithostratigraphic layering and major fault geometry at Yucca Mountain. The GFM contains information about layer thickness and layer contact elevation, and defines fault orientation and displacement. Approximately 40 geologic units and 18 faults are incorporated into the 3-D UZ Flow and Transport Model grids. RPM3.0 (Rock Properties Model) files are used to further define the units, especially the zeolitic zones of CHn. The repository layout data are used to locate areas for enhanced grid resolution.

CRWMS M&O (2000, U0000) also uses inputs of hydrologic unit definitions, fracture data for hydrologic units, and elevation data on the water table and perched water bodies. The hydrologic unit definitions are based on matrix properties (Flint 1998) discussed in Section 2.2.3. Fracture data, discussed in Section 2.2.4, are used to formulate the dual-permeability (dual-k) meshes. The vertical columns in the meshes are from the TCw bedrock to the water table. Water table and perched water elevation data for the lower UZ boundary are discussed in Section 2.2.10.

The final 3-D mesh files for UZ flow fields in Table I-1 are developed with inputs from calibrated property sets, summarized in Section 2.2.11. The areal domain of the UZ models encompasses approximately 40 km² of the Yucca Mountain area. The areal grids are constructed with centers coinciding as close as practical with locations of surface-based boreholes, alcoves and niches, faults, ESF and ECRB drifts, and other domain nodes.

I.3 Infiltration/Climate Data

The USGS (2000, U0005) refines the climate estimates for the next 10,000 years. The climate AMR provides input to the USGS (2000, U0010), *Simulation of Net Infiltration for Modern and Potential Future Climates*. The major inputs and outputs are summarized in Table I-2.

Table I-2. Infiltration/Climate Data for the UZ Model

Data Description	DTN or ACC
Daily precipitation input for 1980-1995 calibration (file MOD3-PPT.DAT)	GS950208312111.001 GS950208312111.002 GS960908312111.004 GS970108312111.001
Summary of the Day Data from the National Climatic Data Center (NCDC) for the Period Ending in 1995: for California, Nevada, Utah, Arizona, New Mexico, Colorado, and Wyoming.	MO9811NCDCSDD0.000
Streamflow records for 5 Yucca Mountain gauging stations (Upper Pagany Wash, Lower Pagany Wash, Wren Wash, Drill Hole Wash, Upper Split Wash).	NWIS Database ATS#YD-200000269
Parameters for SOLRAD subroutine for equations defined in Flint et al. (1996).	GS960908312211.003
Soil-depth-class map (Figure 13, Flint et al., 1996).	GS960908312211.003
Geospatial input parameters acquired from Flint et al. (1996) (elevation, slope, aspect, latitude, longitude, soil type, soil-depth class) (file 30MSITE.INP).	GS960908312211.003
100-year stochastic daily precipitation input (files 4JA.S01 and AREA12.S01).	GS960908312211.003
Calculated flux rates from neutron holes	GS960508312212.008
SO4 infiltration flux	GS910908315214.003 GS931008315214.032
<i>Infiltration map - base case, lower bound, upper bound, CRWMS M&O 2000, U0010</i>	GS000399991221.002

The climate USGS (2000, U0005) also used diatom and ostracode data from Owens Lake 1984-1992 cores, radiometric dating and $\delta^{18}\text{O}$ data from Devils Hole, and earth orbital parameter data for the last 10 million years and the next 100,000 years. The three climate states in VA are replaced by (1) the modern interglacial climate for about the next 400 to 600 years, (2) the monsoon climate for the duration of 900 to 1,400 years, and (3) the glacial-transition climate for the duration of 8,000 to 8,700 years. The modern climate uses data from site and regional meteorological stations. The monsoon climate uses data from Nogales, Arizona, and Hobbs, New Mexico, as upper-bound analogs and present-day site data as lower bound analog. The glacial transition climate uses data from Spokane, Rosalia, and St. John, all in Washington state, as upper-bound analogs and data from Beowawe, Nevada, and Delta, Utah, as lower-bound analogs.

The infiltration USGS (2000, U0010) also used elevation data, bedrock permeability and property data, geology maps, and soil properties as documented in the AMR. Simulation results and averaged values were presented for 123.7 km² area for the net infiltration model domain, for the 38.7 km² area of the UZ Flow and Transport Model domain, and for the 4.7 km² area of the 1999 design potential repository area. Over the potential repository area, the mean net infiltration is 4.7 mm/yr for the modern climate (with 0.4 mm/yr for the mean lower bound and 11.6 mm/yr for the mean upper bound), 12.5 mm/yr for the monsoon climate (with 4.7 mm/yr for the mean lower bound and 20.3 mm/yr for the mean upper bound), and 19.8 mm/yr for the glacial-transition climate (with 2.2 mm/yr for the mean lower bound and 37.3 mm/yr for the mean upper bound).

I.4 Matrix Properties

Matrix properties include permeability, porosity, residual saturation, and the van Genuchten α and m parameters used to describe water retention and relative permeability relationships (van Genuchten 1980, pp. 892–898). The input to the matrix properties for UZ Flow and Transport Model layers to the CRWMS M&O (2000, U0090), *Analysis of Hydrologic Property Data*, is based on the data transmittal listed in Table I-3. The data of Busted Butte cores are used in CRWMS M&O (2000, U0060), *Radionuclide Transport Models under Ambient Conditions*.

Table I-3. Matrix Properties for the UZ Model

Data Description	DTN or ACC
Matrix hydrologic property data	GS960908312231.004
Matrix saturation, water potential and hydrologic property data	GS000399991221.004
Physical and hydraulic properties of core samples from Busted Butte	GS990308312242.007 GS990708312242.008

The sample collection and laboratory measurement methodologies are described by Flint (1998, pp. 11–19) and Rousseau et al. (1999, pp. 19–46). Core samples are grouped and analyzed according to the hydrogeologic units characterized by matrix properties (Flint 1998, pp. 19–46, CRWMS M&O 2000, U0000, Section 6.3, CRWMS M&O 2000, U0090, Section 6.2). Matrix permeability has been measured on 750 core samples from eight surface-based boreholes. Some

samples with permeabilities too low to measure (nondetect results) were retested with a low-detection-limit permeameter. The nondetect results were included in defining the low-permeability units, especially the zeolitic zones of CHn. Matrix porosity values are based on 105°C oven-dried measurements of 4,888 core samples, from 23 shallow boreholes and eight deep boreholes. The residual saturation is determined by relative humidity (RH) porosity and total porosity, with RH porosity determined in a 65°C and 65% RH oven. The RH drying process is designed to remove water contributing flow, leaving only bound water and water in the smallest pores (Flint 1998, p. 17). The van Genuchten parameters are based on desaturation data from 75 samples. Desaturation data, with water potential and saturation measured several times while a core sample is drying, are used to calculate α and m by least-square fitting.

I.5 Fracture Properties, Air Permeabilities, and Liquid Release/Seepage Data

Fracture properties include fracture permeability, fracture porosity, van Genuchten fracture α and m parameters, fracture frequency, intensity, fracture interface area, and fracture aperture. Fracture properties are developed from analyzing fracture survey data and air-injection test data in CRWMS M&O (2000, U0090), *Analysis of Hydrologic Property Data*. The fracture permeability and van Genuchten parameters are updated in CRWMS M&O (2000, U0035), *Calibrated Properties Model*, after calibrations together with core saturation and *in situ* potential data, as summarized in Section 2.2.11. The fracture van Genuchten parameters and porosities are compared with ESF seepage test results for confirmation purposes. The seepage test results and other drift-scale hydrologic testing and air-permeability data are summarized in CRWMS M&O (2000, U0015), *In Situ Field Testing of Processes*. The seepage test results are used in CRWMS M&O (2000, U0080), *Seepage Calibration Model and Seepage Testing Data*. The major inputs and outputs from these AMRs related to fracture properties are tabulated in Table I-4.

Table I-4. Fracture Geometry, Air Permeability, and Liquid Release/Seepage Data

Data Description	DTN or ACC
Fracture type (location, strike, dip, length):	
Sta. 0+60 to 4+00	GS971108314224.020
Sta. 4+00 to 8+00	GS971108314224.021
Sta. 8+00 to 10+00	GS971108314224.022
Sta. 10+00 to 18+00	GS971108314224.023
Sta. 18+00 to 26+00	GS971108314224.024
Sta. 26+00 to 30+00	GS971108314224.025
Sta. 30+00 to 35+00	GS960708314224.008
Sta. 35+00 to 40+00	GS960808314224.011
Sta. 40+00 to 45+00	GS960708314224.010
Sta. 45+00 to 50+00	GS971108314224.026
Sta. 50+00 to 55+00	GS960908314224.014
Sta. 55+00 to 60+00	GS971108314224.028
Sta. 60+00 to 65+00	GS970208314224.003
Sta. 65+00 to 70+00	GS970808314224.008
Sta. 70+00 to 75+00	GS970808314224.010
Sta. 75+00 to 78+77	GS970808314224.012
Sta. 4+00 to 28+00, Alcoves 3 and 4	GS960908314224.020
Alcove 5	GS960908314224.018
Alcove 6	GS970808314224.014
ECRB Cross Drift	GS990408314224.001
	GS990408314224.002
Fracture frequency:	
15 model units from 14 borehole locations	GS970408314222.003
NRG-7a	SNF29041993002.084
SD-12	TM000000SD12RS.012
Fracture type:	
Outcrop survey of Calico Hills formation	GS970308314222.001
Line surveys in the Bullfrog Member of the Crater Flat Tuff from Raven Canyon	GS930608312332.001
Line surveys in the Bullfrog Member of the Crater Flat Tuff from east side of Little Skull Mountain in Yucca Mountain Area	GS930608312332.002

Table I-4. Fracture Geometry, Air Permeability, and Liquid Release/Seepage Data (Continued)

Data Description	DTN or ACC
Air-injection test data:	
surface-based boreholes	GS960908312232.012
	GS960908312232.013
Alcoves 1, 2, 3 (upper TCw, Bow Ridge fault, upper PTn)	GS970183122410.001
Alcove 4 lower PTn fault-matrix interaction test bed	LB980901233124.009
Alcove 5 – single heater test area	LB960500834244.001
Alcove 5 – drift scale test area	LB970600123142.001
	LB980120123142.004
	LB980120123142.005
Alcove 6 fracture-matrix interaction test bed	LB980901233124.004
Niches 3566 and 3650, pre-excavation and post-excavation data	LB980001233124.002
Niches 3107 and 4788, pre-excavation and post-excavation data	LB980901233124.001
Niches, pre-excavation and post-excavation analyses	LB990601233124.001
Niche 4788, Alcoves 4 and 6, cross-hole analyses, and	LB990901233124.004
4 niches and 2 alcoves, statistical analyses	
Niche 3107 and Alcove 5, air-injection, tracer test and fracture porosity data	LB980912332245.002
<i>Fracture properties for the UZ Model grids and uncalibrated fracture and matrix properties for the UZ model layers, CRWMS M&O 2000, U0090</i>	LB99050501233129.001
Seepage and liquid release data:	
Niches 3566 and 3650, pre-excavation liquid-release data, and	LB980001233124.003
Niche 3566, post-excavation seepage data	
Niches 3566, 3650, 3107 and 4788, pre-excavation liquid-release data and analyses, and	LB980901233124.003
Niche 3566, post-excavation seepage analyses	
Niche 3107, post-excavation seepage test data	LB990601233124.002
<i>Seepage Calibration model, software routines and files, CRWMS M&O 2000, U0080</i>	LB990831012027.001

Table I-4. Fracture Geometry, Air Permeability, and Liquid Release/Seepage Data (Continued)

Data Description	DTN or ACC
Infiltration and seepage data, Alcove 1 upper TCw EI Nino test	GS000399991221.003
Water intake rate and wetting front detection data	
Alcove 4 lower PTn fault-matrix interaction test bed	LB990901233124.005
Alcove 6 fracture-matrix interaction test bed	LB990901233124.002

The precalibrated fracture permeabilities are based on air permeabilities from air-injection tests in vertical boreholes and ESF alcoves. For TCw, fracture permeabilities were based on tests in four vertical boreholes (NRG-7/7A, NRG-6, SD-12, and UZ-16) and Alcoves 1, 2, and 3. For PTn, permeability data are from one borehole (NRG-7/7A) and Alcove 3. For TSw, the permeability data are from the four boreholes and the tests at the Single Heater Test and the Drift Scale Test areas in Alcove 5. For CHn, permeability data are from a single sampled interval in borehole UZ-16. No air-injection data are available for the Prow Pass, Bullfrog, and Tram units. For model layers where no data are available, analogs to other units are used. The fracture properties in faults are based on air-injection tests in Alcove 2 for the Bow Ridge fault and in Alcove 6 for the Ghost Dance fault. The fracture permeabilities are used as prior information for the calibrated properties model CRWMS M&O (2000, U0035).

The test-interval lengths between packers were approximately 4 m for vertical boreholes, 1 to 3 m for Alcoves 1, 2, and 3, and 5 to 12 m in the Alcove 5 SHT and DST areas. Extensive air-permeability data on the scale of 0.3 m were measured in the niches (CRWMS M&O 2000, U0015). For Tptpmn, the niche data sets have approximately one order of magnitude lower mean values and two orders of magnitude higher range than the vertical borehole values. In this comparison, only the pre-excavation permeability values from the niche sites are used. The post-excavation data are used in the seepage calibration model CRWMS M&O (2000, U0080).

The detailed line survey (DLS) data along ESF, together with air-permeability data, are the primary data sets used to derive other fracture properties. Borehole fracture data were used only when no data or incomplete data were available from the ESF DLS. Fracture spacing and frequency are calculated from averaging the DLS. The fracture intensity is calculated by dividing the trace length of the fracture by the area surveyed. Fracture interface area is calculated by dividing the fracture area by the volume of the interval surveyed. Fracture apertures are calculated by the cubic law relationship. The van Genuchten fracture m parameter is determined by fitting an analytical solution resulting from the aperture size distribution to the fracture saturation-capillary pressure curve. The fracture alpha parameter (α_f) is related to the aperture by the Young-LaPlace equation. For Tptpmn, the average of $\log(\alpha_f)$ value is -3.17 from the fracture network estimation, compared to the value of -3.16 from averaging over seepage tests in five niche borehole intervals.

Fracture porosities are derived from a combination of field gas-tracer-test data and estimates from the geometry of fracture network. The porosities from gas-tracer tests range from 0.6% to

2%. The porosities from drift seepage tests have the average value of 1.3% from three water-content values determined from seepage front arrival times. The value of 1% is used as an order-of-magnitude estimate for Tptpmn (model layer tsw34). For model layers without field test data, fracture porosities are estimated from aperture and frequency of the fracture network, and relative values are scaled to the tsw34 value.

I.6 Pneumatic Data

The CRWMS M&O (2000, U0035), *Calibrated Properties Model*, uses the borehole pneumatic data in the inversions to calibrate the tuff model-layer and fault properties. The CRWMS M&O (2000, U0015), *In Situ Testing of Processes*, compiled the moisture monitoring data collected along the drifts and in alcoves for the evaluation of moisture removal induced by ventilation operations. Both data sets are summarized in Table I-5.

Table I-5. Pneumatic Data for the UZ Model

Data Description	DTN or ACC
<i>In situ</i> data in surfaced-based boreholes:	
NRG-6 and NRG-7a, pneumatic pressure and temperature	GS950208312232.003 GS951108312232.008 GS960308312232.001 GS960808312232.004
NRG#5, pneumatic pressure	GS960208312261.001
SD-7, pneumatic pressure	GS960908312261.004
UZ-7a, NRG-6, NRG-7a, and SD-12, pneumatic pressure and temperature	GS960308312232.001
UZ#4, UZ#5, UZ-7a, NRG-6, NRG-7a, and SD-12, pneumatic pressure, temperature, and water potential	GS970108312232.002
UZ#4, UZ#5, UZ-7a, NRG-7a, and SD-12, pneumatic pressure, temperature, and water potential:	
1/1/97 - 6/30/97	GS970808312232.005, MOL.19980226.0042-0045
7/1/97 - 9/30/97	GS971108312232.007, MOL.19980226.0607-0614
10/1/97 - 3/31/98	GS980408312232.001, MOL. 19980706.0269

Table I-5. Pneumatic Data for the UZ Model (Continued)

Data Description	DTN or ACC
Moisture monitoring data in underground drifts:	
21+00/LB20, 28+30/LB50, 35+00/LB40	LB960800831224.001
21+00/LB20, 28+30/LB50, 35+00/LB40, 42+50/LB60, 47+00/LB70, 51+73/LB80, 57+50/LB90, 64+59, 67+00, 73+50 10/1/96 – 1/31/97	LB970300831224.001
Before and After the Completion of the ESF	LB970801233124.001
	LB970901233124.002
7+20/GS#3, 10+93/GS#4, 28+93, 51+64, 67+20, 10/1/96 – 1/31/97	GS970208312242.001
2/1/97 – 7/31/97	GS970708312242.002
8/1/97 – 7/31/98	GS980908312242.024
ECRB Cross Drift 0+25, 2+37, 2+88, 3+38, 10+03, 21+07, 24+75, 4/8/98 – 7/31/98	GS980908312242.035
ECRB Cross Drift 14+35, 21+40, 25+55	LB990901233124.006

Pneumatic pressure data measured *in situ* in five boreholes (NRG#5, NRG-6, NRG-7a, SD-7, and SD-12) are used in the 1-D inversion. These boreholes do not intersect known large faults, and thus the pneumatic pressure data are representative of the formation rock of Yucca Mountain. Pneumatic pressure data measured in borehole UZ-7a are used in the 2-D inversion for fault properties. This borehole intersects the Ghost Dance fault, and thus the pneumatic pressure data are representative of the faulted rock of Yucca Mountain.

Thirty days of data from each borehole are used for either the simultaneous inversion of five borehole columns or for the 2-D inversion for fault properties. The data are selected from the time period prior to detection of any influence associated with construction of the ESF. Most of the attenuation and lag of barometric signal occurs within the PTn and not in the fractured TCw or TSw. The data from all PTn instrument stations or ports, along with data from one TCw port (nearest to the bottom) and two TSw ports (uppermost and lowest), are used in the inversions. PTn contains multiple layers and has heterogeneous permeability distributions calibrated by pneumatic inversion.

With the penetration of the ESF drifts underground, atmospheric conditions were introduced into deep tuff units along the drifts. The barometric signals in the TSw ports became less attenuated as the ESF passed by the boreholes. In addition to barometric pressure, relative humidity, temperature, and/or air velocities are monitored along the drifts and in the alcoves, as summarized in Table I-5. The moisture conditions in the drifts are sensitive to the ventilation operations. Ventilation can remove the moisture, dry up the rock, and suppress the seepage. The perturbation to the ambient UZ conditions by the ESF drifts is *de facto* a mountain scale test at Yucca Mountain. UZ model calibration for the ambient conditions does not use the post-penetration data. Detected changes in pneumatic and moisture conditions can be used to validate

the models, assess the impacts of drift construction and operation, and provide inputs to repository design.

I.7 Saturation Data

The CRWMS M&O (2000, U0035), *Calibrated Properties Model*, uses the core saturation data summarized in Table I-6 in the inversions to calibrate the tuff model-layer and fault properties. The CRWMS M&O (2000, U0015), *In Situ Testing of Processes*, compiled the saturation data collected in alcoves and niches. The saturation data sets are summarized in Table I-6.

Table I-6. Saturation Data for the UZ Model

Data Description	DTN or ACC
Saturation data from surface-based borehole cores:	
UZ-7a, UZ-14, UZ#16, SD-7, SD-9, and SD-12	GS000399991221.004
SD-6	GS980808312242.014
WT-24	GS980708312242.010
Saturation data from underground borehole cores	
Alcove 3, 1 borehole	GS980908312242.033
Alcove 4, 2 boreholes	GS980908312242.032
North Ramp, 7+27 – 10+70	GS980308312242.005
South Ramp, 59+65 – 76+33	GS980308312242.003
3 boreholes in Alcove 6,	GS980908312242.029
1 borehole in Alcove 7	GS980908312242.028
Niche 3566, 3 main boreholes, 6 lateral boreholes	GS980908312242.018
Niche 3650, 7 main boreholes	GS980908312242.020
ECRB Cross Drift Starter tunnel, 1 slant borehole below the invert	GS980908312242.030
Time domain reflectometry measurements:	
South Ramp, 8/1/97 - 1/4/98	GS980308312242.001
Crossover point, ESF Main Drift 30+62 below the ECRB Cross Drift, 6/19/98 - 7/16/98	LB980901233124.014

Saturation data measured on core from seven deep boreholes (SD-6, SD-7, SD-9, SD-12, UZ-14, UZ#16, and WT-24) are used for the 1-D inversions. Saturation data measured on core from borehole UZ-7a are used for the 2-D inversions.

Some of the cores from shallow boreholes in alcoves and niches are affected by the drying process, which can decrease the saturation several meters into the rock from the drift walls. The dry samples are not used in UZ model calibrations. The time-domain reflectometry (TDR) sensors are widely used in soil studies and are applied in the ESF boreholes or walls for detection

of saturation changes and wetting front arrivals. Not included in Table I-6 are neutron-hole surveys in the ESF, which were widely used in the infiltration study.

I.8 Water Potential Data

The CRWMS M&O (2000, U0035), *Calibrated Properties Model*, uses the borehole water potential data in the inversions to calibrate the tuff model-layer and fault properties. The CRWMS M&O (2000, U0015), *In Situ Testing of Processes*, compiled the water-potential data in the ESF to evaluate the extent of the drying into the rock and *in situ* profiles along the drifts. The water-potential data sets are summarized in Table I-7.

Table I-7. Water-Potential Data

Data Description	DTN or ACC
<i>In situ</i> water-potential data with psychrometer in surface-based boreholes UZ#4, NRG-6, NRG-7a, SD-12, and UZ-7a	GS950208312232.003 GS951108312232.008 GS960308312232.001 GS960808312232.004 GS970108312232.002 GS970808312232.005 GS971108312232.007 GS980408312232.001
Psychrometer data in underground drifts Niche 3566, 3 main boreholes, 5 lateral boreholes, 5/9/97–10/21/97 Niche 3650, 6 main boreholes, 7/1/97–7/28/97 Niche 3107, 3 main boreholes, 12/22/97–1/8/98 Cross over point, ESF Main Drift 30+62 below the ECRB Cross Drift, 6/19/98–7/16/98 ECRB Cross Drift Starter tunnel, 1 slant borehole below the invert	LB980001233124.001 LB980901233124.014 LB980901233124.014
Heat dissipation probe (HDP) data in underground drifts: Niche 3566, 21 HDP, 11/4/97–7/31/98 Alcove 7, 12/9/97–1/31/98 South Ramp, 8/1/97–1/4/98 ECRB Cross Drift 0+50–7+75, 6 HDP, 4/23/98–7/31/98 ECRB Cross Drift	GS980908312242.022 GS980308312242.007 GS980308312242.002 GS980908312242.036 GS000399991221.001
Filter paper data on cores in underground drifts: Alcove 3, 1 core hole Alcove 4, 2 core holes North Ramp, 18 boreholes, Alcove 4, 3 boreholes, and South Ramp, 46 boreholes, HQ, 2-m length	GS980908312242.033 GS980908312242.032 GS980308312242.004

Five surfaced-based boreholes have enabled continuous measurements of *in situ* water potential with psychrometer since 1997 (see also Table I-5 on pneumatic pressure data). Data measured in four boreholes (UZ#4, NRG-6, NRG-7a, and SD-12) are used in the 1-D inversions for rock formation outside the fault zones. Data from UZ-7a intercepting the Ghost Dance fault are used in the 2-D inversions. The inversions use the *in situ* water-potential data summarized in the first entry of Table I-7 and the core saturation data of Table I-6.

Water-potential data measured in the ESF short boreholes and on cores generally have values substantially different from *in situ* values because of drying by drift ventilation or drying during drilling and/or handling. Drift-ventilation effects are minimized by bulkhead sealing in niches, Alcove 7, and in the second half of the ECRB Cross Drift. Preliminary data indicate that the water-potential values in the lower tuff units are in the range of -1 bar, substantially higher than values measured in the ESF Main Drift and/or sealed intervals in surface-based boreholes.

I.9 Geochemical Data

The CRWMS M&O (2000, U0085), *Analysis of Geochemical Data for the Unsaturated Zone*, and CRWMS M&O (2000, U0100), *Unsaturated Zone and Saturated Zone Transport Properties*, analyze and evaluate the UZ sorption and diffusion parameters for the UZ transport processes.

Table I-8. Geochemical Data for the UZ Model

Data Description	DTN or ACC
Mineralogic data:	
Model input and output files for mineralogic Model "MM3.0" Version 3.0.	LA9908JC831321.001
Mineralogic characterization of the ESF SHT Block	LASL831151AQ98.001
Chloride, chlorine-36, bromide, sulfate data:	
Deep boreholes, halide and ³⁶ Cl analyses NRG-4, NRG-6, and NRG-7/7A	LAJF831222AQ96.005 LAJF831222AQ96.014 LAJF831222AQ96.015 LAJF831222AQ97.007
UZ#16	
UZ-14	
SD-12	
ESF, Cl, ³⁶ Cl, Br, S	LA9909JF831222.010 LA9909JF831222.005 LAJF831222AQ98.004
ESF, CWAT#1, #2, and #3, Cl, Br, S	LAJF831222AQ98.007
Niches 3566 and 3650, Cl, Br, S	LA9909JF831222.012
Tritium data:	
SD-7, SD-9, UZ-14, NRG-7a	GS951208312272.002
Alcoves 2 and 3	GS961108312261.006
Alcove 5 SHT	GS970608312272.005
UZ-14, C#2, C#3, WT##, WT#17, WT-24, 10/06/97 – 07/01/98	GS991108312272.004

Table I-8. Geochemical Data for the UZ Model (Continued)

Data Description	DTN or ACC
DST water and gas chemistry data: CO ₂ gas analyses DST, 4 th , 5 th , and 6 th Qtr. CO ₂ data	LB991215123142.001 LB990630123142.003
UZ diffusion and dispersivity coefficients:	MO9807SPAAREST.000 MO9810SPA00026.000 MO9807SPATBDOC.000
UZ retardation data: Np sorption column measurements Radionuclide elution data through crushed tuff columns and through fractured tuff columns Radionuclide retardation measurements of Ba, CE, Se, Sr, U, Pu, and. Np Kd for zeolitic rocks in UZ transport model	LA000000000034.002 LAIT831341AQ95.001 LAIT831341AQ97.001 LAIT831341AQ96.001 LABR831371DN98.002
Busted Butte UZ transport test data: Tracer Breakthrough Concentrations Radionuclide sorption coefficients of Np, Pu, U, Se Ground penetrating radar	LA9909WS831372.001 LA9909WS831372.002 LA9909WS831372.003 LB990423123112.001 LB990423123112.002 LB000123123112.001
ESF tracer field test data: Alcove 6 fracture-matrix interaction test bed Niche 3650 drift seepage test	LB990901233124.001 LB990601233124.003
Surface water data: Southern Nevada, 8/83 – 8/86, isotope content and temperature of precipitation Fortymile Wash, 1993 water year, water quality data Fortymile Wash, 1995 water year , water quality data	GS920908315214.032 GS940308312133.002 GS960308312133.001

Table I-8. Geochemical Data for the UZ Model (Continued)

Data Description	DTN or ACC
Pore water data:	
Triaxial-Compression Extraction	GS90090123344G.001
NRG-6, NRG7/7a, UZ-14 and UZ-N55, and UZ#16, chemical data from cores	GS950608312272.001
UZ-1, UZ-14, UZ#16, NRG-6, NRG-7a, SD-7, SD-9, Alcove 3 RBT#1, RBT#4, ESF rubble, 94-96	GS961108312271.002
10/1/96 – 1/31/97	GS970208312271.002
NRG-7a, SD-7, SD-9, SD-12, UZ-14, 2/1/97 – 8/31/97	GS970908312271.003
UZ-7a, WT-24, SD-6, SD-7, SD-12, 97 – 98	GS980108312272.004
UZ-14 and UZ-16	GS990208312271.001
Uranium isotopic data:	
SW Nevada–SE California, U isotopic analyses	GS930108315213.004
U and Th analyzed 1/94 – 9/96	GS960908315215.013
Alcove 5, 4/97 – 5/97	GS970508312271.001
12/96 – 12/97	GS980108312322.003
5/89 – 8/97	GS980208312322.006
1/15/98 – 8/15/98	GS980908312322.009
Strontium isotope data:	
4/8/88 – 5/2/89	GS920208315215.012
5/3/89 – 5/9/91	GS910508315215.005
5/10/91 – 2/28/92	GS920208315215.008
11/19/92 – 12/3/93	GS931008315215.029
12/6/93 – 8/17/94	GS941108315215.010
9/7/94 – 5/4/95	GS950608315215.002
SD-7 and ESF calcite	GS970908315215.011
WT-24 and J-13	GS981008315222.004
SD-9 and SD-12	GS990308315215.004
SD-9 and SD-12, X-ray fluorescence elemental compositions	GS990308315215.003
UZ-1 carbon and oxygen data:	
UZ-1, ^{14}C	GS911208312271.009
	GS930108312271.010
	GS930408312271.020
	GS940408312271.005
	GS940408312271.008
UZ-1, $^{13}\text{C}/^{12}\text{C}$	GS911208312271.010
	GS930108312271.009
	GS930408312271.019
UZ-1, $^{13}\text{C}/^{12}\text{C}$ and $^{18}\text{O}/^{16}\text{O}$	GS940408312271.004

Geochemical data are used in the ambient geochemical model for CRWMS M&O (2000, U0050), *UZ Flow Models and Submodels*. Pore-water samples are mainly collected from eight boreholes (NRG-6, NRG-7A, SD-7, SD-9, SD-12, UZ#4, UZ-14, and UZ#16). Chloride concentrations are used in water-infiltration calibration to match the chloride distributions along the ESF and the ECRB Cross Drift. Hydro-geochemical simulations are carried out for the NRS-7A column and for the WT-24 column, with the calcite data available in the second borehole.

The transport properties are used in the CRWMS M&O (2000, U0060), *Unsaturated Zone Radionuclide Transport Model*. The K_d values for radionuclides ^{99}Tc , ^{237}Np , ^{239}U , and its daughter products (including the ^{235}U with modest absorption and long half-life) are among the important parameters used for the transport calculations. Colloidal transport is sensitive to filtration mechanisms, which are evaluated in the CRWMS M&O (2000, U0070), *Unsaturated Zone Colloid Transport Model*.

I.10 Temperature Data

The CRWMS M&O (2000, U0050), *UZ Flow Models and Submodels*, uses temperature profiles for calibration.

Table I-9. Temperature Data for the UZ Model

Data Description	DTN or ACC
<i>In situ</i> temperature data in surface-based boreholes NRG-6, NRG-7a, UZ#4, SD-12, and UZ-7a	GS950208312232.003 GS951108312232.008 GS960308312232.001 GS960808312232.004 GS970108312232.002 GS970808312232.005 GS971108312232.007 GS980408312232.001
Thermal conductivity, grain specific heat	SNT05071897001.012
Heat load data and repository footprint	SN9907T0872799.001
Hydrologic and thermal properties of drift design elements	SN9908T0872799.004
Effective thermal conductivity	SN9907T0872799.002

The recent data from six boreholes (NRG-6, NRG-7A, SD-12, UZ#4, UZ#5, UZ-7) are used for the calibration. The temperature profile data set (Sass et al. 1988) is one of the first sets of data used to indicate that the percolation flux is higher than the low value in the sub-mm/yr range. With low percolation flux, the convective contribution to heat transfer is suppressed. The deviation from conduction-only profiles is used to determine percolation flux.

I.11 Perched Water Data

The CRWMS M&O (2000, U0050), *UZ Flow Models and Submodels*, uses perched water data for calibration.

Table I-10. Perched Water Data for the UZ Model

Data Description	DTN or ACC
Water Table Elevations	MO9609RIB00038.000
Perched Water Elevations	
UZ-14	GS960308312312.005
WT-24	GS98058312313.001
G-2	GS970208312312.003
G-2	GS981008312313.003
SD-9 and NRG-7a	MOL.19980220.0164
SD-7	MOL.19971218.0442

The perched water elevations are used together with matrix liquid saturations and water potentials for the calibration. Perched water may occur where percolation flux exceeds the capacity of the tuff units to transmit vertical flux in the UZ. A permeability-barrier model and an unfractured zeolite model are used to determine the calibrated parameters for the perched water zones.

I.12 Calibrated Property Sets

The CRWMS M&O (2000, U0035), *Calibrated Properties Model*, uses the saturation-potential inversion described in Section 2.3.7 and the pneumatic inversion in Section 2.3.5 to generate the calibrated properties sets summarized in Table I-11. The calibrated property sets are used as inputs to the AMRs on UZ Flow and Transport Field.

Table I-11. Property Sets for the UZ Model

Data Description	DTN or ACC
Flow fields and calibrated hydrologic property set	LB971212001254.006
Top and bottom boundary temperatures, pressure, and boundary elevations	LB990701233129.002
<i>Calibrated 1-D parameter set for the UZ Flow and Transport Model, FY99</i>	
<i>for basecase infiltration</i>	LB997141233129.001
<i>for upper-bound infiltration</i>	LB997141233129.002
<i>for lower-bound infiltration</i>	LB997141233129.003
<i>Drift scale calibrated 1-D property set, FY99</i>	
<i>for basecase infiltration</i>	LB990861233129.001
<i>for upper-bound infiltration</i>	LB990861233129.002
<i>for lower-bound infiltration</i>	LB990861233129.003

Table I-11. Property Sets for the UZ Model (Continued)

Data Description	DTN or ACC
<i>Calibration for CRWMS M&O 2000, U0035 Calibrated Properties Model</i>	
<i>for 1-D, mountain-scale calibration</i>	LB991091233129.001
<i>for 1-D, draft-scale calibration</i>	LB991091233129.002
<i>for 2-D, fault calibration</i>	LB991091233129.003
<i>for 1-D, calibrated fault properties for the UZ Flow and Transport Model</i>	LB991091233129.001

Calibration of the UZ Flow and Transport Model is carried out in a series of steps. For the 1-D, mountain-scale calibration of formation rock (nonfault) parameters and the 2-D fault calibration, first, saturation and potential data are inverted, with permeabilities fixed. Second, the pneumatic data are inverted to calibrate the permeabilities. Third, the calibrated parameters are checked against the saturation and potential data and calibrated if necessary. And fourth, a "final" check against the pneumatic data is performed. The iteration can in principle be carried out with repeated cycles. As a result of the pneumatic inversion, site-scale fracture permeabilities in most of the TSW model layers are increased by almost two orders of magnitude compared to the prior information determined from air-injection tests. The air-injection tests use packed intervals with length a few meters or less, which is closer to the range of drift scale than site scale. In drift-scale calibration, the pneumatic pressure data are excluded. The drift-scale calibrated permeabilities are closer to drift-scale measured values.

The calibrated property sets are used as the starting point in other calibration models for different processes in different scales. The CRWMS M&O (2000, U0050), *UZ Flow Models and Submodels*, uses additional chloride, calcite, temperature and perched water data to formulate the UZ 3-D flow fields. The CRWMS M&O (2000, U0080), *Seepage Calibration Model and Seepage Testing Data*, uses UZ site-scale flow field as boundary conditions for additional drift scale calibration against niche seepage data. The CRWMS M&O (2000, N0120/U0110), *Drift-Scale Coupled Processes (DST and THC Seepage) Models*, uses the calibrated property and is validated against DST results. The CRWMS M&O (2000, U0060), *Unsaturated Zone Radionuclide Transport Model*, uses additional transport properties to evaluate radionuclide and colloid transport.

ATTACHMENT II – List of DTNs for Figures and Tables

The Q-status of the data listed in Tables II-1 and II-2 is provided in the DIRS database for this PMR.

Table II-1. DTNs for Figures

Figure Number	Data Tracking Number (DTN)
1-1.	N/A
1-2.	N/A
2.1-1.	N/A
2.1-2.	MO9901MWDGFM31.000
2.1-3.	MO9901MWDGFM31.000
2.1-4.	MO9901MWDGFM31.000
2.2-1.	LB980930123112.001
2.2-2.	(a) N/A (b) GS000399991221.002
2.2-3.	N/A
2.2-4.	(a) N/A (b) N/A (c) LAJF831222AQ98.004 LA9909JF831222.005 LA9909JF831222.010
2.2-5.	N/A
2.2-6.	(a) N/A (b) N/A (c) N/A (d) LB990901233124.002
2.2-7.	(a) N/A (b) N/A (c) N/A (d) LB990901233124.005
2.2-8.	(a) N/A (b) N/A (c) LB991131233129.002 GS000399991221.003
2.2-9.	N/A
2.2-10.	(a) GS000399991221.002 LB990801233129.003 (b) LB991131233129.001 (c) GS991299992271.001
2.2-11.	(a) N/A (b) GS980908315215.015 GS960908315215.014 (c) LAJF831222AQ98.011 GS991299992271.001
2.2-12.	(a) LB00032412213U.001 (b) N/A (c) N/A
2.2-13.	(a) N/A (b) N/A (c) LB980901123142.006
2.2-14.	N/A
2.4-1.	N/A ^a
2.4-2.	N/A ^a

^a For historical perspective only.

Table II-1. DTNs for Figures (Continued)

2.4-3.	N/A ^a
2.4-4.	N/A ^a
3.2-1.	MO9901MWDGFM31.000
3.2-2.	N/A
3.2-3.	MO9901MWDGFM31.000
3.2-4.	N/A
3.2-5.	N/A
3.2-6.	MO9901MWDGFM31.000
3.2-7.	MO9910MWDISMMM.003
3.3-1.	N/A
3.3-2.	N/A
3.3-3.	N/A
3.3-4.	N/A
3.3-5.	N/A
3.3-6.	N/A
3.3-7.	N/A
3.3-8.	N/A
3.4-1.	N/A
3.4-2.	N/A
3.4-3.	(a) MO9901MWDISMMM.000 (b) MO9910MWDISMMM.003
3.4-4.	(a) MO9901MWDISMRP.000 (b) MO9910MWDISMRP.002
3.4-5.	LB990051233129.001
3.4-6.	(a) N/A (b) LB990501233129.004 (c) LB990701233129.001
3.4-7.	(a) MO9901MWDGFM31.000 (b), (c) LB990701233129.001
3.4-8.	(a) MO9901MWDGFM31.000 (b), (c) LB990701233129.001
3.4-9.	(a) MO9901MWDGFM31.000 (b), (c) LB990501233129.004
3.5-1.	N/A
3.5-2.	(a) N/A (b) GS000399991221.002 (c) N/A
3.5-3.	N/A
3.5-4.	GS000399991221.002
3.5-5.	GS000399991221.002
3.5-6.	SN0003T0503100.001
3.6-1.	N/A
3.6-2.	N/A
3.6-3.	N/A
3.6-4.	LB991091233129.001
3.6-5.	LB991091233129.003
3.6-6.	LB997141233129.001
3.6-7.	LB997141233129.001
3.6-8.	GS960308312232.001 GS980908312242.036 LB990801233129.003 LB991121233129.007
3.6-9.	N/A
3.7-1.	N/A
3.7-2.	N/A
3.7-3.	LB990701233129.001

Table II-1. DTNs for Figures (Continued)

3.7-4.	(a) LB990801233129.003 (b) LB990801233129.015 (c) LB990801233129.009
3.7-5.	N/A
3.7-6.	MO9901MWDGFM31.000
3.7-7.	LB990801233129.003
3.7-8.	(a) LB990801233129.003 (b) LB990801233129.003
3.7-9.	LB990801233129.025
3.7-10.	(a) LB990801233129.003 (b) LB990801233129.003 (c) LB990801233129.004
3.7-11.	(a) LB990801233129.003 (b) LB990801233129.015 (c) LB990801233129.009
3.7-12.	(a) LB990801233129.003 (b) LB990801233129.015 (c) LB990801233129.009
3.7-13.	(a) LB990801233129.003 (b) LB990801233129.003
3.7-14.	LB990801233129.003 LB990801233129.009 LB990801233129.015 GS000399991221.004
3.7-15.	LB991121233129.007 GS960308312232.001
3.7-16.	SN9912T0581699.003 SN0001T0581699.004
3.7-17.	SN9912T0581699.003
3.7-18.	SN9912T0581699.003 SN0001T0581699.004
3.7-19.	N/A
3.8-1.	N/A
3.8-2.	N/A
3.8-3.	GS000399991221.002 LB990801233129.003
3.8-4.	LB991131233129.003
3.8-5.	LB991131233129.003
3.8-6.	LB991131233129.001
3.8-7.	LB991131233129.003
3.8-8.	N/A
3.9-1.	N/A
3.9-2.	N/A
3.9-3.	N/A
3.9-4.	LB990831012027.001
3.9-5.	LB990831012027.001
3.9-6.	LB980001233124.003 LB990831012027.001
3.9-7.	N/A
3.9-8.	N/A
3.9-9.	N/A
3.9-10.	SN9912T0511599.002
3.9-11.	SN9912T0511599.002
3.9-12.	N/A
3.10-1.	N/A
3.10-2.	N/A
3.10-3.	N/A

Table II-1. DTNs for Figures (Continued)

3.10-4	LB991200DSTTHC.002
3.10-5	LB991200DSTTHC.002
3.10-6	LB991200DSTTHC.002
3.10-7	LB991200DSTTHC.002
3.10-8	LB991200DSTTHC.002
3.10-9	LB991200DSTTHC.002
3.10-10	LB991200DSTTHC.002
3.10-11	LB991200DSTTHC.002
3.10-12	LB991200DSTTHC.002
3.10-13	N/A
3.11-1	N/A
3.11-2	N/A
3.11-3	N/A
3.11-4	LB991220140160.012
3.11-5	LB991220140160.012
3.11-6	LB991220140160.012
3.11-7	LB991220140160.017
3.11-8	LB9908T1233129.001
3.11-9	LB9908T1233129.001
3.11-10	LB991220140160.012 LB991220140160.017
3.11-11	N/A
3.11-12	SN9908T0581699.001 LB990901233129.001
3.11-13	SN9908T0581699.001 LB990901233129.001
3.11-14	SN9908T0581699.001 LB990901233129.001
3.11-15	SN9908T0581699.001 LB990901233129.001
3.11-16	N/A
3.12-1	N/A
3.12-2	N/A
3.12-3	LB990701233129.001
3.12-4	LB991201233129.001
3.12-5	LB991201233129.001
3.12-6	LB991201233129.001
3.12-7	LB991201233129.001
3.12-8	LB991201233129.001
3.12-9	LB991201233129.001
3.12-10	LB991201233129.001
3.12-11	LB991201233129.001
3.12-12	LB991201233129.001
3.12-13	LB991201233129.001
3.12-14	LA0004WS831372.002
5.1-1	N/A
5.1-2	N/A
5.1-3	N/A
5.1-4	N/A
5.1-5	N/A

Table II-2. DTNs for Tables

Table	Data Tracking Number (DTN)
1-1.	N/A
1-2.	N/A
1.2-1	N/A
1.2-2.	N/A
1.2-3.	N/A
1.3-1.	N/A
2.3-1.	N/A
2.5-1.	N/A
3.2-1.	N/A
3.2-2.	N/A
3.4-1.	N/A
3.5-1.	N/A
3.5-2.	GS000399991221.002
3.5-3.	GS000399991221.002
3.5-4.	GS000399991221.002
3.7-1.	GS000399991221.002
3.7-2.	LB990801233129.003 LB990801233129.009 LB990801233129.015
3.7-3.	LB990801233129.003 LB990801233129.009 LB990801233129.015
3.7-4.	LB990801233129.003 LB990801233129.009 LB990801233129.015
3.7-5.	LB990801233129.001 LB990801233129.003 LB990801233129.005 LB990801233129.007 LB990801233129.009 LB990801233129.011 LB990801233129.013 LB990801233129.015 LB990801233129.017
3.8-1.	LB991131233129.001
3.9-1.	LB991101233129.001
3.9-2.	SN9912T0511599.002
3.10-1.	LB991200DSTTHC.001
3.10-2.	N/A
3.10-3.	MO9912SPAPAI29.002
3.11-1.	LA0003AM831341.001
3.11-2.	LA0003JC831362.001
3.11-3.	LB991220140160.012
3.11-4.	LA0004WS831372.002
3.12-1.	N/A
3.13-1.	N/A
4.2-1.	N/A
4.3-1.	N/A
5.2-1.	N/A

REFERENCES FOR ATTACHMENT II

CRWMS M&O 2000 (U0100). *Unsaturated Zone and Saturated Zone Transport Properties*. ANL-NBS-HS-000019. Input Transmittal 00104.T. Las Vegas, Nevada: CRWMS M&O. ACC: 20000310.0366.

CRWMS M&O 2000 (U0095). *Analysis of Infiltration Uncertainty*. ANL-NBS-HS-000027 REV 00. Input Transmittal 00113.T. Las Vegas, Nevada: CRWMS M&O. ACC: MOL.20000313.0632.

DTN: GS000399991221.002. Rainfall/Runoff/Runon 1999 Simulations. Submittal date: 03/10/2000.

DTN: GS000399991221.003. Preliminary Alcove 1 Infiltration Experiment Data. Submittal date: 03/10/2000.

DTN: GS000399991221.004. Preliminary Developed Matrix Properties. Submittal date: 03/10/2000.

DTN: GS960308312232.001. Deep Unsaturated Zone Surface-Based Borehole Instrumentation Program Data from Boreholes USW NRG-7A, USW NRG-6, UE-25 UZ#4, UE-25 UZ#5, USW UZ-7A, and USW SD-12 for the Time Period 10/01/95 through 3/31/96. Submittal date: 04/04/1996.

DTN: GS960908315215.014. Uranium and Thorium Isotope Data for ESF Secondary Minerals Collected Between March 1996 and July 1996. Submittal date: 09/25/1996.

DTN: GS980908312242.036. Water Potentials Measured With Heat Dissipation Probes in ECRB Holes from 4/23/98 to 7/31/98. Submittal date: 09/22/1998.

DTN: GS980908315215.015. Uranium and Thorium Isotope Data Including Calculated $^{230}\text{Th}/\text{U}$ Ages and Initial $^{234}\text{U}/^{238}\text{U}$ Activity Ratios for in Situ Microdigestions of Outermost Opal-Rich Mineral Coatings from the Exploratory Studies Facility Analyzed Between 12/01/97 and 09/15/98. Submittal date: 09/23/1998.

DTN: GS991299992271.001. Preliminary Unsaturated Zone Borehole Hydrochemistry Data. Submittal date: 12/23/1999.

DTN: LA0003AM831341.001. Preliminary Revision of Probability for Sorption Coefficients (K_{DS}). Submittal date: 03/29/2000. Submit to RPC URN-0267

DTN: LA0003JC831362.001. Preliminary Matrix Diffusion Coefficients for Yucca Mountain Tuffs. Submittal date: 4/10/2000.

DTN: LA9909JF831222.005. Chlorine-36 Analyses of ESF and Busted Butte Porewaters in FY99. Submittal date: 09/29/1999.

DTN: LA9909JF831222.010. Chloride, Bromide, Sulfate, and Chlorine-36 Analyses of ESF Porewaters. Submittal date: 09/29/1999.

DTN: LA0004WS831372.002. Sorption of Np,Pu, and Am on Rock Samples From Busted Butte, NV. Submittal date: 04/19/2000. Submit to RPC.

DTN: LAJF831222AQ98.004. Chloride, Bromide, Sulfate, and Chlorine-36 Analyses of Salts Leached from ESF Rock Samples. Submittal date: 09/10/1998.

DTN: LAJF831222AQ98.011. Chloride, Bromide, Sulfate and Chlorine-36 Analyses of Springs, Groundwater, Porewater, Perched Water and Surface Runoff. Submittal date: 09/10/1998.

DTN: LB980001233124.003. Liquid Release Tests Performed to Determine if a Capillary Barrier Exists in Niches 3566 and 3650. Submittal date: 04/23/1998.

DTN: LB00032412213U.001. Busted Butte Ground Penetrating Radar Data Collected June 1998 through February 2000 at the Unsaturated Zone Transport Test (UZTT): GPR Velocity Data. Submittal date: 03/24/2000. Submit to RPC

DTN: LB980901123142.006. Laboratory Test Results of Hydrological Properties from Post-Test Dry-Drilled Cores in the Single Heater Test Area for the Final TDIF Submittal for the Single Heater Test. Submittal date: 08/31/1998.

DTN: LB980930123112.001. Surface to ESF Seismic Tomography. Submittal date: 09/30/1998.

DTN: LB990051233129.001. Extent of Vitric Region Used to Assign Material Properties in FY 9 UZ Model Layers; Figure 5 From AMR U0000, "Development of Numerical Grids for UZ Flow and Transport Modeling." Submittal date: 09/24/99.

DTN: LB990501233129.004. 3-D UZ Model Calibration Grids for AMR U0000. "Development of Numerical Grids of UZ Flow and Transport Modeling." Submittal date: 09/24/1999.

DTN: LB990701233129.001. 3-D UZ Model Grids for Calculation of Flow Fields for PA for AMR U0000, "Development of Numerical Grids for UZ Flow and Transport Modeling." Submittal date: 09/24/1999.

DTN: LB990801233129.001. TSPA Grid Flow Simulations for AMR U0050, "UZ Flow Models and Submodels." (Flow Field #1). Submittal date: 11/29/1999.

DTN: LB990801233129.003. TSPA Grid Flow Simulations for AMR U0050, "UZ Flow Models and Submodels." (Flow Field #3). Submittal date: 11/29/1999.

DTN: LB990801233129.004. TSPA Grid Flow Simulations for AMR U0050, "UZ Flow Models and Submodels." (Flow Field #4). Submittal date: 11/29/99.

DTN: LB990801233129.005. TSPA Grid Flow Simulations for AMR U0050, "UZ Flow Models and Submodels." (Flow Field #5). Submittal date: 11/29/1999.

DTN: LB990801233129.007. TSPA Grid Flow Simulations for AMR U0050, "UZ Flow Models and Submodels." (Flow Field #7). Submittal date: 11/29/1999.

DTN: LB990801233129.009. TSPA Grid Flow Simulations for AMR U0050, "UZ Flow Models and Submodels." (Flow Field #9). Submittal date: 11/29/1999.

DTN: LB990801233129.011. TSPA Grid Flow Simulations for AMR U0050, "UZ Flow Models and Submodels." (Flow Field #11). Submittal date: 11/29/1999.

DTN: LB990801233129.013. TSPA Grid Flow Simulations for AMR U0050, "UZ Flow Models and Submodels." (Flow Field #13). Submittal date: 11/29/1999.

DTN: LB990801233129.015. TSPA Grid Flow Simulations for AMR U0050, "UZ Flow Models and Submodels." (Flow Field #15). Submittal date: 11/29/1999.

DTN: LB990801233129.017. TSPA Grid Flow Simulations for AMR U0050, "UZ Flow Models and Submodels." (Flow Field #17). Submittal date: 11/29/1999.

DTN: LB990801233129.025. TSPA Grid Flow Simulations for AMR U0050, "UZ Flow Models and Submodels." Flow Field #25: Present Day Mean Infiltration for Flow-Through Perched-Water Conceptual Model. Submittal date: 3/11/00.

DTN: LB990831012027.001. Input to Seepage Calibration Model AMR U0080. Submittal date: 08/31/1999.

DTN: LB9908T1233129.001. Transport simulations for the low, mean, and upper infiltration scenarios of the present-day, monsoon, and glacial transition climates. Submittal date: 3/11/00.

DTN: LB990901233124.002. Alcove 6 Flow Data for AMR U0015, "In Situ Field Testing of Processes." Submittal date: 11/01/99.

DTN: LB990901233124.005. Alcove 4 Flow Data for AMR U0015, "In Situ Field Testing of Processes." Submittal date: 11/01/99.

DTN: LB990901233129.001. Input and Output Data for Verification of Dual-Continua Particle Tracker (DCPT) for AMR U0155, "Analysis Comparing Advection-Dispersion Transport Solution to Particle Tracking." Submittal date: 10/26/99.

DTN: LB991091233129.001. One-Dimensional, Mountain-Scale Calibration for AMR U0035, "Calibrated Properties Model." Submittal date: 10/22/1999.

DTN: LB991091233129.003. Two-Dimensional Fault Calibration for AMR U0035, "Calibrated Properties Model." Submittal date: 10/22/99.

DTN: LB991101233129.001. Model Input/Output Files Supporting Seepage Model for PA in AMR U0075, "Seepage Model for PA Including Drift Collapse." Submittal date: 11/30/99.

DTN: LB991121233129.007. Calibrated parameters for the present-day, mean infiltration scenario, used for simulations with perched water conceptual model #3 (non-perching) for the mean infiltration scenarios of the present-day, Monsoon and Glacial transition climates. Submittal date: 3/11/00.

DTN: LB991131233129.001. Modeling calcite deposition and percolation. Submittal date: 3/11/00.

DTN: LB991131233129.002. Modeling seepage and tracer tests at Alcove 1. Submittal date: 3/11/00.

DTN: LB991131233129.003. Analytical and Simulation Results of Chloride and Chlorine-36 Analysis. Submittal date: 3/11/00.

DTN: LB991200DSTTHC.001. Pore water composition and CO2 partial pressure input into THC simulations of the Drift Scale Test and the THC Seepage Model, Table 3 of AMR U0110/N0120. Submittal date: 3/11/00.

DTN: LB991200DSTTHC.002. Model Input and Output Files, Excel Spreadsheets and Resultant Figures which are Presented in AMR N0120/U0110, "Drift-Scale Coupled Processes (Drift-Scale Test and THC Seepage) Models." Submittal date: 12/15/99.

DTN: LB991201233129.001. The Mountain-Scale Thermal-Hydrologic Model Simulations for AMR U0105, "Mountain-Scale Coupled Processes (TH) Models." Submittal date: 12/15/99.

DTN: LB991220140160.012. Model Prediction of 3-D Transport, Present-Day Infiltration, #1 Perched Water Model, using EOS9nT Input and Output files. Submittal date: 3/11/00.

DTN: LB991220140160.017. Model Prediction of 3-D Colloid Transport, Present-Day Infiltration, #1 Perched Water Model, using EOS9nT Input and Output files. Submittal date: 3/11/00.

DTN: LB997141233129.001. Calibrated Base-case Infiltration 1-D Parameter Set for the UZ Flow and Transport Model FY99. Submittal date: 07/21/1999.

DTN: MO9901MWDGFM31.000. Geologic Framework Model. Submittal date: 01/06/1999.

DTN: MO9901MWDISMMM.000. Mineralogy Models. Submittal date: 01/22/1999. Submit to RPC.

DTN: MO9910MWDISMMM.003. ISM3.1 Mineralogic Models. Submittal date: 10/01/99.

DTN: MO9901MWDISMRP.000. ISM3.0 Rock Properties Models. Submittal date: 01/22/1999. Submit to RPC.

DTN: MO9910MWDISMRP.002. Rock Properties Model (RPM3.1). Submittal date: 10/06/1999.

DTN: MO9912SPAPAI29.002. PA Initial Abstraction of THC Model Chemical Boundary Conditions. Submittal date: 01/11/2000. Submit to RPC URN-0282.

DTN: SN0001T0581699.004. Supplemental Files to Support Base-case Particle-tracking Analysis for TSPA-SR (Total System Performance Assessment-Site Recommendation) (In Analysis/Model Report U0160, ANL-NBS-HS-000024). Submittal date: 01/06/2000.

DTN: SN0003T0503100.001. Weighting Factors for Low, Middle and High Climate Infiltration Rate Maps. Submittal date: 03/20/2000.

DTN: SN9908T0581699.001. Files to Support 1-D Comparison Between FEHM Particle Tracking and T2R3D Advective-Dispersive Transport Simulations along SD-9. Submittal date: 08/16/99.

DTN: SN9912T0511599.002. Revised Seepage Abstraction Results for TSPA-SR (Total System Performance Assessment-Site Recommendation). Submittal date: 12/15/99.

DTN: SN9912T0581699.003. Files to Support Base-case Particle-tracking Analyses (AMR U0160) for TSPA-SR. Submittal date: 12/13/99.